AARHUS UNIVERSITY

midt
Central Denmark Region

Kinematic investigation of knee osteoarthritis and arthroplasty designs

- employing dynamic radiostereometry

PhD DISSERTATION

Emil Toft Petersen

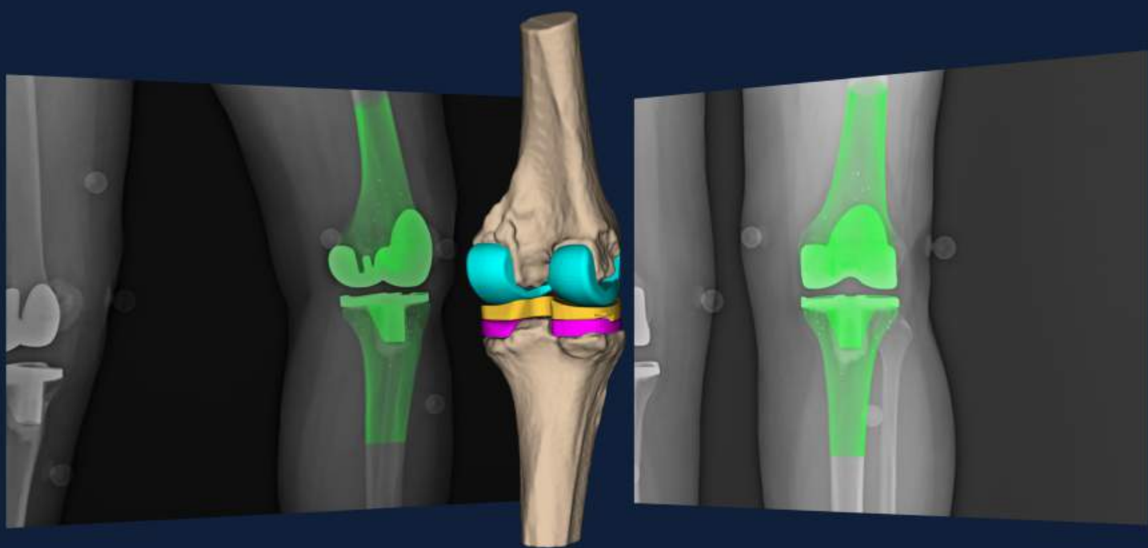

Faculty of Health
Aarhus University
2021

Kinematic investigation of knee osteoarthritis and arthroplasty designs

- employing dynamic radiostereometry

PhD DISSERTATION

Emil Toft Petersen

Faculty of Health

Aarhus University

and

Department of Orthopaedics

Aarhus University Hospital

Correspondence

Emil Toft Petersen, MSc Sports Technology

AutoRSA Research Group

Department of Orthopaedics

Aarhus University Hospital

Palle Juul-Jensens Boulevard 165, J501

DK – 8200 Aarhus N

E-mail: emiltp@clin.au.dk

Phone: + 45 22 88 88 60

PhD DISSERTATION by Emil Toft Petersen

The Graduate School of Health, Aarhus University

Public defence: March 11, 2022

Supervisors

Maiken Stilling, Professor, MD, PhD (*Main Supervisor*)
Department of Orthopaedics, Aarhus University Hospital, Denmark
Department of Clinical Medicine, Aarhus University, Denmark
Email: maiken.stilling@clin.au.dk

Søren Rytter, Associate Professor, MD, PhD
Department of Orthopaedics, Aarhus University Hospital, Denmark
Department of Clinical Medicine, Aarhus University, Denmark
Email: soeren.rytter@rm.dk

Michael Skipper Andersen, MSc, PhD
Department of Materials and Production, Aalborg University, Denmark
Email: msa@mp.aau.dk

Evaluation Committee

Anne Grethe Jurik, Professor, MD, PhD (*Chairman*)
Department of Radiology, Aarhus University Hospital, Denmark
Department of Clinical Medicine, Aarhus University, Denmark
Email: anne.jurik@aarhus.rm.dk

Scott Arthur Banks, Professor, Head of Department, MSc, PhD
Department of Mechanical & Aerospace Engineering
University of Florida, USA
Email: banks@ufl.edu

Elena Gutierrez-Farewik, Professor, MSc, PhD
Department of Mechanics, Director of KTH MoveAbility Lab & KTH BioMEx Center
KTH Royal Institute of Technology Stockholm, Sweden
Email: lanie@kth.se

Acknowledgements

The studies presented in this thesis are based on the scientific work conducted during my enrollment as a PhD student at the Faculty of Health, Aarhus University, in the period from February 2017 to December 2020. All data acquisition work was performed and supported by the University Clinic for Hand, Hip and Knee Surgery at Holstebro Regional Hospital, Denmark. My warmest thanks to Torben Bæk Hansen, Head of Department, for making this possible.

Several people need mentioning for the help they have provided and the role they have played in allowing me to conclude the dissertation. First of all, I would like to express my gratitude to my main supervisor Maiken Stilling and to co-supervisors Søren Rytter, and Michael Skipper for making this project possible and for always providing support and feedback. The journey began quite a few years back during my Masters, which allowed projects in which an external part participated. Here, I met Maiken Stilling, one of the leading researchers in the field of radiostereometric analysis. Maiken, in collaboration with Michael Skipper Andersen, my internal supervisor at the time, enrolled me in both their research societies and fields of research. Just as I concluded my master, Maiken invited me to continue on as a PhD student – which I gladly accepted. I sincerely appreciate that you both believed in me and gave me the opportunity to walk on the path of research. It is inspiring to see how much impact you both have within your respective fields.

Thank you Maiken for the guidance you have provided and the trust that you have shown me; and thank you for the opportunity to work with this exiting topic. Your

enthusiasm for research is infectious and your encouragement has had considerable impact on me, personally as well as professionally.
Thank you, Michael, for the technical insight you have brought to the study. Your technical experience and understanding of knee pathomechanics have been crucial in the development of the work presented in this thesis. I have always been inspired by and thoroughly enjoyed our technical discussions, and I hope we may continue this activity in other research projects in the years to come.
Thank you, Søren, for the clinical insight you have brought to the study. It is a pleasure to work with you and I am grateful for your valuable explanations of various clinical questions and for your essential role in connecting the research findings to the daily clinic.

I also need to mention Anne Dorthe Riedel as you have been essential to this study. Thank you so much for your neurotic need to keep everything organized and your impressive work ethic. Without your help keeping an overview of the patients, analysis, etc. (I could probably go on), this project would not have been possible.
In addition, a special thanks to the knee surgeons for the extra work you contributed by agreeing to include the patients; to Pia Toft Pedersen, for booking all appointments, which I know has been challenging; to all the radiographers at RSA, CT and MRI for the extra hours you have devoted to this project, especially to Michal Nibe Mathiasen and Lars Lindgren for the countless number of hours spent in the RSA rooms; to Torben Svenningsen and Uffe Møller-Pedesen for helping me build equipment for the various exercises; and to the patients and volunteers, for your participation – I can truly say that the project would not have been possible without you.

My daily life as a PhD fellow would not have been the same without the company of our research group and colleagues. I deeply value our group and appreciate your role in making it a pleasure to be at the office.

Finally, I owe heartfelt thanks to my family and friends who have supported and encouraged me. Above all, I need to express my gratitude to my loving wife, Anna-Lena, and our two wonderful daughters Nora and Sofia. You mean the world to me. I could not have done this without your love, support and understanding. I feel truly blessed to be surrounded by such a wonderful family.

Emil Toft Petersen

December 1st, 2021

The work presented in this dissertation was generously supported by Zimmer Biomet, Aarhus University, the Toyota Foundation, the Danish Rheumatism Association, Købmand Sven Hansen og Hustru Ina Hansens Fond, Søster og Verner Lipperts Fond, and Ortopædkirurgisk Forskningsfond i Århus.

List of papers

This dissertation was based on the following four papers:

The papers of this dissertation will be referred to in the text by their Roman numerals (I-IV).

1. R Christensen, **ET Petersen***, JH Jürgens-Lahnstein, S Rytter, L Lindgren, S de Raedt, A Brüel, M Stilling (2021). Assessment of knee kinematics with dynamic radiostereometry: Validation of an automated model-based method of analysis using bone models. Journal of Orthopaedic Research. doi: 10.1002/jor.24875.

2. **ET Petersen**, TD Vind, JH Jürgens-Lahnstein, R Christensen, S de Raedt, A Brüel, S Rytter, MS Andersen, M Stilling (2021). Evaluation of automated radiostereometric image registration in total knee arthroplasty utilizing a synthetic-based volumetric implant model and a CT-based volumetric bone model. Submitted to Journal of Orthopaedic Research.

3. **ET Petersen**, S Rytter, D Koppens, J Dalsgaard, TB Hansen, NE Larsen, MS Andersen, M Stilling (2021). Patients with knee osteoarthritis can be divided into subgroups based on tibiofemoral joint kinematics – an exploratory and dynamic radiostereometric study. Osteoarthritis and Cartilage. doi: 10.1016/j.joca.2021.10.011.

4. **ET Petersen**, S Rytter, D Koppens, J Dalsgaard, TB Hansen, MS Andersen, M Stilling (2021). In vivo kinematic comparison of Medial Congruent and Cruciate Retaining polyethylene designs in total knee arthroplasty - A randomized controlled study of gait using dynamic radiostereometry. Submitted to Knee Surgery, Sports Traumatology, and Arthroscopy.

*I had an essential role in this study and developed the customized program used to process the analysis and method comparisons. In addition, I had an essential role in preparing the study design, data acquisition and management, data interpretation and data presentation. Finally, I provided critical input to the revision of the manuscript.

English summary

Osteoarthritis is a highly prevalent chronic disorder causing degenerative joint changes often associated with joint pain and disability limiting daily activities.[1] The knee is the most commonly affected weightbearing joint in osteoarthritis. The prevalence of painful and disabling knee osteoarthritis (KOA) in adults over 55 years of age is 10%, and a quarter of those affected are severely disabled.[2] Thus, KOA has a considerable impact on the patients' physical and psychosocial health and well-being, but also generates a significant financial burden on the healthcare systems.[3,4] In Denmark, with 60,000-65,000 patients consulting their general practitioner for KOA annually, and with half of these being allocated surgery, the present Danish arthritis-related expenses accrue to 11 billion DKK annually.[5,6] In step with the increasing life expectancy and demographic changes, an increase is expected in the number of patients with disabling KOA and in the ensuing financial healthcare burden.[7–9]

End-stage KOA can be treated surgically with total knee arthroplasty (TKA), which is a well-documented and successful treatment.[10,11] However, up to 20% of patients are dissatisfied with the outcome. Considerable efforts have been devoted to reducing the number of dissatisfied patients; however, these efforts have not yet been successful. The search for ways to enhance patients' health-related quality-of-life, performance and satisfaction have resulted in the widespread application of various TKA implant designs. However, for development of naturally functioning implants, it is fundamental to first understand the normal knee kinematics, the underlying pathomechanics of the osteoarthritis affected knees and the implant designs' influence on knee mechanics.

The overall aim was two-fold: A methodological aim was to evaluate the accuracy of automated dynamic radiostereometric (dRSA) image registration methods; and a clinical aim was to investigate knee pathomechanics in osteoarthritic knees and the mechanical influence of knee arthroplasty designs during gait as a daily activity utilizing dRSA.

Study I presented an automated 2D/3D image registration for dRSA of the knee utilizing computed tomography (CT)-based volumetric bone models which was compared with model-configuration models as gold standard. Two different dRSA setups were evaluated. The image registration accurately measures the tibiofemoral joint kinematics and was not sensitive to the RSA setup. The automated method presented is clinically applicable for functional evaluation of native tibiofemoral joint kinematics and pathomechanics related to specific conditions such as ligament instability and bone dysplasia; and it is applicable for assessment of surgical results. **Study II** presented an automated marker-free bone image registration method using radiostereometric analysis (RSA) for an arthroplasty knee joint in which the radiopaque implant components occluded or replaced a large part of the bone. The results revealed similar accuracy as the gold standard marker-based method. In addition, a synthetic volumetric implant model utilizing digitally reconstructed radiographs (DRR), which may provide more information to the automated registration, was designed and studied. However, in its present form, the volumetric implant model and DRR method did not markedly improve the traditional automated method. **Study III** presented kinematic heterogeneity in patients with KOA during gait. The results revealed four subgroups, each displaying distinguished kinematic gait patterns that relate well to their clinical characteristics. In addition, these subgroups exhibited joint kinematics clearly different from those of healthy volunteers without KOA, including differences that were not present when comparing the entire KOA cohort with the healthy group. **Study IV** demonstrated that the more anatomical

Persona® Medical Congruent® (MC) bearing design changes tibiofemoral joint kinematics compared with the Persona® Cruciate Retaining (CR) bearing. The MC bearing provided an enhanced area of congruency while exhibiting more tibial anterior drawer throughout the gait cycle and greater external tibial rotation during the second half of the swing phase. Thus, the MC bearing design may help prevent so-called paradoxical motion, produce a more effective screw-home movement and contribute more stability during knee motion. This may improve the patient's confidence in knee function during daily activities and thereby potentially lead to improved patient satisfaction.

The four studies together contribute to an enhanced understanding of the native and the artificial knee joint, which may inspire the development of improved and more patient-specific treatment strategies in the future. Furthermore, a method to aid clinicians to evaluate the implant fixation in any TKA patient was developed.

Danish summary

Artrose (slidgigt) er en hyppig degenerativ lidelse, som ofte rammer knæleddet og medfører smerte, stivhed og muskelsvaghed, fejlstilling af knæet og deraf følgende funktionstab. Omkring 10% af voksne over 55 år oplever smertefuld funktionshæmmende knæartrose, og 50% heraf er svært hæmmede. Ud over at patienterne oplever en fysisk begrænsning, påvirkes deres psykosociale helbred også, og sundhedsvæsenet belastes økonomisk. Årligt konsulterer 60.000-65.000 patienter deres praktiserende læge med smerter på grund af knæartrose. Halvdelen af disse patienter har brug for behandling, hvilket medfører en udgift på omkring 11 milliarder kroner om året.

Slutstadiet af knæartrose behandles med et kunstigt knæ, hvilket for langt de fleste medfører smertefrihed. Dog er op mod 20% af patienterne ikke fuldt tilfredse og ca. 6% får foretaget en udskiftning af det kunstige knæ inden for de første 5 år. Årsagen hertil er oftest relateret til løshed, løsning eller slitage af det kunstige knæ og/eller smerter uden umiddelbart forklarlige årsager, hvilket kan give en unormal knæfunktion. I Danmark udføres årligt næsten 11.000 førstegangsoperationer med indsættelse af knæledsprotese og ca. 1.000 udskiftninger af knæledsprotese. Den aldrende befolkning, stigende vægt og ønsket om at vedligeholde en aktiv livsstil langt ind i pensionistalderen vil forventeligt føre til flere patienter med knæartrose og dermed flere operationer med knæledsprotese. Fra år 2017-2019 er antallet af førstegangsoperationer steget med 30% i Danmark, og i USA forventes det at stige med 143% fra 2012 til 2050.

Patienter med artrose er forskellige, men alligevel er det kunstige knæled i udgangspunktet ens for alle patienter, og der tages ikke højde for forskelle i anatomi og funktion. En mere individuel behandling kan potentielt bidrage til større patienttilfredshed. Et nyt knæprotesedesign, som i højere grad tager højde for anatomiske forskelle, er udviklet med henblik på at genskabe en mere naturlig funktion og balance i knæleddet.

Med de hidtil anvendte billeddiagnostiske metoder har det kun været muligt at fremstille knæet stillestående, hvilket ikke har kunnet give informationer om knæleddets funktion under bevægelse, selvom det er her, at patienten oplever sine udfordringer. Der har været efterspørgsel og ønske om nye og mere dynamiske kliniske undersøgelsesmetoder af knæleddet under bevægelse. Dynamisk stereorøntgen (røntgenfilm) kan anvendes til at beregne knæets mekaniske funktion meget nøjagtigt under traditionelle daglige aktiviteter og i netop de situationer, hvor patienten føler smerte.

Formålet med denne afhandling var at undersøge I) en automatisk metode, som kan anvendes til funktionelle undersøgelser af det naturlige knæled, II) en automatisk metode som kan undersøge det kunstige knæled, III) hvorledes patienter med knæartrose kan kategoriseres ud fra deres gangmønster, og IV) hvordan et mere anatomisk knæprotesedesign påvirker knæets mekaniske funktion.
Studie I undersøgte en automatiseret billedregistreringsmetode, som anvendte tredimensionelle knoglemodeller og dynamisk stereorøntgen til at måle knæfunktionen i to forskellige opstillinger. Metoden viste meget nøjagtige målinger af knæets bevægelse for begge opstillinger. Dynamisk stereorøntgen kan således anvendes som et klinisk værktøj til at undersøge forskellige knælidelser, heriblandt artrose. **Studie II** udviklede en automatiseret billedregistreringsmetode til

stereorøntgen, som kan anvende tredimensionelle knogle- og protesemodeller til at undersøge kunstige knæ. Modsat tidligere metoder kan knogleregistreringsmetoden anvendes med samme høje nøjagtighed til alle patienter, mens protesemetoden har en lidt lavere nøjagtighed i forhold til mere manuelle metoder. **Studie III** undersøgte gangmønstre i patienter med knæartrose. Resultaterne viste, at patienterne kunne inddeles i fire grupper ud fra deres gangmønstre. Disse grupper er kendetegnet ved, hvor i knæet der var artrose, graden af artrose og graden af ledbåndsskade. **Studie IV** undersøgte knæmekanikken under gang for et anatomisk protesedesign sammenlignet med et symmetrisk standard-protesedesign. Det anatomiske design viste mere naturlige knæbevægelser, som potentielt kan bidrage til et mere stabilt knæled, hvilket kan medvirke til at genetablere patientens tillid til knæets funktion og dermed føre til større patienttilfredshed.

De fire studier bidrager tilsammen med kliniske værktøjer, som kan anvendes til undersøgelse af knæfunktionen i naturlige og kunstige knæ. Dette vil give knækirurgen bedre mulighed for at tilbyde patienten en mere målrettet behandling. Desuden bidrager studierne med en dybere forståelse af de mekaniske ændringer som følge af artrose samt af, hvordan et anatomisk knæprotesedesign potentielt kan bidrage til styrket patienttilfredshed.

Contents

List of Figures

List of Tables

Abbreviations

ACL	Anterior cruciate ligament
CI	Confidence interval
CR	Persona® Cruciate retaining
CT	Computed tomography
DRR	Digitally reconstructed radiographs
dRSA	Dynamic radiostereometry
FJS	Forgotten Joint Score
KOA	Knee osteoarthritis
KOOS	Knee Injury and Osteoarthritis Outcome Score
LCL	Lateral collateral ligament
LM	Lateral-medial
MC	Persona® Medial Congruent®
MCID	Minimal clinical important difference
MCL	Medial collateral ligament
MRI	Magnetic resonance imaging
OKS	Oxford Knee Score
PCL	Posterior cruciate ligament
RSA	Radiostereometry
SnPM	Statistical non-parametric mapping
SPM	Statistical parametric mapping
TKA	Total knee arthroplasty
VAS	Visual analogue scale

1

Introduction

1.1 Knee osteoarthritis

Knee osteoarthritis (KOA) is the most common form of arthritis in weight-bearing joints and affects millions of individuals worldwide.[8,9] The prevalence of painful and disabling KOA in adults above age 55 years of age is 10%, and a quarter of those affected are severely disabled.[2] KOA affects patients' physical and psychosocial health and generates a significant financial healthcare burden.[3,4] In Denmark, 60,000-65,000 patients see their general practitioner for KOA annually.[5] Fifty percent of these patients are operated, thereby generating Danish arthritis-related expenses in the order of 11 billion DKK annually.[5,6] In step with the increasing life expectancy and demographic changes, an increase in the number of patients with disabling KOA and a corresponding increase in healthcare expenses are expected.[7–9]

1.1.1 Risk factors

Multiple risk factors are associated with KOA. Overall, KOA may be divided into primary osteoarthritis without any apparent underlying cause besides increasing age, female gender, and genetic factors; and secondary osteoarthritis with more apparent reasons (previous joint injury, repetitive joint stress, joint malalignment and obesity).[9,12,13]

Primary knee osteoarthritis: A meta-analysis has presented different risk factors for development and progression of KOA. The authors found a linear association between age below 80 years and the incidence rate of KOA.[13] Females have a two-fold higher risk of KOA than males and a more severe KOA progression.[13,14] This may possibly be related to joint biomechanics, as female knee biomechanics exhibit more knee abduction and hip adduction than male knee biomechanics.[15] Hormonal factors such as estrogen have been hypothesized to play a role in a higher susceptibility for development and progression of KOA in females.[14] The extensor apparatus muscle strength has also been described as a risk factor with an odds ratio of 1.65 for developing KOA in both males and females.[16] Evidence for an association between genetics and a risk of KOA has been inconsistent.[9,17,18] However, genome-wide association studies have proven to be a powerful tool to establish several genes or loci associated with a risk of KOA.[19–21] The gene GDF5 encodes proteins that regulate the development of numerous tissues and cells and promote maintenance and repair of synovial joint tissue, particularly cartilage and bone.[20] It has been shown to have a strong association with self-reported knee pain.[18,20]

Secondary knee osteoarthritis: Persons with previous knee trauma have a four times higher risk of developing KOA than persons without any knee trauma history.[13,22,23] Patients who previously sustained a knee trauma have been suggested to account for approximately 10% of KOA cases.[23,24] The influence of physical activity as a risk factor for KOA is two-sided. On one hand, vigorous physical activity induces cartilage loss; on the other hand, physical activity is a significant factor in maintaining cartilage and a healthy knee joint.[9] Magnetic resonance imaging (MRI) has shown that physical activity resulted in cartilage degeneration for persons with a low baseline cartilage volume or bone marrow lesions, whereas persons with a high baseline cartilage volume and absence of bone marrow lesions either gained, maintained or had only slow degeneration of cartilage in relation to physical activity.[25–27] Former athletes have an up to 30% increased KOA prevalence with soccer being the sport with the largest influence, which is probably explained by increased knee loading and knee trauma such as anterior cruciate ligament (ACL) injuries.[13,28–30] Certain occupational activities increase the risk of developing and aggravating KOA.[31] These occupations are characterized by highly demanding physical activities that include, in particular, kneeling, squatting, lifting and climbing. Among workers exposed to these activities, obese workers have an even higher KOA prevalence.[31,32] Previous obesity has been shown to increase the risk of developing KOA.[33,34] Obesity (Body Mass Index > 25) is associated with a 2.63 times higher risk of KOA progression.[13] Furthermore, body fat has been shown to be a strong predictor of cartilage loss independently of fat-free mass.[35]

1.1.2 Pathogenesis

KOA is a heterogeneous disease with distinct characteristics during various stages of disease progression. Over time, the disease affects the entire knee joint including bone, cartilage, the synovial membrane and fluid, periosteum, and the ligaments and muscles surrounding the knee joint.[9,21] KOA occurs when the dynamic steady state between destructive forces and repair mechanisms inhibits joint homeostasis.[36,37] First, the cartilaginous structure begins to break down from a combination of wear and tear. From this stage, the degenerative process of the cartilage continues, and changes are very evident when compared to the healthy joint.[12,21] Next, the cartilaginous surface of the joint begins to erode, thus narrowing the gap between the bones (joint-space-width), and the viscosity and elasticity of the synovial fluid decreases, which subsequently increases joint friction.[12,21] Finally, osteoarthritis starts to affect the subchondral bone that flattens and, as it starts to repair itself, proteins such as cytokines and chemokines are released into the synovial fluid. The proteins form part of a chain reaction that destroys cartilage and soft tissues. Osteophytes continue to develop – bone moves against bone (attrition) – causing severe pain, stiffness, reduction in range of motion and muscle weakness that limits daily living and quality of life.[12,21,38,39]

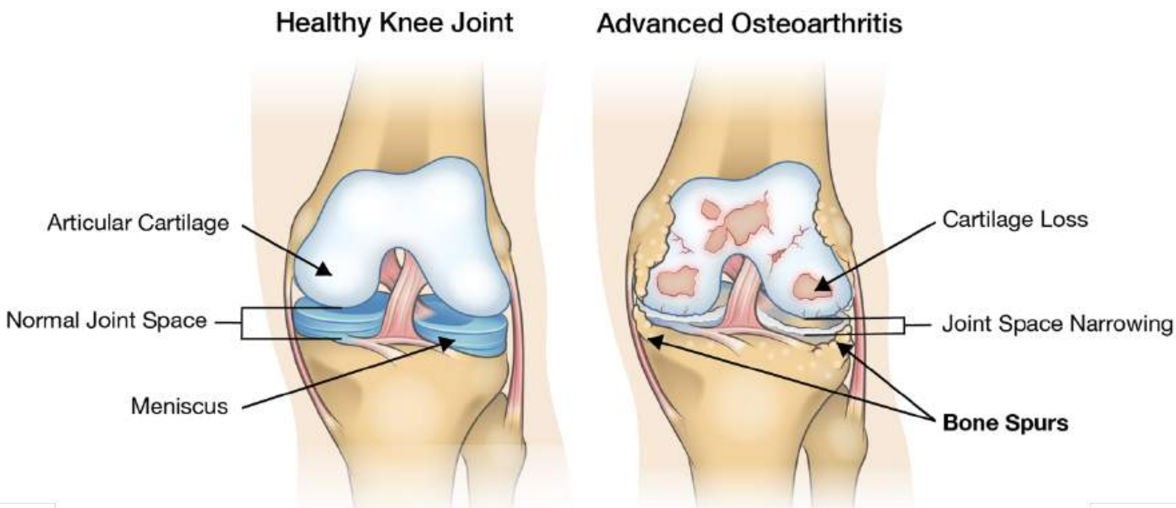

Figure 1-1 The healthy knee (left) and a knee with advanced osteoarthritis (right).[40] The knee consists of the femur, tibia, fibula and patella bones. The articulating areas of the bones are covered with articular cartilage, a smooth and non-fissuring collagen. Furthermore, the knee joint is encapsulated in a synovial membrane containing a viscous synovial fluid aiding in lubricating painless joint movement throughout the range of motion.

1.1.3 Diagnostics and classification

The diagnosis of KOA is based on an overall assessment of risk factors, symptoms and objective and radiological findings. Knee pain and impaired function together with radiographically assessed joint-space-narrowing are commonly used to identify KOA.[41] Several radiographic KOA classifications exist (Table 1-1, Figure 1-2).[42,43]

Figure 1-2 Knee osteoarthritis radiographs showing five examples of the Ahlbäch grading scale.[44]

The Kellgren-Lawrence[42] classification and the Ahlbäch[43] score are two widely used classification schemes. The Kellgren-Lawrence classification is based on radiological grading of osteoarthritis and is oriented on joint-space narrowing, osteophytes and bone sclerosis and deformation. Interobserver precision and arthroscopic correlation are lower for the Kellgren-Lawrence score than for the Ahlbäch score.[45] Originally, the Ahlbäch score was divided into four grades: grade 1, joint-space-narrowing (less than 3 mm) with or without subchondral sclerosis; grade 2, obliteration of joint space; grade 3, minor bone attrition and less than 5 mm joint-space-narrowing; grade 4, moderate bone attrition and 5-10 mm joint-space-narrowing. Subsequently, the Ahlbäch score was appended a fifth grade defined as severe bone attrition and a joint-space narrowing exceeding 10 mm.[46] In this dissertation, the modified version of the Ahlbäch score was used to grade KOA.

Table 1-1 The Ahlbäck classification of radiographic knee osteoarthritis of the tibiofemoral joint and the Kellgren-Lawrence grading system (adapted).[47]

Ahlbäck		Kellgren-Lawrence	
Grade	Definition	Grade	Definition
		'Doubtfull'	Minute osteophyte, doubtful significance
		'Minimal'	Definite osteophyte, unimpaired joint space
1	Joint space narrowing (< 3mm)	'Moderate'	Moderate diminution of joint space
2	Joint space obliteration	'Severe'	Joint space greatly impaired with sclerosis of subchondral bone
3	Minor bone attrition (0-5 mm)	'Severe'	Joint space greatly impaired with sclerosis of subchondral bone
4	Moderate bone attrition (5-10 mm)	'Severe'	Joint space greatly impaired with sclerosis of subchondral bone
5	Severe bone attrition (> 10 mm)	'Severe'	Joint space greatly impaired with sclerosis of subchondral bone

1.1.4 Phenotypes and kinematic subgrouping

Building a deeper understanding of the pathology of patients with KOA is an important part of improving their outcomes following physical therapy and/or surgical intervention. Several studies have demonstrated that patients with KOA cannot be described as a homogeneous group. A systematic review[48] on KOA described high heterogeneity across studies and found that the course of pain and physical functioning were diverse. Other studies have suggested subgrouping of KOA populations – also referred to as phenotypes. Holla et al.[49] identified three subgroups with distinct trajectories of physical functioning over time (good, moderate and poor). Knoop et al.[50] (later confirmed by Esch et al.[51]) identified five homogeneous clinical phenotypes (minimal joint disease phenotype, strong muscle strength phenotype, severe radiographic KOA phenotype, obese phenotype and depressive mood phenotype). Another systematic review proposed six other phenotypes (chronic pain, inflammatory, metabolic syndrome, metabolic bone/cartilage, mechanical overload and minimal joint disease).[52]

Kinematic subgrouping: Kinematic subgrouping has not been investigated directly. Instead, kinematics has been studied in an effort to investigate kinematic alterations within different KOA characteristics. The cohorts have often been stratified into multiple subgroups such as KOA severity[53–55], affected knee compartment[56], ACL deficiency[57] and walking difficulties.[58] Diverse results have been presented. Thus, it was reported that patients with KOA exhibit knee flexion angles greater[54,59], lower[53] and similar[57] to those of healthy controls at initial contact of the foot with the ground during gait. Among these studies, three have investigated adduction and internal rotation. They found greater adduction,[53,54,57] whereas the internal rotation showed both lower[53,54] and similar[57] rotations. Bytyqi et al.[57] and Zeng et al.[54] further investigated tibial anterior translation and found similar and lower translations, respectively. Only Zeng et al.[54] investigated the two remaining parameters, finding a greater tibial lateral shift and joint narrowing. These diverging results may be a consequence of the stratification, which is often based on observer-selected thresholds of different characteristics and often investigated one at the time. Therefore, bias may arise in regard to both the selected threshold and the remaining characteristics within the stratified groups, thereby blurring and inhibiting findings. Thus, an alternative reverse approach to allocating patients into groups based on homogeneous kinematic trajectories may provide more direct information about the multiple characteristics affecting the kinematic motion patterns for these subgroups.

Data clustering: Clustering is such a method that may be used to divide the patient group into multiple subgroups based on homogeneous kinematic trajectories. Clustering is an unsupervised machine learning technique in which the system is given set of data without any prior knowledge after which each data point is automatically allocated into homogeneous subgroups. Several clustering methods exist. They all have different advantages and disadvantages. Some classical ones are K-means, mean-shift, density-based, Gaussian mixture model and Hierarchical methods.[60,61] K-means is easy to understand and fast, though it requires a predefined number of subgroups and may yield various results between runs as a consequence of a random choice of initial cluster centres and due to its iterative approach. In contrast, mean-shift does not require a preselected number of subgroups; however, it does require a preselected window size, which may be non-trivial. Similarly, density-based methods do not require a preselected number of subgroups and are robust to noisy outliers; instead, these methods require a distance threshold and a predefined minimum number of points to define a cluster. Additionally, density-based methods do not perform well on clusters with varying density and high-dimensional data. Gaussian mixture models are less restrictive in terms of the cluster shape compared to, e.g., k-means as they incorporate cluster covariance. However, again, this method requires a predefined number of subgroups, and datapoints may share mixed membership, though with a probabilistic likelihood of each membership. The hierarchical methods do not require a predefined number of subgroups as they construct a dendrogram; even so, subsequently the number of subgroups needs to be determined manually. These methods are sensitive to outliers and characterized by the difficulty of handling various cluster sizes, breaking large clusters and slow computation.[60,61] The k-means clustering method was chosen to allocate our multidimensional data into homogeneous subgroups owing to its simplicity and as it only requires selection of the number of groups. Additionally, it was previously applied to distinguish between subjects with different kinematic trajectories.[62]

1.1.5 Treatment

Currently, no proven disease-modifying agents for treating KOA exist.[63–65] The primary goals of treating osteoarthritis of the knee are to relieve the pain and regain mobility. Conservative and surgical treatments are valid options – and treatment is typically initiated with a conservative treatment strategy. If conservative treatment is insufficient, surgical treatment or a combination are utilized.[7,9,66,67] Conservative treatments includes: weight loss, where even a minimal amount can have a significant influence; exercise and stretching the knee muscles to achieve a more stable and flexible knee joint; pain and anti-inflammatory drugs; steroid injection; unloading or supporting braces; insoles; physical and occupational therapy. Surgical treatment includes overall two procedures: osteotomy, which corrects malalignment by shifting load away from a degenerated knee compartment and total knee arthroplasty (TKA) and unicompartmental knee arthroplasty which replace the articulating part of the bones with artificial parts made from metals and plastic.[7,9,66,67]

1.2 Total knee arthroplasty

The knee joint is one of the most complex weight-bearing joints in the body with complicated movement, stability and functionality. End-stage KOA may be treated surgically with TKA (Figure 1-3). TKA is a well-documented treatment that dates back to the mid-1800s.[10,11,68] One-hundred year later, in the mid-1900s, the first bicompartmental knee arthroplasty (replacing both femur and tibial articular surfaces) was attempted; and in 1970s, the foundation for current concepts and technologies was developed.[68] Two design approaches existed; an anatomical approach that attempted to recreate the native knee anatomy and kinematics preserving most or all the soft tissues of the joint, whereas the other design was a functional approach that attempted to simplify the process, making anatomy secondary to function, and therefore sacrificing the cruciate ligaments.[69]

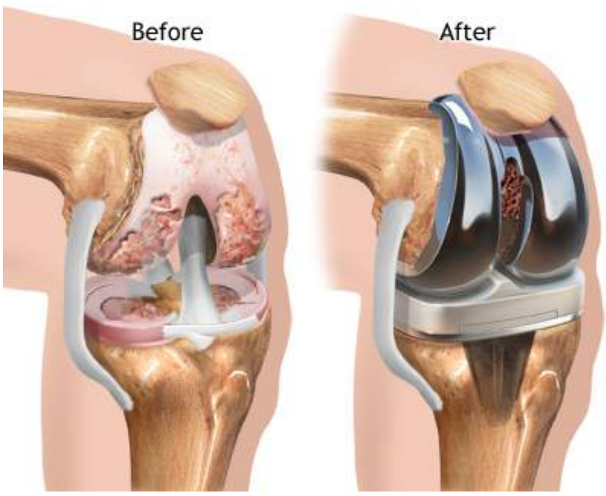

Figure 1-3 Advanced knee osteoarthritis (left) and total knee arthroplasty (right).[70]

1.2.1 Prevalence and risk factors

Currently, in Denmark, about 11,000 primary and 1,000 revision knee arthroplasty surgeries are performed annually.[6] The aging population, higher age before retirement, increasing Body Mass Index and the wish to maintain an active lifestyle will likely increase the amount of primary TKA surgeries and revisions in the future. In Denmark, the amount of primary knee alloplastic surgeries has increased by 30% from 2017-2019. In the United States, using a conservative logistic regression model, the amount of primary TKA surgeries is projected to grow by 143% from 2012 to 2050.[71] The most common indications for TKA revision include instability (26%), infection (24%) and stiffness (18%).[72] Previously, wear-related factors were also a dominating cause of TKA revision. However, major improvement in polyethylene manufacturing and sterilization may have contributed to reducing these wear-related factors.[72]

The search for improvement in patients' health-related quality-of-life, performance and satisfaction has resulted in a widespread application of implant designs. Even so, within the first five years after surgery, 6% of patients require revision[73] and 19% of patients are unsatisfied with their knee surgery outcome after one year.[74,75] Furthermore, the lifetime risk of revision is significantly higher for patients aged under 70 years, especially for middle-aged men (50-54 years).[76] Even though considerable efforts have been devoted to reducing the number of dissatisfied patients, their satisfaction following TKA has not improved during recent decades.[74,77,78] The development of TKA has yielded several designs that may overall be described as symmetric or asymmetric, mobile or fixed-bearing designs in combination with either retaining or sacrificing the posterior cruciate ligament (PCL).[68,69,79–81] Bi-cruciate retaining designs also exit. However, more challenging surgical procedures, strict patient selection and fixation issues have limited clinical application of this design type.[82,83]

1.2.2 Cruciate-retaining versus cruciate-sacrificing designs

The main difference between these two designs is that the PCL is either sacrificed or retained. The anterior cruciate ligament is sacrificed in both designs. For the PCL-sacrificing design, a post-cam was introduced as a posterior stabilizing mechanism, substituting the PCL.[68,69] Traditionally, it is designed with a central peg on the tibial bearing that fits into an intercondylar hole on the femoral component. The PCL-retaining design leaves space for the PCL at the femoral and tibial components to avoid impingement during flexion.[68,69]

Kinematics: In general, during a deep knee flexion, subjects receiving a posterior cruciate-sacrificing implant achieve posterior femoral rollback of their lateral condyle and a normalized tibial rotation, whereas those receiving a posterior cruciate-retaining implant exhibit paradoxical anterior slide and abnormal tibial rotation.[69,80,81,84] However, during the stance phase of gait, both the posterior cruciate-sacrificing and -retaining designs exhibit paradoxical anterior sliding and abnormal tibial rotation. The kinematic differences in high flexion angles between these designs are suggested to be attributed to the sacrificed ACL in the cruciate retaining design. The absence of the ACL simply results in an insufficient contribution of the PCL. For the kinematic similarities during gait, the lower flexion angles may result in an absent post-cam engagement and they therefore do not provide the posterior-stabilizing effect.[84–86] Even so, no differences were found in clinical and patient-reported outcomes between posterior cruciate-retaining and -sacrificing designs in a prospective randomized study.[84]

1.2.3 Mobile- versus fixed-bearing designs

The main difference between these two designs is the fixation of the polyethylene bearing to the tibial tray. In fixed-bearing designs, the bearing is rigidly fixed to the tray using a press-fit click-mechanism or the bearing is molded directly to the tray.[87]

The molded bearing may produce less polyethylene wear owing to non-backside wear. However, it reduces the surgeon's intraoperative opportunity to modify bearing size while being more expensive.[87,88] In the mobile-bearing design, the bearing is movable on the tibial tray, allowing for rotation around the longitudinal axis ("rotating platform") or anterior-posterior translation ("meniscal bearing"). The mobility of the bearing was designed to increase the tibiofemoral contact area to lower polyethylene contact stress while permitting better movement freedom without compromising overload of the implant bone interface.[68,69]

Kinematics: In general, patients with mobile-bearing designs exhibit greater tibial rotation during gait and during deep knee flexion activities than patients with fixed-bearing designs, although these kinematic changes were not reflected in survivorship or clinical outcome.[89–92] Stimulated by findings of no clinical outcome differences, fixed-bearing designs were suggested for younger surgeons because they required less demanding surgical techniques, whereas for more experienced surgeons, it was suggested to select a single surgical protocol and instrumentation rather than focusing on various different designs.[89,90]

1.2.4 Symmetric versus asymmetric designs

These designs are utilized in both PCL-sacrificing and -retaining as well as fixed- and mobile-bearing designs. The asymmetrical designs aim to recreate native knee kinematics, the rationale being that native kinematics will reduce instability thereby providing improved clinical outcomes, function or/and patient satisfaction.[68,83,93] Using increasingly sophisticated technology and knowledge of the native and healthy knee mechanics asymmetric, TKA designs exhibit tibiofemoral kinematics consistent with the intension of the design.[68,69,84,93–97]

Kinematics: Pivoting TKA designs, especially medial pivoting designs, provide well-controlled kinematics and avoid the so-called "paradoxical motion" phenomenon, which is an abnormal kinematic motion in which the femur slides anterior relative to tibia.[80,98,99] Paradoxical motion is associated with mid-flexion instability, which is more evident for CR-bearing designs and has been shown to contribute to dissatisfaction in TKA patients.[100,101] Previously, mainly posterior stabilizing designs have prevented paradoxical motion owing to the presence of the post-cam that substitute the absent PCL. Recent medial pivoting TKA designs have been proposed because they circumvent the risk of polyethylene wear on the post-cam and may potentially approach native knee kinematics.[99,102,103]

1.2.5 Persona® The Personalized Knee System

The new prosthetic knee design Persona® The Personalized Knee System (Zimmer Biomet, Warsaw, Indiana, USA) is a design approach that aims to recreate native knee kinematics with a TKA. The Persona® prosthetic system provides various component sizes, shapes and constraint options and allows for optimized component fit and ligament balancing. The polyethylene bearing of the tibial component is available with a new anatomic design in which the articulating surface is designed in close resemblance with the native knee. The bearing is called the Persona® Medial Congruent® (MC) TKA. Compared with the standard bearing, Persona® Cruciate Retaining (CR), the MC bearing has a higher anterior lib, a more posterior dwell point and a more congruent articulation with the femoral component (Figure 1-4). Expectedly, this will normalize kinematics during knee movements compared with the standard CR polyethylene-bearing prosthetic knee design. The tibial, femoral and patella components of Persona® are identical for the MC and CR bearing designs. No studies examining the MC bearing existed at the time of initiating this dissertation. Thus, it was not investigated whether the MC bearing design complies with its rationale, and whether its kinematics are superior to those of CR bearing designs. However, in the meantime, a handful of studies have been published with promising results regarding the MC bearing. Thus, compared with CR, MC tended to reproduce more native kinematics, achieved greater mid-flexion stability, prevented paradoxical motion, yielded a similar or improved range of motion, clinical outcome and higher patient satisfaction, showed no difference in relation to a posterior stabilizing design even though PCL was sacrificed, and had no effect on migration.[102,104–108]

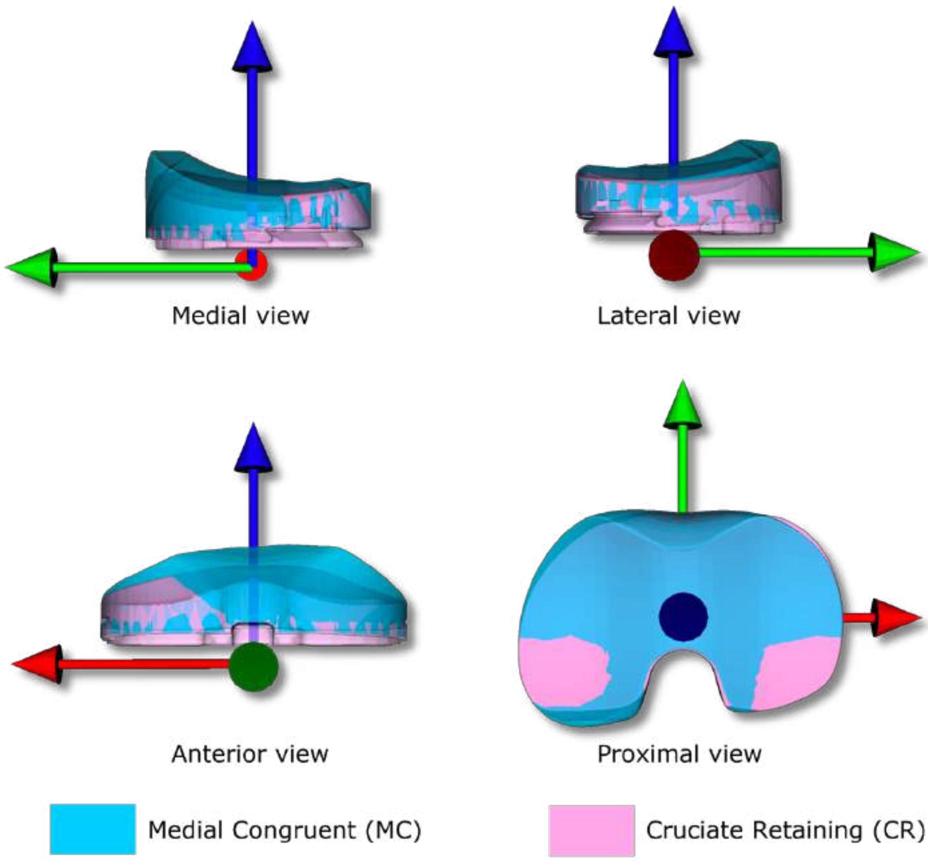

Figure 1-4 Superimposed illustration of right knee Persona® Medial Congruent® (MC) and Cruciate Retaining (CR) bearing designs in different views. The axis directions are red for lateral, green for anterior and blue for proximal.[109]

1.3 Gait analysis

Gait is the style and manner of walking. It depends on repeated motions of synovial joints of the lower limbs that advances the body in a desired direction (locomotion) while maintaining balance. Gait is the most common and also one of the most conservative kinds of locomotion in terms of physiologic energy use.[110] As with many other motion functions, its effectiveness depends on joint mobility and a well-functioning musculoskeletal system that is selective in both timing and intensity. Gait is often described in terms of a cycle extending between two successive initial foot contacts of the ipsilateral limb. The gait cycle may be divided into a stance phase, approximately the initial 60%, and a swing phase, approximately the final 40% (Figure 1-5).[111] It is important to evaluate knee joint mechanics during activities that persons actually perform during daily living as these activities reflects the typical joint function that the person experiences.

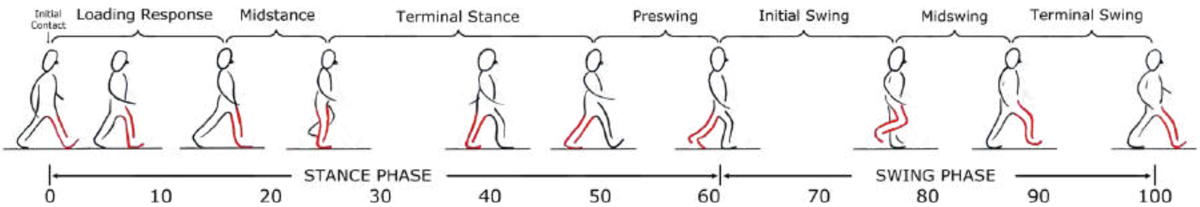

Figure 1-5 Gait cycle description from 0-100%. *Initial Contact*, point where the foot initially contacts the ground; *Loading Response*, point of the initial double limb stance; *Midstance*, point of initial single leg support; *Terminal Stance*, point where the supporting heel rises from the ground; *Preswing*, point of the second initial double limb support; *Initial Swing*, point of initial single limb support of the opposite limb; *Midswing*, point of initial maximum knee flexion; *Terminal Swing*, point where tibia is vertical.

1.3.1 Optical marker-based

Optical marker-based gait analysis is a common method to investigate dynamic joint mechanics. The markers are directly attached to either specific anatomical landmarks of the human body or to corresponding body segments using clusters of markers. Typically, infrared cameras are used to determine the three-dimensional (3D) position of the markers, thus enabling registration of the position and orientation of the segments, which can be used to calculate 3D joint kinematics.[112] Although optical marker-based gait analysis is a power full tool, it comes with several limitations.[112] Skin-attached markers are always associated with inaccuracies in determining the underlying bone and joint kinematics due to the soft tissue artifacts of wobbling masses.[113,114] This is a concern for obese subjects, in particular. In relation to this dissertation, which focuses on patients with KOA and TKA, more accurate joint kinematics estimates were essential, not least because obesity is common in KOA.[9]

Furthermore, similar marker placement between test persons is based on surface anatomy, which is inaccurate.[115] As a solution, radiographic imaging may be applied to assess the underlying bone pose in a 3D space.[116–124]

1.3.2 Radiographic imaging

Computed tomography: Traditional computed tomography (CT) is a fast-spinning radiographic imaging modality that produces high-quality cross-sectional two-dimensional (2D) images of the body stacked in a 3D space. CT enables accurate estimates of bone positions in three dimensions.[125] However, only one static bone pose is produced, and although the method provides considerable anatomical detail, it does not yield information about the dynamics of the knee joint. Furthermore, the patient is in a supine position with unloaded knee joints during the scan and the radiation dose of CT is high why multiple scans in several joint positions is not feasible. A newer four-dimensional CT method provides dynamic evaluation of joints. However, this method exposes patients to high radiation dose similar to those of traditional CT and provides only a relatively low frame rate of 5 Hz. Additionally, it does not allow for investigation of weight-bearing exercises as related to daily activities.

Radiostereometric analysis: Radiostereometric analysis (RSA) is another radiographic imaging modality that utilizes 2D synchronized dual radiographs – so-called stereoradiographs – to provide 3D pose information of an object. The RSA setup requires two x-ray sources pointing at each of their detector (Figure 1-6). The object of interest is positioned at the cross-light of the x-ray beams. To enable spatial calculations, a box containing a known grid of radiopaque markers is used for calibration.[126] The calibration box can be included simultaneously with the recording of the object or before/after the recording as long as the system is untouched during the period of recording and calibration. The RSA method has been proven to be a valid and accurate technique for measuring 3D object poses.[127,128] Owing to submillimetre accuracy and precision, RSA requires only small sample sizes to identify small differences between groups.[129,130] Furthermore, RSA has been widely utilized in randomized studies evaluating longitudinal implant fixation of hip and knee arthroplasty joints with a strong early predictive power for later aseptic component loosening.[127,131–133] The method has even been proposed as one of the initial investigations in the step-wise introduction of new implants.[134]

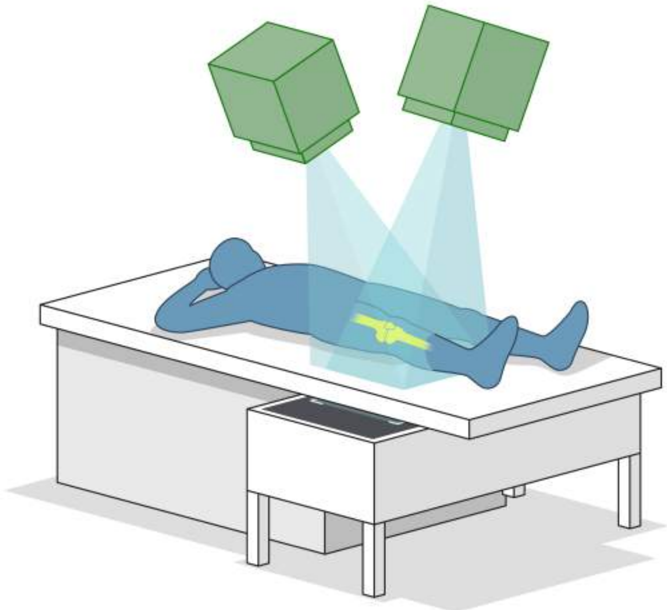

Figure 1-6 Standard static uniplanar radiostereometric analysis (RSA) setup with the patient in a supine position. The setup includes two x-ray sources that irradiate through the calibration box with embedded detectors positioned in one plane next to each other. The knee joint of interest is positioned in the crossing field of the two x-ray beams.

Originally, RSA depended solely on tantalum markers attached to the implants and inserted into the periprosthetic bone during surgery. Implant-embedded markers have several downsides, including expense, need for new regulatory approval of the implants and a possible impact on fixation.[135] Instead, a commercially available surface-based method has been introduced. This method allows for implant tracking without implant-embedded markers at the expense of a slight accuracy loss.[116,135] The surface-based method registers a triangulated surface model of the implant to manually selected contours of the implant. However, the requirement for markers as bone reference and the lack of full analysis automatization restrict the general use of RSA for clinical monitorization of implant loosening.[127,133,136] These two methods, markers to assess the bone reference and surface-model and contour matching are considered the gold standard.

A potential substitute for the marker-based method: Automated 2D/3D image registration of bone-models in TKA patients has previously provided poor results.[137,138] However, none of these methods has utilized digitally reconstructed radiographs (DRR) methods. DRR methods may potentially provide sufficient information to maintain a high accuracy even though important bone geometry has either been resected or hidden behind the radiopaque metal implant component.[139]

A potential improvement of the surface-based method: Automated 2D/3D image registration techniques for radiographic imaging have been studied intensively. Even so, the registration techniques often utilize silhouette projections of triangulated surface models without including inner contours.[116,122,140–145] Image registration of CT-based bone models have successfully utilized DRR images taking advantage of the high contrast intensity differences in the images and thereby the inner projection contours.[120,124,146] From a surface model, it is possible to generate a synthetic volumetric representation of the implant with constant predefined voxel values within the surface shell. This allows for utilization of DRR and may improve image registration accuracy as it will include more information from the inner contours in the similarity metric rather than only utilizing the silhouette projection.

Dynamic radiostereometric analysis: During recent decades, 2D/3D image registration has turned single and dual fluoroscopy systems into 3D analysis tools of joint kinematics (Figure 1-7).[119–122] In addition, radiographic technology advancements have made it possible to obtain clear-pulsed radiographic images providing a radiographic film.[118,147,148] This is similar to fluoroscopy, but with improved image quality, resolution and recording area. Automated image registration techniques for this analysis are essential in a research perspective but also in the clinic, as image registration is very time consuming. The analysis was obtained from RSA (single stereographic imaging). Thus, it is referred to as dynamic RSA (dRSA). The AutoRSA research group in Aarhus, Denmark, has developed an automated software system (AutoRSA software, Orthopedic Research Unit, Aarhus, Denmark) capable of analysing in an automated fashion the large series of stereoradiographs that a dynamic recording produces. The wide applicability of the AutoRSA software has been shown in studies of the hip, elbow and wrist joints.[123,149,150] However, its application for estimating tibiofemoral joint kinematics has not previously been assessed.

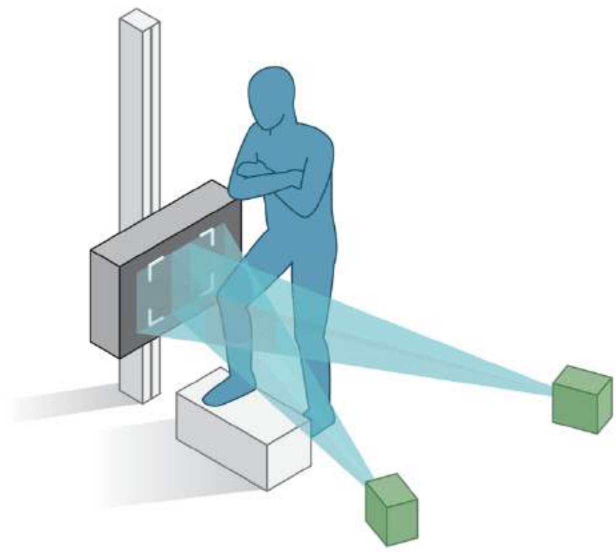

Figure 1-7 Standard dynamic uniplanar radiostereometric analysis (dRSA) setup for a knee recording during a step-up motion. Two x-ray sources irradiate through the calibration box with embedded detectors positioned in one plane next to each other. The joint of interest, here the knee joint, is positioned in the crossing field of the two x-ray beams.[151]

1.3.3 Statistical parametric mapping

Studies investigating kinematic parameters have often acquired trajectories containing a high number of values per recording. Typically, hypothesis testing has been conducted using observer-selected individual discrete time points, excursion, maximum, minimum, etc., reducing the information available. This has been performed to avoid excessive statistical multiple comparisons at each discrete time point, which needs to be accounted for using, e.g., Bonferroni adjustment, which is basically an overestimate of the alpha-level to avoid type-II errors. Consequently, Bonferroni adjustment may introduce type-I error. Statistical parametric mapping was recently suggested as an alternative statistical approach that outlines the analysis in a continuous manner directly on the original trajectory. SPM allows for non-directed hypothesis testing of the entire one-dimensional time series of trajectories. SPM exploits the fact that spatiotemporal data are correlated owed to local smoothness and thereby avoid issues of selection bias and multiple comparison.[152–154] It uses Gaussian random field theory to calculate the threshold that only the significance level of equivalently smooth Gaussian random fields would cross when the null hypothesis is true.

1.4 Motivation for the PhD dissertation

Even though TKA surgery is a widely accepted treatment of KOA and considerable effort has been devoted to reducing the number of dissatisfied patients, approximately 20% of unsatisfied patients remain one year after their knee surgery. This share has stayed unchanged in recent decades.[74,75] Function is a great contributor to satisfaction in patients with TKA, which is underlined by the fact that knee joint instability and stiffness are major reasons for revisions. Therefore, understanding knee joint mechanics in healthy knees, the pathomechanics in osteoarthritic knees and the mechanical impact of knee arthroplasty designs is essential in improving outcomes following TKA.[72,74]

1.4.1 Validation of dynamic radiostereometry for tibiofemoral joint kinematics

The amount of data provided by dRSA is significant. One six-second recording produces 90 stereographs at a frame rate of 15 Hz. Manually, dRSA analysis is a very time-consuming task, and with improved technology the framerate may increase, resulting in even higher workloads. Therefore, a need exists for automated analysis. Furthermore, automated image registration may promote the application and feasibility of radiostereometry, extending dRSA from being used as a research tool to serving as a clinical tool.

1.4.2 Validation of automated marker-free radiographic imaging

Currently, no method is available to assess the fixation of *in vivo* TKA patients in the absence of surgically implanted tantalum markers. It remains unknow whether CT-based bone models may replace the markers. A marker-free RSA method may be an extra clinical tool with which to assess implant bone interface properties. Identifying the problem is the first step to helping the patient by offering secondary treatment options.

1.4.3 Understanding the knee pathomechanics of osteoarthritis

Heterogeneity and clinical phenotyping have previously been proposed for KOA patients as have targeted treatments towards selective phenotypes for improvement of outcomes.[67] Kinematic phenotyping within the KOA patient group has yet to be investigated and may contribute to expand existing knowledge and yield a better understanding of patient characteristics and their relation to different kinematic motion patterns.

1.4.4 Mechanical influence of total knee arthroplasty implant design

Emerging evidence suggests that achieving normalized kinematic patterns in prosthetic knees may improve functional knee performance.[68,155] This has led to asymmetrical and more anatomical prosthetic knee designs that resemble the native knee. When the work on this dissertation was initiated, no available studies had explored the MC bearing design, Thus, no evidence was available that the MC bearing design provided improved knee mechanics compared with the standard CR bearing. This comparison, where the only group difference was the polyethylene bearing, keeping the femoral and tibial bone fixation and interface identical, may contribute to our knowledge of the joint surface congruency influence on knee mechanics.

2

Aim of the dissertation

The methodological aim of this dissertation was to evaluate the accuracy of automated dRSA image registration methods. The clinical aim of this dissertation was to investigate the knee pathomechanics in osteoarthritic knees and the mechanical impact of knee arthroplasty designs during gait utilizing dRSA. Rather than evaluating discrete kinematic features, SPM was utilized. This allowed for non-direct hypothesis testing of the entire kinematic trajectory and thereby minimized the risk of type-II error and selection bias.

The specific aims for each of the four studies were:

2.1.1 Study I:

The aims of this *in vitro* study were (1) to evaluate accuracy of an automated CT-based volumetric bone model method against the gold standard of marker-based RSA for measurement of tibiofemoral joint kinematics in dRSA recordings, (2) to evaluate pose estimation of the femoral and tibial bones and (3) to compare the accuracy of a uniplanar and biplanar radiographic setup.

2.1.2 Study II:

The aim of this *in vitro* study was to investigate the accuracy of automated image registration methods of implant components from TKA and tibial and femoral bone models from CT scans using silhouette projections and DRR. As reference, accuracy was investigated for tantalum markers implanted in the femur and tibia.

2.1.3 Study III:

In this study, full trajectory knee joint kinematics were investigated during level gait in patients with KOA to identify: 1) subgroups of KOA patients based on knee kinematics through clustering, and 2) features of knee kinematics unique to the identified subgroup, linking kinematics to the patient characteristics of the subgroups. The results from KOA patients were compared with data from a group of healthy volunteers with asymptomatic non-arthritic knees.

2.1.4 Study IV:

The aim of this study was to compare the Persona® anatomic prosthetic medial congruent knee design (MC) with the symmetric knee design (CR) using dRSA during gait at a one-year follow-up after TKA surgery. It was hypothesized that 1) the tibiofemoral kinematics differed between the MC and the CR bearing designs, and that 2) the MC bearing enhances articular congruency compared with CR bearing designs.

3 Materials and Methods

The following sections provide a presentation of ethical issues, study design, patient cohorts and experimental protocols including an outcome overview. Subsequently, a description is provided of relevant methodologies applied in the three studies. An overview of the four studies is presented in Table 3.1.

Table 3-1 Method overview.

	Cohorts	Design	Exercise	Modalities	Analysis method	Outcome measures (primary)	Outcome measures (secondary)	Statistics (primary)	Statistics (secondary)
Study I	Native knees (n=8)		Cycle-motion	•Preoperative (CT, x-rays, dRSA)	autorsa-bone marker-configuration	Accuracy of tibiofemoral joint kinematics	Accuracy of femur and tibia bone pose, and a uniplanar and a biplanar RSA setup	Bland-Altman plot with t-test assessing mean bias	Bland-Altman plot with t-test assessing mean bias
Study II	TKA specimens (n=8)		Static pose in two views: anteroposterior and mediolateral	•Preoperative (CT) •Postoperative (sRSA)	marker mbrsa autorsa-surface autorsa-volume autorsa-bone	Translation accuracy of alle methods		Bland-Altman plot	
Study III	KOA (n=66) Healthy (n=15)	Preoperative cross-sectional design	Treadmill gait at 0.83 m/s	•Preoperative CT, MRI, x-rays, dRSA	autorsa-bone	Tibiofemoral kinematics (6 dof)	Ahlbäck score, KOA affected compartment, ACL lesion grade, ligament presents (PCL, LCL, MCL), PROMs (OKS, FJS, KOOS)	Statistical parametric mapping	ANOVA for continuous variables, ordinal logistic regression for categorical variables, and logistic regression for binary variables. Bonferroni correction was applied for group differences.
Study IV	TKA patients • MC (n=31) • CR (n=33)	Double-blinded randomized controlled design	Treadmill gait at 0.83 m/s	•Preoperative MRI, x-rays •Postoperative One-year FU dRSA	autorsa-surface	Tibiofemoral kinematics (6dof) and joint articulation	Assessed pre- and postoperative: Ahlbäck score, KOA affected compartment, ACL lesion grade, ligament presents (PCL, LCL, MCL), PROMs (OKS, FJS, KOOS)	Statistical parametric mapping	ANOVA for continuous variables, ordinal logistic regression for categorical variables, and logistic regression for binary variables. Bonferroni correction was applied for group differences.

RSA: radiostereometic analysis, CT: computed tomography, MRI: magnetic resonance imaging, X-ray: conventional radiographs, KOA: knee osteoarthritis, dRSA: dynamic radiostereometric analysis, dof: degrees-of-freedom, ACL: anterior cruciate ligament, PCL: posterior cruciate ligament, LCL: lateral collateral ligament, MCL: medial collateral ligament, PROMs: patient-reported outcome measures, OKS: Oxford Knee Score, FJS: Forgotten Joint Score, KOOS: Knee Osteoarthritis Outcome Score, ANOVA: One-way analysis of variance, MC: Persona® Medial Congruent™, CR: Persona® Cruciate Retaining, TKA: total knee arthroplasty, sRSA: static radiostereometric analysis.

3.1 Ethical issues

All studies followed the Helsinki II Declaration and handled data according to the General Data Protection Regulation.[156,157] Prior to study initiation, the protocols were reviewed and approved by the relevant authorities. In the patient studies (III and IV), patients were informed about the research study and data collection before written consent was obtained.

The Central Denmark Region Committee on Biomedical Research Ethics:

Studies I and II: journal no. 1-10-72-236-19, issued 21st November 2019

Studies III and IV: journal no. 1-10-72-303-16, issued 28 February 2017

The Danish Data Protection Agency:

Studies I and II: journal no. 1-16-02-410-19, issued 2nd December 2019

Studies III and IV: journal no. 1-16-02-582-16, issued 31st October 2016

ClincialTrials.gov:

Studies III and IV: NCT03633201

3.1.1 Radiation dose estimates

Application of radiographic examinations will expose subjects to ionizing radiation in addition to the background radiation. This is particularly relevant for dynamic stereoradiographs, which produce a large series of dual radiographs. Similarly, CT will expose subjects to ionizing radiation in addition to the background radiation. Awareness of measures to limit the amount of additional radiation to which patients are exposed is important.

The effective radiation dose of the stereoradiographs produced by our equipment was estimated by our local medicotechnical advisors at Aarhus University Hospital. A static stereoradiograph was estimated to produce an effective radiation dose of 0.623 μSv, and one frame from a dynamic stereoradiograph was estimated to produce an effective dose of 0.02288 μSv. For a dynamic series of approximately six seconds at a frame rate of 15 Hz, the effective radiation dose was 2.0592 μSv (a total of 90 stereoradiographs). In the dynamic RSA setup, it was not possible to limit exposure to a single knee alone – the contralateral knee will also be exposed due to leg-crossing during gait. Thus, the effective dose for each patient was doubled for the dynamic recordings, resulting in a total of 0.004 mSv per patient for a dynamic RSA recording of gait.

The effective dose contribution from the CT was estimated based on the dose-length product (mGy·cm) registered for daily patient CTs. Dose-length-product was the volume CT dose index times the length of the CT. The expected dose-length product for each joint was: ankle = 25, knee = 225 and hip = 50. The dose-length-product estimates were converted into effective dose using a conversion coefficient (mSv/(mGy·cm)): ankle = 0.0002, knee = 0.0004 and hip = 0.0106 for adults.[158] The effective dose contributed by the CT of the hip, knee and ankle was estimated to 0.625 mSv, whereas an isolated CT dose of the knee was estimated to 0.09 mSv.

The total effective radiation dose for studies III and IV was 0.629 mSv and 0.004 mSv, respectively. For studies I and II, it was not relevant to estimate the total effective dose to which that each specimen was exposed. Rather, the clinically relevant effective radiation dose needed to conduct a dynamic RSA analysis of a prosthetic knee is important. To acquire the bone volume of the femur and tibia, a CT is required. If the hip and ankle joint centres are included to provide the mechanical axis for the kinematic measures, it was estimated to an effective dose of approximately 0.625 mSV (Study I). If the hip and ankle joint centres were not included, the effective dose was reduced to approximately 0.090 mSV (Study II). It was only necessary to acquire the CT once. Thus, for the stereoradiographs, the effective radiation dose accumulates to approximately 0.000623 mSv for a dynamic recording with a duration of six seconds (90 stereoradiographs).

According to the International Commission on Radiological Protection standard, the accumulated effective radiation dose for the patients and healthy volunteers (Studies III and IV) falls into category IIa.[159] This corresponds to an induced theoretical lethal cancer risk of approximately 1 in 100,000. In other words, at a 5% increased risk of cancer for each Sievert (Sv), the additional radiation exposure of 0.633 mSv in relation to the general Danish population increases from 25% to 25.0032%. Or elaborated in another manner, the amount of effective dose corresponds to less than eight months of background radiation when living in Denmark.[159]

3.2 Design and patients

3.2.1 Studies I and II

Studies I and II were methodological studies evaluating image registration methods *in vitro,* utilizing eight fresh-frozen hemi-pelvis doner legs with a 1:1 male:female ratio and a mean age of 85 years (80-93 years).

3.2.2 Studies III and IV

Studies III and IV were based on the same patient cohort and employed the same inclusion/exclusion criteria (Table 3-2). Study III assessed the preoperative data and Study IV assessed the postoperative data at a one-year follow-up (Appendix I). The consort flow chart of studies III and IV is presented in Figure 3-1. Study III is a cross-sectional study of 66 patients aged 18-80 years of age, diagnosed with KOA and scheduled for TKA. For comparison, in Study III, a control group was included comprising 15 healthy, age-similar volunteers with asymptomatic knees and no radiographic KOA (Table 3-2). Study IV was a prospective randomized controlled double-blinded study investigating two different designs of Vitamin E Infused Technology polyethylene bearings for TKA at a one-year follow-up. The appropriate group sizes were determined by post-hoc power analysis using data variation from published knee kinematics of patients with TKA.[160] Assuming a threshold for observing a difference of three degrees (for rotation) and three millimetres (for translation), an alpha value of 0.05 and a power of 0.80, group sizes of n = 29 were required. A total of 66 subjects were enrolled in the period from 2017 to 2019. The subjects were randomized into two groups with the different polyethylene bearing designs MC and CR. Block randomization (blocks of ten) was performed during surgery using concealed opaque envelopes. The patients and the analyst were blinded to type of bearing. The blinded analyst, the author, performed all data recordings and analyses. The type of bearing was first released once all recordings and analyses were completed. This was possible because the radiolucency of the polyethylene bearings.

Table 3-2 Inclusion and exclusion criteria.[161]

	Patient group	**Healthy control group**
Inclusion	Age above 18 years but no more than 80 years of age. Informed and written consent. Primary knee osteoarthritis in capable men and women. Indication for cruciate-retaining total knee arthroplasty.	Age above 18 years but no more than 80 years of age. Informed and written consent. Asymptomatic knees and no radiographic osteoarthritis.
Exclusion	Patients with a thigh circumference exceeding 60 cm. Patients with conditions that severely compromise their gait other than knee osteoarthritis in the affected knee. Patients with previous severe fractures at the knee level or severe malalignment at the knee level. Surgically implanted metallic parts or pacemaker. Patients with a need for an augmentation and/or stem extension. Patients who cannot perform the exercises.	Patients with a thigh circumference exceeding 60 cm. Patients with conditions that severely compromise their gait. Patients with previous fractures or severe malalignment at the knee level. Surgically implanted metallic parts or pacemaker. Patients who cannot perform the exercises.

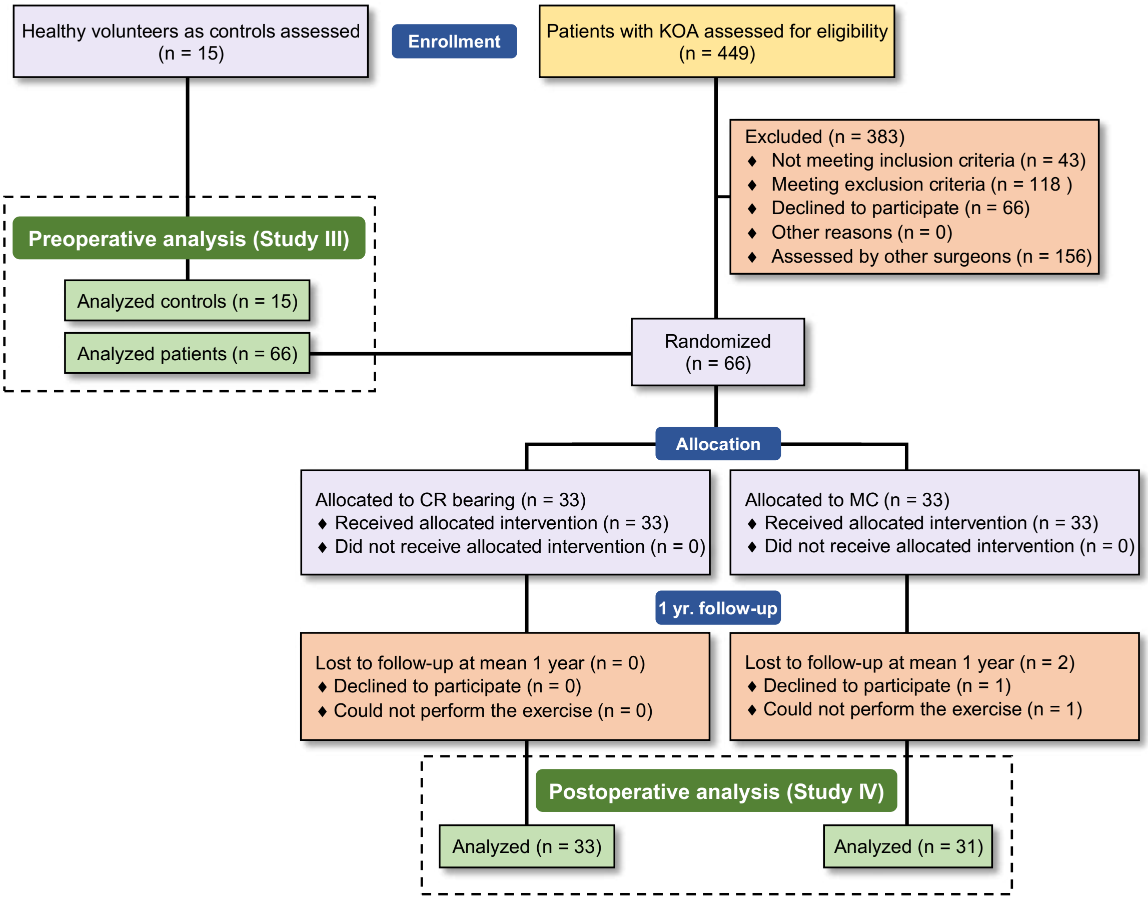

Figure 3-1 Consort flow chart of the patients and healthy volunteers investigated in Studies III and IV.[109]

3.3 Experimental protocols

3.3.1 Studies I and II - preparation

Preoperatively, the knee of each specimen was CT scanned (SOMATOM Definition Flash; Siemens Healthcare, Erlangen, Germany) including 15 cm proximally and distally to the joint line including the femoral head and ankle joint. The CT were conducted using a standard protocol with axial slices at a peak voltage of 120 kVp and exposure of 183 mAs, slice thickness of 0.6 mm, slice increments of 1 mm and a pixel width of 0.29 × 0.29 mm. Subsequently, all specimens were disarticulated at the hip and ankle joints, and the proximal femoral and distal tibial bone were dissected for soft tissue to ensure rigid fixation of the specimen. Approximately 8-13 tantalum beads (X-medics, Sweden) were inserted through a 4 mm cortical bone drill hole in each of the distal femoral and proximal tibial bones using a bead gun (Kulkanon, Wennbergs Finmek AB, Sweden). Beads were placed in a systematic pattern intending a wide-spread 3D marker distribution. For Study I, the specimens were again CT scanned at 120 kVp, exposure 200 mAs, slice thickness 0.6 mm, slice increment 0.8 mm, and pixel spacing 0.29 × 0.29 mm, with the application of metal artifact reduction.

3.3.2 Study I

Radiographic setup: The stereoradiographs were recorded utilizing a dedicated RSA system (AdoraRSA; NRT X-Ray A/S, Hasselager, Denmark). The system uses two ceiling-mounted x-ray tubes positioned horizontally at an inter-tube angle of 40 degrees and a source-to-image distance of 320 cm (Figure 3-2). Two different RSA setups were investigated – a uniplanar and a biplanar setup. For the uniplanar setup, the flat panel detectors (CXDI-50RF, Canon Inc., Tokyo, Japan) were slotted behind a uniplanar calibration cage (Box 24, Medis Specials, Leiden, Netherlands). For the biplanar setup, the detectors were placed angulated on a free stand approximately orthogonally to the rays from each x-ray tube. In dynamic-image mode, full detector size was acquired with images dimensioned 1104 x 1334 pixels and a quadric pixel width of 0.32 mm using exposure settings of 90 kVp and 0.6 mA. Subsequently, a static image of the calibration cube was conducted (2208 x 2668 pixels, 0.16 mm quadric pixel width).

Experimental procedure: A customized fixture was constructed to simulate a flexion-extension movement (Figure 3-2). The proximal part of the femoral bone was fixed to a plywood board attached to the system with a mobile fitting, whereas the distal portion of the tibial bone was attached to a functional pedal with a crank arm of 10 cm. The vertical height of the femoral bone fixation could be adjusted to fit specimens of variable length. With the crank arm, the pedal had freedom of rotation around an axis in the medial-lateral direction. A rope was used to manually apply force to the pedal in an upward direction, making the specimens perform a standardized knee flexion motion in the 0–70° range. The average angular velocity of knee flexion and extension was approximately 12 deg/s.

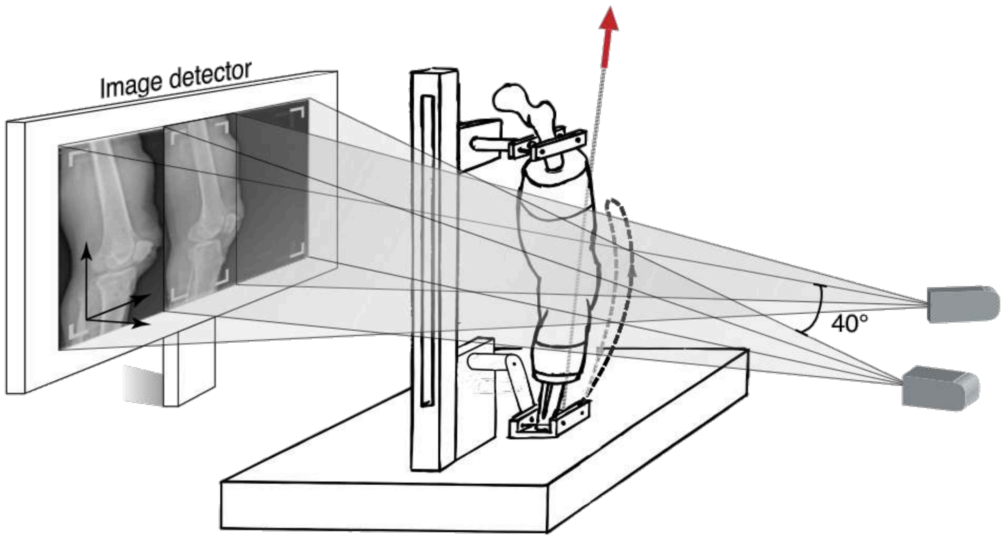

Figure 3-2 Illustration of the uniplanar radiostereometric setup and fixture. Flat-panel image detectors were slotted in the detector panel behind the calibration boxes. Roentgen tubes were positioned at 40° relative to each other in both setups. The knee joint of the specimen was positioned at the crossing of x-ray beams to form stereoradiographs. The dashed line shows the path of movement during knee flexion when traction (arrow) was applied to the mobile mechanical fixture.[124]

Outcomes: For each RSA setup, the tibiofemoral joint kinematics were estimated using the CT-based bone volumetric method (*autorsa*) and the CT-based marker configuration model method as gold standard method. The individual bone pose was evaluated for the femoral and tibial bones. The difference in pose estimation was calculated in all six degrees of freedom for each dRSA image. Additionally, the total difference in pose estimation was computed by the magnitude of the resultant vector for each image using the 3D Pythagorean Theorem. For rotations, this is only allowed for small values which were expected.

3.3.3 Study II

Surgical procedure: For Study II, each specimen underwent TKA surgery. One experienced knee arthroplasty surgeon used a standard operative total knee arthroplasty procedure according to the manufacturer's surgical technique with an anterior midline incision and medial parapatellar arthrotomy.[162] All specimens received the cemented (Palacos®R+G, Heraeus, Medial GmbH, 61273, Wehrheim, Germany) Triathlon® Knee System (Stryker, Kalamazoo, MI, USA) for the femur, tibia and patella.

Radiographic setup: The stereoradiographs were recorded utilizing a dedicated RSA system (AdoraRSA; NRT X-Ray A/S, Hasselager, Denmark). The system uses two ceiling-mounted x-ray tubes positioned vertically at an inter-tube angle of 40 degrees and a source-to-image distance of 160 cm (Figure 3-3). The flat panel detectors (CXDI-50RF, Canon Inc., Tokyo, Japan) were slotted behind a uniplanar calibration cage (Box 24, Medis Specials, Leiden, Netherlands). In single-image mode, full detector size was acquired with images dimensioned 2208 x 2668 pixels with a quadric pixel width of 0.16 mm using exposure settings of 120 kVp and 1.2 mAs.

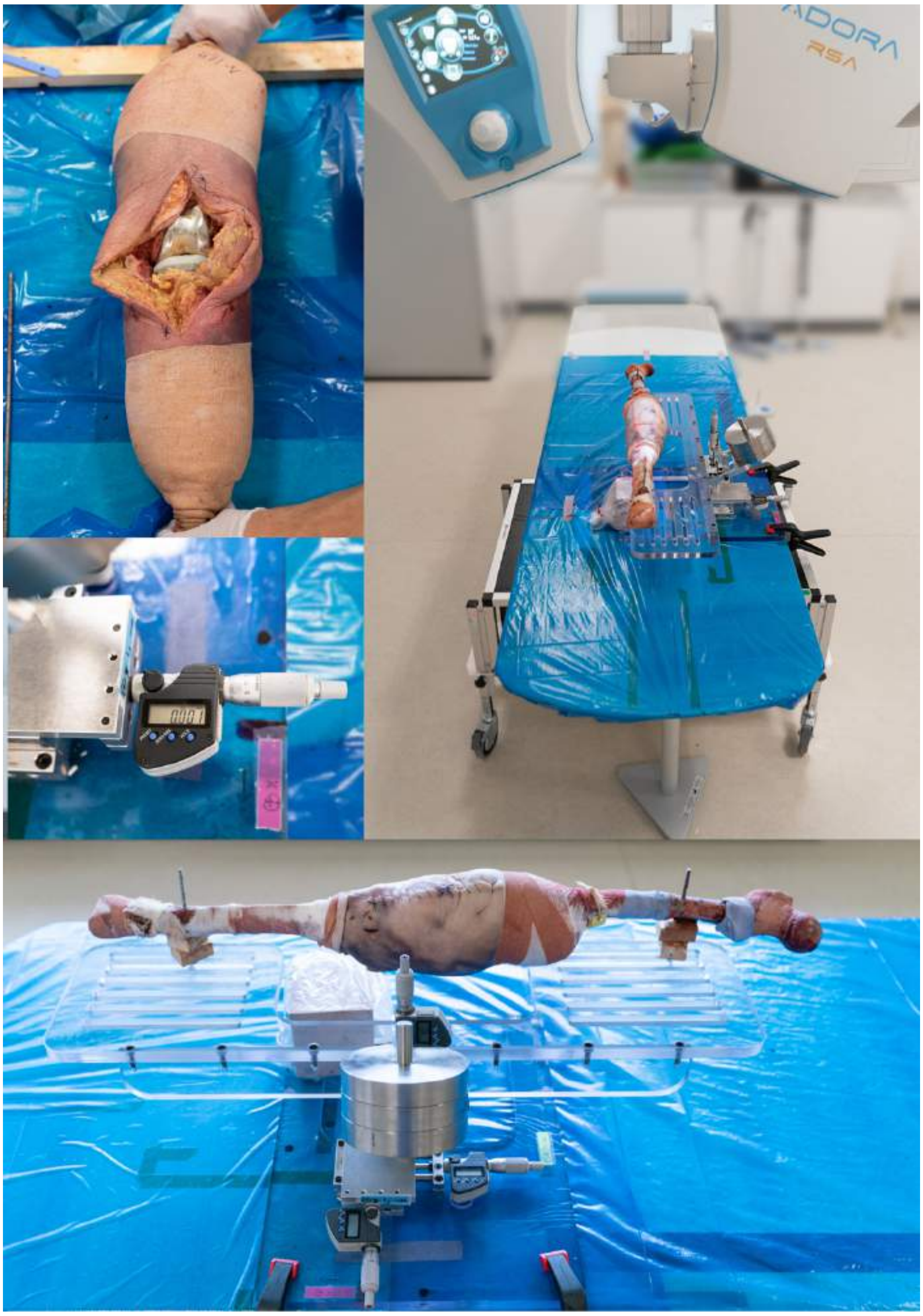

Figure 3-3 Illustration of the radiostereometric setup, the fixture, total knee arthroplasty knee before wound closure and the micrometre measurement unit on the fixture.[163]

Experimental procedure: A customized fixture with an axial movable plexiglass plate was built and ensured rigid fixation of the knee specimen (Figure 3-3). Accommodating optimal radiographic imaging, a hole was cut out of the plexiglass at the knee level, ensuring free passage of the x-ray beams. The plate was moved in three directions (x, y, z) using digital dial micrometres, each with a resolution of 0.001 mm

(Hofmann GmbH, Achim, Germany). The fixture was oriented approximately orthogonally to the reference frame of the RSA setup (calibration cage). First, the knee was positioned in the anterior-posterior (AP) plane, replicating a patient in a supine position. Second, the knee was positioned in a lateral-medial (LM) view to investigate the influence of a different view. Recordings were obtained in all directions (x, y, z) at 16 positions. Each series included five recordings at baseline. Second, two recordings were obtained each at 10, 20, 30, 40, 50, 100, 200, 300, 400, 500, 1,000, 2,000, 3,000, 4,000 and 5,000 micrometres. The corresponding measured displacement was established by the difference between the median of the estimated positions at baseline and the corresponding estimated position. The error was determined by subtracting the actual (micrometre) displacement from the measured (RSA) displacement.

Outcomes: The accuracy of the bone and implant were analysed for both the tibia and femur using five different registration methods. In terms of gold standard, the Model-based RSA (version 4.2, RSAcore, Leiden, the Netherlands) was utilized to estimate bone and implant using a marker-based (*marker*) and a surface-based (*mbrsa*) method, respectively. The position of the marker model was estimated as the centroid of the marker positions. AutoRSA software system was used for the remaining three methods. Two methods estimated the implant poses using either a surface- or a volume-based (*autorsa-surface*, *autorsa-volume*) method, respectively. The final method used a volume-based (*autorsa-bone*) method to estimate the bone poses. The five different registration methods are summarized in Figure 3.4.

3.3.4 Studies III and IV

All patients were set to complete repeated protocols before and after surgery at the one-year follow-up. The healthy control subjects completed the same protocol. The participants walked barefoot on a levelled treadmill (Sole F63, Jonesboro, AR, USA) to

Figure 3-4 Overview of the radiostereometric analysis methods.[163]

Name	Software	Method	Description	Illustration
marker	MBRSA	Hugh circle detector	The actual marker projections were detected using Hugh circle detector based on manually applied parameters. **Marker-method**: utilizing the actual markers on the stereoradiographs to estimate a 3D position of each marker by minimizing the crossing-line-distance of the marker for each view. **Marker-configuration model**: utilizing a predefined 3D marker-model estimating its 3D pose by minimizing the difference between its projected marker positions and the actual markers on the stereoradiographs.	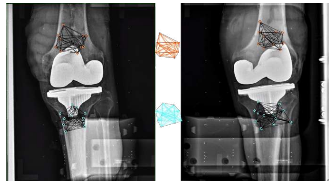
mbrsa	MBRSA	Canny edge detector	Contours were automatically detected in the stereoradiographs by canny edge detection based on manually applied parameters and region of interest. From these the relevant contours of the object of interest were manually selected. Coarser to finer optimization algorithms were applied to estimate the poses by minimizing the error between the virtual projections of the bone models and the manually selected contours.	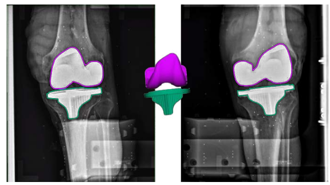
autorsa-surface	AutoRSA	Silhouette-projection	This automated image registration method utilizes silhouette-projection of surface models that are matched to the actual object silhouette-projection using Sobel edge detection algorithm. The similarity metric was determined as the average of the horizontal and vertical gradients normalized cross-correlation between the actual stereoradiographs and the virtually generated projections. Coarser to finer optimization algorithms and image resolution were applied and an automated mask image were used to determine region of interest.	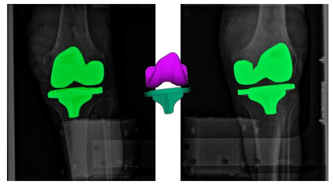
autorsa-volume	AutoRSA	Digitally reconstructed radiographs	This automated image registration method utilizes digitally reconstructed radiographs of synthetic generated volumetric models that are matched to the actual object stereoradiographs using Sobel edge detection algorithm. The similarity metric was determined as the average of the horizontal and vertical gradients normalized cross-correlation between the actual stereoradiographs and the virtually generated projections. Coarser to finer optimization algorithms and image resolution were applied and an automated mask image were used to determine region of interest.	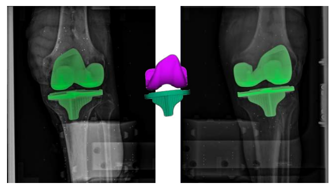
autorsa-bone	AutoRSA	Digitally reconstructed radiographs	This automated image registration method utilizes digitally reconstructed radiographs of CT-based volumetric models that are matched to the actual object stereoradiographs using Sobel edge detection algorithm. The similarity metric was determined as the average of the horizontal and vertical gradients normalized cross-correlation between the actual stereoradiographs and the digitally reconstructed radiographs. Coarser to finer optimization algorithms and image resolution were applied and an automated mask image were used to determine region of interest and excluding the other implant.	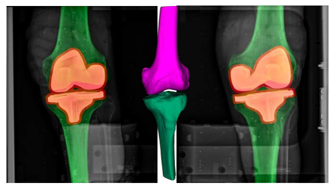

Abbreviations: MBRSA – Model-Based RSA (RSAcore, Leiden, the Netherlands); AutoRSA – AutoRSA software, Orthopedic Research Unit, Aarhus, Denmark; 3D – three-dimensional; CT – computed tomography mimic level gait (Figure 3-5). They were afforded a habituation period to gain familiarity with the test environment, with slowly increasing speed reaching a final speed of 0.83 m/s. This is slightly slower than average walking speed (1.25 m/s)[164] and was chosen to avoid exclusion of gait-disabled patients while facilitating sufficient dRSA data generation throughout the entire gait cycle. When the subject felt comfortable, data collection was initiated. Up to seven coherent gait cycles were obtained. For precaution and anticipating loss of balance during testing, subjects had a rail they could hold on to. Only none-rail-supported gait trials were included for further analysis. Subsequently, the patients' pain intensity perception during the trial using a horizontal visual analogue scale (VAS) (transformed into a 0-10 range) and their strength using a leg-extension power rig (Bio-Med International, Nottingham, UK) were registred.[165,166]

Gait analysis setup: The gait trials were recorded with a dedicated dRSA system (AdoraRSA; NRT X-Ray A/S, Hasselager, Denmark). To utilize the largest recording area possible, a biplanar setup was used in which the detectors were placed on individual stands at a relative angle of 40 degrees; one in front of the subject and one to the side of the limb of interest (Figure 3-5). The source image distance was 250 cm (frontal view) and 300 cm (side view). The system was acting in a plane parallel to the floor at a patient-specified height to centralize the knee joint in the radiographic images throughout the entire recording. The setup was mirrored for left/right knees to accommodate the investigated knee as close as possible to the side view. The radiation exposure parameters were set at 90 kVp, 600 mA and a pulse-width of 2.5 ms, utilizing the highest frame rate of 15 Hz without compromising the image size of 1,104 x 1,344 pixels (quadratic pixel width of 0.32).

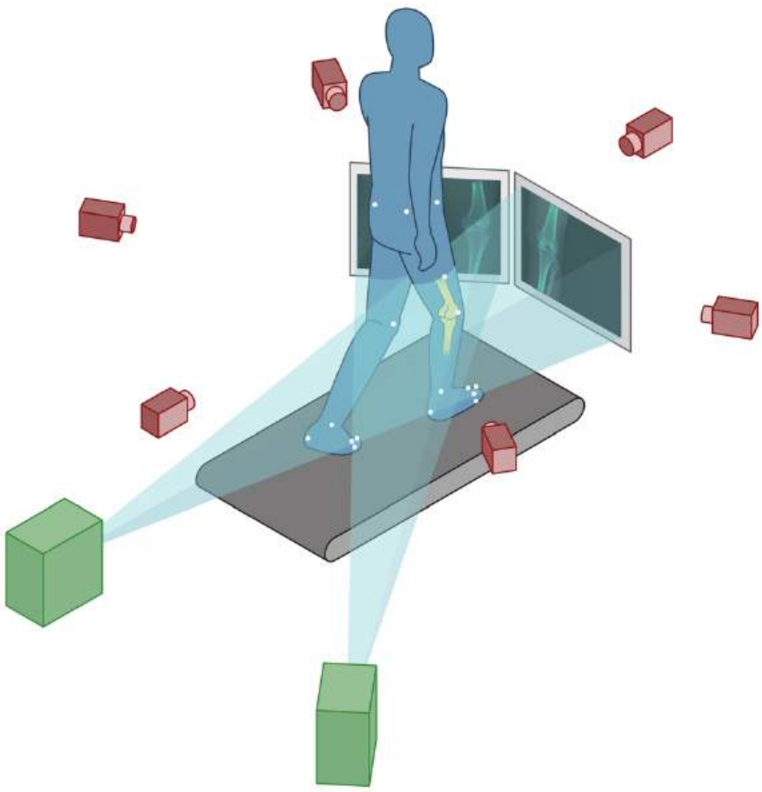

Figure 3-5 Illustration of the treadmill setup utilizing dynamic radiostereometry and optical motion capture.[161]

Simultaneously with the dRSA system, a minimum of six OptiTrack Prime 13 motion cameras (NaturalPoint, Corvalis, OR, USA) and Motive software (Motive v.2.0.0, NaturalPoint, USA) were used to assess the trajectories of skin-attached reflective markers (diameter: 10 mm). The optical cameras were positioned strategically surrounding the subject to avoid occluded markers during reflective marker analysis. The markers were attached at the subjects' pelvis, lower limb and feet; three cluster markers at the thigh, two at the knee epicondyles, three cluster markers at the shank, two at the ankle malleolus, one at the heel, three at the metatarsals (1, 3, 5) and one at the first distal phalanx. Prior to usage, the entire recording area was calibrated using an OptiTrack CW-500 Calibration Wand (NaturalPoint, USA). Furthermore, a custom-programmed Raspberry Pi 3 Model B (Linux Mini PC, Broadcom BCM2837 1.2 GHz Quad-Core 64-bit, 1 Gb LPDDR2 RAM) was used to time synchronize data from the dRSA and the optical marker systems using pulse information from both systems.

Volumetric imaging: Preoperatively, all participants including the healthy control subjects underwent a CT (Revolution EVO, GE Medical Systems, Milwaukee, WI, US) and an MRI (1.5 T Avanto, SIEMENS, Erlangen, Forchheim, DE). For the CT, a helical scan protocol with the reconstruction kernel "boneplus" was used to cover 15 cm of the most distal and proximal part of the femur and tibia, respectively. The knee scans were acquired with axial slices at a peak voltage of 100 kVp and 200 mAs, a slice thickness of 0.625 mm and a pixel spacing of 0.48 x 0.48 mm. To reduce radiation dose exposure, the femoral head and ankle were acquired with a slice thickness of 2.5 mm. For the ankle, the voltage was additionally reduced to 80 kVp. For the detailed MRI, a modified version of the Osteoarthritis Initiative Protocol[167] based on GE scanner recommendations was used (T2 SAG de3D DESS WE acquisition with 0.7 mm slice thickness and T1 COR fl3D WE with 1.5 mm slice thickness).

Conventional radiographs, clinical characteristics and patient-reported outcome measures: All participants underwent conventional weight-bearing radiographs of their native knee and classified their KOA according to the modified version of the Ahlbäck Score (grade 1-5).[43,46] Additionally, the MRI provided information to register the affected tibiofemoral compartment as lateral or/and medial and ligament lesions. The following knee ligaments were evaluated: ACL, PCL, the medial collateral ligament (MCL), and the lateral collateral ligament (LCL). The ACL was graded as 0 (no lesion), 1 (partial lesion), and 2 (total lesion). PCL, MCL, and LCL were registered as 0 (no lesion) or 1 (lesion). Furthermore, a series of questionnaires on patient-reported outcome measures (PROMs) were collected pre- and postoperatively for the patient cohort and the healthy controls. The PROMs included the Oxford Knee Score (OKS)[168], the Knee Injury and Osteoarthritis Outcome Score (KOOS)[169], and the Forgotten Joint Score (FJS)[170]. Finally, any postoperative complications were registered during the one-year follow-up period.

Surgical procedure and rehabilitation: For Study IV, all included patients with KOA underwent a TKA procedure. Three experienced knee arthroplasty surgeons used a standard operative procedure with an anterior midline incision and medial parapatellar arthrotomy. The surgeries were performed according to the manufacturer's surgical techneque.[171] All patients received cemented CR femoral implants (standard or narrow), tibial implants with either a MC or CR bearing, and patella resurfacing with all-polyethylene patella implants. The patients followed the same postoperative routine rehabilitation regime and were discharged according to well-defined clinical and functional criteria.

Outcomes – Study III: First, the tibiofemoral joint kinematics were compared between the KOA patient cohort and the healthy controls. Second, the tibiofemoral joint kinematics were compared between the KOA subgroups that were allocated based on homogeneous tibiofemoral joint kinematics. Third, the subgroups kinematic patterns were related to their clinical characteristics. The preoperative clinical characteristics included: KOA grade, KOA-affected compartment, ligament lesion grade (ACL, PCL, MCL, LCL), PROMs (OKS, KOOS, FJS), leg-extension power and pain assessed by VAS during gait examination.

Outcomes – Study IV: First, a comparison was made of the tibiofemoral joint kinematics and articulation between the MC and CR TKA groups one year after surgery. Second, a comparison was made of the MC and CR TKA groups' clinical characteristics preoperatively and postoperatively at the one-year follow-up. The clinical characteristics included: KOA grade, KOA-affected compartment, ligament lesion grade (ACL, PCL, MCL, LCL), PROMs (OKS, KOOS, FJS), leg-extension power, and pain assessed by VAS during gait examination.

3.4 Data processing and quantification measures

This section provides elaborated descriptions of the applied methods. Conducting RSA and dRSA in particular is a time-consuming task that requires multiple steps before the final measures may be assessed (Figure 3-6).

3.4.1 Bone model segmentation and reconstruction

The most accurate 3D representation of bone structures and anatomy is obtained from a CT. For all studies, except Study IV, the bone structure was extracted from the CT volume using a fully automated graph-cut segmentation method employing the Insight Segmentation and Registration Toolkit (Kitware, Clifton Park, New York).[172,173] This method uses eigen analysis of the hessian matrix to identify the sheet-like structure (strong edges) of the cortical bone separating the bone from the surrounding soft tissue.[172] Subsequently, a sheetness measure is formulated, which is used in a graph-cut optimization.[174] From the segmentation, femur and tibia models were extracted as volumes and surface representations (Figure 3-7). The volume models were 3D volumes consisting of the CT image intensities of the representative bones. The surface models were 3D triangulated models of the representative bones' shape as vertices and faces generated utilizing the marching cubes algorithm on the segmentation.[175]

3.4.2 Anatomical coordinate systems

For Studies I, III and IV, it was essential to describe the tibiofemoral joint kinematics in clinically relevant terms. The individual bone was assigned an anatomical coordinate system, which was automatically generated, using a modified version described by Miranda et al. that implemented the mechanical axis (Figure 3-7).[148,176] For the femur: the lateral-medial axis was defined as the centre line of a least-square fitted cylinder to the knee condyles, the proximal-distal axis was defined as an orthogonal

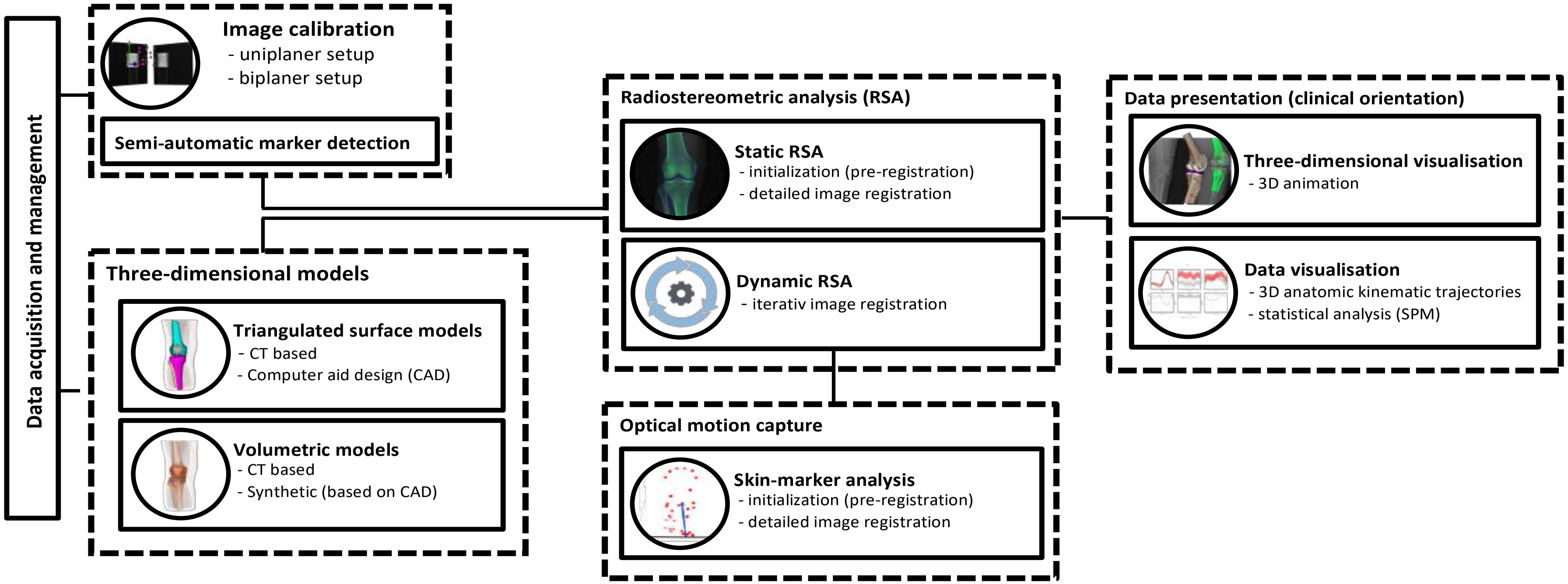

Figure 3-6 Illustration of the multiple steps that were required to conduct RSA and dRSA – from data management to final kinematic analysis. First, data acquisition and organizing and labeling the data from the different radiographic modalities (radiostereometry and computed tomography). Second, the radiostereometric images were calibrated and bone models (surface and volume) were extracted from the computed tomography and assigned an anatomical coordinate system. Third, the images were analysed for the static recordings in Study II the five analysis methods described in Appendix II were used. While for the dynamic recording in Studies I and III *autorsa-bone* method were used, and in study IV *autorsa-surface* were used. For the dynamic recordings the reflective skin-marker trajectories form the optical motion capture system were used to initialize each frame prior to image registration. Finally, the results be presented as kinematic measures (Study I, III, and IV).

projection from the medial-lateral axis to the centre of a least-square fitted sphere at the femoral head. The anterior-posterior axis was defined as the cross product of the medial-lateral axis and the proximal-distal axis. The origin was defined as the midpoint between the medial-lateral axis surface intersections. For the tibia, the origin was defined as the centroid of the tibial plateau proximal of the largest cross section. The medial-lateral axis was defined as the first principal component axis. The proximal-distal axis was defined as an orthogonal projection from the medial-lateral axis to the midpoint between the ankle malleoli. The anterior-posterior axis was defined as the cross product of the medial-lateral axis and the proximal-distal axis.

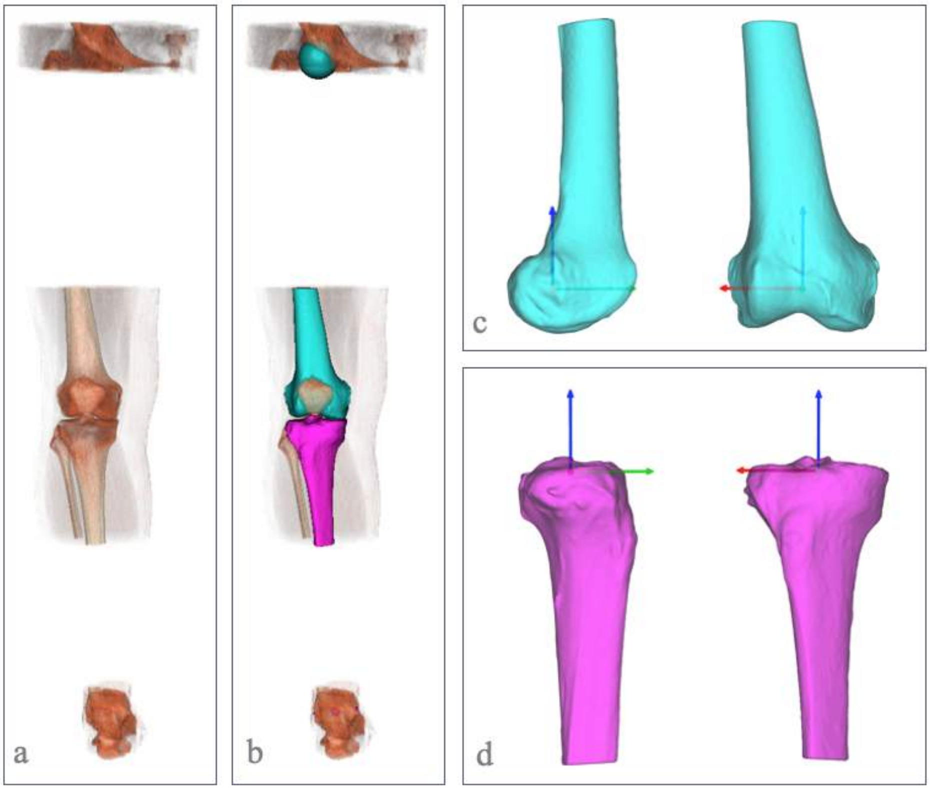

Figure 3-7 Model segmentation, reconstruction and anatomical coordinate systems. Illustration of the right leg of a CT (a), bone segmentation along with marked hip and ankle centres (b), anatomical coordinate system (c-d) and knee joint coordinate system (e). (a) Volume rendering of a hip-knee-ankle CT. (b) Bone segmentation of the femur (cyan) and tibia (magenta). (c-d) 3D bone models of the femur (c) and tibia (d) bones in a sagittal and frontal view illustrating the anatomical coordinate system.[177]

3.4.3 Radiostereometry image calibration

Registration and spatial measurements in the 2D images require calibration of each recording for image orientation in the 3D space. Two different calibration methods were utilized, a non-simultaneous and a simultaneous image calibration acquisition method. The calibration required precise selection and identification of each calibration-marker projection for both methods.

Figure 3-8 Non-simultaneous calibration images of a biplanar setup with landscape-oriented detectors and identified and labelled calibration markers. Cube-markers (green) and reflective sphere-markers (red).

Non-simultaneous image calibration: The non-simultaneous image calibration method was used for the biplanar setup in Studies I, III and IV (Figure 3-8). Subsequently, the dynamic recording, a static image in single-image mode (2,208 x 2,788 pixels with 0.16 mm quadratic pixel width), was conducted of a custom-made calibration cube. The single-image mode provides higher image resolution and, thus, better calibration. Importantly, no interaction with the roentgen tubes or the detectors was allowed during or in-between recording calibration-image acquisitions. The calibration cube was an acrylic cube containing a grid of 23 unique radiopaque tantalum beads (0.8 mm) at known locations. The 3D bead-marker positions were determined with a tolerance of +/- 0.003 mm (ATOS Triple Scan, Zebicon, Billund, Denmark). For this setup, Model-based RSA was not optional to perform the entire calibration; however, the Model-based RSA software was utilized to manually select and label the 23 cube beads projections on each of the two static radiographs before application of a custom-written program utilizing the *stereocalibrate* modules in OpenCV-Python (v. 3.1.0.5). This program calculates the x-ray source position and image pose (calibration) based on the manually selected projections and the known 3D bead positions.

Simultaneous image calibration: The simultaneous image calibration method was used for the uniplanar setup in Studies I and II (Figure 3-9). This was possible as the detectors were slotted behind the calibration box during the recording. Hence, the calibration markers are present within the stereoradiograph. The calibration box includes two layers (fiducials and controls) of radiopaque tantalum beads within a known grid. For the static images, the stereoradiograph was used directly (Study II), whereas for the dynamic images with a lower resolution, an average of the entire image series was used for calibration (Study I). This enhances the static objects (calibration markers) and blurs moving objects (leg). For this method, the entire calibration acquisition was conducted using Model-based RSA, which transforms the image pixels into the fiducial layer.

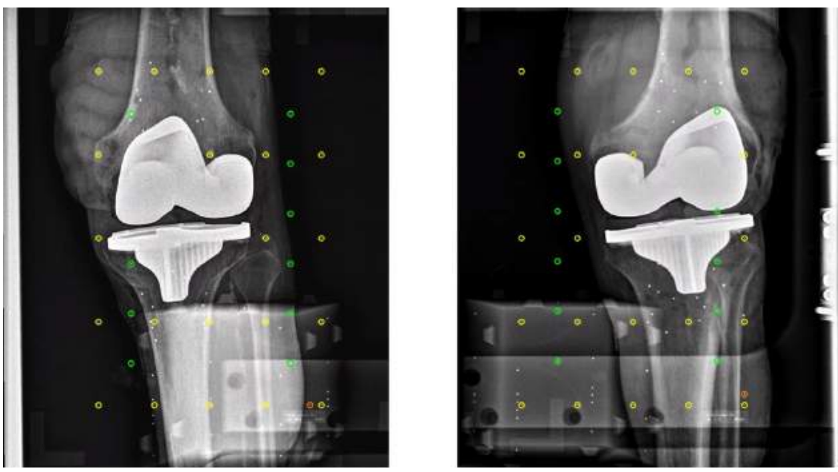

Figure 3-9 Simultaneous calibration images of a uniplanar setup with portrait-oriented detectors and identified and labelled calibration markers. Fiducials (yellow) and controls (green).

3.4.4 Gold standard radiostereometric analysis

Marker-based method. For Studies I and II, the marker-based method from Model-based RSA was used as a gold standard reference for the bone poses (*marker*, Figure 3-10). The tantalum markers inserted into the femur and tibia were identified in the radiographic images. To accommodate the recommendation of the RSA guidelines, the condition numbers for the different specimens were well below a maximum accepted value of 130, and the maximum rigid body error was below 0.35.[129,178,179]

The marker configuration model was used in Study I and a traditional marker-model was used in Study II.[180,181] The difference between the two methods was that the marker configuration method utilized a 3D model that fits its projected marker-positions to the actual marker positions, whereas the traditional marker method estimated a 3D representation of each marker by minimizing the crossing-line distance between the actual marker positions of the two views. It was important for the traditional method that the same markers were identified within each series, which was the strength of the marker configuration method, as there was no requirement to have the matched marker projections identified in each view within a stereoradiograph.

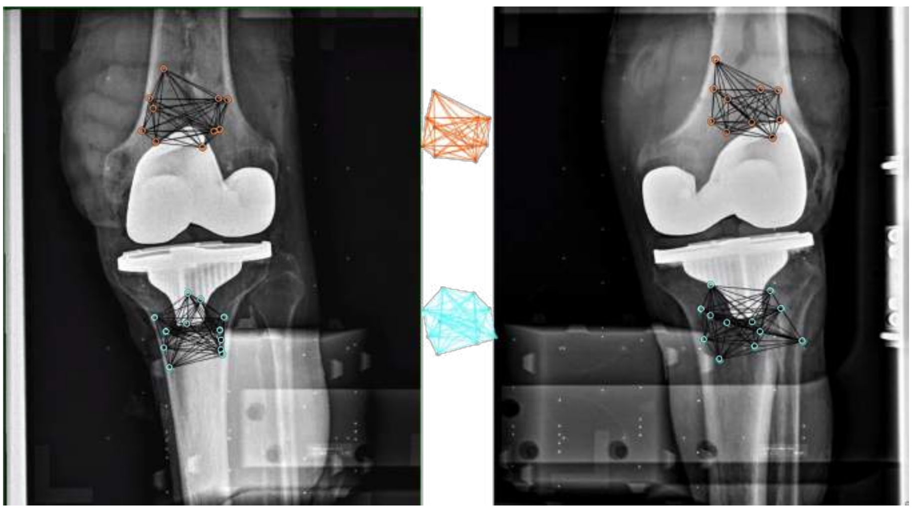

Figure 3-10 Illustration of the stereoradiographs and the radiostereometrically analysed projection of the *marker* method. Images display the tantalum bead projections and the three-dimensional reconstructed *marker* model.[163]

Alignment between marker configuration model and anatomical coordinate system: For Study I, the tibiofemoral joint kinematics were evaluated using the marker configuration model as gold standard. The marker configuration models were constructed based on the post-marker-inserted CT of the specimens. From this, each marker was carefully segmented in the volume image using a manually applied threshold followed by manual refinement. The marker centres were subsequently obtained by fitting a sphere to each of the marker segmentations.

To quantify and describe the tibiofemoral joint kinematics (rotations and translations) of the model configuration method using the anatomical coordinate system previously described, a transformation was required to account for alteration in the position of the specimen within the scanner since bone models were generated from baseline CTs and marker configuration models were generated from post-insertion CTs. This transformation was defined by superimposing and matching 3D/3D image registrations of both scans using the Elastix toolbox for registration of images applying normalized mutual information metrics.[182] This process was performed for each target bone region since the translation and rotation of the knee pose could not be assumed to be identical between scans.

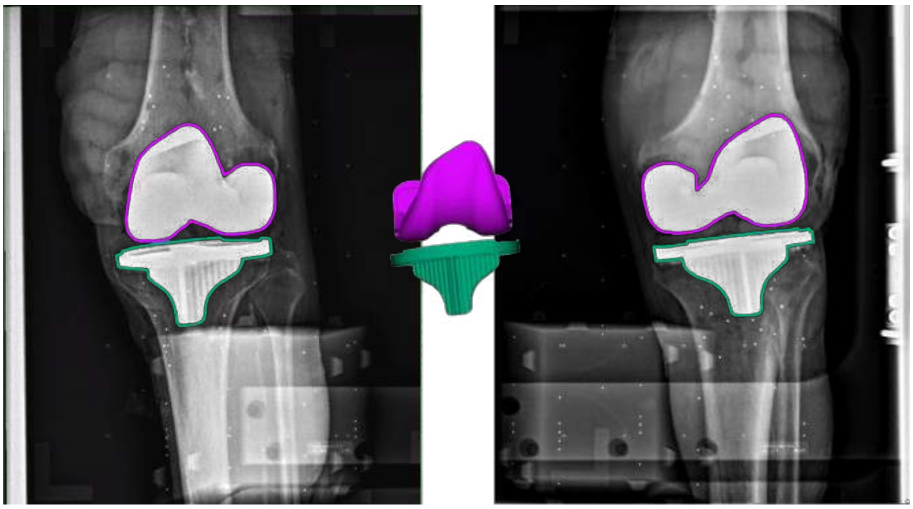

Figure 3-11 Illustration of the stereoradiographs and the radiostereometrically analysed projection of the *mbrsa* method. The images display the implant-projected contours (enhanced contours for improved visualization) and the three-dimensional implant model.[163]

Surface-based method. For Study II, a semi-automated surface-based method from Model-based RSA was used as a gold standard reference for the implant poses (*mbrsa*, Figure 3-11). Based on manually applied parameters and regions of interest, the contours were automatically detected in the stereoradiographs using the Canny Edge Detector (RSAcore, Leiden, The Netherlands). Then, from these contours, the contours for the femur and tibia implants were selected manually. Coarser to finer algorithms (IIPM, DIFDHSAnn, and DIFDoNLP) were applied to estimate the poses by minimizing the error between the virtual projections of the bone models and the manually selected contours.[117] An effort was made to identify as much of the implant silhouette as possible.

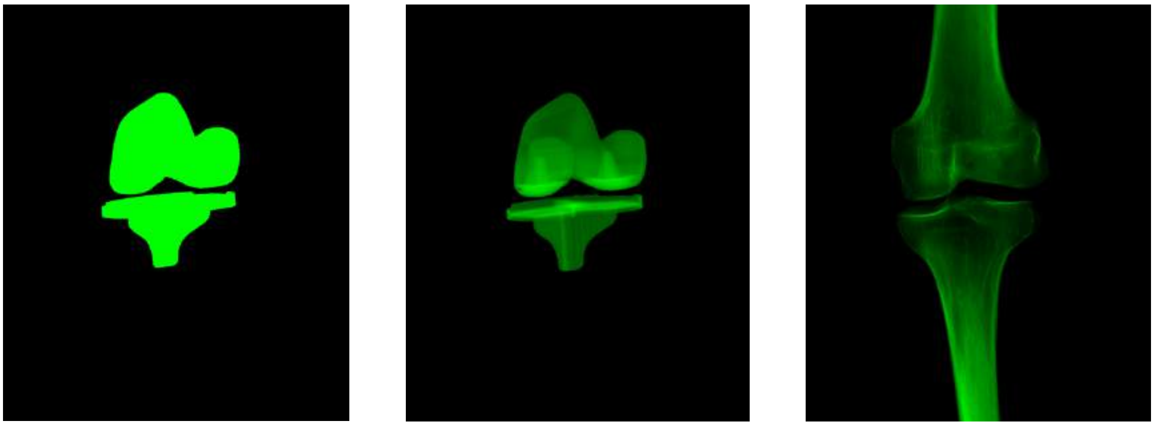

Figure 3-12 Illustration of the model projections. From left, silhouette projection of a surface implant model (*autorsa-surface*), digitally reconstructed radiographs of a synthetic volumetric implant model (*autorsa-volume*) and digitally reconstructed radiographs of a CT-based volumetric bone model (*autorsa-bone*).

3.4.5 Automated radiostereometric image registration

For all studies, the AutoRSA image registration system was utilized to analyse the stereoradiographs. This software system includes two analysis methods, both of which apply a pin-hole camera model accommodating perspective projection for improved depth measures and ray casting; one utilizing silhouette projection of surface models (surface based), and one utilizing DRR projection of volume models (volume based) (Figure 3-12). To estimate the 3D model pose, the surface-based method utilizes only the model silhouette, whereas the volume-based method utilizes the DRR by calculating the cumulative attenuation of the ray by each pixel it passes through the CT volume. The image registration processes were accelerated utilizing the graphics processing unit for speed improvement.

Synthetic volume model: To utilize the AutoRSA volume-based method, a synthetic volumetric representation of the implant models was generated. This was accomplished by assigning the voxels in a 3D isometric volume image inside the surface of the implant model to a value of 3,000 and outside values to zero (Figure 3-13). The volume images with a voxel spacing of 0.4x0.4x0.4 were centralized, oriented and dimensioned according to the implants' coordinate systems and bounding boxes using visualization Toolkit (Kitware).

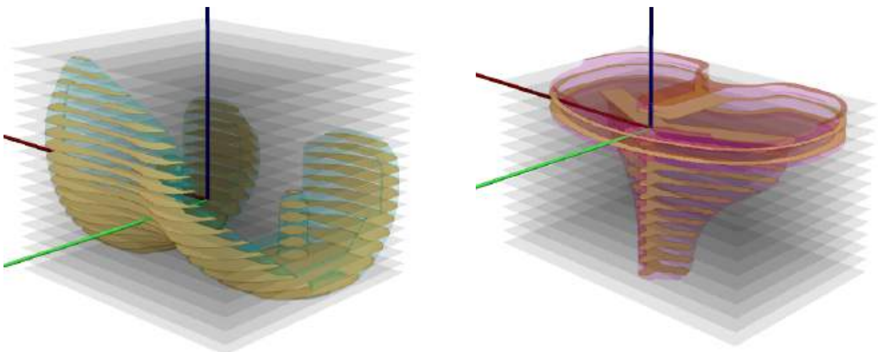

Figure 3-13 Illustration of the synthetically generated volumetric models. The voxels with the high-intensity-assigned value of 3,000 are represented with the copper colour at each slice. A transparent representation of the surface models was superimposed onto each of the volume images to illustrate the outline of the models. Low-resolution volumetric models are presented for visualization (slice thickness 3 mm rather than 0.4 mm).[163]

Similarity metric: For 2D/3D registration, according to previous metric evaluation and initial tests using CT-based volumetric models, the normalized gradient correlation worked best when comparing the virtually generated projections with the actual stereoradiographs.[123,183] The gradients were automatically determined using the Sobel edge detection algorithm.[184] This algorithm calculated 2D spatial gradient measures at each pixel utilizing 3x3 convolution kernels, producing horizontal and vertical gradient images. (Figure 3-14) The similarity metric was then determined as the average of the horizontal and vertical gradients' normalized cross-correlation between the actual radiographs and the virtually generated projection.

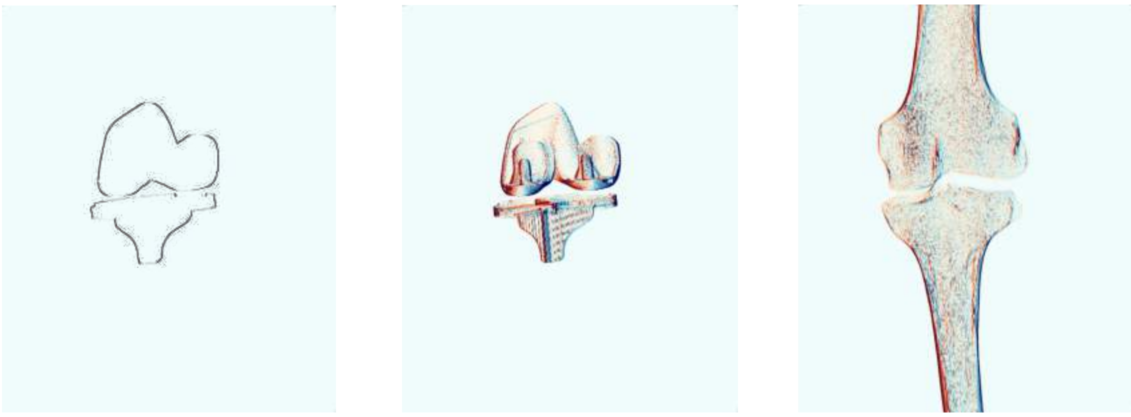

Figure 3-14 Horizontal Sobel gradient images of the left view.[184] From left; silhouette projection of a surface implant model (*autorsa-surface*), digitally reconstructed radiographs of a synthetic volumetric implant model (*autorsa-volume*) and digitally reconstructed radiographs of a CT-based volumetric bone model (*autorsa-bone*).[163]

Mask images: The software allowed for application of a mask image to exclude part of the image from the registration process. This benefits the registration in case of non-relevant high image contrasts, which was found to influence the registration during initial tests. Two methods were optional in combination or separately: 1) a predefined fixed mask image that may be used for excluding high-intensity objects like metallic objects, and 2) a dynamic mask image ensuring analysis of the region of interest only. The dynamic mask image was automatically defined as the initial dilated model projection, thereby excluding the remaining part of the image.

Optimization algorithms: Several optimization algorithms were optional. For our studies, the program's robust optimization scheme was applied consisting of a two-stage registration process using the implemented nonlinear optimization library

NLopt (Steven G. Johson, Boston, Massachusetts). First, a global optimizer (controlled random search algorithm with local mutations). Second, a local optimizer that refined the registration (Nelder-Mead Simplex).[185,186] This was first applied to images at half of the full resolution; and for the final optimization in full resolution, only the local optimizer was applied. The optimization was performed individually for each model.

Analysis application in the studies: For the *in vitro* and *in vivo* native knee studies (Studies I and III), the CT-based volume model (*autorsa-bone*) was used to analyse the femoral and tibial bones, with the dynamic mask applied during the refined optimization in full image resolution. For the *in vitro* TKA study (Study II), first, the implants of the femur and tibia were analysed using both the surface-based (*autorsa-surface*) and the volume-based (*autorsa-volume*) method. For both methods, the dynamic mask was applied during the refined local optimizer in full image resolution. Second, the bone models were analysed using the volume-based (*autorsa-bone*) method in the same order. With information from the pre-analysed implants poses, the fixed mask was used to exclude the surgically removed bone and the metallic part of the implant from the registration. The fixed mask was produced automatically by dilating the implant silhouette projection obtained from the previous implant analysis. The fixed mask was applied during the global optimizer in half resolution and applying a combination of the fixed and dynamic mask during the refined local optimizer in full resolution. For the *in vivo* TKA study (Study IV), the *autorsa-surface* method was used to analyse the femoral and tibial implants in the same way as in Study II. The same desktop computer with a quad-core processor (Intel Xeon E5-1620, 3.60 GHz), 8 GB of DDR4 RAM and a dedicated graphics processing unit (GeForce GTX 960, 4 GB GDDR5) completed the registration for all studies.

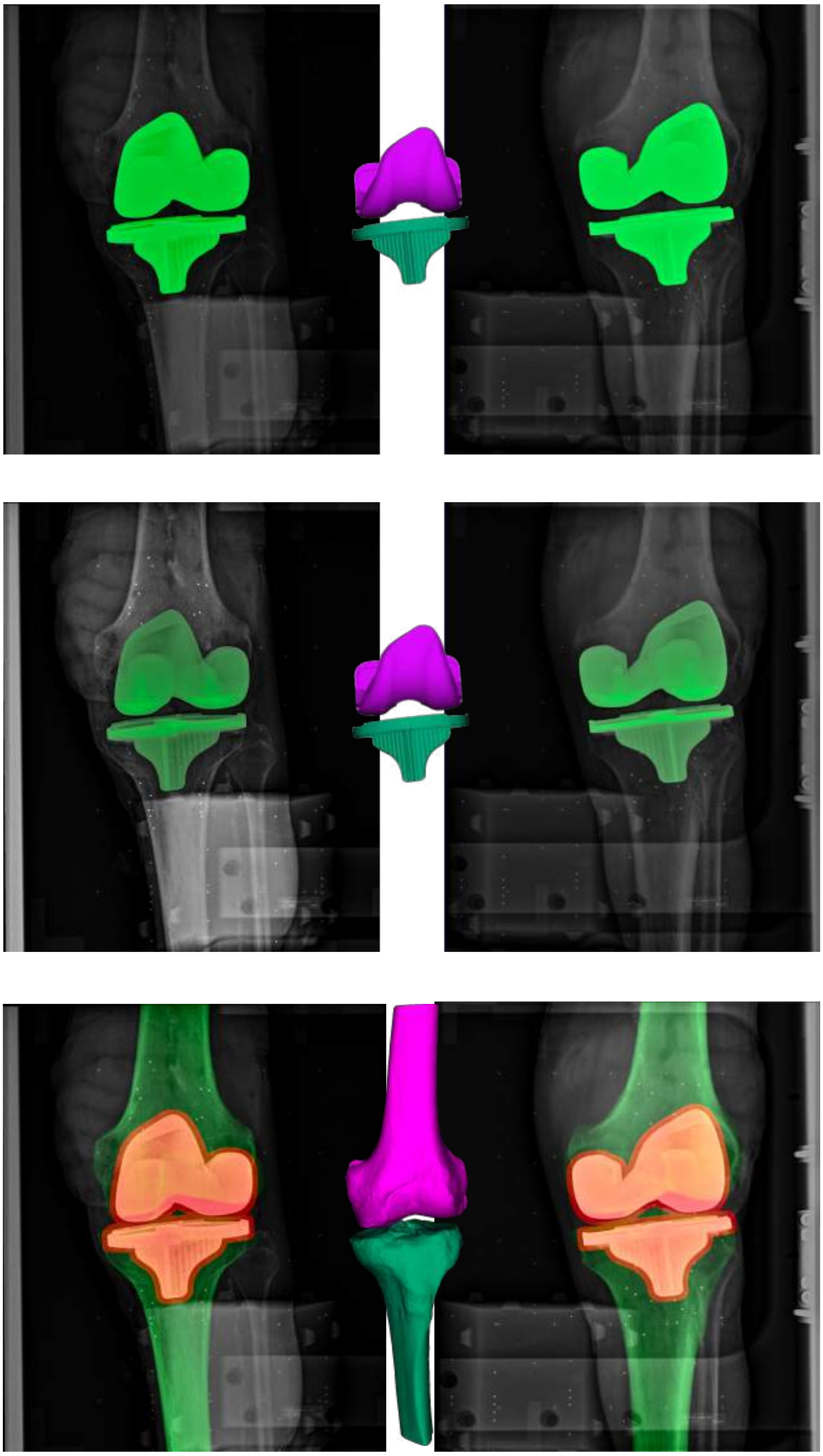

Figure 3-15 Illustration of the stereoradiographs and the radiostereometrically analysed projection of the three automated AutoRSA methods. From the top: The *autorsa-surface* method displays the superimposed silhouette projection of the implant and the three-dimensional implant model. The *autorsa-volume* method displays the superimposed, digitally reconstructed radiographs of the implant and the three-dimensional surface representation of the implant model. The *autorsa-bone* method displays the superimposed digitally reconstructed radiographs and the fixed mask (dilated implant silhouette projection) with a three-dimensional surface representation of the bone model.[163]

3.4.6 Pose initialization

In Studies I, III and IV, dynamic recordings were utilized. These recordings consist of a large number of stereoradiographs that are time-consuming to analyse manually. The automized 2D/3D image registration process requires an approximated initialization to achieve global convergence of the optimization, i.e., correct bone pose. For the *in vitro* study (Study I), the initialization was predicted as the 3D extrapolation of the previous solved images. With initialization being predicted between frames, only the first frame required manual initialization. For the *in vivo* studies (Studies II and IV), it was experienced that the changes in directions occasionally were too sudden, which resulted in poor initialization predictions. Instead, the bone pose initialization was acquired automatically by means of the kinematic trajectories of the reflective markers, analysed prior to the 2D/3D image registration process. As the kinematics trajectories and stereoradiographs were time synchronized, an approximate bone position could be estimated for the new frame using the relative transform for the markers and bone pose in the previous frame. Similar to the *in-vitro* study (Study I), the stereoradiographic series were conducted automatically. Even so, all recordings were visually evaluated, and cases with a clear offset between the digitally generated projection and the actual projection at the radiograph were manually initialized and the bone pose was reoptimized.

3.4.7 Alignment of reference frames between RSA and optical motion capture

For the *in vivo* (Studies III and IV), the kinematic trajectories for the reflective markers and bone trajectories for the dRSA were obtained within different reference frames. Therefore, a transformation between these reference frames needed to be established in order to utilize the marker trajectories as pose initialization for the image registration. To establish this transformation, the reflective markers attached to the calibration cube were recorded using the optical motion capture system simultaneously with the radiographic calibration image acquisition. Then, the reflective marker positions were determined. In the reference frame of the optical motion capture system, this was done using the Motive software system, whereas the RSA reference frame relied on 2D/3D fitting of elementary, geometrically shaped sphere models in the Model-based RSA software system. Finally, the relative transformation was achieved by least-square matching of the calibration cube attached reflective marker positions in the two reference frames (Figure 3-16).

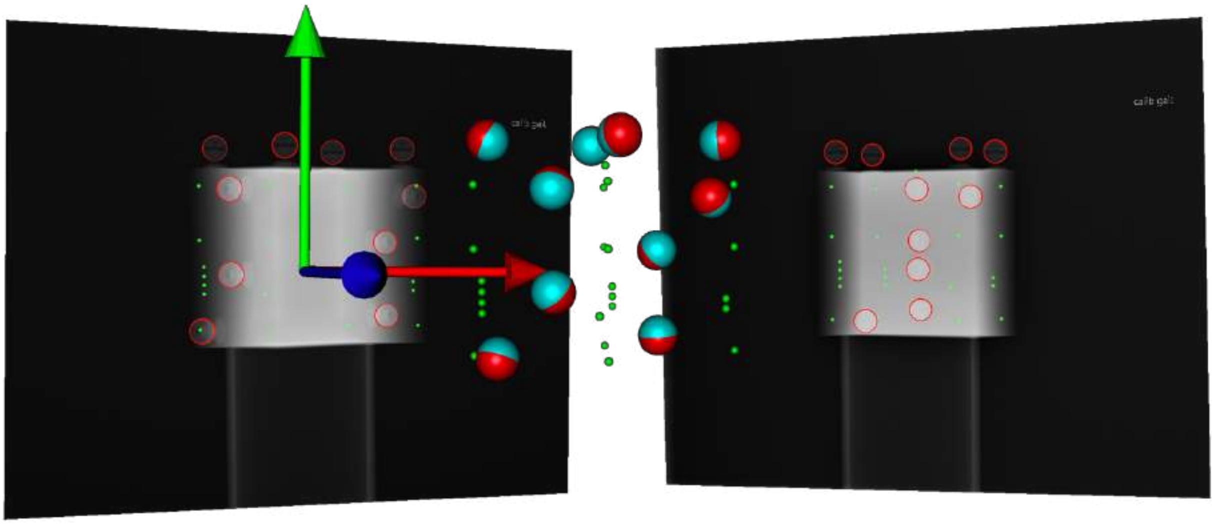

Figure 3-16 Illustration of the alignment between the RSA system (red) and the optical motion capture system (cyan). The spheres represent the reflective markers from each system in the three-dimensional space after the systems were aligned. Additionally, the left and right calibration images of the biplanar setup with the detectors oriented in landscape mode are presented with the selected contours of the reflective markers (red) and cube-markers (green).

3.4.8 Estimating initial contact during gait

For studies III and IV, each dRSA recording contained a series of gait cycles to evaluate and compare the gait patterns between patients; these cycles needed to be identified. One gait cycle started and ended with two successive initial foot contacts of the ipsilateral limb. The initial contact was estimated using a foot velocity algorithm similar to that proposed by O'Conner et al. (Figure 3-17).[187] In short, the method utilizes the velocity trajectory of a virtual foot marker defined midway between the heel marker and the 2nd metatarsal head. The initial contact was estimated using the minima of the foot velocity trajectory complying heel marker closeness to the ground. The closeness to the ground was defined using a threshold level set to 35% of the range of heel heights encountered during the trial. From this point, the heel marker minima were identified within a 0.4 s window. The toe-off was estimated as the foot velocity maxima. From this point, the minimum of the toe marker was identified within a window of 0.4 s as this similarly matched the force determining toe-off best.

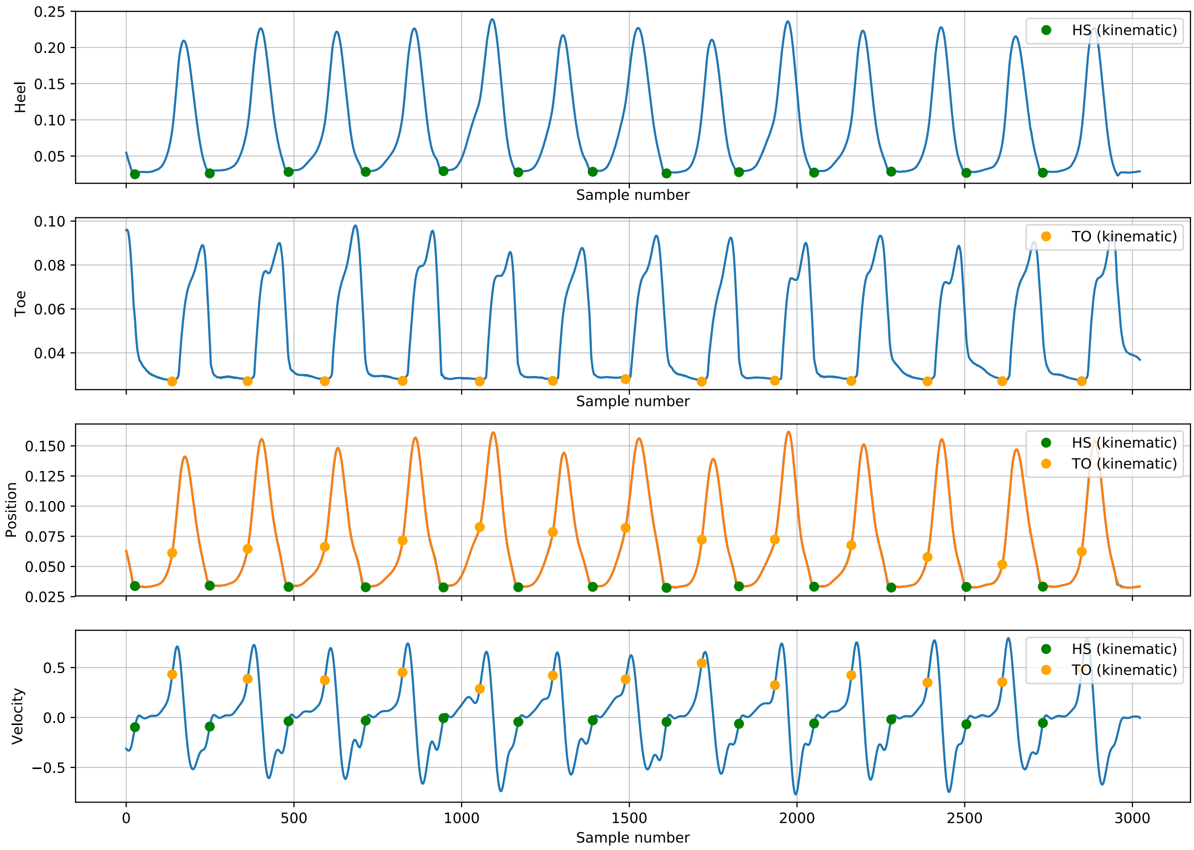

Figure 3-17 A gait cycle example with estimated initial contact of the foot with the ground (HS) and toe-off (TO). The marker trajectories placed at the foot; from top: heel marker, distal phalanx, foot position (midway between the heel marker and 2nd metatarsal head).

Ensuring correct implementation and closeness to a gold standard, a few preliminary tests were conducted. Utilizing the force platform as the gold standard, a threshold of 10 N was used to determine contact between the foot and the ground (force platform). These tests displayed a performance similar to that reported by O'Connor et al. who presented an accuracy of 16 ± 15 ms for initial contact and 9 ± 15 ms for toe-off (Figure 3-17).

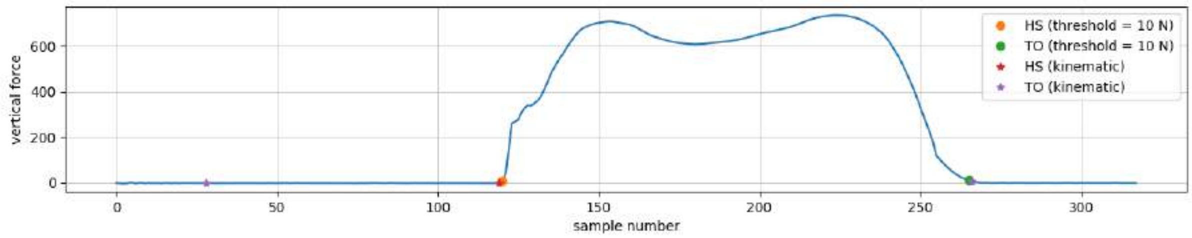

Figure 3-18 Illustration of the knee joint coordinate system used for kinematic pose assessment of the femoral and tibial bones considered in relation to each bone.

3.4.9 Quantification of tibiofemoral joint kinematics

For studies I, II and IV, the tibiofemoral joint kinematics from the dRSA-obtained bone poses was implementing using the Grood and Suntay joint coordinate system (Figure 3-19).[188] Accounting for possible hyper-extension and -flexion, the modified equations proposed by Dabirrahmani and Hogg were applied.[189] The relative motion in all six degrees of freedom (rotation and translation) of the body-fixed anatomical coordinate systems was computed for each frame. The translation was quantified in mm with medial tibial shift, tibial anterior drawer and joint distraction as positive directions. Rotations were measured in sequence as presented and quantified in degrees with flexion, adduction and tibial internal rotation as positive directions. Kinematic values were divided into gait cycles with a gait cycle starting and ending with two successive initial foot contacts of the ipsilateral limb. To estimate the most representative gait cycle pattern, the kinematic measures were time-normalized to 21 points representing the gait cycle from 0-100% and the median across trials for each subject were calculated. The median is a robust measure with which to estimate the central trend of the trajectories when only few samples are available as it compensates for outliers.

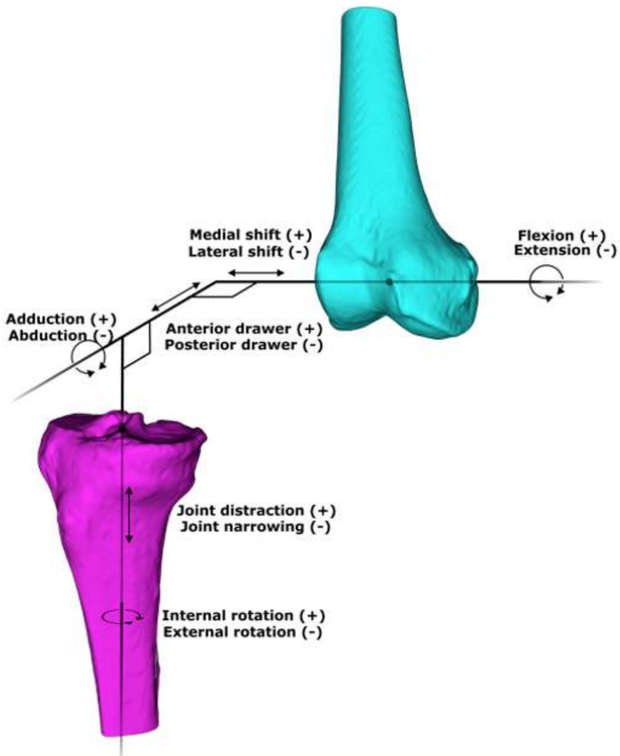

Figure 3-19 Illustration of the knee joint coordinate system used for kinematic pose assessment of the femoral and tibial bones considered in relation to each.[177]

3.4.10 Subgroup allocation

In Study III, the KOA patients were divided into subgroups based on their kinematic trajectories using k-means. K-means is a centroid-based clustering algorithm.[190] In an unsupervised machine learning manner, k-means allocates multidimensional data into clusters based on a Euclidean distance measure without any prior knowledge of group allocation, except the number of clusters. K-means clustering is an iterative algorithm that randomly allocates every data point to the nearest cluster while minimizing the sum of squared Euclidian distance between every data point and its cluster's centroid. Due to random seeding of the initial allocation, the k-means algorithm may not reach the ideal global optimum, but it may instead converge at a local optimum. To address this limitation, the ideal allocation may be chosen as the one with the least sum of squared Euclidian distance of multiple clustering processes with different randomly allocated seeds. Below, this is referred to as a *clustering process*. Another challenge of the k-means approach is to determine the number of clusters (k). The number of clusters (*k*) may be determined by investigating the repeatability and quality for *k* number of clusters. Cluster repeatability may be investigated by tracking differences in cluster allocations for *clustering processes* with increasing *k* clusters. Furthermore, cluster quality may be assessed using the Silhouette value. This is basically a similarity measure describing how well each subject is allocated within a cluster in relation to all other clusters. The Silhouette value ranges from -1 to 1, where a greater value indicates a stronger association to its allocated cluster, and a greater negative value indicates greater association to other clusters.

The skleans[61] implementation of k-means in Python was used to divide our patients with KOA into subgroups based on their kinematic gait patterns. The median kinematic trajectories of each patient were used to construct a 126 by 66 feature matrix (M) containing the 126 trajectory kinematic feature points (6 kinematic parameters x 21 time-points) for each of the 66 patients. Feature point ordering was consistent across all participants in the matrix. The features were standardized to avoid different weightages between features. The standardization included that each feature was subtracted from the respective mean values and divided by the standard deviation. One *clustering process* was defined as 50 repetitions of a single k-means with randomly allocated seeds and 2-5 number of subgroups were investigated (*k*). Subgroup repeatability was evaluated based on repeating ten *clustering processes*. The subgroup quality of the 2-5 *k* subgroups was assessed using the Silhouette value of the best *clustering process* - the one with the lowest sum of squared error of the ten repetitions.

3.4.11 Quantification of tibiofemoral artificial joint articulation

For Study IV, the joint articulation was estimated by constructing a distance map between the femur implant and the tibia bearing. Since the tibia bearing is radiolucent, a rigid relation to the radiopaque tibia implant was assumed to estimate its pose. The distance mapping was obtained by assigning each mesh point on the tibia bearing with the value of its shortest distance to the femur implant model within a distance range limit of -0.5 to 0.5 mm. The distance mapping was computed for each frame. To compare the participants' different implant sizes and types, each bearing was scaled to a fixed width of 68 mm, representing a mid-implant size. Subsequently, a 70x70 point grid was defined with a point distance of 1 mm. It was centred around the Z axis and oriented in the XY plane (coronal) of the tibia implant coordinate system. The grid points were coloured according to the cell colour of which its orthogonal projection intersects the bearing. (Figure 3-20)

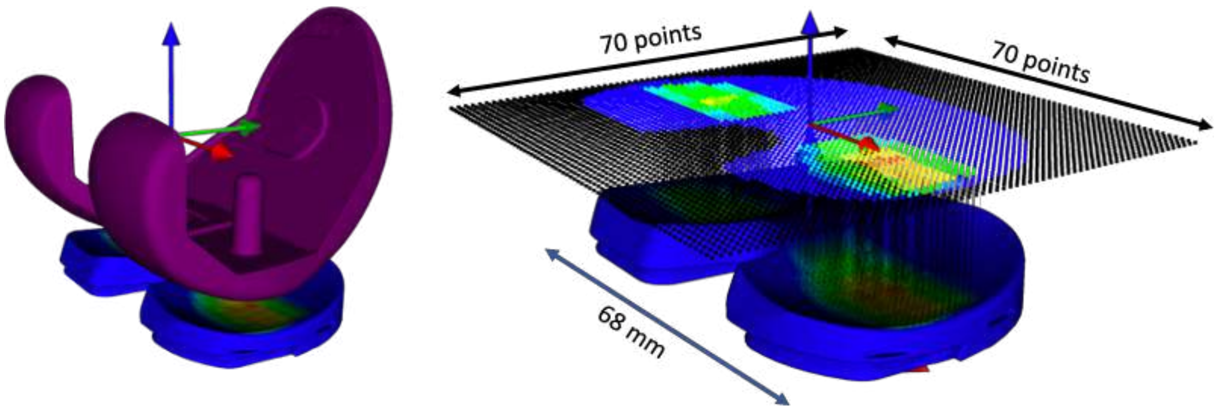

Figure 3-20 Quantification of joint articulation; left) Illustration of the distance colour map determined by the shortest distance from each point on the tibial bearing to the femoral implant. The spacing between the bearing and the implant is increased to enhance the visualization. right) Illustration of the 3D colour map transformation to the 2D point grid that was used in the statistical parametric mapping (SPM) analysis to quantify the difference between the Persona® Medial Congruent® (MC) and Persona® Cruciate Retaining (CR) bearing.[109]

3.4.12 Alignment of reference frames between RSA and specimen fixture

When positioning the fixture at the cross-section of the x-ray tubes, the fixture reference frame was oriented meticulously (defined by the displacements of the three axial micrometres), as closely as possible to the RSA reference frame (defined by the calibration cage). Even so, the coordinate systems were not completely aligned. To accomplish error investigation for each direction individually, the axial direction was defined according to a linear fit of the 25 marker displacements for each series individually (Figure 3-21). Then, the investigated position coordinate of the models, expressed in the RSA reference frame, were projected to the fitted micrometres' axial direction.

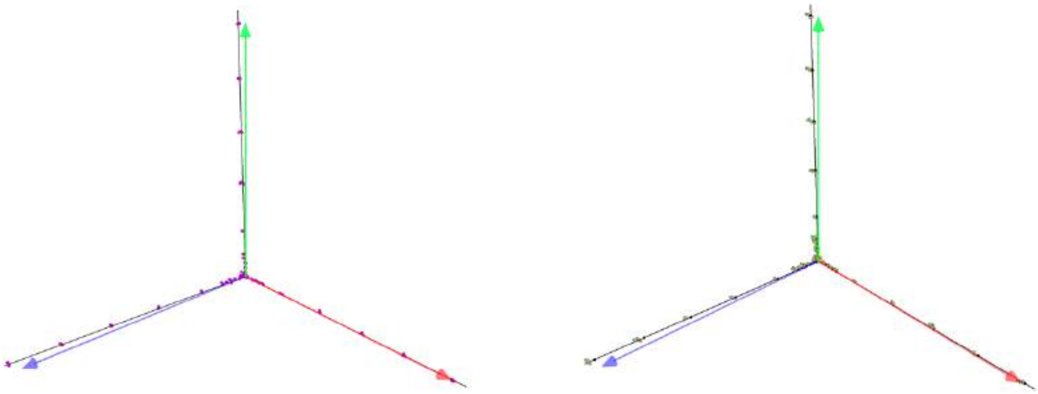

Figure 3-21 An example of the offset between the RSA system (coloured) and the fixture axes (black). Left figure: presents the marker positions that were used to determine the fixture axis as a linear fit. Right figure: presents the estimated position of the five methods for these series.

3.4.13 Patient-reported outcome measures

PROMs are a widely used tool to assess patients' perceptions of their treatment in relation to their health and daily function. Three traditional knee questionnaires were registered: the OKS, the KOOS and the FJS. Below, each questionnaire is described with its minimal clinical important difference (MCID). The MCID is the minimal change in scoring measures that demonstrate an effect of a procedure.

Oxford Knee Score: The OKS was developed and validated specifically for measuring outcomes of knee replacement surgery. It consists of 12 items capturing the intensity of the subject's own perception of the given term. The summary score ranges from 0 to 48 (high is best).[168] Subscales that are standardized from 0 to 100 (high is best) can also be derived for pain (items 2, 3, 7, 11, 12) and function (item 1, 4, 5, 6, 8, 9, 10).[191] The MCID of the OKS is 5.0 (95 % CI 4.4–5.5) points.[192]

Knee Injury and Osteoarthritis Outcome Score: The KOOS was developed specifically to assess the patient's opinion about their knee and associated problems.

It is divided into five subscales (pain, function, activities of daily living, sport and recreation, and knee-related quality of life. In total, the questionnaire consists of 42 items capturing the intensity of the subject's own perception of the given term. The five subscales of the KOOS are scored, evaluated and standardized individually. The standardized scale ranges from 0 to 100 (high is best).[169] The MCIDs are 15.4 points for KOOS pain, 15.1 points for KOOS function, 17 points for KOOS activities of daily living, 11.2 points for KOOS sports and recreation and 16.5 points for KOOS quality of life.[193]

Forgotten Joint Score: FJS is a newer assessment tool that attempts to provide more distinct measures for well-performing patients, in particular, by assessing the patient's joint awareness – his or her ability to forget the artificial joint. In total, the questionnaire consists of 12 items capturing the intensity of the subject's own perception of the given term. This standardized scale ranges from 0 to 100 (high is best).[170] The MCID of the FJS is 16.6 (95 % CI 8.9-24.3) points.[194]

3.4.14 Ligament lesion grading from magnetic resonance imaging

MRI is non-invasive and one of the preferred modalities for assessing the knee pathology to provide information for patient management and treatment.[195] The imaging technique obtains high-resolution images displaying soft tissue structures such as the menisci, ligaments and tendons. In recent decades, technological advancements have improved the method. Generally, MRI provides good diagnostics for larger structures but less so for minor structures.[196] The sensitivity and specificity for the ACL fell in the 83–95% and 95–100% range, respectively. For the PCL, the corresponding numbers were 94% and 92%, respectively.[195,196] For MCL, the accuracy and sensitivity was 86.4%.[197]

3.4.15 Leg-extension power rig

The leg-extension power represents an objective functional measure of the patient's lower extremity muscle strength and was assessed using a leg-extension power rig (Bio-Med International, Nottingham, UK). The affected leg was tested preoperatively (Study III) and one-year after TKA (Study (IV). The subject was seated with back-support and the foot placed on a movable footplate. The seat position was adjusted ensuring that the leg could be fully extended without allowing hyper-extension but ensuring comfortable knee and hip flexion. The test rig determines the amount of power that the leg extension provides. The subjects were instructed to extend their leg as forcefully and quickly as possible. Before data acquisition, the subject performed a few warm-up attempts to get familiar with the rig. Each subject performed a minimum of five and a maximum of ten trials separated by a short 15-second recovery period. The test session was concluded if two trails were lower than the previous or if the subject reported knee pain.[166] The maximum recorded measurement for each subject was used in the subsequent analysis.

3.4.16 Method agreement

Accuracy describes the ability to determine the true value. Whereas precision describes the ability to reproduce the measurement within a short period of time – precision and repeatability considers synonyms. For these studies (Studies I and II), only the accuracy was assessed. To assess a methods' accuracy, ideally the true value must be known; however, the true value typically remains unknown. Instead, the best possible method is used to determine the true value, often referred to as gold standard method. The variation between two methods consists of systematic variation (bias) and random variation. Bland-Altman plots are traditionally used to assess method agreement by plotting the average against the difference of the methods.[198] The mean difference of the methods is the bias, and the random variation is the standard deviation of the differences. If the 95% confidence interval of the bias does not include zero, no difference, the investigated method displays a systematic bias. The limit of agreement is estimated as the mean difference plus/minus 1.96 standard deviations and is expected to contain 95% of future measurements on similar subjects and setup. Whereas the bias may be adjusted for if well established, the limit of agreement cannot be adjusted for. A highly accurate gold standard is important, at least one that is superior to the investigated method as the investigated method can be determined only within the accuracy of the gold standard. Both the bias and limit of agreement of the gold standard relative to the true value affect the bias and limit of agreement of the investigated method.

3.5 Statistics

3.5.1 Study I

The accuracy of the tibiofemoral joint kinematics was presented in Bland-Altman plots facilitating the presentation of mean bias and limits of agreement with a significance level of 0.05. The tibiofemoral joint kinematics and individual bone poses (femur and tibia) were evaluated for both RSA setups, uniplanar and biplanar. The mean difference (bias) was compared against the null hypothesis of no difference from zero using a simple t test. Statistical calculations were performed using (Stata/IC 16.0, StataCorp, TX, USA) with a significance level of 0.05.

3.5.2 Study II

Accuracy measures were presented in Bland-Altman plots facilitating the presentation of mean bias and limits of agreement at a significance level of 0.05. Each of the following five methods RSA were presented separately for the femur and tibia, respectively: marker-based of bones (*marker*), contour-based of implants (*mbrsa*), surface-based of implants (*autorsa-surface*), volume-based of implants (*autorsa-volume*) and volume-based of bones (*autorsa-bone*). Statistical differences were not investigated between methods. For this study, it was not relevant to determine whether methods were statistically different from one another. What relevant were the accuracy of the method in the context of its clinical application. Even so, to provide a visual overview of the methods, their mean bias and limits of agreement are summarized graphically.

3.5.3 Study III and IV

Overall, the same statistics and a significance level of 0.05 were applied in Studies III and IV. Differences in tibiofemoral joint kinematics across the entire gait cycles (Studies III and IV) and for the 2D articulation measure on the entire grid map at each time point during the gait cycles (study IV) were examined using one-dimensional SPM with the open-source code spm1d (spm1d.org, v.0.4.2) for Python (Python Software Foundation, v.3.6). In both cases, QQ-plots revealed that our kinematic data were not normally distributed. Thus, the non-parametric equivalent was used. Statistical non-parametric mapping (SnPM) deals with smoothness implicitly and estimates the test statistics through permutation[199]. First, a Hotelling test was implemented on the entire vector field. Then, the post-hoc Hotelling test was applied to each vector component if the vector field level reached statistical significance.

In Study III, we compared demographically and clinically characteristic differences between subgroups using one-way analysis of variance (ANOVA) for continuous variables, ordinal logistic regression for categorical variables and logistic regression for binary variables. When significant differences were detected, the Bonferroni correction was applied for group differences. Visual inspection of QQ-plots verified normally distributed data.

In Study IV, we compared demographical and clinical characteristics, PROMs, VAS, leg-extension power and contact point range-of-motion differences between groups using Student's T-test for continuous variables, ordinal logistic regression for categorical variables and chi-squared for binary variables. Visual inspection of QQ-plots verified normally distributed data.

4

Results

4.1 Study I

A total of 1,520 radiostereometric images (760 uniplanar, 760 biplanar) were analysed and included for statistical comparison of the automated CT-based volume models and the marker configuration models. The results described in the text below refer to the uniplanar radiographic setup.

4.1.1 Method agreement for tibiofemoral kinematics (uniplanar setup)

The agreement of the *autorsa-bone* and *marker* analysis of tibiofemoral kinematics in a dRSA recording of one specimen during one tibiofemoral flexion cycle is reported

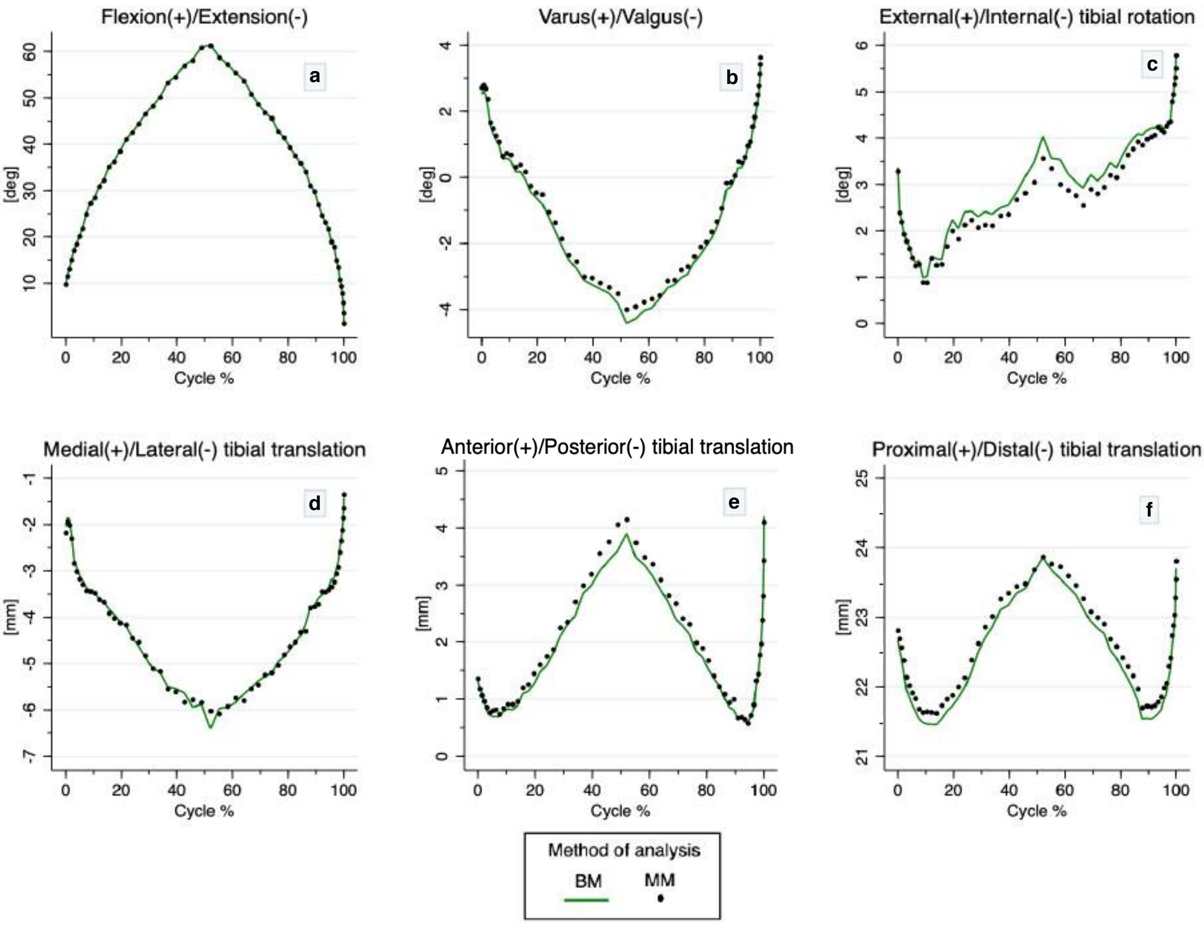

Figure 4-1 Difference during the movement cycle. A comparison between the CT-based bone volume (*autorsa-bone*, solid green lines) and the marker configuration method (marker, black dots) for a single recording; Cadaver ID C, uniplanar calibration setup. (A–C) Rotations. (D–F) Translations.[124]

graphically as a general example (Figure 4-1). The plots show a high method agreement with a very small bias of the *autorsa-bone* compared with the *marker* method. The agreement between the methods in tibiofemoral joint kinematic assessment for all eight specimens is demonstrated in Bland-Altman plots for the six degrees of freedom (Figure 4-2). The bias and limit of agreement are listed in a box within each plot. A systematic bias was found for the *autorsa-bone* in all six degrees of freedom ($p < 0.001$); however, excellent agreement was still observed as bias ranged between -0.04 to 0.04° for all rotations and from -0.19 to 0.18 mm for all translations. The poorest precision was ±0.42 mm for anterior-posterior translation and ±0.33° for external-internal rotation.

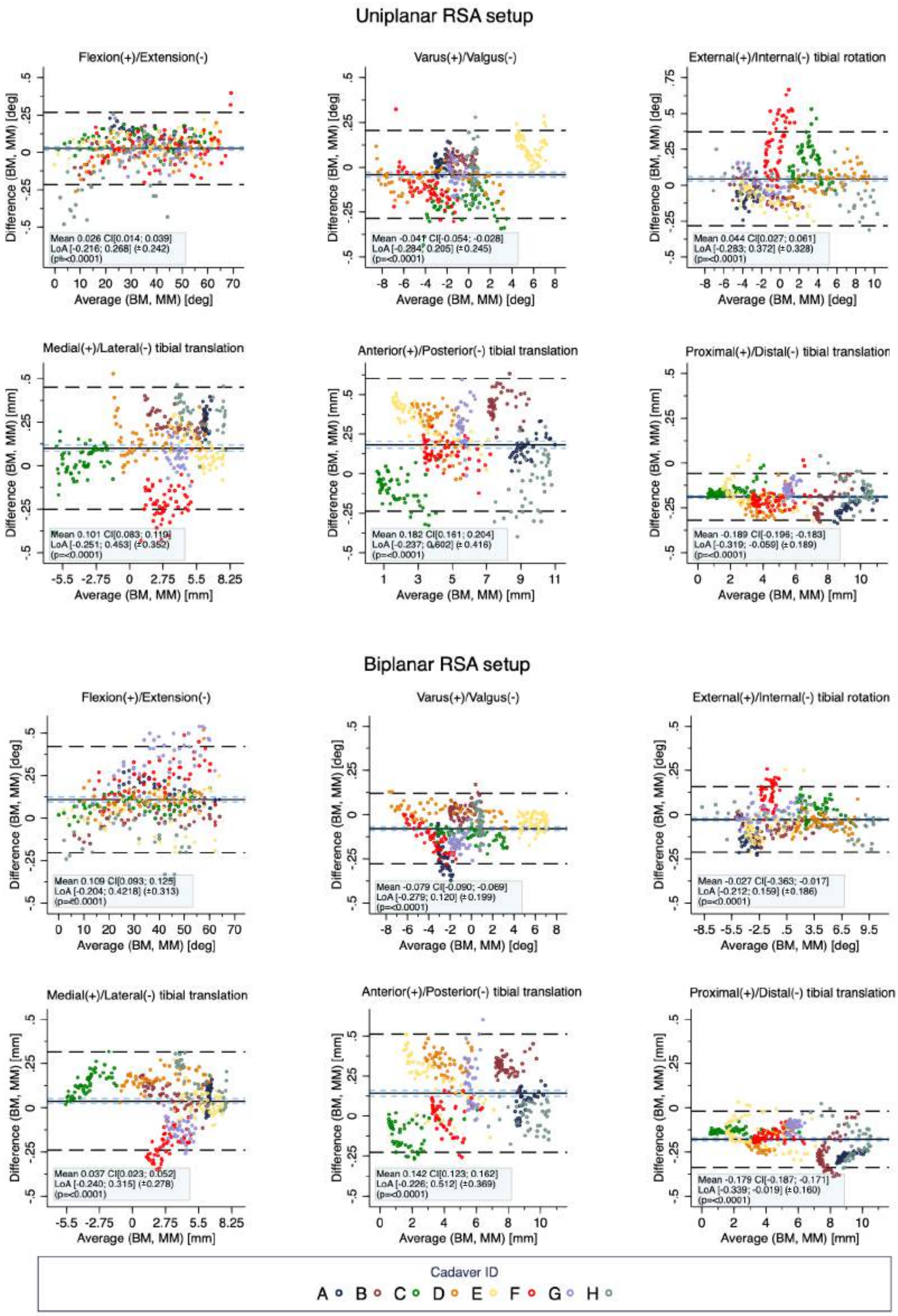

Figure 4-2 Bland-Altman plots for kinematic measurements in uniplanar (top) and biplanar (bottom) setup comparing the CT-based bone method (*autorsa-bone*) with the marker configuration method (*marker*). The scatter colours represent each specimen (A-H). The solid black horizontal line represents the mean difference (bias), dashed blue lines show the CI of the mean differences and the dashed black lines show the limit of agreement.[124]

4.1.2 Method agreement for individual bone pose estimation

Femoral bone poses for the *autorsa-bone* in comparison with the *marker* method showed a largest observed bias of -0.13 mm for translations and -0.19° for rotations, with limits of agreement falling within ±0.50 mm for translation in medial-lateral axis and ±0.34° for rotation about anterior-posterior axis (Table 4-1). The pose of the tibial bone had a bias of up to 0.09 mm for translations and -0.21° for rotations, with limits of agreements of ±0.38 mm and ±0.24° for translation in and rotation about the medial-lateral axis, respectively. Overall, the bias was lower and the limits of agreement better for the pose of the tibial bones than for the femoral bones. Adding to this, less variation of mean total difference (total bias) for tibial bone translations than femoral bone translations was found when specimens were considered individually (Figure 4-3).

Table 4-1 Bias of the CT-based bone model (*autorsa-bone*) for individual bone pose estimates.[124]

	Translation precision (mm)					Rotational precision (°)				
	Tx	**Ty**	**Tz**	**Total[I]**	***p-value***	**Rx**	**Ry**	**Rz**	**Total**	***p-value***
Uniplanar (*n= 380*)										
Femoral bone										
Mean difference	-0.125*	-0.107	-0.085	0.302	< 0.001	-0.191	-0.026	-0.015	0.273	< 0.001
± 95% CI	0.026	0.011	0.010	0.010		0.012	0.008	0.007	0.016	
SD	0.252	0.101	0.932	0.099		0.120	0.174	0.071	0.114	
± LoA	0.495	0.198	0.183	0.195		0.236	0.341	0.139	0.223	
Tibial bone										
Mean difference	0.094	0.055	0.054	0.226	< 0.001	-0.211	0.035	-0.003*	0.267	< 0.001
±95% CI	0.019	0.009	0.004	0.010		0.013	0.011	0.007	0.009	
SD	0.191	0.888	0.037	0.097		0.124	0.110	0.072	0.084	
±LoA	0.375	0.174	0.074	0.191		0.243	0.216	0.141	0.165	
Biplanar (*n =380)*										
Femoral bone										
Mean difference	0.055	0.066	-0.536	0.227	< 0.001	-0.126	-0.038	-0.004*	0.198	< 0.001
±95% CI	0.021	0.011	0.011	0.014		0.014	0.014	0.006	0.011	
SD	0.199	0.100	0.099	0.136		0.140	0.105	0.055	0.105	
±LoA	0.392	0.196	0.195	0.267		0.270	0.206	0.107	0.206	
Tbial bone										
Mean difference	0.106	0.129	0.167	0.304	< 0.001	-0.232	0.051	-0.054	0.278	< 0.001
±95% CI	0.019	0.007	0.005	0.009		0.013	0.010	0.008	0.011	
SD	0.191	0.071	0.044	0.839		0.120	0.093	0.073	0.102	
±LoA	0.375	0.135	0.086	0.165		0.236	0.186	0.143	0.201	

Note: n Indicates the number of matched items. Abbreviations: SD – standard deviation; CI – confidence interval; LoA – limit of agreement. [I] Mean total difference (total bias) for all specimens, approximated using the Pythagorean theorem.

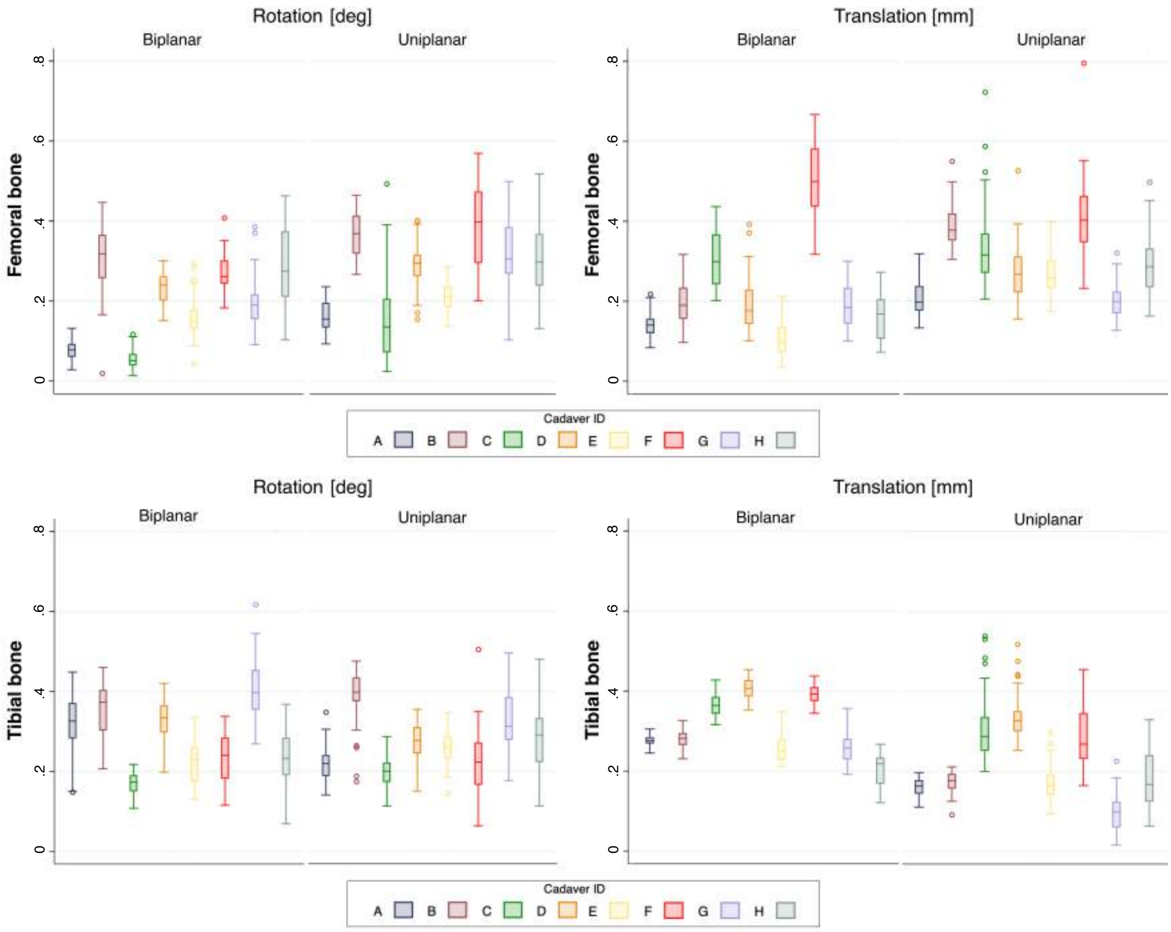

Figure 4-3 Total bias of the CT-based bone model (*autorsa-bone*) in the pose of the femoral (top) and tibial bone (bottom). The mean total difference (total bias) for rotations and translations was computed using the Pythagorean theorem for all individual recordings. Uniplanar and biplanar recordings are shown side-by-side for comparison. Boxes are drawn from the 25th percentile (lower hinge) to the 75th percentile (upper hinge). Whiskers extend to upper and lower adjacent values and contain all values not considered outliers. Abbreviations: A to H - donor specimens; DRR – digitally reconstructed radiographs.[124]

4.1.3 Agreement of radiographic setup configuration

The biplanar setup was slightly less accurate in determining kinematic flexion-extension with a bias of 0.11 mm and limits of agreements of ±0.31° compared with 0.03 mm and ±0.24° in the uniplanar setup (Figure 4-2). However, for external-internal rotation of specimens C and F, the Bland-Altman plots showed a wider observation cluster in the uniplanar setup than the biplanar setup (Figure 4-2). Overall, no consistent effect on bias or limits of agreement of the *autorsa-bone* was found to be caused by radiographic setup configuration (Table 4-1 and Figure 4-2).

4.2 Study II

The results include 205 recordings on eight specimens yielding a total of 1,640 stereoradiographs. This included displacement series of two views (AP and LM) in three directions (x, y, z) with one series consisting of 35 stereoradiographs. Seven series were excluded due to non-methodology issues such as a missing image in the recording or unlabelled takes, leaving a total of 1,395 analysed stereoradiographs.

The results of each registration method are presented as Bland-Altman plots for the femur and tibia separately and revealed no bias for any of the analysed methods (Figure 4-4). The best limits of agreements were obtained for the *marker* and *autorsa-bone* registration with similar results for both the femur and tibia. The poorest limits of agreement was found for the *autorsa-surface* method for the femoral implant, whereas the *autorsa-surface* and *autorsa-volume* methods showed equally large limits of agreements for the tibial implant. The *autorsa-volume* method displayed similar limits of agreement for analysis of the femoral implant as the *mbrsa* method. The *mbrsa* method displayed slightly poorer limits of agreement values than the *marker* and *autorsa-bone* methods (Figure 4-5).

For future power calculations, detailed results of the individual directions calculated separately for each view are presented in Table 4-2 and Table 4-3, and data for the two views are combined in Table 4-4 for femoral and tibial models. In general,
poorer accuracies were found in the z direction for the AP view and in the x direction for the LM view, with the LM view yielding the poorest results. When data for the two views were combined, the tibia generally displayed a slightly poorer accuracy.

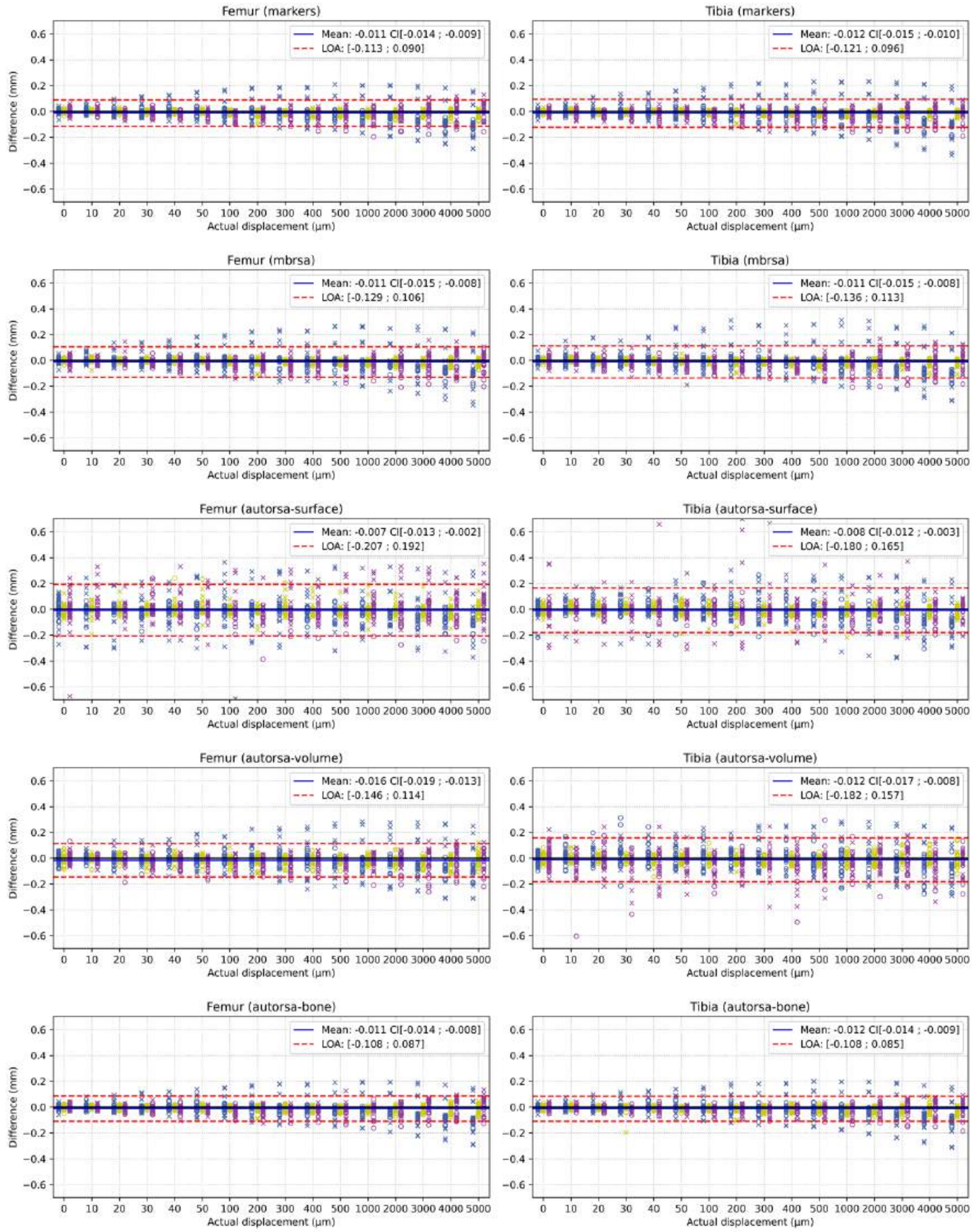

Figure 4-4 Bland-Altman plots for each method with the colours representing x (blue), y (yellow) and z (purple). The "o" and "x" represent the anterior-posterior and lateral-medial view, respectively. From the top row: *marker*, *mbrsa*, *autorsa-surface*, *autorsa-volume* and *autorsa-bone*. The first column presents the data of the femur and the second column presents data of the tibia. Abbreviations: LOA – limits of agreement, CI – confidence interval.[163]

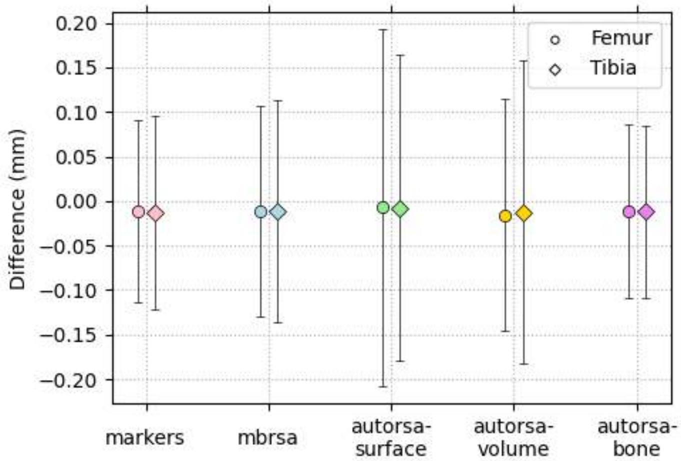

Figure 4-5 Presentation of the limit of agreement for each method for the femur and tibia.[163]

Table 4-2 Presenting the femur mean and standard deviation of the different views in the three directions. The red text presents the highest standard deviations for each method and view. The bold-red text presents the highest standard deviation for each method in both views.[163]

	Anterior-posterior view			Lateral-medial view		
	x	y	z	x	y	z
marker	-0.027 (0.043)	-0.011 (0.018)	-0.028 (0.049)	**-0.002 (0.102)**	-0.001 (0.016)	-0.005 (0.041)
mbrsa	-0.027 (0.042)	-0.009 (0.015)	-0.038 (0.052)	**0.004 (0.123)**	-0.004 (0.019)	-0.003 (0.049)
autorsa-surface	-0.027 (0.054)	-0.006 (0.031)	0.036 (0.074)	**-0.018 (0.161)**	0.001 (0.051)	0.026 (0.149)
autorsa-volume	-0.023 (0.049)	-0.013 (0.033)	-0.050 (0.070)	**-0.000 (0.127)**	-0.009 (0.030)	-0.010 (0.049)
autorsa-bone	-0.026 (0.040)	-0.010 (0.021)	-0.027 (0.044)	**-0.003 (0.098)**	-0.004 (0.018)	-0.002 (0.040)

Table 4-3 Presenting the tibia mean and standard deviation of the different views in the three directions. The red text presents the highest standard deviations for each method and view. The bold-red text presents the highest standard deviation for each method in both views.[163]

	Anterior-posterior view			Lateral-medial view		
	x	y	z	x	y	z
marker	-0.026 (0.043)	-0.008 (0.013)	-0.035 (0.046)	**0.003 (0.114)**	-0.008 (0.015)	-0.006 (0.043)
mbrsa	-0.026 (0.045)	-0.008 (0.016)	-0.031 (0.056)	**0.011 (0.126)**	-0.009 (0.023)	-0.010 (0.059)
autorsa-surface	-0.020 (0.072)	-0.003 (0.025)	-0.029 (0.058)	**0.007 (0.131)**	-0.010 (0.040)	0.004 (0.131)
autorsa-volume	-0.006 (0.084)	-0.008 (0.039)	-0.032 (0.107)	**0.015 (0.120)**	-0.007 (0.025)	-0.035 (0.105)
autorsa-bone	-0.022 (0.039)	-0.014 (0.020)	-0.024 (0.041)	**-0.002 (0.101)**	-0.010 (0.023)	-0.002 (0.034)

Table 4-4 Presenting the combined mean and standard deviation of both views in the three directions for the femur and tibia. The red text presents the highest standard deviations for each method and bone. The bold-red text presents the highest standard deviation for each method in both bones.[163]

	Femur			Tibia		
	x	y	z	x	y	z
marker	-0.015 (0.077)	-0.006 (0.018)	-0.014 (0.046)	**-0.013 (0.085)**	-0.008 (0.015)	-0.005 (0.041)
mbrsa	-0.012 (0.091)	-0.006 (0.017)	-0.017 (0.053)	**-0.009 (0.094)**	-0.008 (0.020)	-0.018 (0.059)
autorsa-surface	-0.023 (0.117)	-0.002 (0.043)	**0.002 (0.129)**	-0.008 (0.104)	-0.006 (0.034)	-0.009 (0.110)
autorsa-volume	-0.013 (0.094)	-0.011 (0.031)	-0.026 (0.061)	-0.003 (0.102)	-0.007 (0.032)	**-0.034 (0.106)**
autorsa-bone	-0.016 (0.074)	-0.007 (0.020)	-0.011 (0.043)	**-0.013 (0.075)**	-0.012 (0.022)	-0.010 (0.038)

4.3 Study III

4.3.1 Subgroup allocation

The quality and repeatability analyses are presented in Figure 4-6. Silhouette values [mean (standard deviation)] across ten k-means cluster repetitions were: *k*=2 [0.178 (0.002)]; *k*=3 [0.140 (0.006)]; *k*=4 [0.128 (0.004)]; and *k*=5 [0.125 (0.005)]. The individual subgroup allocation across the ten consecutive repetitions showed identical subgroup allocation for *k*=2. Individual data allocation was more variable for *k*=3 and *k*=4 with three and ten individuals switching subgroups, respectively. No consistent pattern of subgroup allocation could be identified for the *k*=5 solution. Noticeably, the second (*k*=3) and third (*k*=4) solutions allocated two identical subgroups (G3, G4), whereas the third (k=4) solution separated the remaining subgroup into two subgroups (G1, G2). All of this indicates that four subgroups may represent the optimal solution for separating the present dataset into the largest number of subgroups with the highest quality possible and a reasonable repeatability. Consequently, the third (*k*=4) solution was chosen for further analysis; G1 (n=20), G2 (n=17), G3 (n=10), and G4 (n=19).

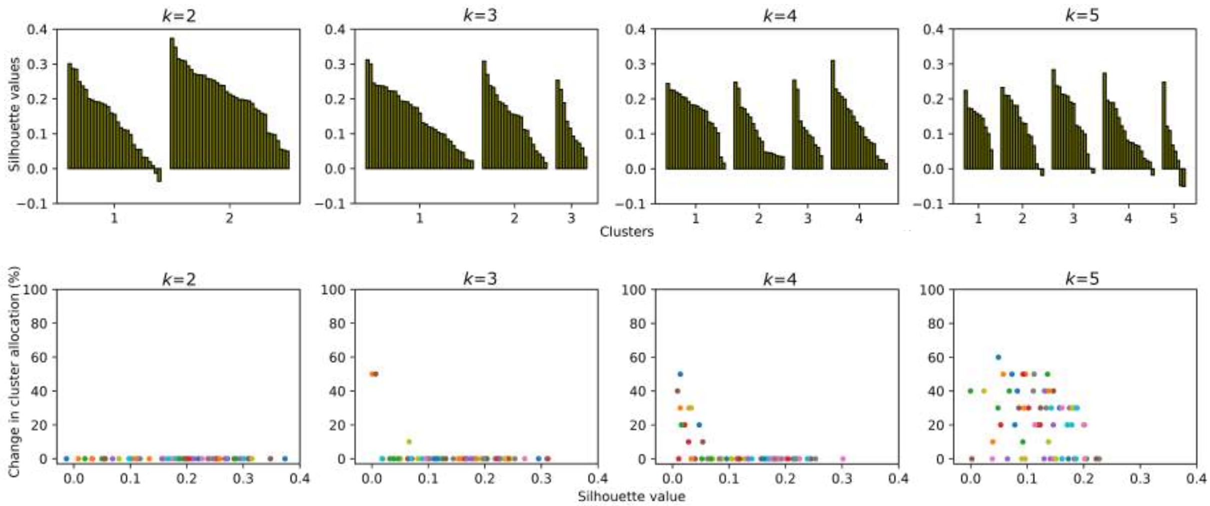

Figure 4-6 Presentation of cluster allocation for *k*-values ranging from 2 to 5. Top row: Silhouette values of each subject of the repetition that showed the best mean square error of the ten repetitions. Bottom row: change in cluster allocation across the ten repetitions with respect to each subject's silhouette value.[177]

4.3.2 Kinematic and clinical characteristics

The tibiofemoral joint kinematic trajectories for the entire patient cohort showed increased tibial external rotation, tibial lateral shift and joint narrowing compared with the healthy group (Figure 4-7). The four gait-trajectory-based subgroups (G1, G2, G3 and G4) are compared with the healthy group in Figure 4-8 and Table 4-5c (colour-code highlights the main differences). The in-between subgroup kinematic comparison is presented in Appendix II. Clinical differences and a schematic overview of the most relevant differences between subgroups and the healthy control group are presented in Table 2.

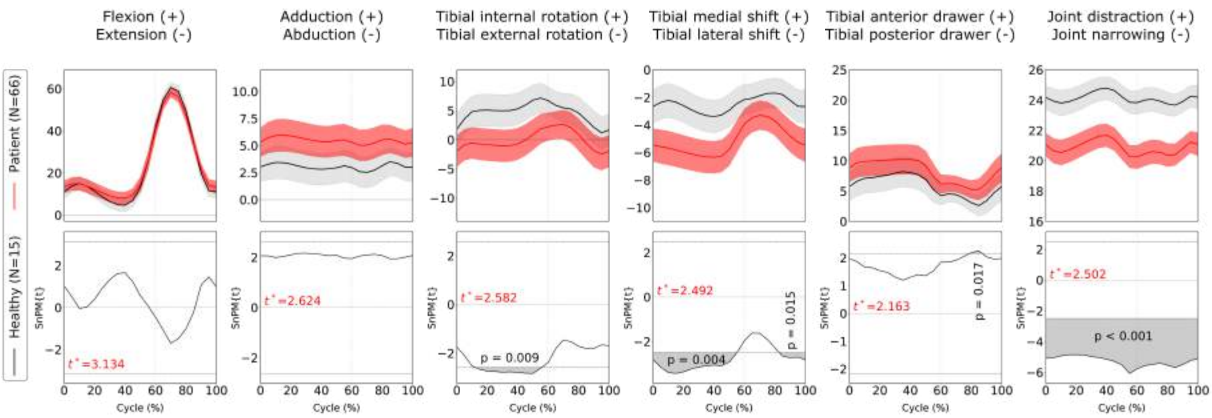

Figure 4-7 Kinematic comparison of the entire patient group with the healthy control group. The top row presents the mean trajectories of the two groups with confidence interval as the shaded area. The bottom row presents the post hoc non-parametric scalar field t tests (SnPM{t}), depicting where patients show higher (+) and lower (-) values than healthy subjects. The thin dotted lines indicate the critical thresholds for significance. The grey-shaded areas show when a critical threshold is exceeded, thus determining a significant difference.[177]

<u>G1 – *The flexion group*: </u>This was the only subgroup revealing different knee flexion when compared with the healthy group. Increased knee flexion was identified at initial contact, terminal stance and in the terminal swing phase. Additionally, throughout the entire gait cycle, this subgroup showed greater adduction and joint narrowing than the healthy group. The clinical characteristics revealed that this subgroup consisted primarily of cases with medial tibiofemoral osteoarthritis. In relation to the other subgroups, this group displayed a larger flexion angle than *the anterior group* (loading

response and initial swing phase) and *the external rotation group* (swing phase). Additionally, this subgroup displayed the largest internal rotation of any group.

G2 – *The abduction group:* This was the only subgroup revealing greater abduction than the healthy group. This was identified throughout the entire gait cycle. In addition, this subgroup showed greater joint narrowing throughout the gait cycle and anterior drawer during the loading response and terminal swing phase. The clinical characteristics revealed that it was the only subgroup that included cases with lateral tibiofemoral osteoarthritis. In relation to the other subgroups, this group displayed the largest abduction. It also revealed a larger anterior drawer than *the flexion group* (stance, initial swing and terminal swing) and *the external rotation group* (initial contact to mid-stance and terminal stance). It was only second in this respect to *the anterior drawer group*.

G3 – *The anterior drawer group:* This was the only subgroup revealing severe anterior drawer throughout the gait cycle. Furthermore, this subgroup showed the largest external tibial rotation and lateral tibial shift throughout the motion (similar to G4) and larger adduction and joint narrowing than the healthy group. The clinical characteristics revealed that this subgroup consisted primarily of cases with medial tibiofemoral osteoarthritis, with partial and total ACL lesion and the largest KOA score of any group. In relation to the other subgroups, this group displayed the largest anterior drawer and, during the swing phase, the largest joint narrowing of any group. In addition, like *the external rotation group,* it showed the largest adduction, external rotation and tibial lateral shift. For this subgroup, increased lateral tibial shift was not observed during mid swing, whereas increased external rotation was not found during mid-swing, but this only applied when compared with *the abduction group*.

G4 – *The external rotation group:* This subgroup revealed, similar to G3, more external tibial rotation and lateral tibial shift than the health group, but no anterior drawer was observed. In addition, this subgroup showed more adduction and joint narrowing throughout the gait cycle. The clinical characteristics of this subgroup included the cases with the largest proportion of MCL and PCL lesions. Like *the anterior drawer group*, this group displayed the largest adduction, external rotation and tibial lateral shift. For this subgroup, increased lateral shift was not observed during the swing phase compared with *the abduction group*, whereas increased external rotation was observed only when compared with *the abduction group*. Similar to lateral shift, no difference in external rotation was found during mid-swing between this subgroup and *the abduction group*.

All subgroups reported larger VAS pain scores during gait than the healthy group, with the exception of *the abduction group*, which was due to considerable variation in this group. However, no differences between subgroups were identified. Similarly, all subgroups had poorer clinical scores than the healthy group. Although the entire KOA patient group displayed a higher Body Mass Index than the healthy group, and *the adduction group* included younger patients than did *the flexion group*, no other differences between groups were found in terms of potentially confounding variables (age, height, weight, side and gender) (Table 4-5a).

Table 4-5 Group summary and comparison.[177]

	Healthy (n=15)	KOA patients (n=66)	G1 (n=20)	G2 (n=17)	G3 (b=10)	G4 (n=19)	P-value*	P-value**
a) Demographics with means and confidence intervals for continuous parameters and percentage for categorical parameters.								
Age	65.1 (60.1;70.1)	63.2 (61.1;65.2)	66.8 (64.2;69.4)^{G2}	57.5 (54.0;60.9)^{G1}	64.3 (56.3;72.3)	63.8 (59.8;67.9)	0.419	0.007
Side (left %)	46.7	54.6	45.0	76.5	30.0	57.9	0.581	0.131
Gender (female %)	26.7	39.4	40.0	41.2	20.0	47.4	0.348	0.536
Height	172.0 (167.3;176.7)	172.5 (170.9;174.6)	173.1 (169.3;176.9)	175.5 (172.4;178.5)	173.2 167.0;179.3)	169.3 (165.3;173.4)	0.794	0.236
Weight	78.1 (71.7;84.4)	86.5 (82.8;90.1)	87.75 (82.5;93.0)	88.3 (80.9;95.7)	81 (71.1;90.9)	86.3 (77.1;95.6)	0.044	0.211
Body Mass Index	26.2 (25.1;27.4)^{P}	29.0 (27.6;30.1)^{H}	29.3 (27.6;31.1)	28.7 (26.3;31.1)	26.8 (24.7;29.0)	30.0 (27.2;32.8)	0.001	0.075
Thigh circumference	51.5 (49.2;53.8)	52.1 (50.7;53.5)	51.9 (49.2;54.6)	53.3 (50.3;56.2)	50.2 (46.6;53.8)	52.2 (49.5;55.0)	0.711	0.700
b) Clinical characteristics with means and confidence intervals for continuous parameters and percentages for categorical parameters (except for the OA Ahlbeck score, which is presented with mean and confidence interval).								
ACL deficiency (0/1/2) %	73 / 27 / 0$^{P, C2, C3}$	30 / 38 / 32^{H}	45 / 35 / 20^{C3}	24 / 41 / 35^{H}	**0 / 30 / 70$^{H, C1}$**	37 / 42 / 21	0.004	<0.001
PCL deficiency (%)	6.7	12.1	10.0	11.8	10.0	15.8	0.544	0.943
MCL deficiency (%)	0.0	7.6	0.0	5.9	0.0	21.5	0.271	0.174†
LCL deficiency (%)	6.8	6.1	5.0	11.8	0.0	5.3	0.930	0.866†
OA Ahlbeck grade	0.7 (0.3;1.0) $^{C1, C2, C3, C4}$	2.8 (2.5;3.1)	2.7 (2.4;3.0)$^{H, C3}$	2.2 (1.8;2.7)$^{H, C3}$	**3.9 (3.4;4.4)$^{H, C1, C2}$**	2.8 (2.2;3.4)^{H}	-†	<0.001
OA medial (%)	53.3	72.7	95.0^{C2}	29.4$^{C1, C4}$	60.0	94.7^{C2}	0.142	<0.001
OA lateral (%)	0.00	9.09	0.00	**35.29**	0.00	0.00	0.225	-†
OA medial+lateral (%)	6.7	16.7	5.0	29.4	40.0	5.3	0.970	0.029
FJS	98.6 (97.1;100.1)$^{P, C1, C2, C3, C4}$	16.0 (12.3;19.7)^{H}	15.3 (9.2;21.4)^{H}	12.3 (6.7;17.8)^{H}	20.0 (3.2;36.8)^{H}	17.9 (10.6;25.2)^{H}	<0.001	<0.001
OKS	47.8 (47.6;48.0)$^{P, C1, C2, C3, C4}$	23.5 (21.9;25.0)^{H}	23.15 (20.4;25.9)^{H}	23.4 (20.3;26.4)^{H}	22.5 (15.7;29.3)^{H}	24.5 (22.0;26.9)^{H}	<0.001	<0.001
KOOS SYMPTOMS	98.6 (97.1;100.0)$^{P, C1, C2, C3, C4}$	48.9 (44.6;53.2)^{H}	49.5 (40.5;58.4)^{H}	40.5 (33.7;47.4)^{H}	52.9 (39.3;66.4)^{H}	53.8 (45.5;62.0)^{H}	<0.001	<0.001
KOOS PAIN	99.6 (99.1;100.2)$^{P, C1, C2, C3, C4}$	43.5 (39.8;47.2)^{H}	39.4 (33.0;45.8)^{H}	42.6 (37.0;48.3)^{H}	46.4 (28.7;64.0)^{H}	46.9 (40.4;53.4)^{H}	<0.001	<0.001
KOOS ADL	99.7 (99.4;100.0)$^{P, C1, C2, C3, C4}$	51.5 (48.1;55.0)^{H}	49.1 (43.3;54.9)^{H}	49.4 (43.1;55.7)^{H}	56.6 (43.1;70.1)^{H}	53.3 (46.6;60.1)^{H}	<0.001	<0.001
KOOS SPORT/REC	96.3 (92.9;99.7)$^{P, C1, C2, C3, C4}$	15.1 (11.5;18.6)^{H}	13.8 (8.4;19.1)^{H}	15.9 (7.5;24.2)^{H}	15.0 (2.0;28.0)^{H}	15.8 (8.8;22.8)^{H}	<0.001	<0.001
KOOS QOL	97.9 (95.8;100.1)$^{P, C1, C2, C3, C4}$	27.4 (24.5;30.3)^{H}	23.4 (19.0;27.9)^{H}	28.3 (22.8;33.8)^{H}	28.1 (16.9;39.3)^{H}	30.3 (24.1;36.4)^{H}	<0.001	<0.001
VAS – gait	0.0 (0.0;0.0)$^{P, C1, C3, C4}$	2.4 (1.5;2.5)^{H}	2.9 (1.7;4.1)^{H}	1.5 (0.5;2.6)	2.3 (1.1;3.5)^{H}	2.9 (1.8;4.0)^{H}	<0.001	<0.001
OPR bilateral	0.0	9.9	15.0	5.9	30.0	5.3	0.156	0.242
c) Kinematic characteristics with overall difference when compared with the healthy group. The superimposed colour-squares, which are identical to those in Figure 6, highlight trajectories with similar differences when compared with the healthy control group.								
Flexion (+) / Extension (-)			**↑ Flexion (sections)**				-	-
Adduction (+) / Abduction (-)			↑ Adduction (full)	**↑ Abduction (full)**	↑ Adduction (full)	↑ Adduction (full)	-	-
Internal rotation (+) / External rotation (-)		↑ External (section)			↑ External (full)	↑ External (full)	-	-
Medial shift (+) / Lateral shift (-)		↑ Lateral (sections)			↑ Lateral (sections)	↑ Lateral (full)	-	-
Anterior drawer (+) / Anterior drawer (-)				↑ Anterior (sections)	**↑ Anterior (full)**	**No anterior**	-	-
Joint distraction (+) / Joint narrowing (-)		↑ Narrowing (full)	↑ Narrowing (full)	↑ Narrowing (full)	↑ Narrowing (full)	↑ Narrowing (full)	-	-

The superscript: H (the healthy group), P (the KOA-patient group) C1 (*the flexion group*), C2 (*the abduction group*), C3 (*the anterior drawer group*), and C4 (*the external rotation group*) show to which groups a significant difference was identified after Bonferroni adjustment.
The bold-cell data illustrate results of high importance.
*Comparison between the healthy group and the entire KOA patient group using either a t-test or a chi-squared test.
**Comparison between the healthy group and the clusters using either one-way analysis of variance, ordinal logistic regression or logistic regression.
†Statistical difference could not be estimated for groups without events.

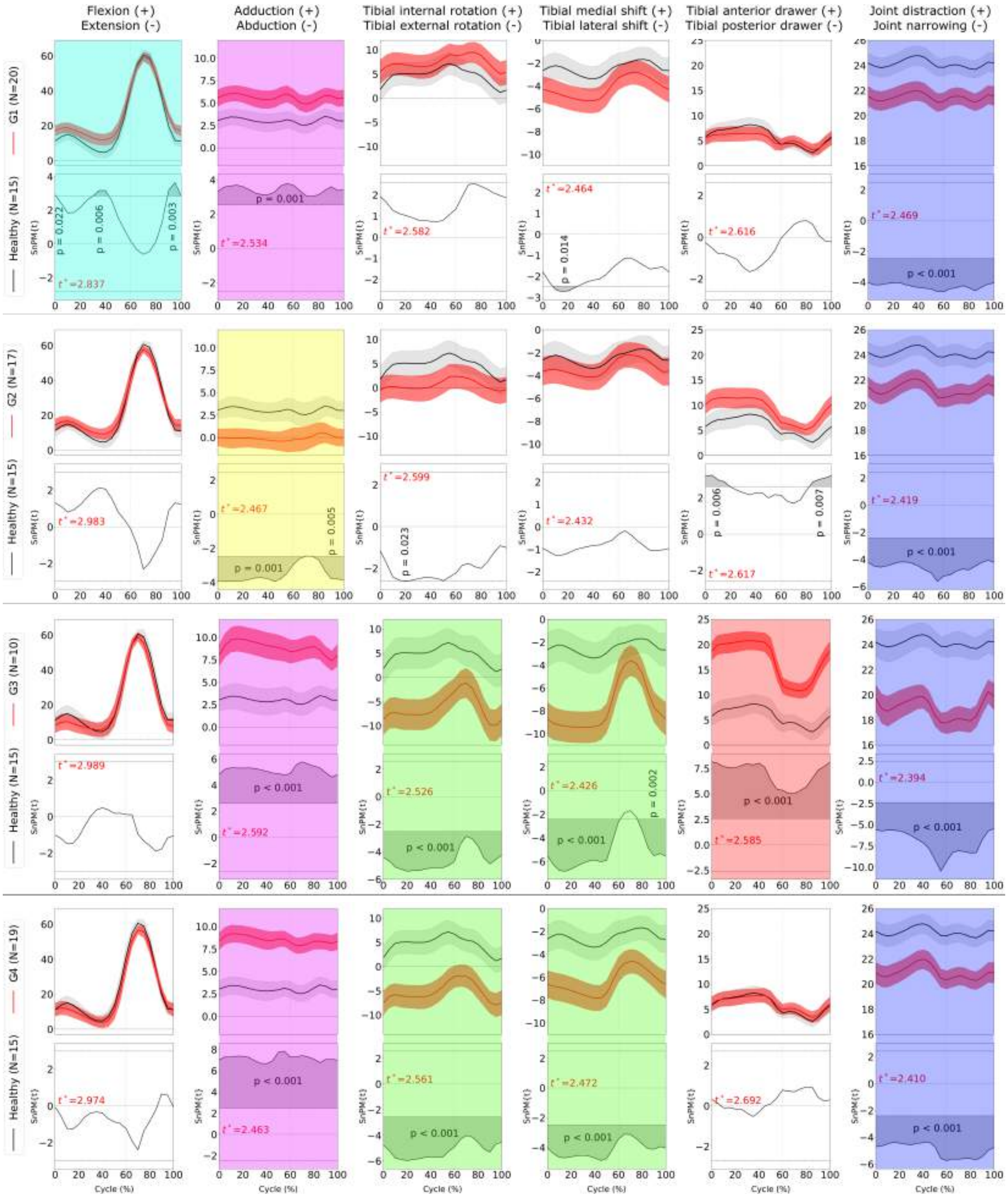

Figure 4-8 Statistical parametric mapping of all kinematic parameters (flexion/extension, adduction/abduction, internal/external tibial rotation, medial/lateral tibial shift, anterior/posterior tibial drawer and joint distraction/narrowing) for each cluster compared with the healthy control group. For each cluster comparison, the top row presents the mean trajectories of the two groups with confidence interval shown as the shaded area. The bottom row presents the post hoc non-parametric scalar field t tests (SnPM{t}), depicting where patients show more (+) and less (-) than healthy controls. The thin dotted lines indicate the critical thresholds of significance. The grey-shaded areas illustrate when the critical threshold is exceeded; thus, a significant difference is present. The superimposed colour-squares highlight trajectories with similar differences when compared with the healthy control group: cyan presents increased flexion angle trajectories; magenta presents increased adduction angle trajectories; yellow presents abduction angle trajectories; green presents increased tibial external rotation and tibial lateral shift trajectories; red presents increased tibial anterior drawer; blue presents increased joint narrowing. The significance level was set to 5%.[177]

4.4 Study IV

4.4.1 Tibiofemoral joint kinematics and articulation

The comparison of the tibiofemoral joint kinematic trajectories for the MC and CR bearings are presented in Figure 4-9. The MC bearing displayed an offset with a statistically significantly greater anterior tibial drawer during the entire motion and more tibial external rotation from the mid-swing to end of the gait cycle.

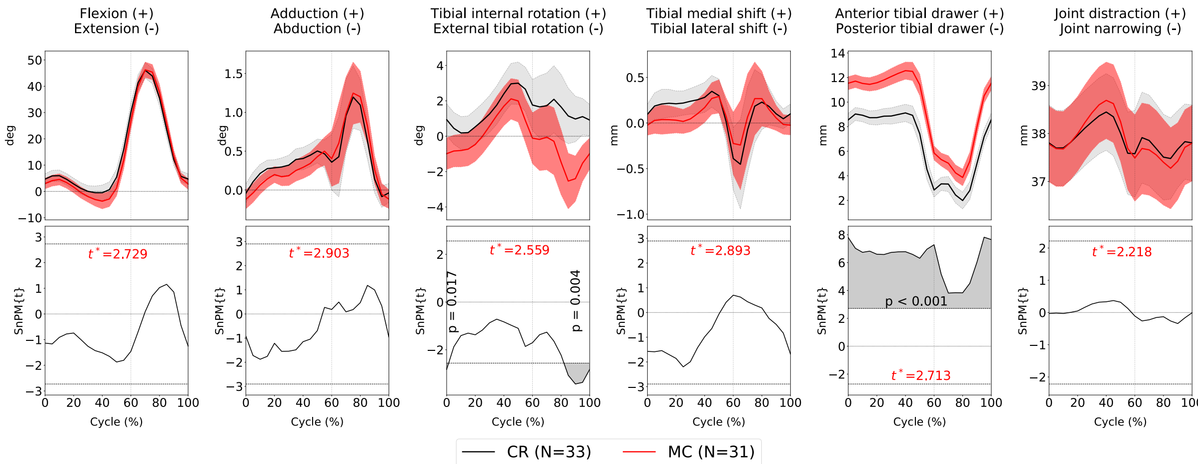

Figure 4-9 Statistical parametric mapping of tibiofemoral joint kinematics. Kinematic comparison of the MC bearing group (red) with the CR bearing group (grey). The top row presents the mean trajectories of the two groups with confidence interval as the shaded area. The bottom row presents the post hoc non-parametric scalar field t tests (SnPM{t}), depicting where the MC group shows higher (+) and lower (-) than the CR group. The thin dotted lines indicate the critical thresholds for significance. The grey-shaded areas illustrate when the critical threshold is exceeded, thus determining a significant difference.[109]

The congruency area in the joint articulation was statistically significantly greater during approximately 80% of the gait cycle for the MC than for the CR bearing. (Figure 4-10). This included most of the stance phase and the mid-swing to the end of the gait cycle. The greater congruency occurred during the same gait phases for both knee compartments; for the lateral compartment, it was mostly medially pronounced, whereas for the medial compartment, the area of congruency moved during the gait cycle. For the medial compartment, the greater area of congruency was pronounced posterolaterally at initial contact of the foot. During loading response, the greater congruency area moved so that it also included the anterolateral area of the bearing until it resolved during pre-swing, first posterolaterally and then anterolaterally. During mid-swing, the greater congruency area appeared again, this time anterolaterally and it moved posterolaterally during the terminal swing. Furthermore, the femoral low-point kinematics for the MC bearing group showed a 1.8 mm [CI 0.8;2.8] ($p<0.001$) more limited range of motion for the medial compartment when compared with the CR bearing (Table 4-6c)

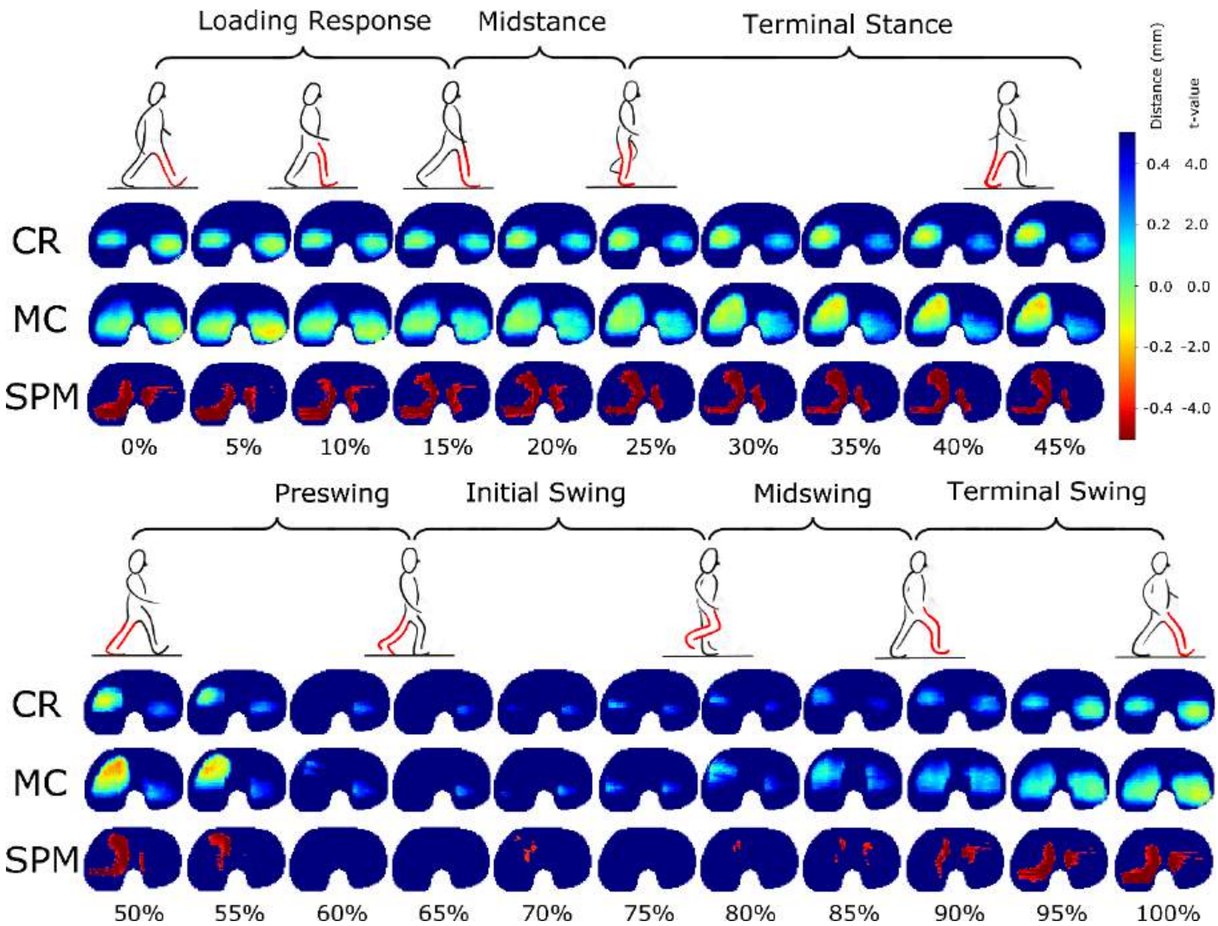

Figure 4-10 Statistical parametric mapping of tibiofemoral joint articulation. Illustration of the tibiofemoral articulation analysis of a right knee throughout the gait cycle represented by the distance point grid (70x70 pixels). The columns represent each of the 21 normalized discrete time points corresponding to the same time points used for the kinematic analysis. The rows represent from the top the Persona® Cruciate Retaining (CR) bearing, the Persona® Medial Congruent® (MC) bearing, and the results of the statistical parametric mapping (SPM) analysis. The red areas of the SPM row show where statistical significance was reached between the MC and CR grid-point maps.[109]

4.4.2 Clinical characteristics, PROMs and complications

Between groups, no differences were found in demographics, clinical characteristics, implant size or implant type ($p>0.320$). Furthermore, the three surgeons operated a similar number of patients in both groups ($p=0.367$). Both groups improved significantly regarding PROMs ($p<0.001$), VAS ($p<0.001$) and leg-extension power rig ($p<0.004$). However, no differences in improvement were found between groups ($p>0.351$). In the first year after TKA, five patients had knee manipulations under anaesthesia for joint stiffness (brisement forcé), five in the MC group and two in the CR group ($p=0.197$). Among those, an intraarticular corticosteroid injection was administered in one patient per group. Aspiration of the knee due to joint effusion was performed in three patients, one in the MC group and two in the CR group. Cultures were negative for bacterial growth, and no knee revisions or recognized deep infections were observed during the one-year follow-up period.

Table 4-6 Group summary and comparison.[109]

	CR (n=33)	MC (n=31)	P-value*
a) Demographics with means and confidence intervals for continuous parameters and percentages for categorical parameters.			
Age (years)	62.0 (59.2;65.9)	64.8 (61.8;67.9)	0.182
Side (left %)	45.5	64.5	0.126
Gender (female %)	39.4	38.7	0.955
Height (cm)	173.5 (170.5;176.6)	171.9 (169.5;174.5)	0.420
Weight (kg)	87.9 (82.7;93.2)	85.9 (80.5;91.2)	0.576
Body Mass Index (kg/m²)	29.2 (27.6;30.7)	29.0 (27.2;30.8)	0.913
Thigh circumference (cm)	52.9 (50.9;54.8)	51.4 (49.3;53.6)	0.484
b) Clinical characteristics with means and confidence intervals for continuous parameters and percentages for categorical parameters (except for the KOA Ahlbäck Score, which is presented with mean and confidence interval).			
ACL lesion (0/1/2) %	27 / 36 / 36	35 / 42 / 23	0.474
PCL lesion (%)	12.1	12.9	0.925
MCL lesion (%)	9.1	6.5	0.694
LCL lesion (%)	9.1	3.2	0.333
KOA Ahlbäck grade	3.0 (2.6;3.4)	2.6 (2.2;3.0)	0.071
KOA medial (%)	64.6	80.7	0.130
KOA lateral (%)	12.1	6.5	0.437
KOA medial+lateral (%)	21.2	12.9	0.379
FJS (preop)	16.1 (11.0;21.2)	16.5 (10.5;22.4)	0.522
OKS (preop)	24.3 (22.2;26.5)	23.1 (20.8;25.4)	0.775
KOOS SYMPTOMS (preop)	47.4 (41.5;53.4)	51.0 (44.1;57.9)	0.417
KOOS PAIN (preop)	42.5 (37.5;47.5)	45.4 (39.6;51.2)	0.438
KOOS ADL (preop)	49.7 (44.5;54.9)	53.7 (48.9;58.6)	0.250
KOOS SPORT/REC (preop)	14.8 (9.9;19.8)	16.1 (10.6;21.6)	0.726
KOOS QOL (preop)	29.0 (25.0;32.9)	26.8 (22.4;31.3)	0.459
VAS – gait (preop)	2.3 (1.6;3.1)	2.5 (1.6;3.5)	0.729
LEPR (preop) (W/kg)	1.5 (1.3;1.7)	1.5 (1.3;1.7)	0.731
FJS (follow-up)	55.4 (43.6;67.3)	58.9 (47.7;70.2)	0.668
OKS (follow-up)	39.0 (36.2;41.8)	39.0 (36.4;41.8)	0.986
KOOS SYMPTOMS (follow-up)	71.4 (64.6;78.2)	75.0 (68.6;81.4)	0.441
KOOS PAIN (follow-up)	82.9 (76.2;89.6)	82.6 (76.8;88.5)	0.946
KOOS ADL (follow-up)	83.2 (77.4;88.9)	84.8 (79.3;90.3)	0.672
KOOS SPORT/REC (follow-up)	46.5 (38.5;54.5)	49.5 (39.2;59.8)	0.638
KOOS QOL (follow-up)	64.4 (55.8;72.9)	65.3 (58.0;72.7)	0.306
VAS – gait (follow-up)	0.2 (-0.1;0.4)	0.0 (-0.0;0.1)	0.354
LEPR (follow-up) (W/kg)	1.8 (1.5;2.0)	1.8 (1.6;2.0)	0.712
c) Range of motion of the femoral low-point kinematics. Measured for both the lateral and medial compartment in both directions; x (lateral [+] and medial [-]) and y (anterior [+] and posterior [-]). The means and confidence intervals are presented for each group.			
Lateral low-point (x)	1.9 (1.7;2.1)	1.8 (1.6;2.0)	0.381
Lateral low-point (y)	4.7 (4.1;5.3)	4.0 (3.5;4.5)	0.076
Medial low-point (x)	1.4 (1.2;1.6)	1.4 (1.2;1.6)	0.883
Medial low-point (y)	6.4 (5.6;7.2)	4.6 (4.1;5.1)	**<0.001**

ACL: anterior cruciate ligament, PCL: posterior cruciate ligament, MCL: medial collateral ligament, LCL: lateral collateral ligament, KOA: knee osteoarthritis, FJS: Forgotten Joint Score, OKS: Oxford Knee Score, KOOS: Knee Osteoarthritis Outcome Score, ADL: activity of daily living, QOL: quality of life, VAS: visual analogue scale, LEPR: leg extension power rig, W/kg; watt/kilogram, MUA: manipulation under anaesthesia, preop: preoperative, follow-up: 1-year follow-up.
Demographics, clinical characteristics and preoperative PROMs have previously been published [196].

5

Discussion

The aim of this dissertation was first to evaluate the accuracy of automated dRSA image registration methods to investigate the native and artificial knee; and, second, to investigate knee pathomechanics in the osteoarthritic knees and the mechanical impact of knee arthroplasty designs during gait utilizing dRSA.

5.1 Key findings

5.1.1 Study I

This *in vitro* study investigated the accuracy of an automated CT-based volumetric 2D/3D image registration method for dRSA against a marker configuration method as gold standard. A knee flexion exercise was evaluated in a uniplanar and biplanar dRSA setup. A slight bias with a good limit of agreement was observed for the kinematic parameters with no greater bias than 0.19mm for translation and 0.11 degrees for rotation, and limits of agreement of 0.42 mm for translations and 0.33 degrees for rotation.

5.1.2 Study II

This *in vitro* study had two main findings. First, it demonstrated that an automated marker-free RSA method utilizing CT-obtained volumetric bone models provided similar accuracy as the gold standard *marker* method. Second, the study showed that an automated image registration method utilizing synthetic volumetric implant models could not take advantage of the additional information to markedly improve an automated silhouette projection method of implant surface models - at least not in its present form.

5.1.3 Study III

This clinical cohort study investigated the kinematic heterogeneity within patients with KOA. The results revealed four subgroups each with distinguished kinematic gait patterns that related well to their clinical characteristics. In addition, these subgroups revealed joint kinematics clearly different from those the healthy volunteers without KOA. These differences were not present when comparing the entire KOA cohort with the healthy group.

5.1.4 Study IV

This double-blinded clinical randomized trial demonstrated that the MC bearing, which has a medial congruent anatomical design, had tibiofemoral joint kinematics that were different from those of the standard symmetrical CR bearing. Compared with the CR bearing, the MC bearing design enhanced the area of congruency, had more tibial anterior drawer throughout the gait cycle and greater external tibial rotation during the second half of the swing phase.

5.2 The pathway of radiostereometry method validation

This section offers a chronological account of my engagement with the validation of registration methods for radiostereometry; in what context my conception was shaped – and how it influenced the study designs for validating the AutoRSA Software System; I first discuss the dynamic setup and later why it was extended by an investigation of a static setup.

5.2.1 Preconception

I was first introduced to RSA and dRSA in 2015 when I participated in a validation study of a contour-based registration of CT surface bone models using canny edge detection.[118] Similar to Study I, the objective of this study was to assess the tibiofemoral joint kinematics during a flexion movement. For this study, *markers* were used as gold standard. Thus, a relationship between the anatomical coordinate system and the markers was required. This relationship could be established based on a single stereoradiograph; however, to eliminate variance, this was determined in a least square manner using a series of stereoradiographs.[118,178] Even though the accuracies were evaluated in other stereoradiographs, the gold standard was largely dependent on the investigated method.

5.2.2 Study I - gold standard considerations

A crucial part of validation is to establish an accurate and reliable gold standard. A consequence of incorporating the investigated method into the process of establishing the gold standard method (as was done in the previously described study[118]) is that this may introduce unwanted bias. Therefore, Study I utilized a gold standard method that was more independent of the investigated method. Tantalum markers were used as gold standard, and the relationship between the markers and the anatomical coordinate system was established using CT to allow comparison with the investigated bone model. This validation method was similar to the methods used in other image registration validation studies.[120,200–202] Even so, the present validation methods differed slightly from those of the previous studies. These prior studies conducted CT of the specimens with markers and replaced the intensities of the markers with their surrounding intensities to avoid influence of the markers during the image registration.[120,200–202] The present study obtained two CTs, one with and one without the markers, in order to obtain an unedited CT of the specimens. Next, these two CTs were matched utilizing 3D-3D matching, thereby establishing a relation between the markers and the anatomical coordinate system.[182]

5.2.3 Study I - dynamic radiostereometry accuracy of the native knee

This study demonstrated a superior limit of agreement for the DRR CT-based bone volume method compared with the contour-based registration of CT (my first RSA study).[118] The contour-based method included inner contours to improve the registration. However, the present results suggest that the DRR method and utilization of the entire bone intensities provide more valuable information that may improve registration. The present results demonstrated a superior bias and limit of agreement compared with a DRR high-speed biplanar fluoroscopy study of tibiofemoral joint kinematics of running.[120] Furthermore, compared with a second DRR biplanar fluoroscopy study of patellofemoral joint kinematics, the present results demonstrated a superior bias and limit of agreement, but with a similar femoral individual bone pose and a superior individual patellar bone pose.[202] This suggests that the accuracy of image registration may be affected by object velocity, bone size and bone shape. The influence of the bone geometrical properties was confirmed in a hip study utilizing the same DRR method as the present study; the hip study demonstrated a superior limit of agreement for the pelvis compared with the proximal femoral bone.[123] One of the benefits of this method is that it can easily be applied to other joints. However, the accuracy cannot be transferred directly to other joints. Thus, the target object velocity and bone geometrical properties should be accounted for when utilizing the methods in other joints.

5.2.4 Study II – gold standard considerations

Initially, the present study intended to evaluate the automated registration of the implant in a dynamic setting identical to that of Study I. However, even though metal artifact reduction was added to the CT of the marker-inserted bones, the markers could appear slightly elliptical, and it was somewhat difficult to segment the beginning and the end of the marker when scrolling through the CT image volume. Therefore, a concern was raised: To which extent was the accuracy of the investigated model attributed to error caused by limitations of the gold standard? For validation, it is essential that the gold standard is more accurate than the investigated method. Therefore, alternative gold standard methods were considered. One study used a computer-assisted kinematics system as gold standard.[142] They used an active probe to detect the outer geometry of the actual object and determined the reference to the RSA-measured data by fitting these points to the surface model of interest. Others have estimated the accuracy by measuring no motion.[140,201–204] This is used in traditional RSA studies that measure implant migration and determine the clinical validity of the study setup and method by evaluating the difference in implant migration on two images, taken on the same day a short time period apart (double examination). The difference is often referred to as “accuracy of zero motion” or “detection limit”.[129,134,179] In addition, for identical image registration method, a previous study has demonstrated superior accuracy for sawbones compared with human *in-vitro* specimens.[205] This suggests that sawbones may simulate the conditions too ideally and, therefore, may not demonstrate a clinically relevant accuracy of the investigated method. For the present study, both the image registration methods and the *marker* method were of interest. Thus, all investigated methods were evaluated independently according to the true displacement induced by a highly accurate micrometre screw, as in a previous study.[146] The main difference between these studies was that Miranda et al. used the average of 20 stereoradiographs to estimate a baseline reference, whereas the present study used the median of five stereoradiographs. With no proportional bias, five recordings were shown to be a sufficient baseline.

5.2.5 Study II - accuracy of static radiostereometry

Application of the micrometre screws allowed for a completely independent evaluation of the various registration methods. The similar limit of agreement observed for the *marker* method as for the *autorsa-bone* method (even with bone removal) suggested that the *autorsa-bone* method has potential to replace the *marker* method that has traditionally been used as a gold standard for radiostereometry. This comparison has not previously been made. Further research is needed to confirm these results and to investigate rotations.

5.2.6 Partial bone registration in artificial joint

A few other studies have investigated semi-automated bone registration for TKA.[137,138] Their accuracies were inferior to that of the method presented here. Seehause et al. showed migration that exceeded the accuracy of the traditional *marker* method to such an extent that they precluded the feasibility of using their method in the presented form, whereas Kim et al. presented repeatability ranging up to 0.289 mm.[137,138] Both methods utilized silhouette projection and the canny edge detection method. This may have attributed to the inferior results compared with those of the DRR method which takes advantage of the intensity information within the entire bone structure.[124] Furthermore, compared with the other studies, a risk may exist that the bone silhouette projection and the postoperative articulating surface part of the actual implant may coincide and thereby inhibit the optimizer from reaching the global optima. On the contrary, to avoid that the high implant intensities inhibited the optimizer, the present DRR method excluded the implant from the registration by utilizing a mask image generated from the pre-completed implant registration.

5.2.7 Synthetically generated volumetric implant model

The enhanced information from the DRR failed to improve image registration. This suggests that, in its present form, the metric inadequately utilized the gradient information. This may be attributed to the radiopaque nature of the implants. However, visually, the stereographs of this implant displayed clear intensity differences and the correlation images showed that some of this information was included in the metric. Therefore, other metrics may potentially better promote the intrinsic implant gradients. Previous studies have suggested other similarity metrics; one combined the gradient and radiographic images, and another study suggested a cross-correlation residual entropy of intensity-based edge-enhanced images.[122,206] Continuous research is needed to investigate if other similarity metrics may utilize the intrinsic implant projection gradients better to improve automated implant registration.

5.2.8 Conclusion

The CT-based bone volume model offers an automated, fast and non-invasive method for measuring tibiofemoral joint kinematics with dRSA and a marker-free bone reference for migration calculation with RSA. Furthermore, joint kinematics was insensitive to alteration in the configuration of the radiographic setup. The automatic methods presented with these studies are clinically applicable for functional evaluation of native tibiofemoral joint kinematics and pathomechanics related to conditions such as ligament instability and bone dysplasia, as well as in the assessment of surgical results.

5.3 The heterogeneity of patients with knee osteoarthritis

5.3.1 Kinematic subgrouping

The reversed approach used in this study allowed us to divide the KOA patient cohort into subgroups without applying an observer-biased threshold of certain clinical characteristics or discrete kinematic values. The gait knee kinematics in patients with KOA observed in previous studies have shown diverse results.[53,54,57] Thus, compared with healthy controls, at the initial contact of the foot during gait, patients with KOA displayed greater[54,59], lower[53] and similar[57] flexion angles; greater[53,54,57] adduction angles; lower[53,54] and similar[57] tibial internal rotations; and similar[57] and lower[54] tibial anterior translation. In addition, a systematic review[48] of KOA has described a high heterogeneity across studies and found that the courses of pain and physical functioning were diverse. In the present study (Study III), when the entire KOA cohort was compared with a healthy cohort, the results did not confirm the previous gait studies. Instead, when the four identified subgroups and the healthy cohort were compared, differences were shown for all kinematic parameters. This suggests that the cohort of patients with KOA comprised different kinematic subgroups and that the diversity in previous studies reflected specific compositions of kinematic subgroups included but not controlled for.

5.3.2 Multifactorial subgrouping

Even though the four subgroups presented distinct gait patterns, kinematic subgrouping cannot stand alone as an explanation of the KOA patient group's heterogeneity. The quality and repeatability of the subgrouping in combination with the clinical scores indicated an overlap between these kinematic subgroups. This suggests that a different clustering algorithm may potentially provide better allocation or that other factors than gait kinematics are important to include as features to improve the allocation. The heterogeneity within the KOA patient group is well known.[207] However, the heterogeneity of KOA patients has only recently been investigated with the intent of distinguishing these patients and establishing different phenotype classifications.[49–52] These studies did not include kinematic parameters. The typical phenotyping has addressed various functional scores and clinical characteristics.[49–52] Holla et al.[49] identified three subgroups with distinct trajectories of physical functioning over time (good, moderate and poor). Knoop et al.[50] (whose findings were subsequently confirmed by Esch et al.[51]) identified five homogeneous clinical phenotypes (minimal joint disease phenotype, strong muscle strength phenotype, severe radiographic KOA phenotype, obese phenotype and depressive mood phenotype) based on k-means clustering analysis of data from the Osteoarthritis Initiative. A systematic review proposed six other phenotypes (chronic pain, inflammatory, metabolic syndrome, metabolic bone/cartilage, mechanical overload and minimal joint disease) based on studies that aimed to identify KOA phenotypes.[52] The authors defined a strong evidence for existence of a specific phenotype if the evidence was supported by at least two high-quality studies. These phenotypes may potentially explain the observed overlap of kinematic and clinical phenotyping. Thus, combining multiple characteristics including clinical, biomechanical, psychosocial and genetic factors may potentially better describe the heterogeneous pathology and multifactorial nature of patients with KOA.

5.3.3 The potential of subgrouping

Overall, TKA is a successful treatment for pain in patients with KOA. However, up to 20% of the patients are dissatisfied with the outcome of TKA, and more than 50% have residual knee symptoms.[74,77] Although considerable efforts have been devoted to increasing patient satisfaction, this has not yet been accomplished. Considering the heterogeneity within the KOA patient group and that various implant designs often do not exhibit differences in patient-reported function and satisfaction, we speculate that different patient groups may have to undergo different interventions or be more suitable for certain implant designs than others. Phenotype classification may contribute to such targeted treatment, which has previously been suggested to stimulate improved outcomes.[67] One approach to investigate this may be to evaluate the patients' postoperative outcome measures individually within phenotypically categorised subgroups. Various outcome measures may be evaluated: kinematics, function, PROMs, and - maybe best of all - patient satisfaction.

5.3.4 Conclusion on subgrouping

Patients with KOA can be divided into four subgroups with distinct gait patterns. These subgroups feature meaningful clinical characteristics of KOA-affected compartments, KOA progression and knee ligament lesions. Phenotyping of patients with KOA may benefit from a deeper understanding of their pathomechanics, which may inspire improved and more patient-specific treatment strategies in the future.

5.4 The influence of congruency on total knee arthroplasty

Because of the novelty of the MC bearing design, the number of studies on the MC bearing is limited; so far, one intraoperative study[106], one kinematic study[104], four clinical studies[105,107,208,209], one radiological and one migration study[108] have been published.

5.4.1 Congruency and kinematics

The intraoperative study[106] showed that in MC knees, the femoral position was more posterior to the tibia and had less anterior-posterior range of motion than in CR knees. Furthermore, the MC knees exhibited more tibial external rotation at full extension than CR knees.[106] Our study confirmed both of these findings, which may be the result of design differences between the bearings. The increased anterior lip height and a more posterior dwell point in MC bearings as compared to CR bearings likely caused the more posterior femoral position relative to the tibia and provided anterior-posterior stability. This construction may contribute to preventing the so-called "paradoxical motion" phenomenon, which is an abnormal kinematic motion in which the femur slides anteriorly relative to the tibia.[98] This phenomenon has been found to be more evident for cruciate-retaining designs and less so for posterior-stabilizing TKA designs. Furthermore, the paradoxical motion has been associated with mid-flexion instability, which may be a contributing factor to dissatisfaction in cruciate-retaining TKA patients.[100,101] A radiological study[102] and a simulation study[210] support this finding of more anterior-posterior stability among patients with the MC bearing. The radiological study compared the MC design with a posterior-stabilizing design and highlighted that the different designs provided similar stability in knee flexion, even though the PCL was removed in both patient groups.[102] On the other hand, the simulation study investigated the kinematic effect of sagittal and coronal congruency and demonstrated that both tibial anterior-posterior translation and tibial internal rotation depend on sagittal congruency.[210] The more externally rotated tibia during extension observed in both the intraoperative studies and the present studies may be the result of increased congruency and the articulating design *per se*. This motion may be associated with the so-called "screw-home" movement as is seen for healthy knees. Therefore, these results indicate that patients with the MC bearing reproduce the screw-home movement more effectively than patients with the CR bearing design.

The kinematic study[104] used a skin-based optical motion capture technique to compare the MC bearing design with the posterior-stabilizing design during a complete gait cycle. The authors found that the MC bearing group exhibited a greater peak internal rotation moment than in the posterior-stabilizing group. Furthermore, the patients with the MC bearing tended towards more extended knees at heel-strike and midstance with less peak knee flexion moment.[104] The present results and a different medial pivoting design confirmed this tendency of more extended knees from early to midstance.[211] Ghirardelli et al. related the tendency of greater knee flexion angles and moments in patients with a posterior-stabilizing design compared with the MC design to a "flexion contracture".[104] This contracture has previously been reported during loading response in patients following ACL reconstruction and TKA as a strategy to limit the demands placed on the quadriceps muscle.[212,213] Furthermore, Ghirardelli et al. hypothesized that this was a result of an intrinsic instability during early stance that led to recruitment of hamstring contraction as a secondary anterior-posterior stabilizer. The present results showed enhanced congruency for patients with the MC compared with the CR bearing design and, therefore, expectedly a higher intrinsic stability for the MC bearing group. In addition, patients with the MC bearing demonstrated that the enhanced area of congruency position changed during the gait cycle, which may be related to the intrinsic force distribution in the knee. Previous studies have described several occurrences of antero-posterior directed movement within the tibiofemoral joint during stance.[214–216]

Figure 5-1 Tibiofemoral load cases. Load case 1: a posterior load of the femur on the tibia corresponding to the extensor mechanism pulling at the tibia. Load case 2: an anterior load of the femur on the tibia corresponding to the braking action of the tibia. Load case 3: an anterior load of the femur on the tibia, corresponding to the increased moment from the centre of gravity's forward movement and contraction of the gastrocnemius.[109]

Three load cases have been described (Figure 5-1); at initial contact and during late midstance, a posterior load of the femur on the tibia corresponding to the extensor mechanism pulling at the tibia (case 1); during loading response, the femur applies an anterior load on the tibia corresponding to the braking action of the tibia (case 2); during terminal stance and pre-swing, an anterior load of the femur is applied on the tibia corresponding to the increased moment from the centre of gravity's forward movement and contraction of the gastrocnemius (case 3).[214–216] The position and movement of the greater area of congruency observed for the patients with the MC bearing compared with the CR bearing corresponded to the occurrence of these load cases during the gait cycle. The only time there were no correspondence with a load case and the area of congruency was during late midstance when the knee extends back. Here, load case 1 was not observed as there was no greater posterior congruency area for the MC bearing compared to the CR. One explanation may be that during single-leg support, the entire load of the body and the knee flexion angle result in complete congruency between the bearing and the femoral implant. Importantly, the greater congruency is not necessarily a result of anterior-posterior relative movement of the femur and tibia implants, but more likely the results of a greater anterior-posterior constraint. This is supported by the present results of the femoral low-point kinematics that showed a lower medial range of motion for the MC than for the CR bearing. Thus, the present study confirms the findings of the kinematic study: that the articulating design of the MC bearing may provide increased intrinsic stability of the knee and thereby potentially reduce demands on ligaments and muscles (as other knee stabilizers), which may be experienced by patients as a more natural knee function and more stability.

5.4.2 Congruency and component fixation

Along with a more congruent knee design follows a potential risk of increasing the stress in the implant-bone interface, resulting in overload and implant loosening. Therefore, investigation of the migration pattern of the TKA components in relation to the periprosthetic bone over time is crucial. In fact, when introducing new implants and designs, investigation of the migration patterns has been suggested as part of a stepwise introduction.[127,136] A randomized controlled study of migration patterns for 60 patients with the MC bearing design compared with the CR bearing design utilized RSA to investigate the migration pattern at three months, one year and two years after surgery.[108] The authors found a similar migration pattern for both the femoral and tibial component at any follow-up.[108] However, further studies confirming these promising findings and studies with a longer follow-up are required. Furthermore, dRSA studies on the Persona® knee in relation to fixations have not been conducted but may provide important information on inducible micromotion of the femoral and tibial components upon patient activity loading.[217]

5.4.3 Congruency and polyethylene wear

Polyethylene wear may be a second risk factor for a more congruent bearing design. Polyethylene measurements are time dependent. Firstly, the wear must be large enough to measure. Secondly, a "bedding in" period exists where the polyethylene creep deformation reaches a steady state. Therefore, estimating valid wear measures usually requires more than a few years of follow-up. In addition to this, cruciate-retaining TKA deigns have displayed low wear rates at midterm follow-up; and yet the osteolysis threshold for polyethylene wear of TKA is unknown.[88,218]

A wear simulation study investigated the effect of different conformities on wear while including the polyethylene deformations over time within the analysis.[210] The authors found that sagittal conformity was more sensitive than coronal conformity, and more sagittal conformity resulted in an increased wear rate, wear area and contact area. In contrast, the maximum accumulated sliding distance and linear wear showed the lowest values for the higher sagittal conformity designs after 10 million cycles.[210] Mobile-bearing TKA designs are completely non-constrained, and one of the expected benefits was lower polyethylene wear.[68,69] Long-term results show no detectable wear after 15 years.[219] These results cannot be extrapolated to the MC bearing design but show that wear is affected by conformity. Wear of the MC bearing design has yet to be investigated. In particular, comparing wear patterns in MC bearing designs with those of wear patterns in a mobile-bearing design would provide interesting information.

5.4.4 Congruency and patient-reported outcome measures

Two clinical studies from the same research group matched 50 patients with a MC bearing to either a posterior-stabilizing design or a different medial pivoting "ball-in-socket" with a single-radius femoral design (GMK).[105,208] In line with the present results, both studies reported no differences in PROMs after two years. In contrast, functionally, the MC bearing group exhibited an increased range of motion; 3 degrees compared with the posterior-stabilizing design and 7 degrees when compared with the GMK design.[105,208] A third study compared 327 patients with either an MC (n=96), a CR (n=70) or a posterior-stabilizing bearing design (n=161) at two weeks, six weeks, three months and one year follow-up.[107] The patients with the MC bearing displayed higher range of motion (4.9 degrees) at two weeks and lower VAS at all time points than the group with the posterior-stabilizing bearing design. Conversely, the MC group had higher FJS than the CR group at one-year follow-up. Furthermore, compared with patients undergoing procedures with the posterior-stabilizing TKA design, a larger share of MC knee patients reported that they were "very satisfied" and a smaller share reported that they were "not at all satisfied".[107] In summary, the literature agrees that patients with MC bearings exhibit either equal or better PROMs, equal or higher satisfaction and equal or larger range of motion than patients with CR, GMK and a posterior-stabilizing bearing designs. In contrast, the present study did not report knee flexion range of motion but demonstrated more cases of knee manipulation under anaesthesia for joint stiffness for the MC than for the CR group, although the difference between the two groups was not statistically significant, indicating for these cases an over constrained knee. It is therefore important to be aware that the mechanically more constrained features and kinematic stability of the MC bearing does not inhibit knee flexion range of motion. This difference may reflect the patient groups' preoperative conditions, their rehabilitation, surgical technique or other potential confounders. Thus, further research concerning this is warranted.

5.4.5 Conclusion

The MC bearing design changes the tibiofemoral kinematics and provides an increased area of congruency compared with the CR bearing design. This may ensure improved control of paradoxical motion, produce a more effective screw-home movement and contribute to a more stable knee motion. Collectively, this may, in turn, restore the patient's confidence in knee function during daily activities and potentially enhance patient satisfaction.

5.5 Limitations and methodological considerations

5.5.1 Generalizability and bias

One of the most important considerations following this study is generalizability.

***In-vitro* (Studies I and II)**: For both studies, the use of specimens is a limitation, and the high age of the donors may affect the bone models. In relation to bone models, the accuracy of the DRR method is primarily dependent on bone shape, size and intensity. The size does not change with age, but the risk of osteophytes increases with age due to expectancy of some KOA, and the cortical and trabecular bone volume decreases.[220] The osteophytes may provide arbitrary bone projections on the stereoradiographs that may improve registration, whereas reduction of the cortical and trabecular bone may impair the registration. Thus, the obtained accuracies likely represent the accuracies in the *in vivo* studies (Studies III and IV).

***In-vivo* (Studies III and IV)**: The results only represent the study group and cannot be extrapolated directly to patients outside the study criteria. Among patient exclusions, the most important ones are obese patients and those with gait dysfunction so severe that they were unable to participate. These patients may potentially append additional subgroups to the four subgroups presented in Study III. Additionally, the size of the cohort is relatively small in relation to the prevalence of KOA. However, the cohort size in the present studies (Studies III and IV) is relatively large or similar to the cohort sizes employed in previous studies.[53,54,57,104] However, the cohort size may potentially influence the results. For Study IV, because of the KOA patient group's heterogeneity, there is no guarantee that a different or larger cohort would have displayed similar kinematic differences between the MC and CR bearing designs. However, the randomized study design and the sample size calculation estimates reduce such a risk.

5.5.2 Clustering method

Even though four distinct gait patterns were identified within this patient cohort, the cluster quality and repeatability revealed some overlap. K-means is a simple clustering method in which only the number of groups needs to be specified. However, it does not necessarily provide identical results per run; the runs were handled by defining one *clustering process* as the best of 50 repetitions. Other clustering methods might have yielded different results. It would be expected that patients may fall in between two subgroups. Thus, the Gaussian mixture model may potentially be an alternative. This clustering method would be less restrictive in terms of the cluster shape than the k-means approach, and it incorporates the cluster covariance and provides probabilistic likelihood, making shared membership possible. Even so, Gaussian mixture model requires, like k-means, subjective selection of the number of subgroups and adds complexity as other parameters can be tweaked.

5.5.3 Gait pattern acquisition

The patients walked barefooted on a treadmill, which might not be compared directly to walking on the ground. Furthermore, it is debatable whether the sample frequency of 15 Hz is sufficiently high to obtain the entire frequency domain from gait kinematics. According to the Nyquist theorem, the sampling rate must be twice the maximum frequency of the gait to avoid insufficient sampling and aliasing.[221] Aliasing occurs when data are lost and the discrete time points cannot reproduce the original trajectory; instead, it aliases with a lower frequency and appears "slower".[221] The typical frequency of normal gait kinematics is 4-6 Hz and spectral power analysis from barefoot walking shows that 98% of the spectral power is below 10 Hz and over 90% below 5 Hz.[222] Random samples of the patients' lower limb skin-attached markers confirmed this spectral power analysis using Fast Fourier Transform.[223]

5.6 Perspectives and future research

5.6.1 Radiostereometry validation

The next step in validation is to validate the automated image registration method of implants in a dynamic setting and evaluate different metrics. Even though the marker configuration models possibly were inhibited by the metal artefacts on the marker segmentation, utilizing the same method and setup on the same specimens would provide valuable information on the accuracy of the implant registration methods. Furthermore, evaluation of the DRR method using pre- and postsurgical bone models, with and without cement, would be interesting in a clinical perspective utilizing static and dynamic recordings. Finally, a completely automated calibration and registration method with no need for manual initialization would significantly improve clinical usability.

5.6.2 Clinical investigation

In addition to the presented data in this dissertation, the patient cohort in Studies III and IV walked on a declined treadmill and stepped up and down on a force plate. Furthermore, full lower lib MRI scans were conducted of each patient with the purpose of generating subject-specific musculoskeletal models. Given the data obtained on this patient cohort, several investigations would be of great interest. First, a further investigation of the KOA cohort during other and more demanding functional tasks would be interesting: Is it possible to identify the same subgroups? If this is not the case; how and why do new subgroups deviate? Further issues worth exploring are: What are the internal forces in KOA knees, and may these forces be linked to the subgroups? Additionally, a further investigation of the TKA cohort during other and more demanding functional tasks could be conducted to answer the following question: Does the medial pivot appear more consistent during deeper knee flexion angles for the MC bearing and is the intrinsic force distribution different? Furthermore, it would be interesting to conduct a pre- and postoperative comparison at a one-year follow-up: How do the four subgroups alter their gait kinematics following TKA? Do one or more subgroups yield results that come closer to their preoperative gait pattern or closer to those of the healthy controls? Is there coherence between kinematic patterns and patients' improvement in PROMs or kinematics? How do patients who have had manipulation under anaesthesia due to knee stiffness deviate from the remaining KOA cohort? Finally, a five-year follow-up would be interesting in which it was evaluated whether the kinematic differences had evolved and if there were differences in migration and wear patterns between the MC and CR bearing design.

6

Bibliography

1. Davis MA, Ettinger WH, Neuhaus JM, Mallon KP. Knee osteoarthritis and physical functioning: Evidence from the NHANES I epidemiologic followup study. *J Rheumatol*. 1991;18(4):591-598.

2. Peat G, McCarney R, Croft P. Knee pain and osteoarthritis in older adults: a review of community burden and current use of primary health care. *Ann Rheum Dis*. 2001;60(2):91-97. doi:10.1136/ard.60.2.91

3. Gupta S, Hawker GA, Laporte A, Croxford R, Coyte PC. The economic burden of disabling hip and knee osteoarthritis (OA) from the perspective of individuals living with this condition. *Rheumatology*. 2005;44(12):1531-1537. doi:10.1093/rheumatology/kei049

4. Veronese N, Stubbs B, Solmi M, et al. Association between lower limb osteoarthritis and incidence of depressive symptoms: Data from the osteoarthritis initiative. *Age Ageing*. 2017;46(3):470-476. doi:10.1093/ageing/afw216

5. Authority Danish Health. *Knæartrose - Nationale Kliniske Retningslinjer Og Faglige Visitationsretningslinjer*.; 2012. Accessed October 4, 2021. https://www.sst.dk/~/media/CD7B016D7F9C4766A1530172473FD5F2.ashx

6. Odgaard A. Danish Knee Arthroplasty Register. Published online 2020.

7. Egloff C, Hügle T, Valderrabano V. Biomechanics and pathomechanisms of osteoarthritis. *Swiss Med Wkly*. 2012;142(JULY). doi:10.4414/smw.2012.13583

8. Turkiewicz A, Petersson IF, Björk J, et al. Current and future impact of osteoarthritis on health care: A population-based study with projections to year 2032. *Osteoarthr Cartil*. 2014;22(11):1826-1832. doi:10.1016/j.joca.2014.07.015

9. Martel-Pelletier J, Barr AJ, Cicuttini FM, et al. Osteoarthritis. *Nat Rev Dis Prim*. 2016;2. doi:10.1038/nrdp.2016.72

10. Nemes S, Rolfson O, A WD, et al. Historical view and future demand for knee arthroplasty in Sweden. *Acta Orthop*. 2015;86(4):426-431. doi:10.3109/17453674.2015.1034608

11. Hawker G, Wright J, Coyte P, et al. Health-related quality of life after knee replacement. *J Bone Jt Surg (American Vol*. 1998;80(2):163-173. http://www.ncbi.nlm.nih.gov/entrez/query.fcgi?cmd=Retrieve&db=PubMed&dopt=Citation&list_uids=9486722

12. Heidari B. Knee osteoarthritis prevalence, risk factors, pathogenesis and features: Part 1. *Casp J Intern Med*. 2011;2(2):205-212.

13. Blagojevic M, Jinks C, Jeffery A, Jordan KP. Risk factors for onset of osteoarthritis of the knee in older adults: a systematic review and meta-analysis. *Osteoarthr Cartil*. 2010;18(1):24-33. doi:10.1016/j.joca.2009.08.010

14. Zhang Y, Jordan JM. Epidemiology of Osteoarthritis. *Clin Geriatr Med*. 2010;26(3):355-369. doi:10.1016/j.cger.2010.03.001

15. Phinyomark A, Osis ST, Hettinga BA, Kobsar D, Ferber R. Gender differences in gait kinematics for patients with knee osteoarthritis. *BMC Musculoskelet Disord*. 2016;17(1):157. doi:10.1186/s12891-016-1013-z

16. Øiestad BE, Juhl CB, Eitzen I, Thorlund JB. Knee extensor muscle weakness is a risk factor for development of knee osteoarthritis. A systematic review and meta-analysis. *Osteoarthr Cartil*. 2015;23(2):171-177. doi:10.1016/j.joca.2014.10.008

17. Zhai G, Stankovich J, Ding C, Scott F, Cicuttini F, Jones G. The Genetic Contribution to Muscle Strength, Knee Pain, Cartilage Volume, Bone Size, and Radiographic Osteoarthritis: A Sibpair Study. *Arthritis Rheum*. 2004;50(3):805-810. doi:10.1002/art.20108

18. Rodriguez-Fontenla C, Calaza M, Evangelou E, et al. Assessment of osteoarthritis candidate genes in a meta-analysis of nine genome-wide association studies. *Arthritis Rheumatol*. 2014;66(4):940-949. doi:10.1002/art.38300

19. Valdes AM, Spector TD. Genetic epidemiology of hip and knee osteoarthritis. *Nat Rev Rheumatol*. 2011;7(1):23-32. doi:10.1038/nrrheum.2010.191

20. Meng W, Adams MJ, Palmer CNA, et al. Genome-wide association study of knee pain identifies associations with GDF5 and COL27A1 in UK Biobank. *Commun Biol*. 2019;2(1). doi:10.1038/s42003-019-0568-2

21. He Y, Li Z, Alexander PG, et al. Pathogenesis of osteoarthritis: Risk factors, regulatory pathways in chondrocytes, and experimental models. *Biology (Basel)*. 2020;9(8):1-32. doi:10.3390/biology9080194

22. Muthuri SG, McWilliams DF, Doherty M, Zhang W. History of knee injuries and knee osteoarthritis: A meta-analysis of observational studies. *Osteoarthr Cartil*. 2011;19(11):1286-1293. doi:10.1016/j.joca.2011.07.015

23. Thomas AC, Hubbard-Turner T, Wikstrom EA, Palmieri-Smith RM. Epidemiology of posttraumatic osteoarthritis. *J Athl Train*. 2017;52(6):491-496. doi:10.4085/1062-6050-51.5.08

24. Brown TD, Johnston RC, Saltzman CL, Marsh JL, Buckwalter JA. Posttraumatic osteoarthritis: A first estimate of incidence, prevalence, and burden of disease. *J Orthop Trauma*. 2006;20(10). doi:10.1097/01.bot.0000246468.80635.ef

25. Teichtahl AJ, Wluka AE, Wang Y, et al. Effect of long-term vigorous physical activity on healthy adult knee cartilage. *Med Sci Sports Exerc*. 2012;44(6):985-992. doi:10.1249/MSS.0b013e318245c849

26. Teichtahl AJ, Wang Y, Heritier S, et al. The interaction between physical activity and amount of baseline knee cartilage. *Rheumatol (United Kingdom)*. 2016;55(7):1277-1284. doi:10.1093/rheumatology/kew045

27. Doré DA, Winzenberg TM, Ding C, et al. The association between objectively measured physical activity and knee structural change using MRI. *Ann Rheum Dis*. 2013;72(7):1170-1175. doi:10.1136/annrheumdis-2012-201691

28. Bjordal JM, Arnøy F, Hannestad B, Strand T. Epidemiology of anterior cruciate ligament injuries in soccer. *Am J Sports Med*. 1997;25(3):341-345. doi:10.1177/036354659702500312

29. Madaleno FO, Santos BA, Araújo VL, Oliveira VC, Resende RA. Prevalence of knee osteoarthritis in former athletes: a systematic review with meta-analysis. *Brazilian J Phys Ther*. 2018;22(6):437-451. doi:10.1016/j.bjpt.2018.03.012

30. Thomas AC, Hubbard-Turner T, Wikstrom EA, Palmieri-Smith RM. Epidemiology of posttraumatic osteoarthritis. *J Athl Train*. 2017;52(6):491-496. doi:10.4085/1062-6050-51.5.08

31. Palmer KT. Occupational activities and osteoarthritis of the knee. *Br Med Bull*. 2012;102(1):147-170. doi:10.1093/bmb/lds012

32. Rytter S, Egund N, Jensen LK, Bonde JP. Occupational kneeling and radiographic tibiofemoral and patellofemoral osteoarthritis. *J Occup Med Toxicol*. 2009;4(1). doi:10.1186/1745-6673-4-19

33. Yoshimura N, Nishioka S, Kinoshita H, et al. Risk Factors for Knee Osteoarthritis in Japanese Women: Heavy Weight, Previous Joint Injuries, and Occupational Activities. *J Rheumatol*. 2004;31(1):157-162. http://ovidsp.ovid.com/ovidweb.cgi?T=JS&PAGE=reference&D=emed6&NEWS=N&AN=2004024791

34. Yoshimura N, Kinoshita H, Hori N, et al. Risk factors for knee osteoarthritis in Japanese men: A case-control study. *Mod Rheumatol*. 2006;16(1):24-29. doi:10.1007/s10165-005-0450-6

35. Ding C, Stannus O, Cicuttini F, Antony B, Jones G. Body fat is associated with increased and lean mass with decreased knee cartilage loss in older adults: A prospective cohort study. *Int J Obes*. 2013;37(6):822-827. doi:10.1038/ijo.2012.136

36. Kääb MJ, Ito K, Rahn B, Clark JM, Nötzli HP. *Effect of Mechanical Load on Articular Cartilage Collagen Structure: A Scanning Electron-Microscopic Study SEM Scanning Electron Microscopy*. Vol 167.; 2000. http://www.charite.de/unfallchirurgieABCFax+41613061234E-Mailkarger@karger.chwww.karger.comwww.karger.com/journals/cto

37. Eyre DR. Collagens and cartilage matrix homeostasis. In: *Clinical Orthopaedics and Related Research*. Lippincott Williams and Wilkins; 2004. doi:10.1097/01.blo.0000144855.48640.b9

38. Kumm J, Tamm A, Lintrop M, Tamm A. Diagnostic and prognostic value of bone biomarkers in progressive knee osteoarthritis: A 6-year follow-up study in middle-aged subjects. *Osteoarthr Cartil*. 2013;21(6):815-822. doi:10.1016/j.joca.2013.03.008

39. Sellam J, Berenbaum F. The role of synovitis in pathophysiology and clinical symptoms of osteoarthritis. *Nat Rev Rheumatol*. 2010;6(11):625-635. doi:10.1038/nrrheum.2010.159

40. Spring Loader. Accessed October 21, 2021. https://springloadedtechnology.com/guide-to-severe-knee-osteoarthritis/

41. Bekkers JEJ, Creemers LB, Dhert WJA, Saris DBF. Diagnostic Modalities for Diseased Articular Cartilage—From Defect to Degeneration: A Review. *Cartilage*. 2010;1(3):157. doi:10.1177/1947603510364539

42. Kellgren JH, Lawrence JS. Radiological Assessment of Osteo-Arthrosis. *Ann Rheum Dis*. 1957;16(4):494-502. doi:10.1136/ard.16.4.494

43. Ahlbäck S. Osteoarthrosis of the knee. A radiographic investigation. *Acta Radiol Diagn (Stockh)*. Published online 1968:Suppl 277:7—72. http://europepmc.org/abstract/MED/5706059

44. Zambianchi F, Daffara V, Negri A, Franceschi G, Schiavon G, Catani F. Preoperative Osteoarthritic Grade Affects Forgotten Joint Status and Patient Acceptable Symptom State After Robotic Arm-Assisted Unicompartmental Knee Arthroplasty. *J Arthroplasty*. 2021;36(11):3650-3655. doi:10.1016/j.arth.2021.06.028

45. RW W. Osteoarthritis Classification Scales: Interobserver Reliability and Arthroscopic Correlation. *J Bone Joint Surg Am*. 2014;96(14):1145-1151. doi:10.2106/JBJS.M.00929

46. Keyes GW, Carr AJ, Miller RK, Goodfellow JW. The radiographic classification of medial gonarthrosis: Correlation with operation methods in 200 knees. *Acta Orthop*. 1992;63(5):497-501. doi:10.3109/17453679209154722

47. Petersson IF, Boegård T, Saxne T, Silman AJ, Svensson B. Radiographic osteoarthritis of the knee classified by the Ahlbäck and Kellgren & Lawrence systems for the tibiofemoral joint in people aged 35-54 years with chronic knee pain. *Ann Rheum Dis*. 1997;56:493-496.

48. De Rooij M, Van Der Leeden M, Heymans MW, et al. Prognosis of Pain and Physical Functioning in Patients with Knee Osteoarthritis: A Systematic Review and Meta-Analysis. *Arthritis Care Res*. 2016;68(4):481-492. doi:10.1002/acr.22693

49. Holla JFM, Van Der Leeden M, Heymans MW, et al. Three trajectories of activity limitations in early symptomatic knee osteoarthritis: A 5-year follow-up study. *Ann Rheum Dis*. 2014;73(7):1369-1375. doi:10.1136/annrheumdis-2012-202984

50. Knoop J, Van Der Leeden M, Thorstensson CA, et al. Identification of phenotypes with different clinical outcomes in knee osteoarthritis: Data from the osteoarthritis initiative. *Arthritis Care Res*. 2011;63(11):1535-1542. doi:10.1002/acr.20571

51. Van der Esch M, Knoop J, van der Leeden M, et al. Clinical phenotypes in patients with knee osteoarthritis: A study in the Amsterdam osteoarthritis cohort. *Osteoarthr Cartil*. 2015;23(4):544-549. doi:10.1016/j.joca.2015.01.006

52. Dell'Isola A, Allan R, Smith SL, Marreiros SSP, Steultjens M. Identification of clinical phenotypes in knee osteoarthritis: a systematic review of the literature. *BMC Musculoskelet Disord*. 2016;17(1):1-12. doi:10.1186/s12891-016-1286-2

53. Nagano Y, Naito K, Saho Y, et al. Association between in vivo knee kinematics during gait and the severity of knee osteoarthritis. *Knee*. 2012;19(5):628-632. doi:10.1016/j.knee.2011.11.002

54. Zeng X, Ma L, Lin Z, et al. Relationship between Kellgren-Lawrence score and 3D kinematic gait analysis of patients with medial knee osteoarthritis using a new gait system. *Sci Rep*. 2017;7(1):1-8. doi:10.1038/s41598-017-04390-5

55. Zeni JA, Higginson JS. Differences in gait parameters between healthy subjects and persons with moderate and severe knee osteoarthritis: A result of altered walking speed? *Clin Biomech*. 2009;24(4):372-378. doi:10.1016/j.clinbiomech.2009.02.001

56. Farrokhi S, Tashman S, Gil AB, Klatt BA, Fitzgerald GK. Are the kinematics of the knee joint altered during the loading response phase of gait in individuals with concurrent knee osteoarthritis and complaints of joint instability? A dynamic stereo X-ray study. *Clin Biomech*. 2012;27(4):384-389. doi:10.1016/j.clinbiomech.2011.10.009

57. Bytyqi D, Shabani B, Lustig S, Cheze L, Karahoda Gjurgjeala N, Neyret P. Gait knee kinematic alterations in medial osteoarthritis: Three dimensional assessment. *Int Orthop*. 2014;38(6):1191-1198. doi:10.1007/s00264-014-2312-3

58. Na A, Piva SR, Buchanan TS. Influences of knee osteoarthritis and walking difficulty on knee kinematics and kinetics. *Gait Posture*. 2018;61:439-444. doi:10.1016/j.gaitpost.2018.01.025

59. Favre J, Jolles BM. Gait analysis of patients with knee osteoarthritis highlights a pathological mechanical pathway and provides a basis for therapeutic interventions. *EFORT Open Rev*. 2016;1(10):368-374. doi:10.1302/2058-5241.1.000051

60. Jain AK, Murty MN, Flynn PJ. Data Clustering: A Review. *ACM Comput Surv*. 2000;31(3):1999.

61. Pedregosa F, Varoquaux G, Gramfort A, et al. *Scikit-Learn: Machine Learning in Python*. Vol 12.; 2011. http://scikit-learn.sourceforge.net.

62. Kuntze G, Nettel-Aguirre A, Ursulak G, et al. Multi-joint gait clustering for children and youth with diplegic cerebral palsy. *PLoS One*. 2018;13(10). doi:10.1371/journal.pone.0205174

63. Springer BD. Management of the Bariatric Patient. What Are the Implications of Obesity and Total Joint Arthroplasty: The Orthopedic Surgeon’s Perspective? *J Arthroplasty*. 2019;34:s30-s32. doi:10.1016/j.arth.2018. 12.021

64. Elsiwy Y, Jovanovic I, Doma K, Hazratwala K, Letson H. Risk factors associated with cardiac complication after total joint arthroplasty of the hip and knee: A systematic review. *J Orthop Surg Res*. 2019;14(1). doi:10.1186/s13018-018-1058-9

65. Lundgren-Nilsson Å, Dencker A, Palstam A, et al. Patient-reported outcome measures in osteoarthritis: A systematic search and review of their use and psychometric properties. *RMD Open*. 2018;4(2). doi:10.1136/rmdopen-2018-000715

66. Bruyère O, Cooper C, Pelletier JP, et al. An algorithm recommendation for the management of knee osteoarthritis in Europe and internationally: A report from a task force of the European Society for Clinical and Economic Aspects of Osteoporosis and Osteoarthritis (ESCEO). *Semin Arthritis Rheum*. 2014;44(3):253-263. doi:10.1016/j.semarthrit.2014.05.014

67. Bijlsma JWJ, Berenbaum F, Lafeber FPJG. Arthritis 1 Osteoarthritis: an update with relevance for clinical practice. *Lancet*. 2011;377:2115-2141.

68. Causero A, Di Benedetto P, Beltrame A, Gisonni R, Cainero V, Pagano M. Design evolution in total knee replacement: which is the future? *Acta Biomed*. 2014;85(2):5-19.

69. Comitini S. Evolution in Knee Replacement Implant. *Single Cell Biol*. 2015;04(02). doi:10.4172/2168-9431.1000109

70. Edmonton Journal.

71. Inacio MCS, Paxton EW, Graves SE, Namba RS, Nemes S. Projected increase in total knee arthroplasty in the United States – an alternative projection model. *Osteoarthr Cartil*. 2017;25(11):1797-1803. doi:10.1016/j.joca.2017.07.022

72. Le DH, Goodman SB, Maloney WJ, Huddleston JI. Current modes of failure in TKA: Infection, instability, and stiffness predominate. *Clin Orthop Relat Res*. 2014;472(7):2197-2200. doi:10.1007/s11999-014-3540-y

73. Odgaard A, Hospital G. *Dansk Knæalloplastikregister, Årsrapport 2016*.; 2016. https://www.sundhed.dk/content/cms/99/4699_dkr-rapport-2016.pdf

74. Bourne RB, Chesworth BM, Davis AM, Mahomed NN, Charron KDJJ. Patient satisfaction after total knee arthroplasty: Who is satisfied and who is not? *Clin Orthop Relat Res*. 2010;468(1):57-63. doi:10.1007/s11999-009-1119-9

75. Baker PN, Van Der Meulen JH, Lewsey J, Gregg PJ. The role of pain and function in determining patient satisfaction after total knee replacement - data from the national joint registry for England and Wales. *J Bone Jt Surg [Br]*. 2007;8989(7):893-900. doi:10.1302/0301-620X.89B7

76. Bayliss LE, Culliford D, Monk AP, et al. The effect of patient age at intervention on risk of implant revision after total replacement of the hip or knee: a population-based cohort study. *Lancet*. 2017;389(10077):1424-1430. doi:10.1016/S0140-6736(17)30059-4

77. Nam D, Nunley RM, Barrack RL. Patient dissatisfaction following total knee replacement: A growing concern? *Bone Jt J*. 2014;96B(11):96-100. doi:10.1302/0301-620X.96B11.34152

78. Nunley RM, Nam D, Berend KR, et al. New Total Knee Arthroplasty Designs: Do Young Patients Notice? *Clin Orthop Relat Res*. 2015;473(1):101-108. doi:10.1007/s11999-014-3713-8

79. Dennis DA, Komistek RD, Mahfouz MR, Haas BD, Stiehl JB. Conventry Award Paper: Multicenter Determination of In Vivo Kinematics After Total Knee Arthroplasty. *Clin Orthop Relat Res*. 2003;416(416):37-57. doi:10.1097/01.blo.0000092986.12414.b5

80. Dennis DA, Komistek RD, Mahfouz MR. In Vivo Fluoroscopic Analysis Of Fixed-Bearing Total Knee Replacements. *Clin Orthop Relat Res*. 2003;410(410):114-130. doi:10.1097/01.blo.0000062385.79828.72

81. Banks SA, Harman MK, Bellemans J, Hodge WA. Making sense of knee arthroplasty kinematics: news you can use. *J Bone Joint Surg Am*. 2003;85-A Suppl(suppl 4):64-72. http://jbjs.org/content/85/suppl_4/64.abstract

82. Trecci A. Bicruciate retaining. *Ann Transl Med*. 2016;4(7):128-128. doi:10.21037/atm.2016.01.27

83. Baumann F. Bicruciate-retaining total knee arthroplasty compared to cruciate-sacrificing TKA: what are the advantages and disadvantages? *Expert Rev Med Devices*. 2018;15(9):615-617. doi:10.1080/17434440.2018.1514256

84. Victor J, Banks S, Bellemans J. Kinematics of posterior cruciate ligament-retaining and -substituting total knee arthroplasty: a prospective randomised outcome study. *J Bone Joint Surg Br*. 2005;87(5):646-655. doi:10.1302/0301-620X.87B5.15602

85. Zingde SM, Leszko F, Sharma A, Mahfouz MR, Komistek RD, Dennis DA. In vivo determination of cam-post engagement in fixed and mobile-bearing TKA knee. *Clin Orthop Relat Res*. 2014;472(1):254-262. doi:10.1007/S11999-013-3257-3

86. Banks SA, Meneghini RM. Achieving More Natural Motion, Stability, and Function With a Dual-Pivot ACL-substituting Total Knee Arthroplasty Design. *Tech Orthop*. 2018;33(1). www.techortho.com

87. Makhdom AM, Parvizi J. Modular versus nonmodular tibial inserts in total knee arthroplasty: What are the differences? *Ann Transl Med*. 2017;5(10). doi:10.21037/atm.2017.02.25

88. Torle J, Thillemann JK, Petersen ET, Madsen F, Søballe K, Stilling M. Less polyethylene wear in monobloc compared to modular ultra-high-molecular-weight-polyethylene inlays in hybrid total knee arthroplasty: A 5-year randomized radiostereometry study. *Knee*. 2021;29:486-499. doi:10.1016/j.knee.2021.02.033

89. Huang C-H, Liau J-J, Cheng C-K. Fixed or mobile-bearing total knee arthroplasty. *J Orthop Surg Res*. 2007;2:1. doi:10.1186/1749-799X-2-1

90. Fransen BL, van Duijvenbode DC, Hoozemans MJM, Burger BJ. No differences between fixed- and mobile-bearing total knee arthroplasty. *Knee Surgery, Sport Traumatol Arthrosc*. 2017;25(6):1757-1777. doi:10.1007/s00167-016-4195-x

91. Amaro JT, Novaretti JV, Astur DC, et al. Higher Axial Tibiofemoral Rotation and Functional Outcomes with Mobile-Bearing Compared with Fixed-Bearing Total Knee Arthroplasty at 1-but Not at 2-Year Follow-Up-A Randomized Clinical Trial. *J Knee Surg*. 2020;33(5):474-480. doi:10.1055/s-0039-1678675

92. Park CH, Kang SG, Bae DK, Song SJ. Mid-term clinical and radiological results do not differ between fixed- and mobile-bearing total knee arthroplasty using titanium-nitride-coated posterior-stabilized prostheses: a prospective randomized controlled trial. *Knee Surgery, Sport Traumatol Arthrosc*. 2019;27(4):1165-1173. doi:10.1007/s00167-018-5095-z

93. Banks SA, Deckard E, Hodge WA, Meneghini RM. Rationale and Results for Fixed-Bearing Pivoting Designs in Total Knee Arthroplasty. *J Knee Surg*. 2019;32(7):590-595. doi:10.1055/s-0039-1679924

94. Dennis DA, Komistek RD, Mahfouz MR, Haas BD, Stiehl JB. Multicenter Determination of in Vivo Kinematics after Total Knee Arthroplasty. In: *Clinical Orthopaedics and Related Research*. Lippincott Williams and Wilkins; 2003:37-57. doi:10.1097/01.blo.0000092986.12414.b5

95. Mikashima Y, Tomatsu T, Horikoshi M, et al. In vivo deep-flexion kinematics in patients with posterior-cruciate retaining and anterior-cruciate substituting total knee arthroplasty. *Clin Biomech*. 2010;25(1):83-87. doi:10.1016/j.clinbiomech.2009.09.009

96. Digennaro V, Zambianchi F, Marcovigi A, Mugnai R, Fiacchi F, Catani F. Design and kinematics in total knee arthroplasty. *Int Orthop*. 2014;38(2):227-233. doi:10.1007/s00264-013-2245-2

97. Roberti di Sarsina T, Alesi D, Di Paolo S, et al. In vivo kinematic comparison between an ultra-congruent and a posterior-stabilized total knee arthroplasty design by RSA. *Knee Surgery, Sport Traumatol Arthrosc*. Published online 2021. doi:10.1007/s00167-021-06629-1

98. Dennis DA, Komistek RD, Colwell CE, et al. *In Vivo Anteroposterior Femorotibial Translation of Total Knee Arthroplasty: A Multicenter Analysis*. Vol 356. Lippincott Williams & Wilkins; 1998. http://journals.lww.com/clinorthop

99. Indelli PF. Is Normal Knee Biomechanics Reproduced by Modern Total Knee Arthroplasty Designs? The Role of Fluoroscopy. *Osteol Rheumatol Open J*. 2016;1(1):6-9. doi:10.17140/ORHOJ-1-103

100. Martin JW, Whiteside LA. *The Influence of Joint Line Position on Knee Stability After Condylar Knee Arthroplasty*. http://journals.lww.com/clinorthop

101. Hasegawa M, Naito Y, Yamaguchi T, Wakabayashi H, Sudo A. Factors Contributing to Patient Satisfaction and Expectations following Computer-Assisted Total Knee Arthroplasty. *J Knee Surg*. 2018;31(5):448-452. doi:10.1055/S-0037-1604144

102. Stramazzo L, Bassi N, Ghirardelli S, Amoroso T, Osti L, Indelli PF. Posterior stability in posterior-stabilized vs medially congruent total knee replacement: A radiological comparison of two polyethylene designs in a single model. *J Orthop Trauma Rehabil*. Published online December 11, 2020:221049172097898. doi:10.1177/2210491720978988

103. Dolan MM, Kelly NH, Nguyen JT, Wright TM, Haas SB. Implant design influences tibial post wear damage in posterior-stabilized knees. In: *Clinical Orthopaedics and Related Research*. Vol 469. Springer New York LLC; 2011:160-167. doi:10.1007/s11999-010-1515-1

104. Ghirardelli S, Asay JL, Leonardi EA, Amoroso T, Indelli PF, Andriacchi TP. Kinematic comparison between medially congruent and posterior-stabilized third-generation tka designs. *J Funct Morphol Kinesiol*. 2021;6(1). doi:10.3390/jfmk6010027

105. Indelli PF, Morello F, Ghirardelli S, Fidanza A, Iannotti F, Ferrini A. No clinical differences at the 2-year follow-up between single radius and J-curve medial pivot total knee arthroplasty in the treatment of neutral or varus knees. *Knee Surgery, Sport Traumatol Arthrosc*. 2020;28(12):3949-3954. doi:10.1007/s00167-020-05854-4

106. Tsubosaka M, Ishida K, Kodato K, et al. Mid-flexion stability in the anteroposterior plane is achieved with a medial congruent insert in cruciate-retaining total knee arthroplasty for varus osteoarthritis. *Knee Surgery, Sport Traumatol Arthrosc*. 2021;29(2):467-473. doi:10.1007/s00167-020-05927-4

107. Frye BM, Patton C, Kinney JA, Murphy TR, Klein AE, Dietz MJ. A Medial Congruent Polyethylene Offers Satisfactory Early Outcomes and Patient Satisfaction in Total Knee Arthroplasty. *Arthroplast Today*. 2021;7:243-249.e0. doi:10.1016/j.artd.2020.11.003

108. Christensson A, Tveit M, Kesteris U, Flivik G. Similar migration for medial congruent and cruciate-retaining tibial components in an anatomic TKA system: a randomized controlled trial of 60 patients followed with RSA for 2 years. *Acta Orthop*. Published online 2021. doi:10.1080/17453674.2021.1983709

109. Petersen ET, Rytter S, Koppens D, et al. In vivo kinematic comparison of Medial Congruent and Cruciate Retaining polyethylene designs in total knee arthroplasty - A randomized controlled study of gait using dynamic radiostereometry. *Manuscr Submitt Publ*. Published online 2021.

110. Saunders JBIM, Inman VT, Eberhart HD, Francisco S. The major determinants in normal and pathological gait. *J Bone Jt Surg*. 1953;35-A(3):543-558. http://journals.lww.com/jbjsjournal

111. Cuccurullo SJ. *Physical Medicine and Rehabilitation Board Review*.; 2004.

112. Klöpfer-Krämer I, Brand A, Wackerle H, Müßig J, Kröger I, Augat P. Gait analysis – Available platforms for outcome assessment. *Injury*. 2020;51:S90-S96. doi:10.1016/J.INJURY.2019.11.011

113. Schmitt S, Günther M. Human leg impact: energy dissipation of wobbling masses. *Arch Appl Mech 2010 817*. 2010;81(7):887-897. doi:10.1007/S00419-010-0458-Z

114. Benoit DL, Ramsey DK, Lamontagne M, Xu L, Wretenberg P, Renström P. Effect of skin movement artifact on knee kinematics during gait and cutting motions measured in vivo. *Gait Posture*. 2006;24(2):152-164. doi:10.1016/j.gaitpost.2005.04.012

115. Della Croce U, Cappozzo A, Kerrigan DC. Pelvis and lower limb anatomical landmark calibration precision and its propagation to bone geometry and joint angles. *Med Biol Eng Comput*. 1999;37(2):155-161. doi:10.1007/BF02513282

116. Kaptein BL, Valstar ER, Stoel BC, Rozing PM, Reiber JHC. A new model-based RSA method validated using CAD models and models from reversed engineering. *J Biomech*. 2003;36(6):873-882. doi:10.1016/S0021-9290(03)00002-2

117. Kaptein BL, Valstar ER, Stoel BC, Rozing PM, Reiber JHC. Evaluation of three pose estimation algorithms for model-based roentgen stereophotogrammetric analysis. *Proc Inst Mech Eng H*. 2004;218(4):231-238. doi:10.1243/0954411041561036

118. Stentz-Olesen K, Nielsen ET, De Raedt S, et al. Validation of static and dynamic radiostereometric analysis of the knee joint using bone models from CT data. *Bone Jt Res*. 2017;6(6):376-384. doi:10.1302/2046-3758.66.BJR-2016-0113.R3

119. You BM, Siy P, Anderst W, Tashman S. In vivo measurement of 3-D skeletal kinematics from sequences of biplane radiographs: Application to knee kinematics. *IEEE Trans Med Imaging*. 2001;20(6):514-525. doi:10.1109/42.929617

120. Anderst W, Zauel R, Bishop J, Demps E, Tashman S. Validation of three-dimensional model-based tibio-femoral tracking during running. *Med Eng Phys*. 2009;31(1):10-16. doi:10.1016/j.medengphy.2008.03.003

121. Komistek RD, Dennis DA, Mahfouz M. In vivo fluoroscopic analysis of the normal human knee. In: *Clinical Orthopaedics and Related Research*. Lippincott Williams and Wilkins; 2003:69-81. doi:10.1097/01.blo.0000062384.79828.3b

122. Mahfouz MR, Hoff WA, Komistek RD, Dennis DA. A Robust Method for Registration of Three-Dimensional Knee Implant Models to Two-Dimensional Fluoroscopy Images. *IEEE Trans Med Imaging*. 2003;22(12):1561-1574. doi:10.1109/TMI.2003.820027

123. Hansen L, De Raedt S, Jørgensen PB, Mygind-Klavsen B, Kaptein B, Stilling M. Marker free model-based radiostereometric analysis for evaluation of hip joint kinematics. *Bone Jt Res*. 2018;7(6):379-387. doi:10.1302/2046-3758.76.BJR-2017-0268.R1

124. Christensen R, Petersen ET, Jürgens-Lahnstein J, et al. Assessment of knee kinematics with dynamic radiostereometry: Validation of an automated model-based method of analysis using bone models. *J Orthop Res*. Published online 2020. doi:10.1002/jor.24875

125. Wu D, Sofka M, Birkbeck N, Zhou SK. Segmentation of multiple knee bones from CT for orthopedic knee surgery planning. In: *Lecture Notes in Computer Science (Including Subseries Lecture Notes in Artificial Intelligence and Lecture Notes in Bioinformatics)*. Vol 8673 LNCS. ; 2014:372-380. doi:10.1007/978-3-319-10404-1_47

126. Jürgens-Lahnstein JH, Petersen ET, Laursen M, et al. Development, construction, and validation of a thinner uniplanar calibration cage for radiostereometry. *J Orthop Res*. Published online 2021. doi:10.1002/jor.25193

127. Pijls BG, Valstar ER, Nouta K-A, et al. Early migration of tibial components is associated with late revision: a systematic review and meta-analysis of 21,000 knee arthroplasties. *Acta Orthop*. 2012;83(6):614-624. doi:10.3109/17453674.2012.747052

128. Kärrholm J. Radiostereometric analysis of early implant migration – a valuable tool to ensure proper introduction of new implants. *Acta Orthop*. 2012;83(6):551-552. doi:10.3109/17453674.2012.745352

129. Valstar ER, Gill R, Ryd L, Flivik G, Börlin N, Kärrholm J. Guidelines for standardization of radiostereometry (RSA) of implants. *Acta Orthop*. 2005;76(4):563-572. doi:10.1080/17453670510041574

130. ISO 16087:2013. Implants for surgery — Roentgen stereophotogrammetric analysis for the assessment of migration of orthopaedic implants.

131. Kärrholm J, Borssén B, Löwenhielm G, Snorrason F. Does early micromotion of femoral stem prostheses matter? 4-7-year stereoradiographic follow-up of 84 cemented prostheses. *J Bone Joint Surg Br*. 1994;76(6):912-917. http://www.ncbi.nlm.nih.gov/pubmed/7983118

132. Ryd L, Albrektsson BE, Carlsson L, et al. Roentgen stereophotogrammetric analysis as a predictor of mechanical loosening of knee prostheses. *J Bone Jt Surg Br*. 1995;77(3):377-383. http://www.ncbi.nlm.nih.gov/entrez/query.fcgi?cmd=Retrieve&db=PubMed&dopt=Citation&list_uids=7744919

133. Pijls B. Evidence based introduction based introduction of orthopaedic implants RSA, implant quality and patient safety. Published online 2013:1-191. doi:10.13140/RG.2.1.4552.3602

134. Nelissen RGHH, Pijls BG, Kärrholm J, Malchau H, Nieuwenhuijse MJ, Valstar ER. RSA and Registries: The Quest for Phased Introduction of New Implants. *J Bone Jt Surg*. 2011;3:62-65.

135. Valstar ER, De Jong FW, Vrooman H a., Rozing PM, Reiber JHC. Model-based Roentgen stereophotogrammetry of orthopaedic implants. *J Biomech*. 2001;34(6):715-722. doi:10.1016/S0021-9290(01)00028-8

136. Nelissen RG, Piljs BG, Kärrholm J, Malchau H, Nieuwenhuijse MJ, Valstar ER. RSA and Registries: The Quest for Phased Introduction of New Implants. *J Bone Jt Surg*. 2011;3:62-65.

137. Kim Y, Kim K Il, Choi JH, Lee K. Novel methods for 3D postoperative analysis of total knee arthroplasty using 2D-3D image registration. *Clin Biomech*. 2011;26(4):384-391. doi:10.1016/j.clinbiomech.2010.11.013

138. Seehaus F, Olender GD, Kaptein BL, Ostermeier S, Hurschler C. Markerless Roentgen Stereophotogrammetric Analysis for in vivo implant migration measurement using three dimensional surface models to represent bone. *J Biomech*. 2012;45(8):1540-1545. doi:10.1016/j.jbiomech.2012.03.004

139. Zhu Z, Li G. An automatic 2D-3D image matching method for reproducing spatial knee joint positions using single or dual fluoroscopic images. *Comput Methods Biomech Biomed Engin*. 2012;15(11):1245-1256. doi:10.1080/10255842.2011.597387

140. Banks SA, Hodge WA. *Accurate Measurement of Three-Dimensional Knee Replacement Kinematics Using Single-Plane Fluoroscopy*. Vol 43.; 1996.

141. Zuffi S, Leardini A, Catani F, Fantozzi S, Cappello A. A model-based method for the reconstruction of total knee replacement kinematics. *IEEE Trans Med Imaging*. 1999;18(10):981-991. doi:10.1109/42.811310

142. Lebel BP, Pineau V, Gouzy SL, et al. Total knee arthroplasty three-dimensional kinematic estimation prevision. From a two-dimensional fluoroscopy acquired dynamic model. *Orthop Traumatol Surg Res*. 2011;97(2):111-120. doi:10.1016/j.otsr.2011.01.003

143. Wu J, Fatah EEA, Mahfouz MR. Fully automatic initialization of two-dimensional–three-dimensional medical image registration using hybrid classifier. *J Med Imaging*. 2015;2(2):024007. doi:10.1117/1.JMI.2.2.024007

144. Yamazaki T, Watanabe T, Nakajima Y, et al. Improvement of depth position in 2-D/3-D registration of knee implants using single-plane fluoroscopy. *IEEE Trans Med Imaging*. 2004;23(5):602-612. doi:10.1109/TMI.2004.826051

145. Guan S, Gray HA, Keynejad F, Pandy MG. Mobile biplane X-Ray imaging system for measuring 3D dynamic joint motion during overground gait. *IEEE Trans Med Imaging*. 2016;35(1):326-336. doi:10.1109/TMI.2015.2473168

146. Miranda DL, Schwartz JB, Loomis AC, Brainerd EL, Fleming BC, Crisco JJ. Static and Dynamic Error of a Biplanar Videoradiography System Using Marker-Based and Markerless Tracking Techniques. *J Biomech Eng*. 2011;133(12). doi:10.1115/1.4005471

147. K H, BL K, L R, PB J, M S. Dynamic RSA for the evaluation of inducible micromotion of Oxford UKA during step-up and step-down motion. *Acta Orthop*. 2017;88(3):275-281. doi:10.1080/17453674.2016.1274592

148. Nielsen ET, Stentz-Olesen K, de Raedt S, et al. Influence of the Anterolateral Ligament on Knee Laxity: A Biomechanical Cadaveric Study Measuring Knee Kinematics in 6 Degrees of Freedom Using Dynamic Radiostereometric Analysis. *Orthop J Sport Med*. 2018;6(8). doi:10.1177/2325967118789699

149. Hemmingsen CK, Thillemann TM, Elmengaard B, et al. Elbow Biomechanics, Radiocapitellar Joint Pressure, and Interosseous Membrane Strain Before and After Radial Head Arthroplasty. *J Orthop Res*. 2020;38(3):510-522. doi:10.1002/jor.24488

150. Thillemann JK, De Raedt S, Hansen TB, Munk B, Stilling M. Distal radioulnar joint stabilization with open foveal reinsertion versus tendon graft reconstruction: an experimental study using radiostereometry. *J Exp Orthop*. 2021;8(1). doi:10.1186/s40634-021-00329-y

151. Valstar ER, Nelissen RGHH, Reiber JHC, Rozing PM. The use of Roentgen stereophotogrammetry to study micromotion of orthopaedic implants. *ISPRS J Photogramm Remote Sens*. 2002;56(5-6):376-389. Accessed January 10, 2016. http://www.sciencedirect.com/science/article/pii/S0924271602000643

152. Pataky TC. One-dimensional statistical parametric mapping in Python. *Comput Methods Biomech Biomed Engin*. 2012;15(3):295-301. doi:10.1080/10255842.2010.527837

153. Pataky TC, Robinson MA, Vanrenterghem J. Vector field statistical analysis of kinematic and force trajectories. *J Biomech*. 2013;46(14):2394-2401. doi:10.1016/j.jbiomech.2013.07.031

154. Pataky TC. Generalized n-dimensional biomechanical field analysis using statistical parametric mapping. *J Biomech*. 2010;43(10):1976-1982. doi:10.1016/J.JBIOMECH.2010.03.008

155. Victor J, Bellemans J. A comparative study on the biomechanics of the native human knee joint and total knee arthroplasty. *Dep Orthop Fac Med*. 2009;PhD:168.

156. World Medical Association. World Medical Association declaration of Helsinki: Ethical principles for medical research involving human subjects. *JAMA - J Am Med Assoc*. 2013;310(20):2191-2194. doi:10.1001/jama.2013.281053

157. European Commission. 2018 reform of EU data protection rules. Published 2018. Accessed June 17, 2019. https://ec.europa.eu/commission/sites/beta-political/files/data-protection-factsheet-changes_en.pdf

158. Saltybaeva N, Jafari ME, Hupfer M, Kalender W a. Estimates of effective dose for CT scans of the lower extremities. *Radiology*. 2014;273(1):153-159. doi:10.1148/radiol.14132903

159. The Danish National Committee on Health Research Ethics. *Guidelines on the Use of Ionising Radiation in Health Research Projects - Appendix 2.*; 2018.

160. Guan S, Gray HA, Schache AG, Feller JA, de Steiger R, Pandy MG. In vivo six-degree-of-freedom knee-joint kinematics in overground and treadmill walking following total knee arthroplasty. *J Orthop Res*. 2017;35(8):1634-1643. doi:10.1002/JOR.23466

161. Petersen ET, Rytter S, Koppens D, et al. Patients with knee osteoarthritis can be divided into subgroups based on tibiofemoral joint kinematics of gait – an exploratory and dynamic radiostereometric study. *Osteoarthr Cartil*. 2021;1st revisi.

162. Stryker. *Triathlon ® Knee System.*; 2015.

163. Petersen ET, Vind TD, Jürgens-Lahnstein JH, et al. Evaluation of automated radiostereometric image registration in total knee arthroplasty utilizing a synthetic-based volumetric implant model and a CT-based volumetric bone model. *Manuscr Submitt Publ*. Published online 2021.

164. Bohannon RW, Williams Andrews A. Normal walking speed: A descriptive meta-analysis. *Physiotherapy*. 2011;97(3):182-189. doi:10.1016/j.physio.2010.12.004

165. Lee JS, Hobden E, Stiell IG, Wells GA. Clinically important change in the visual analog scale after adequate pain control. *Acad Emerg Med*. 2003;10(10):1128-1130. doi:10.1111/J.1553-2712.2003.TB00586.X

166. Aalund PK, Larsen K, Hansen T, Bandholm T. Normalized knee-extension strength or leg-press power after fast-track total knee arthroplasty: which measure is most closely associated with performance-based and self-reported function? *Arch Phys Med Rehabil*. 2013;94(2):384-390. doi:10.1016/J.APMR.2012.09.031

167. Peterfy CG, Schneider E, Nevitt M. The osteoarthritis initiative: report on the design rationale for the magnetic resonance imaging protocol for the knee. *Osteoarthr Cartil*. 2008;16(12):1433-1441. doi:10.1016/j.joca.2008.06.016

168. Dawson J, Fitzpatrick R, Murray D, Carr A. Questionnaire on the perceptions of patients about total knee replacement. *J Bone Joint Surg Br*. 1998;80(1):63-69. doi:10.1302/0301-620x.80b1.7859

169. Roos E. *The 2012 User's Guide to: The Knee Injury and Osteoarthritis Outcome Score.*; 1998. doi:10.1097/00005131-200609001-00018

170. Behrend H, Giesinger K, Giesinger JM, Kuster MS. The "Forgotten Joint" as the Ultimate Goal in Joint Arthroplasty. Validation of a New Patient-Reported Outcome Measure. *J Arthroplasty*. 2012;27(3). doi:10.1016/j.arth.2011.06.035

171. Zimmer Biomet. *Persona® The Personalized Knee® - Surgical Technique.*; 2017.

172. Krčah M, Székely G, Blanc R. Fully automatic and fast segmentation of the femur bone from 3D-CT images with no shape prior. *Proc - Int Symp Biomed Imaging*. Published online 2011:2087-2090. doi:10.1109/ISBI.2011.5872823

173. De Raedt S, Mechlenburg I, Stilling M, et al. Reliability of computer-assisted periacetabular osteotomy using a minimally invasive approach. *Int J Comput Assist Radiol Surg*. 2018;13(12):2021-2028. doi:10.1007/s11548-018-1802-y

174. Boykov Y, Funka-Lea G. Graph cuts and efficient N-D image segmentation. *Int J Comput Vis*. 2006;70(2):109-131. doi:10.1007/s11263-006-7934-5

175. Schroeder W, Martin K, Lorensen B. *The Visualization Toolkit An Object-Oriented Approach To 3D Graphics Edition 4.1.*

176. Miranda DL, Rainbow MJ, Leventhal EL, Crisco JJ, Fleming BC. Automatic determination of anatomical coordinate systems for three-dimensional bone models of the isolated human knee. *J Biomech*. 2010;43(8):1623-1626. doi:10.1016/j.jbiomech.2010.01.036

177. Petersen ET, Rytter S, Koppens D, et al. Patients with knee osteoarthritis can be divided into subgroups based on tibiofemoral joint kinematics of gait – an exploratory and dynamic radiostereometric study. *Osteoarthr Cartil*. Published online October 2021. doi:10.1016/j.joca.2021.10.011

178. Söderkvist I, Wedin PÅ. Determining the movements of the skeleton using well-configured markers. *J Biomech*. 1993;26(12):1473-1477. doi:10.1016/0021-9290(93)90098-Y

179. Ryd L, Yuan X, Löfgren H. Methods for determining the accuracy of radiostereometric analysis (RSA). *Acta Orthop Scand*. 2000;71(4):403-408. doi:10.1080/000164700317393420

180. Kaptein BL, Valstar ER, Stoel BC, Rozing PM, Reiber JHC. A new type of model-based Roentgen stereophotogrammetric analysis for solving the occluded marker problem. *J Biomech*. 2005;38(11):2330-2334. doi:10.1016/j.jbiomech.2004.09.018

181. Hurschler C, Seehaus F, Emmerich J, Kaptein BL, Windhagen H. Comparison of the Model-Based and Marker-Based Roentgen Stereophotogrammetry Methods in a Typical Clinical Setting. *J Arthroplasty*. 2009;24(4):594-606. doi:10.1016/j.arth.2008.02.004

182. Klein S, Staring M, Murphy K, Viergever MA, Pluim JPW. Elastix: A toolbox for intensity-based medical image registration. *IEEE Trans Med Imaging*. 2010;29(1):196-205. doi:10.1109/TMI.2009.2035616

183. Van Der Bom IMJ, Klein S, Staring M, Homan R, Bartels LW, Pluim JPW. Evaluation of optimization methods for intensity-based 2D-3D registration in x-ray guided interventions. In: Dawant BM, Haynor DR, eds. *Medical Imaging 2011: Image Processing*. Vol 7962. SPIE; 2011:657-671. doi:10.1117/12.877655

184. Sobel I, Feldman G. A 3x3 Isotropic Gradient Operator for Image Processing. *Stanford Artif Intell Proj*. Published online 1986. https://www.researchgate.net/publication/239398674

185. Kaelo P, Ali MM. Some Variants of the Controlled Random Search Algorithm for Global Optimization. *J Optim Theory Appl 2006 1302*. 2006;130(2):253-264. doi:10.1007/S10957-006-9101-0

186. Nelder JA, Meadf R. *A Simplex Method for Function Minimization*.

187. O'Connor CM, Thorpe SK, O'Malley MJ, Vaughan CL. Automatic detection of gait events using kinematic data. *Gait Posture*. 2007;25(3):469-474. doi:10.1016/j.gaitpost.2006.05.016

188. Grood ES, Suntay WJ. A joint coordinate system for the clinical description of three-dimensional motions: application to the knee. *J Biomech Eng*. 1983;105(2):136-144. Accessed July 31, 2015. http://www.ncbi.nlm.nih.gov/pubmed/6865355

189. Dabirrahmani D, Hogg M. Modification of the Grood and Suntay Joint Coordinate System equations for knee joint flexion. *Med Eng Phys*. 2017;39:113-116. doi:10.1016/j.medengphy.2016.10.006

190. Lloyd SP. Least Squares Quantization in PCM. *IEEE Trans Inf Theory*. 1982;28(2):129-137. doi:10.1109/TIT.1982.1056489

191. Harris K, Dawson J, Doll H, et al. Can pain and function be distinguished in the Oxford Knee Score in a meaningful way? An exploratory and confirmatory factor analysis. *Qual Life Res*. 2013;22(9):2561-2568. doi:10.1007/s11136-013-0393-x

192. Clement ND, MacDonald D, Simpson AHRW. The minimal clinically important difference in the Oxford knee score and Short Form 12 score after total knee arthroplasty. *Knee Surgery, Sport Traumatol Arthrosc*. 2014;22(8):1933-1939. doi:10.1007/s00167-013-2776-5

193. Jacquet C, Pioger C, Khakha R, et al. Evaluation of the "Minimal Clinically Important Difference" (MCID) of the KOOS, KSS and SF-12 scores after open-wedge high tibial osteotomy. *Knee Surgery, Sport Traumatol Arthrosc*. 2021;29(3):820-826. doi:10.1007/s00167-020-06026-0

194. Clement ND, Scott CEH, Hamilton DF, MacDonald D, Howie CR. Meaningful values in the Forgotten Joint Score after total knee arthroplasty. *Bone Jt J*. 2014;103(7):96-907. doi:10.1302/0301-620X.103B5

195. Nacey NC, Geeslin MG, Miller GW, Pierce JL. Magnetic resonance imaging of the knee: An overview and update of conventional and state of the art imaging. *J Magn Reson Imaging*. 2017;45(5):1257-1275. doi:10.1002/jmri.25620

196. Koch JEJ, Ben-Elyahu R, Khateeb B, et al. Accuracy measures of 1.5-tesla MRI for the diagnosis of ACL, meniscus and articular knee cartilage damage and characteristics of false negative lesions: a level III prognostic study. *BMC Musculoskelet Disord*. 2021;22(1). doi:10.1186/s12891-021-04011-3

197. Halinen J, Koivikko M, Lindahl J, Hirvensalo E. The efficacy of magnetic resonance imaging in acute multi-ligament injuries. *Int Orthop*. 2009;33(6):1733-1738. doi:10.1007/s00264-008-0689-6

198. Bland JM, Altman DG. Statistical methods for assessing agreement between two methods of clinical measurement. *Lancet*. 1986;1(8476):307-310. doi:10.1016/S0140-6736(86)90837-8

199. Nichols TE, Holmes AP. Nonparametric permutation tests for functional neuroimaging: A primer with examples. *Hum Brain Mapp*. 2002;15(1):1-25. doi:10.1002/hbm.1058

200. Tashman S, Anderst W. In-vivo measurement of dynamic joint motion using high speed biplane radiography and CT: application to canine ACL deficiency. *J Biomech Eng*. 2003;125(2):238-245. doi:10.1115/1.1559896

201. Bey MJ, Zauel R, Brock SK, Tashman S. Validation of a new model-based tracking technique for measuring three-dimensional, in vivo glenohumeral joint kinematics. *J Biomech Eng*. 2006;128(4):604-609. doi:10.1115/1.2206199

202. Bey MJ, Kline SK, Tashman S, Zauel R. Accuracy of biplane x-ray imaging combined with model-based tracking for measuring in-vivo patellofemoral joint motion. *J Orthop Surg Res*. 2008;3:38. doi:10.1186/1749-799X-3-38

203. Papaioannou G, Nianios G, Mitrogiannis C, Fyhrie D, Tashman S, Yang KH. Patient-specific knee joint finite element model validation with high-accuracy kinematics from biplane dynamic Roentgen stereogrammetric analysis. *J Biomech*. 2008;41(12):2633-2638. doi:10.1016/j.jbiomech.2008.06.027

204. Bonanzinga T, Signorelli C, Bontempi M, et al. Evaluation of RSA set-up from a clinical biplane fluoroscopy system for 3D joint kinematic analysis. *Joints*. 2016;4(2):121-125.

205. de Bruin PW, Kaptein BL, Stoel BC, Reiber JHC, Rozing PM, Valstar ER. Image-based RSA: Roentgen stereophotogrammetric analysis based on 2D-3D image registration. *J Biomech*. 2008;41(1):155-164. doi:10.1016/j.jbiomech.2007.07.002

206. Scarvell JM, Pickering MR, Smith PN. New registration algorithm for determining 3D knee kinematics using CT and single-plane fluoroscopy with improved out-of-plane translation accuracy. *J Orthop Res*. 2010;28(3):334-340. doi:10.1002/jor.21003

207. Driban JB, Sitler MR, Barbe MF, Balasubramanian E. Is osteoarthritis a heterogeneous disease that can be stratified into subsets? *Clin Rheumatol*. 2010;29(2):123-131. doi:10.1007/s10067-009-1301-1

208. Indelli PF, Risitano S, Hall KE, Leonardi E, Migliore E. Effect of polyethylene conformity on total knee arthroplasty early clinical outcomes. *Knee Surgery, Sport Traumatol Arthrosc*. 2019;27(4):1028-1034. doi:10.1007/s00167-018-5170-5

209. Sabatini L, Risitano S, Parisi G, et al. Medial Pivot in Total Knee Arthroplasty: Literature Review and Our First Experience. *Clin Med Insights Arthritis Musculoskelet Disord*. 2018;11. doi:10.1177/1179544117751431

210. Zhang Q, Chen Z, Zhang J, et al. Insert conformity variation affects kinematics and wear performance of total knee replacements. *Clin Biomech*. 2019;65:19-25. doi:10.1016/J.CLINBIOMECH.2019.03.016

211. Miura K, Ohkoshi Y, Ino T, et al. Kinematics and center of axial rotation during walking after medial pivot type total knee arthroplasty. *J Exp Orthop*. 2020;7(1). doi:10.1186/s40634-020-00286-y

212. Lewek M, Rudolph K, Axe M, Snyder-Mackler L. The effect of insufficient quadriceps strength on gait after anterior cruciate ligament reconstruction. *Clin Biomech*. 2002;17(1):56-63. doi:10.1016/S0268-0033(01)00097-3

213. Mizner RL, Petterson SC, Stevens JE, Vandenborne K, Snyder-Mackler L. Early quadriceps strength loss after total knee arthroplasty: The contributions of muscle atrophy and failure of voluntary muscle activation. *J Bone Jt Surg - Ser A*. 2005;87(5):1047-1053. doi:10.2106/JBJS.D.01992

214. Lafortune MA, Cavanagh PR, Sommer HJ, Kalenak~i A. *Three-Dimensional Kinematics of the Human Knee during Walking*. Vol 25.; 1992.

215. Dyrby CO, Andriacchi TP. Secondary motions of the knee during weight bearing and non-weight bearing activities. *J Orthop Res*. 2004;22(4):794-800. doi:10.1016/J.ORTHRES.2003.11.003

216. Kozanek M, Hosseini A, Liu F, et al. Tibiofemoral kinematics and condylar motion during the stance phase of gait. *J Biomech*. 2009;42(12):1877-1884. doi:10.1016/j.jbiomech.2009.05.003

217. Bragonzoni L, Russo A, Loreti I, Montagna L, Visani A, Marcacci M. The stress-inducible displacement detected through RSA in non-migrating UKR. *Knee*. 2005;12(4):301-306. doi:10.1016/j.knee.2004.09.006

218. Stilling M, Mechlenburg I, Jepsen CF, et al. Superior fixation and less periprosthetic stress-shielding of tibial components with a finned stem versus an I-beam block stem: a randomized RSA and DXA study with minimum 5 years' follow-up. *Acta Orthop*. 2019;90(2):165-171. doi:10.1080/17453674.2019.1566510

219. Jenny JY, Saragaglia D. No Detectable Polyethylene Wear 15 Years After Implantation of a Mobile–Bearing Total Knee Arthroplasty With Electron Beam–Irradiated Polyethylene. *J Arthroplasty*. 2019;34(8):1690-1694. doi:10.1016/j.arth.2019.03.054

220. Boskey AL, Coleman R. Critical reviews in oral biology & medicine: Aging and bone. *J Dent Res*. 2010;89(12):1333-1348. doi:10.1177/0022034510377791

221. Lévesque L. Nyquist sampling theorem: Understanding the illusion of a spinning wheel captured with a video camera. *Phys Educ*. 2014;49(6):697-705. doi:10.1088/0031-9120/49/6/697

222. Jagos H, Oberzaucher J, Reichel M, Zagler WL, Hlauschek W. A multimodal approach for insole motion measurement and analysis. In: *Procedia Engineering*. Vol 2. Elsevier Ltd; 2010:3103-3108. doi:10.1016/j.proeng.2010.04.118

223. Cooley JW, Tukey JW. *An Algorithm for the Machine Calculation of Complex Fourier Series*. https://www.ams.org/journal-terms-of-use

Appendices

Appendix I

Patient appointment and data acquisition flow chart (studies III and IV).

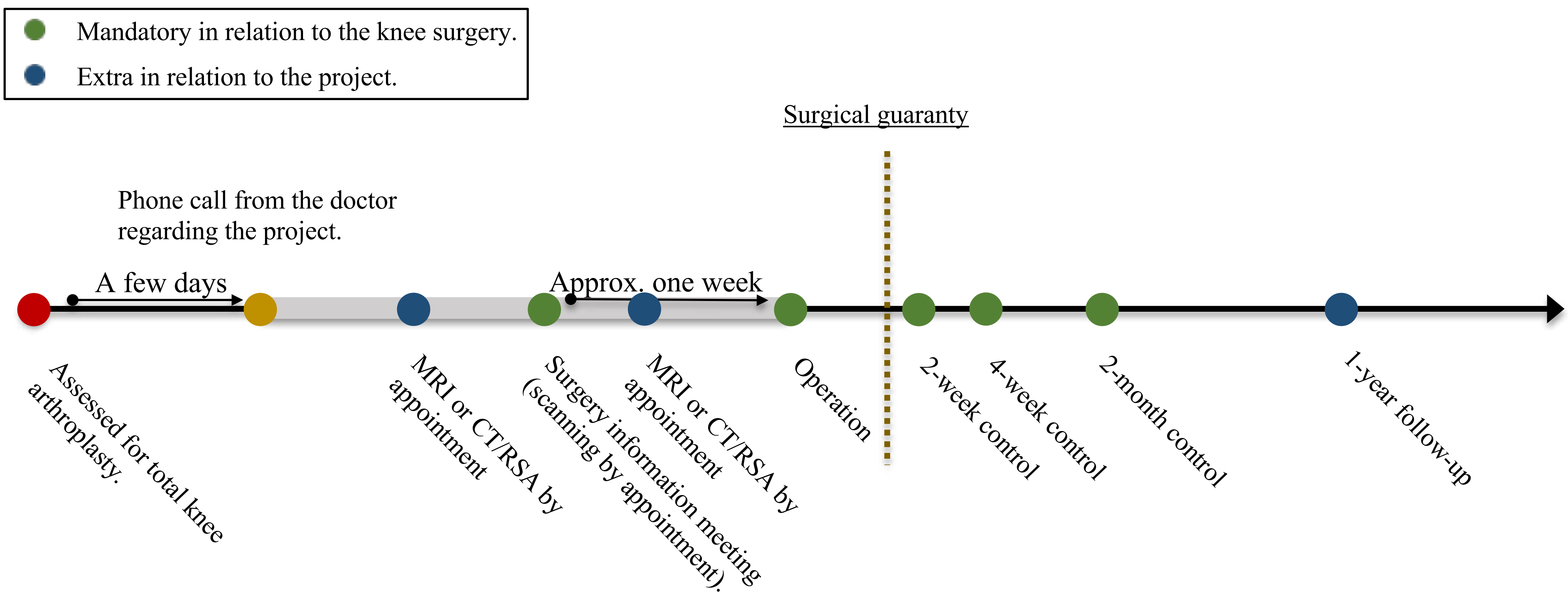
Mandatory in relation to the knee surgery.
Extra in relation to the project.
Surgical guaranty
Phone call from the doctor regarding the project.
A few days
Approx. one week
Assessed for total knee arthroplasty.
MRI or CT/RSA by appointment
Surgery information meeting (scanning by appointment).
MRI or CT/RSA by appointment
Operation
2-week control
4-week control
2-month control
1-year follow-up

Appendix II

In-between subgroup comparison for study III.[177]

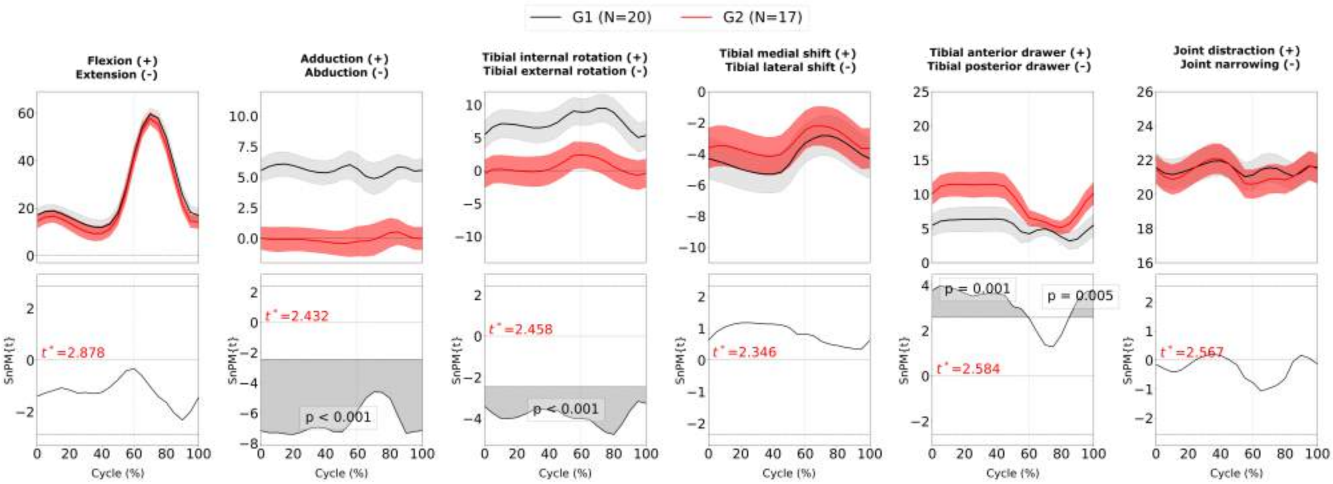

G1 (N=20)
G2 (N=17)
Flexion (+)
Extension (-)
Adduction (+)
Abduction (-)
Tibial internal rotation (+)
Tibial external rotation (-)
Tibial medial shift (+)
Tibial lateral shift (-)
Tibial anterior drawer (+)
Tibial posterior drawer (-)
Joint distraction (+)
Joint narrowing (-)
SnPM{t}
t* =2.878
t* =2.432
p < 0.001
t* =2.458
p < 0.001
t* =2.346
p = 0.001
p = 0.005
t* =2.584
t* =2.567
Cycle (%)

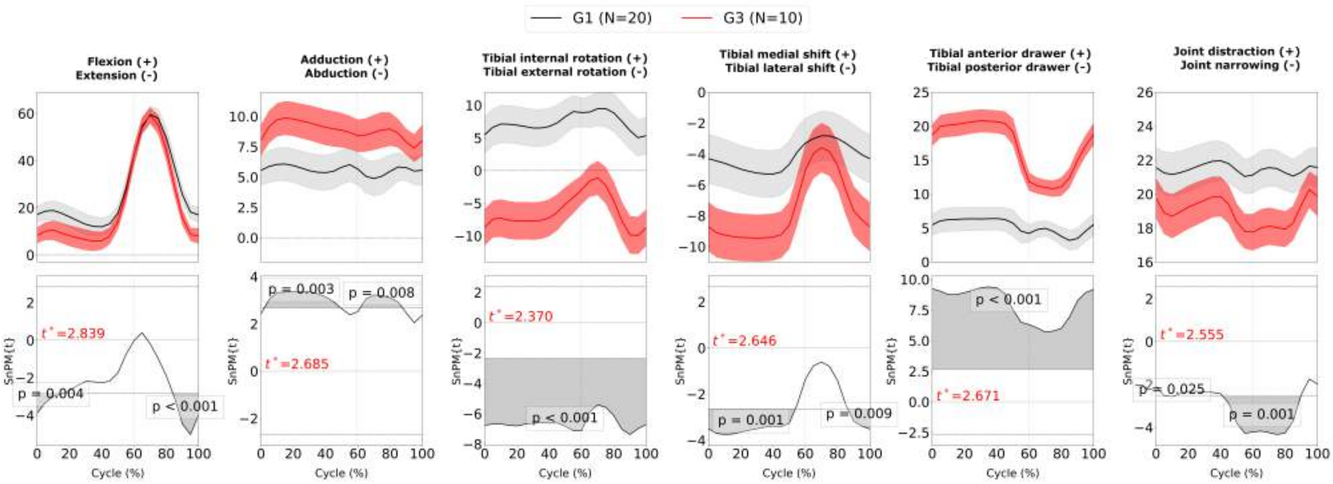

G1 (N=20)
G3 (N=10)
Flexion (+)
Extension (-)
Adduction (+)
Abduction (-)
Tibial internal rotation (+)
Tibial external rotation (-)
Tibial medial shift (+)
Tibial lateral shift (-)
Tibial anterior drawer (+)
Tibial posterior drawer (-)
Joint distraction (+)
Joint narrowing (-)
SnPM{t}
t* =2.839
p = 0.004
p < 0.001
p = 0.003
p = 0.008
t* =2.685
t* =2.370
p < 0.001
t* =2.646
p = 0.001
p = 0.009
p < 0.001
t* =2.671
t* =2.555
p = 0.025
p = 0.001
Cycle (%)

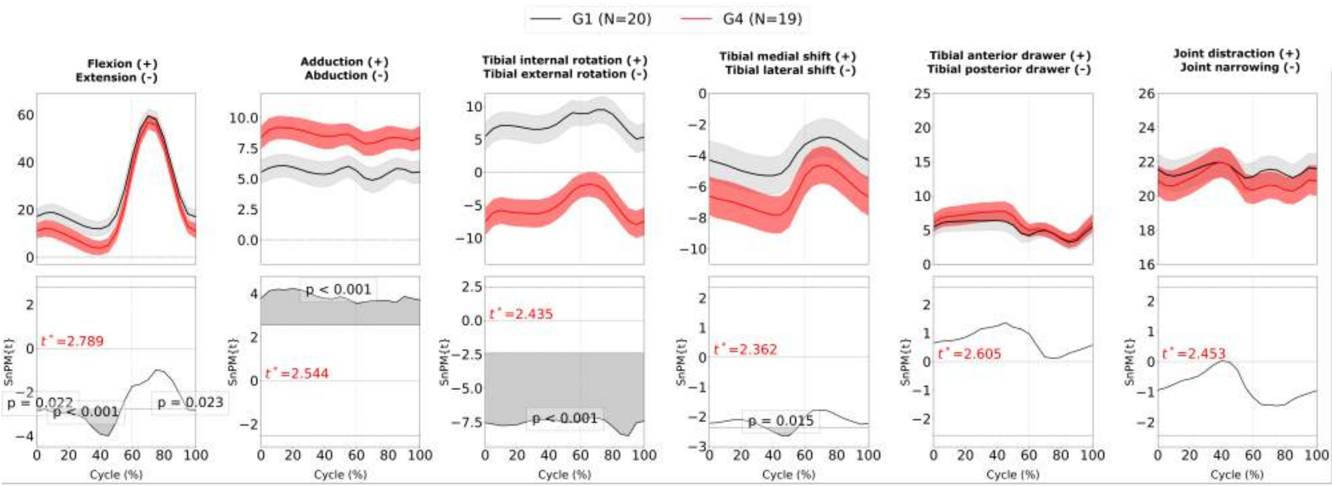

G1 (N=20)
G4 (N=19)
Flexion (+)
Extension (-)
Adduction (+)
Abduction (-)
Tibial internal rotation (+)
Tibial external rotation (-)
Tibial medial shift (+)
Tibial lateral shift (-)
Tibial anterior drawer (+)
Tibial posterior drawer (-)
Joint distraction (+)
Joint narrowing (-)
SnPM{t}
t* =2.789
p = 0.022
p < 0.001
p = 0.023
p < 0.001
t* =2.544
t* =2.435
p < 0.001
t* =2.362
p = 0.015
t* =2.605
t* =2.453
Cycle (%)

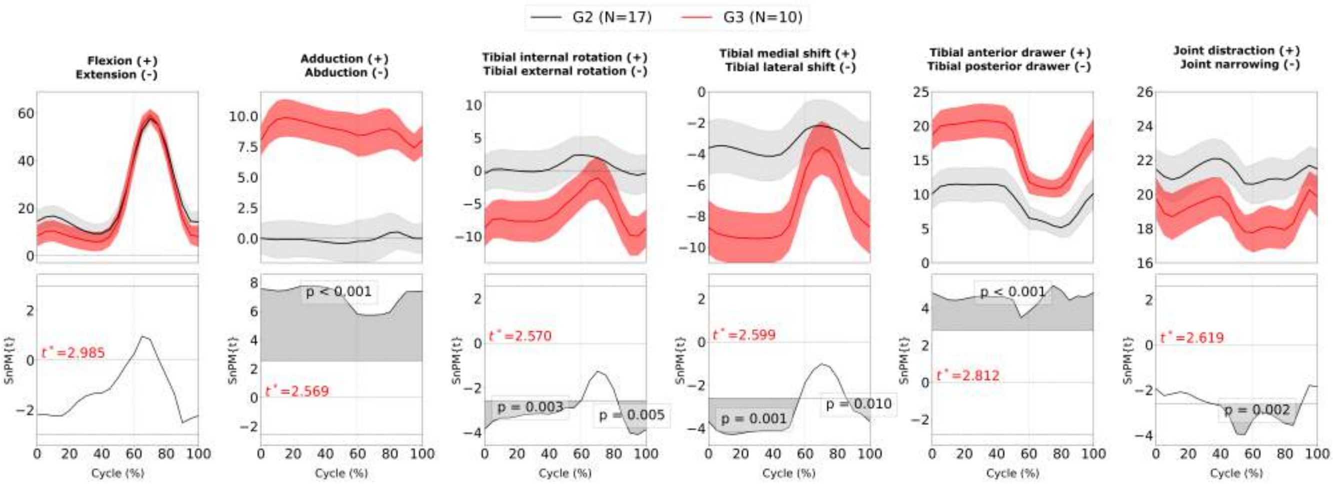
G2 (N=17)
G3 (N=10)
Flexion (+)
Extension (-)
Adduction (+)
Abduction (-)
Tibial internal rotation (+)
Tibial external rotation (-)
Tibial medial shift (+)
Tibial lateral shift (-)
Tibial anterior drawer (+)
Tibial posterior drawer (-)
Joint distraction (+)
Joint narrowing (-)
SnPM{t}
t* =2.985
t* =2.569
p < 0.001
t* =2.570
p = 0.003
p = 0.005
t* =2.599
p = 0.001
p = 0.010
t* =2.812
p < 0.001
t* =2.619
p = 0.002
Cycle (%)

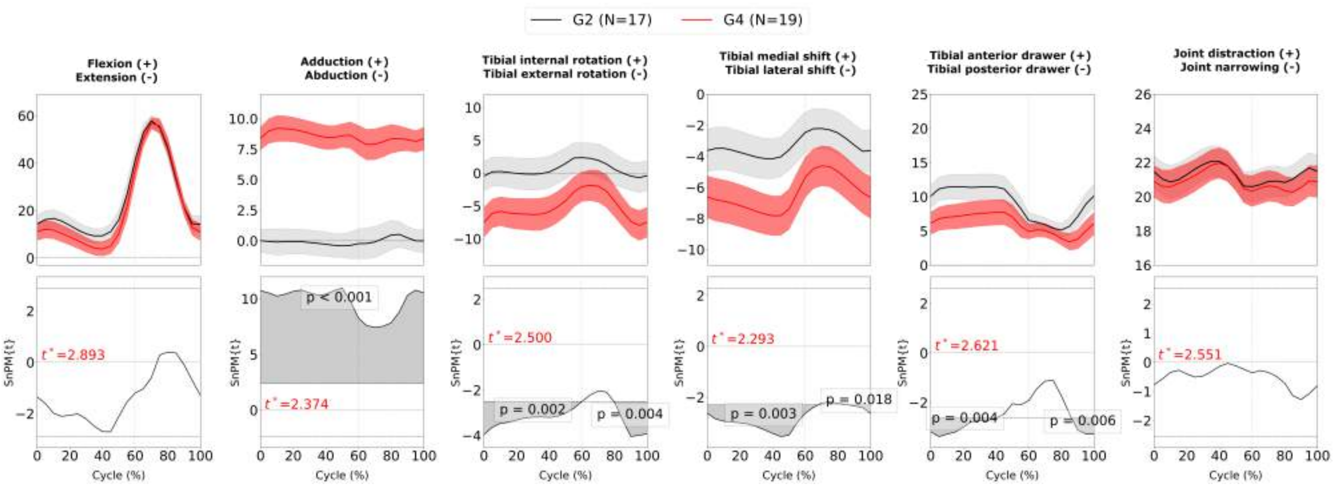
G2 (N=17)
G4 (N=19)
Flexion (+)
Extension (-)
Adduction (+)
Abduction (-)
Tibial internal rotation (+)
Tibial external rotation (-)
Tibial medial shift (+)
Tibial lateral shift (-)
Tibial anterior drawer (+)
Tibial posterior drawer (-)
Joint distraction (+)
Joint narrowing (-)
SnPM{t}
t* =2.893
t* =2.374
p < 0.001
t* =2.500
p = 0.002
p = 0.004
t* =2.293
p = 0.003
p = 0.018
t* =2.621
p = 0.004
p = 0.006
t* =2.551
Cycle (%)

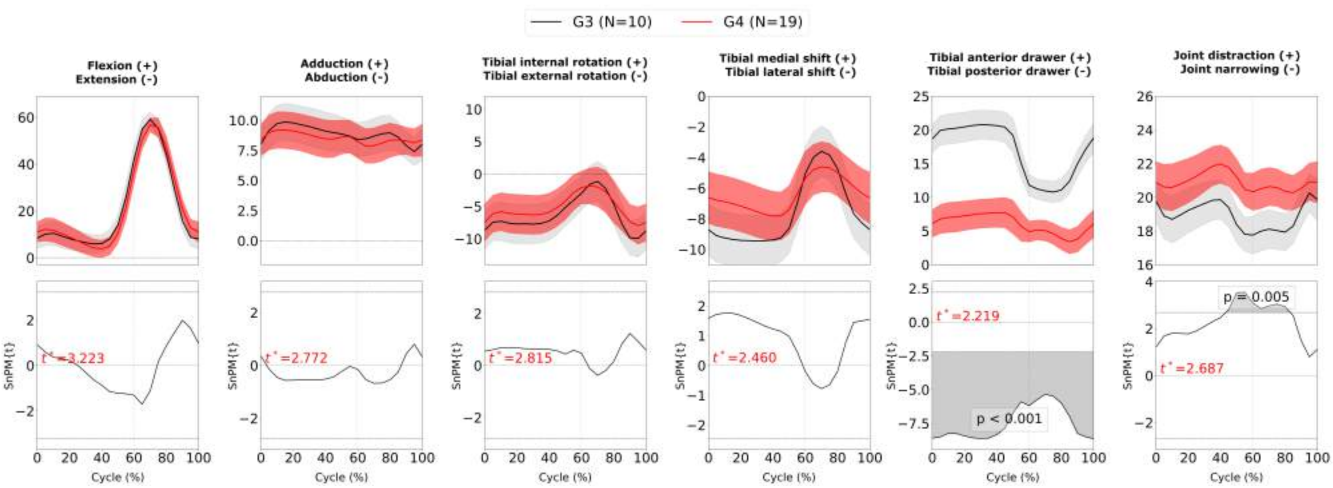
G3 (N=10)
G4 (N=19)
Flexion (+)
Extension (-)
Adduction (+)
Abduction (-)
Tibial internal rotation (+)
Tibial external rotation (-)
Tibial medial shift (+)
Tibial lateral shift (-)
Tibial anterior drawer (+)
Tibial posterior drawer (-)
Joint distraction (+)
Joint narrowing (-)
SnPM{t}
t* =3.223
t* =2.772
t* =2.815
t* =2.460
t* =2.219
p < 0.001
t* =2.687
p = 0.005
Cycle (%)

Appendix III

Other authored and co-authored publications and proceedings during the PhD.

Co-authored publications in peer-reviewed journals during the PhD

1. CK Hemmingsen, TM Thillemann, B Elmengaard, S de Raedt, **ET Nielsen**, SB Mosegaard, K Stentz-Olesen, M Stilling (2020). Elbow Biomechanics, Radiocapitellar Joint Pressure, and Interosseous Membrane Strain Before and After Radial Head Arthroplasty. J Orthop Res. doi: 10.1002/jor.24488.
2. J Torle, JK Thillemann, **ET Petersen**, F Madsen, K Søballe, M Stilling (2021). Less polyethylene wear in monobloc compared to modular ultra-high-molecular-weight-polyethylene inlays in hybrid total knee arthroplasty: A 5-year randomized radiostereometry study. Knee. doi: 10.1016/j.knee.2021.02.033.
3. JH Jürgens-Lahnstein, **ET Petersen**, M Laursen, CH Iversen, BL Kaptein, L Lindgren, M Stilling (2021). Development, construction, and validation of a thinner uniplanar calibration cage for radiostereometry. J Orthop Res. doi: 10.1002/jor.25193.
4. JK Thillemann, S de Raedt, **ET Petersen**, KB Puhakka, TB Hansen, M Stilling. Normal Values of Distal Radioulnar Joint Kinematics During a Dynamic Press Test. J. Wrist Surg. [accepted – 2021]

Publications authored for proceedings during the PhD

1. JH Jürgens-Lahnstein, **ET Petersen**, S Rytter, F Madsen, K Søballe, M Stilling. Measuring polyethylene migration in total knee arthroplasty: A 5-6 year randomized radiostereometry study. J Arthroplasty. [submitted – 2021]
2. JK Thillemann, S de Raedt, **ET Petersen**, KB Puhakka, TB Hansen, M Stilling. Kinematics of the distal radioulnar joint before and after open reinsertion of the foveal triangular fibrocartilage complex and in comparison to normal joints. Acta Orthop. [submitted – 2021]

Presentations made during the PhD

3. **ET Petersen**, K Stentz-Olesen, S de Raedt, PB Jørgensen, OG Sørensen, BL Kaptein, MS Andersen, M Stilling. Influence of anterolateral ligament on knee laxity during flexion-internal rotation. A biomechanical cadaver study using dynamic radiostereometric analysis. 2017. 5th International RSA Meeting, Adelaide, Australia.
4. **ET Petersen**, OG Sørensen, K Stentz-Olesen, M Stilling. Measurement of knee kinematics during examiner applied pivot-shift test. A dynamic radiostereometric cadaver study. 2019. 6th International RSA Meeting, Aarhus, Denmark.
5. **ET Petersen**, S Rytter, D Koppens, J Dalsgaard, TB Hansen, NE Larsen, MS Andersen, M Stilling. Patients with knee osteoarthritis can be divided in subgroups based on tibiofemoral joint kinematic clustering of gait – An exploratory and dynamic radiostereometric study. 2021, 7th International RSA Meeting, Oslo, Norway, ***Winner Best Paper, 1000€.***
6. **ET Petersen**, S Rytter, D Koppens, J Dalsgaard, TB Hansen, NE Larsen, MS Andersen, M Stilling. Patients with knee osteoarthritis can be divided in subgroups based on tibiofemoral joint kinematic clustering of gait – An exploratory and dynamic radiostereometric study. DOS Conference 2021, Copenhagen, Denmark.

Paper I

Received: 22 April 2020 | Revised: 26 July 2020 | Accepted: 6 October 2020

DOI: 10.1002/jor.24875

RESEARCH ARTICLE

Journal of Orthopaedic Research®

Assessment of knee kinematics with dynamic radiostereometry: Validation of an automated model-based method of analysis using bone models

Rasmus Christensen[1,2] | Emil Toft Petersen[1,2,3] | Jonathan Jürgens-Lahnstein[1,2] | Søren Rytter[1,2,4] | Lars Lindgren[1,5] | Sepp De Raedt[1,6] | Annemarie Brüel[7] | Maiken Stilling[1,2,4]

[1]AutoRSA Research Group, Orthopaeadic Research Unit, Aarhus University Hospital, Aarhus N, Denmark

[2]Department of Clinical Medicine, Aarhus University, Aarhus N, Denmark

[3]University Clinic for Hand, Hip and Knee Surgery, Holstebro Central Hospital, Holstebro, Denmark

[4]Department of Orthopaedic Surgery, Aarhus University Hospital, Aarhus N, Denmark

[5]Department of Radiology, Aarhus University Hospital, Aarhus N, Denmark

[6]NRT X-RAY, Hasselager, Denmark

[7]Department of Biomedicine, Aarhus University, Aarhus C, Denmark

Correspondence

Rasmus Christensen, MD, AutoRSA Research Group, Orthopaedic Research Unit, Aarhus University Hospital, Palle Juul-Jensens Blvd 165, 8200 Aarhus N, Denmark.
Email: rasmus.c@aol.com

Funding information

Fonden til Lægevidenskabens Fremme, Grant/Award Number: 19-L-0017; Orthopaedic Research Found at Aarhus University Hospital

Abstract

Radiostereometic analysis (RSA) is a precise method for the functional assessment of joint kinematics. Traditionally, the method is based on tracking of surgically implanted bone markers and analysis is user intensive. We propose an automated method of analysis based on models generated from computed tomography (CT) scans and digitally reconstructed radiographs. The study investigates method agreement between marker-based RSA and the CT bone model-based RSA method for assessment of knee joint kinematics in an experimental setup. Eight cadaveric specimens were prepared with bone markers and bone volume models were generated from CT-scans. Using a mobile fixture setup, dynamic RSA recordings were obtained during a knee flexion exercise in two unique radiographic setups, uniplanar and biplanar. The method agreement between marker-based and CT bone model-based RSA methods was compared using bias and LoA. Results obtained from uniplanar and biplanar recordings were compared and the influence of radiographic setup was considered for clinical relevance. The automated method had a bias of −0.19 mm and 0.11° and LoA within ±0.42 mm and ±0.33° for knee joint translations and rotations, respectively. The model pose estimation of the tibial bone was more precise than the femoral bone. The radiographic setup had no clinically relevant effect on results. In conclusion, the automated CT bone model-based RSA method had a clinical precision comparable to that of marker-based RSA. The automated method is non-invasive, fast, and clinically applicable for functional assessment of knee kinematics and pathomechanics in patients.

KEYWORDS

digitally reconstructed radiographs, dynamic stereoradiographs, kinematics, knee arthroplasty, radiostereometry

1 | INTRODUCTION

The interest for functional assessment of knee joint kinematics in both native and prosthetic knee joints is increasing. Radiostereometric analysis (RSA) is a highly accurate and precise method for quantifying the motion of a rigid body based on stereoscopic images from two roentgen tubes and corresponding detectors in a calibrated setup.[1,2] However, some limitations make the method less attractive in clinical practice. Most importantly, traditional marker-based RSA involves the insertion of radiopaque tantalum beads and requires substantial user interaction during analysis, while other factors such as prolonged surgery, risk of loose beads or poor bead placement further impede clinical use.[3] In recent years, new approaches using dynamic RSA (dRSA) to precisely measure the motion of bones and migration of implants have been researched.[4–10] New RSA methods are based on virtual software matching of three-dimensional (3D) models of either bones or implants to two-dimensional (2D) images of dRSA recordings, so-called model-based RSA. Bone models have an anatomical coordinate system (ACS), are individual for each patient, and can be generated from computed tomography (CT) scans, readily available in clinical practice. On the contrary, the insertion of beads is a surgical procedure and markers provide a bone reference with no relation to the bone ACS. Therefore, model-based tracking of CT-derived bone models has obvious advantages over traditional marker-based RSA, in which application outside joint replacement surgery remains limited. With the model-based technique, diagnostic assessment of native knee kinematics and pathomechanics, as well as arthroplasty dysfunction and instability, are possible. The method has a place in preoperative planning of knee surgery and in comparing preoperative function to postoperative result. Limitations of the model-based method include the need for a high-quality CT scan of the knee joint adding additional radiation dose and a possible effect of patient-specific parameters such as variation in bone density and contour geometrics. A functional dRSA recording produces a great number of images with a substantial amount of data to be processed. This creates a need for a precise and automated software-based method of analysis with minimal need for user interaction.

The aims of this experimental cadaver study were (1) to evaluate the method agreement in terms of bias and precision of an automated CT bone model-based RSA method (AutoRSA) against the gold standard of marker-based RSA for measurement of knee joint kinematics in dRSA recordings, (2) to assess the bias and precision of pose estimation of the femoral and tibial bones, and (3) to compare the bias and precision of a uniplanar and biplanar radiographic setup.

2 | METHODS AND MATERIALS

2.1 | Specimens and preparation

Eight cadaveric legs showing no visual or fluoroscopic signs of previous injury, surgery, or severe degenerative osteoarthritis were acquired from Caucasian donors; male:female ratio 1:1, ages 80–93 (mean 85 years). Specimens were full legs including hemipelvis, hip, knee, ankle, and foot. Relevant approvals from the Central Denmark Committee on Biomedical Research Ethics (case number 1-10-72-236-19, issued November 21st 2019) and the Data Protection Agency (case number 1-16-02-410-19, issued December 2nd 2019) were obtained.

Before specimen preparation and dissection, eight baseline spiral ultrahigh resolution CT-scans (SOMATOM Definition Flash; Siemens Healthcare, Erlangen, Germany) of the full lower extremity were carried out using axial slices at a peak voltage of 120 kVp and exposure of 183 mAs, slice thickness of 0.6 mm, slice increment of 1 mm and pixel spacing of 0.29 × 0.29 mm. Full leg scans were performed to obtain hip and ankle centers required to define local ACS for each specimen.[11,12] In addition, baseline scans were used to generate 3D volumetric bone models of the distal 15 cm of the femoral bone and the proximal 15 cm of the tibial bone for each specimen, using a fully automated graph-cut segmentation method.[13–15] Bone models were used in model-based analysis, defined as the bone model method (BM).

To prepare for RSA recordings, 8–13 1-mm tantalum beads (X-medics, Sweden) were inserted in through a 4 mm cortical bone drill hole in each of the distal femoral and proximal tibial bones using a bead gun (Kulkanon, Wennbergs Finmek AB, Sweden). Beads were placed in a systematic pattern intending a wide-spread 3D marker distribution. Next, all specimens were disarticulated at the hip and ankle joints, and tissue on the proximal femoral and distal tibial bones was removed. After this, specimens were CT-scanned at 120 kVp, exposure 200 mAs, slice thickness 0.6 mm, slice increment 0.8 mm, and pixel spacing 0.29 × 0.29 mm, with the application of metal artifact reduction. From these scans, a 3D marker-model was generated and used for marker-based reference, defined as the marker-model method (MM).

2.2 | Experimental setup

A mobile fixture for the specimens was constructed for use during dRSA recordings (Figure 1). The proximal part of the femoral bone was fixed to a plywood board attached to the system with a mobile fitting, whereas the distal portion of the tibial bone was attached to a functional pedal with a crank arm of 10 cm. The vertical height of the femoral bone fixation could be adjusted to fit specimens of variable length. With the crank arm, the pedal had freedom of rotation around an axis in the medial-lateral direction. A rope was used to manually apply force to the pedal in an upward direction, making the specimens preform a standardized knee flexion motion in the range of 0–70°. Average angular velocity of knee flexion and extension was approximately 12 deg/s. The experimental setup simulated a weight-bearing step-up exercise used in clinical dRSA of the knee.[16,17]

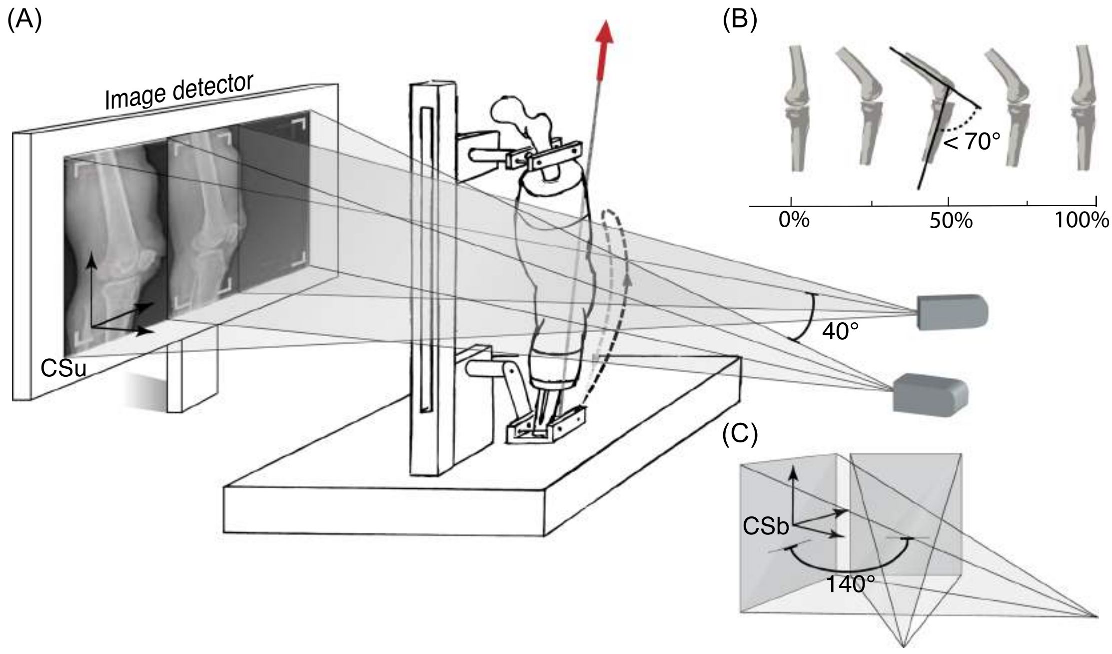

FIGURE 1 Illustration of mobile fixture and radiostereometric setup. (A) Uniplanar recording. Flat-panel image detectors were slotted in the detector panel behind the calibration boxes. Roentgen tubes were positioned at 40° relative to each other in both setups. The knee joint of the specimen was positioned at the crossing of roentgen beams to form stereo-images. The dashed line shows the path of movement during knee flexion when traction (arrow) was applied to the mobile mechanical fixture. (B) The movement pattern of the specimen during one simulated flexion exercise; flexion upon applied force (0%–50%) followed by passive extension against resistance (50%–100%). (C) Biplanar setup. Image detectors were positioned at 140° relative to each other. Roentgen tubes were focused on image detectors, still arranged at an intersection angle of 40° in the horizontal plane. CSu/CSb represent the position of coordinate systems in both the unipanar (CSu) and the biplanar (CSb) calibration setups [Color figure can be viewed at wileyonlinelibrary.com]

2.3 | Radiographic setup

Series of dRSA were recorded using a dedicated system (AdoraRSA; NRT X-Ray A/S, Hasselager, Denmark). The system uses two ceiling-mounted roentgen tubes and flat-panel detectors (CXDI-50RF, Canon Inc, Tokyo, Japan), with individual options for positioning. Recordings were made in both a uniplanar and a biplanar setup (Figure 1). For the uniplanar setup, the detectors were slotted behind a uniplanar calibration box (Carbon Box 14; Medis Specials, Leiden, The Netherlands). For the biplanar setup, the detectors were placed on a free stand and static images of a custom-made calibration phantom were taken following each recording. It was ensured that neither the roentgen tubes nor the detectors were touched during recording and subsequent calibration. The phantom was an acrylic cube containing 23 unique radiopaque beads (0.8 mm) at known locations. For both calibration setups, tubes were oriented at an angle of 40° to each other in the horizontal plane with a distance of 3200 mm from source to detectors and approximately 2400 mm from source to skin. The system was set to record with synchronized pulsed radiation at 15 frames per second with an exposure of 90 kVp, 600 mA and a resolution of 1104 × 1344 pixels for the dynamic recordings and 2208 × 2688 pixels for static biplanar calibration images. One trial per specimen was recorded in both the uniplanar and the biplanar calibration setup for a total of 16 trials.

2.4 | Analysis of radiographs

2.4.1 | Calibration

The first step in the analysis was to calibrate the resulting pairs of dynamic images for the individual setup. Each uniplanar recording was calibrated by identifying fiducial and control markers of the calibration box in a single processed image of averaged pixel intensity over the image sequence. The origin of the calibration box coordinate system was placed in the lower-left corner of the image (Figure 1A). The biplanar setup was calibrated by identifying the 23 beads of the phantom centered in the static RSA image. The identified beads and their known 3D grid configuration were input parameters for calibration in a custom-written program utilizing stereocalibration modules in OpenCV-Python (ver. 3.1.0.5).[18] The calibration output was the estimated relative pose of the two roentgen focal points and 2D RSA images, with the calibrated coordinate system centered and orientated with respect to the left image (Figure 1C).

2.4.2 | Bone model method

An automated custom software system of model-based analysis based on digitally reconstructed radiographs (DRR) was developed at our institution (AutoRSA software, Orthopaedic Research Unit, Aarhus, Denmark). The software is a graphics processing unit (GPU) accelerated and estimates the pose of bones from virtually generated projections using mathematical optimization algorithms as previously described in more detail.[19,20] A two-step analysis was used to first determine an initial pose using a global optimizer (Controlled Random Search with local mutations) at half image resolution and subsequently the pose was refined by a local optimizer (Nelder-Mead Simplex) at full resolution.[21,22] Registration used a local bounding box (BB) coordinate system based on the CT volume bone model (Figure 2C). The optimal pose was found by comparing the virtually generated DRR images to the dRSA images using the normalized gradient correlation.[19,23] Analysis requires the user to set the primary initialization by matching bone models to the initial image

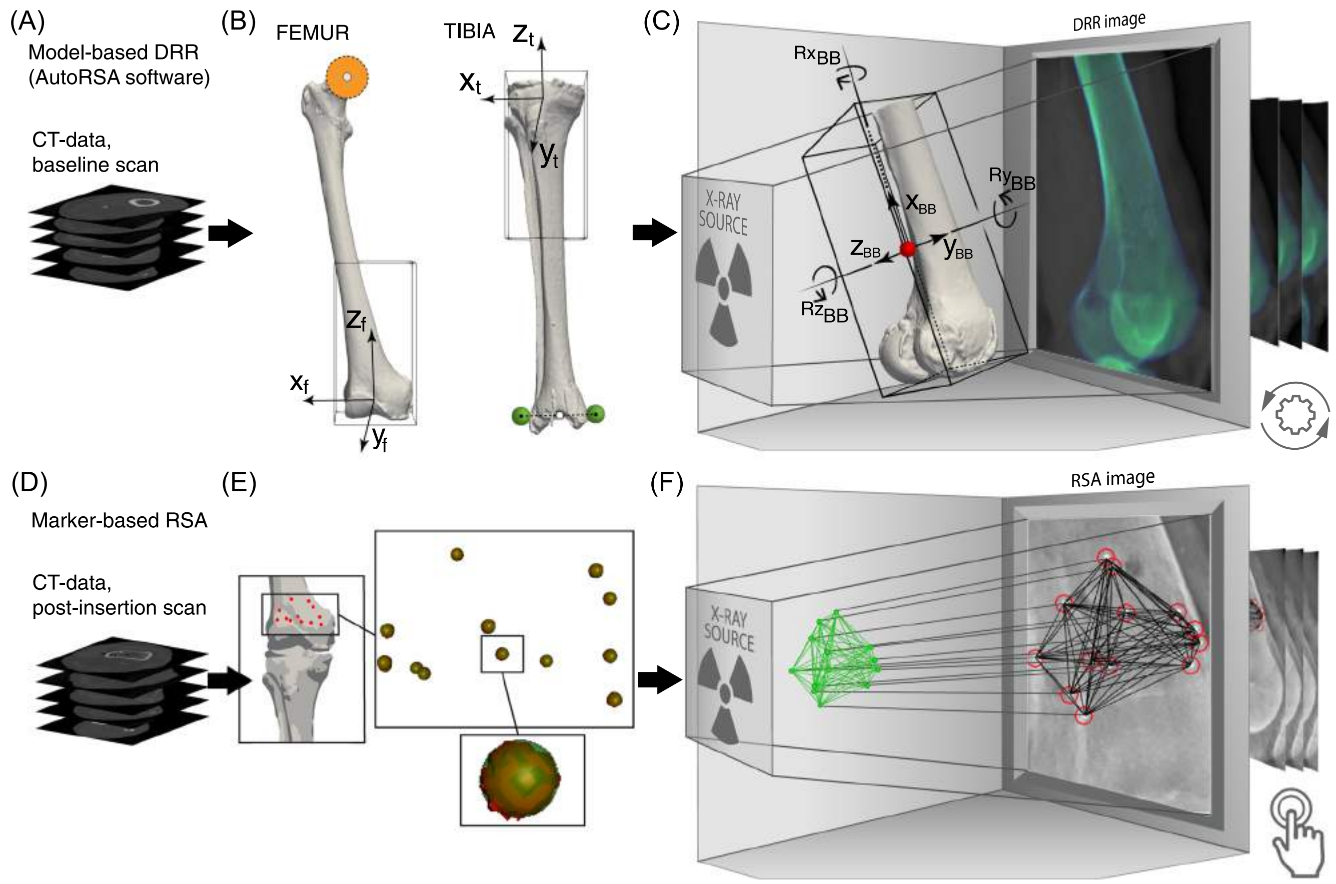

FIGURE 2 Overview of workflow for pose estimation using bone model-based DRR (A–C) and marker-based (D–F) methods. (A) Acquisition of baseline CT-data for segmentation and generation of CT volume bone models. (B) 3D bone models of femoral and tibial bones in frontal view including overlaid anatomical coordinate systems (ACS) with *x*-, *y*- and *z*-axes in medial-lateral, anterior–posterior, and proximal–distal direction, respectively. Anatomical landmarks were used for placing the *z*-axis in a modified version of Miranda et al:[24] Hip-center: a sphere was fitted to the femoral head from polygonal mesh data to mark the hip center (orange sphere). Ankle-joint center: medial and lateral malleolus were marked manually onto a digital 3D bone model surface (green spheres) and the midpoint of the trans-epicondylar line was defined to determine the ankle-joint center. (C) Process of bone model-based DRR tracking (BM) of the femoral bone on successive dRSA image frames in the AutoRSA software. The bounding box (BB) is outlined around the CT image volume. For the BB, the centroid was marked as the center point of diagonal intersection (red sphere) and a local BB coordinate system was assigned from this origin; the *x*-axis (x_{BB}) defined as the longest axis from origin to any BB-plane, the *y*-axis (y_{BB}), the second-longest, and *z*-axis (z_{BB}) the shortest. In AutoRSA, the DRR-match process was carried out by evaluating candidate poses generated from rotation and translation of the CT volume bone model (within BB) during virtual exposure, that is, applying individual rotation and translation from the BB coordinate system in each iteration. After initialization, the process of DRR pose estimation ran all images of the series automatically with no need for user interaction. (D) Acquisition of post-insertion CT-data containing tantalum beads within the bones. (E) 3D-rendering of a marker-model segmented from CT-data (red, uneven sphere) and fitted spheres (green, even sphere). For marker-based pose estimation, center coordinates of the fitted spheres were used, to obtain the remaining CT data from interpolation. (F) Marker-based tracking (MM) of a biplanar image (no calibration box markers) in MBRSA software; the image is identical to the one shown for DRR-registration in (C). The marker-model (green) is projected onto manually marked tantalum beads (red circles). After automatic detection, picking of markers and initial model-fitting was done manually for all images in the series. Note that DRR and RSA images are zoomed to show only the matching of the femoral bone in a single image of the paired radiographs. AutoRSA, local software, Orthopaedic Research Unit, Aarhus, Denmark; BB, bounding box; CT, computed tomography; DRR, digitally reconstructed radiographs; MBRSA, commercial software, RSAcore, Leiden, Netherlands; RSA, radiostereometric analysis [Color figure can be viewed at wileyonlinelibrary.com]

of the dRSA sequence. For each subsequent image, the software sets initialization on 3D extrapolation of trajectory based on previously solved images and analysis runs in an automated process. The hardware used was a desktop computer with a quad-core processor (Intel Xeon E5-1620, 3.60 GHz), 8 GB of DDR4 RAM, and a dedicated GPU (GeForce GTX 960, 4 GB GDDR5). The time to solve a single dual projection was approximately 3–4 min.

To quantify and describe relative rotation and translation of bone models in clinically relevant terms as defined in general biometrics, subject-specific ACS were assigned locally to each of the volumetric bone models generated from baseline CT-scans.[11,12] ACS was defined using a modified version of the system described by Miranda et al,[24] as the bone mechanical axis was used to define the proximal-distal axis (Figure 2B).

2.4.3 | Marker-model method

MBRSA software (RSAcore, ver. 4.2, Leiden University Medical Center, the Netherlands) was used for MM analysis. The accuracy and precision of this analysis are dependent on the marker configuration. The quality of the marker distribution can be considered by the condition number (CN).[25,26] With a commonly accepted maximum value of 130,[3] the mean CN for the femoral bone was 29 (range 23–33) and for the tibial bone, it was 25 (range 22–30). All beads were segmented from CT-data and a 3D surface model of beads was reconstructed. To this surface model, virtual spheres were fitted and center coordinates were used for MM analysis (Figure 2E). Images were extracted for every 2° of movement. Before optimization, two observers manually fitted the pose of the marker-model to the markers in the femoral and tibial bones appearing on the dRSA images. Optimization algorithms were used to optimize the pose of the marker-model in MBRSA software (DIFDoNLP)[27] (Figure 2F). Estimated time to solve a single dual projection was 25–30 min with manual bead marking and pose estimation being the most time-consuming tasks.

To quantify and describe the relative rotation and translation of marker-models using the ACS generated from the individual bone models, a transformation was required to account for alteration in the position of the specimen within the scanner since bone models were generated from baseline CT-scans and marker-models were generated from postinsertion CT-scans. This transformation was defined by superimposing and matching 3D image registrations of both scans using the Elastix toolbox for registration of images applying Normalized Mutual Information metrics.[28] This process was performed for each target bone region since the translation and rotation of the knee pose could not be assumed identical between scans.

2.4.4 | Dose calculations

Dose calculations were performed on real-time dRSA recordings of cadaveric legs. At an average of 172 ± 11 frames per recording, the calculated effective dose was 3.94 ± 0.25 µSv per dRSA recording in either setup. CT-scans added an additional 0.625 mSv of effective dose per scan. Thus, the calculated total efficient dose per specimen was 1.26 ± 0.01 mSv. The clinically relevant dosage per specimen was 0.63 ± 0.01 mSv, as only one CT-scan and one dRSA recording is required for clinical application.

2.5 | Data assessment and statistical considerations

The method agreement of the bone model-based DRR method (BM) of pose estimation in an automated software package (AutoRSA) was compared to the best available gold standard; a marker-model RSA method (MM) of pose estimation in semiautomated software. In this process, the pose was defined as absolute translation (mm) and rotation (°) of the 3D model, when the projection of either the bone model or the marker-model was matched to the observed 2D RSA images. To facilitate comparison, all resulting coordinates were transformed to the ACS.

Knee kinematics were evaluated as the relation between the pose of the femoral and tibial bones in each dRSA image. Thus, bias and precision of knee kinematic measurements were dependent on individual pose estimation of the femoral and tibial bones. Results were described in the knee joint coordinate system for kinematics as defined by Grood and Suntay (Figure 3).[12] To assess bias, the difference in kinematic measurements between the BM and MM method was calculated for all dRSA images included in the analysis, and bias was expressed as the mean of difference over all images in

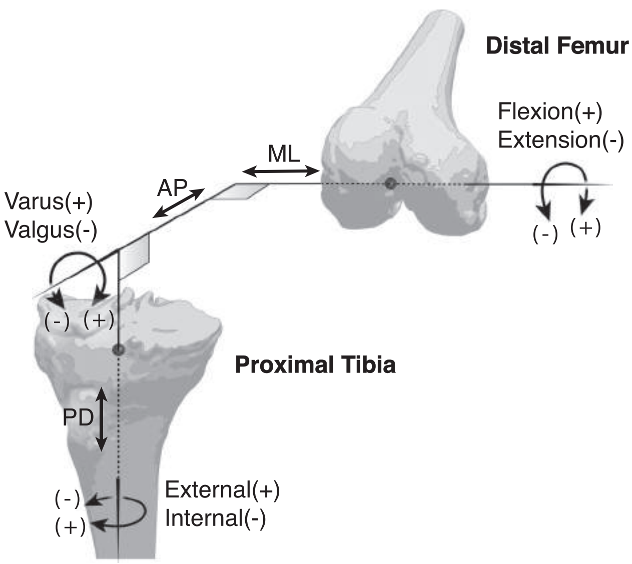

FIGURE 3 Knee joint coordinate system for description of kinematics. Modified from Grood and Suntay.[12] Pose of the femoral and tibial bones considered in relation to each other for kinematic assessment. Note all six degrees of freedom are present, that is, three translations (abbreviated) and three rotations (spelled out). AP, anterior–posterior axis; ML, medial-lateral axis; PD, proximal-distal axis

each radiographic setup. Precision was assessed by calculating the limits of agreement (LoA) of the mean difference.

The individual bone pose was evaluated for the femoral and tibial bones. The difference in pose estimation was calculated in all six degrees of freedom (DoF) for each dRSA image. In addition, the total difference in pose estimation was computed by the magnitude of the resultant vector for each image using the 3D Pythagorean theorem; $d_{total} = \sqrt{\Delta x^2 + \Delta y^2 + \Delta z^2}$, with x, y, and z denoting respective rotations and translations in bone ACS (Figure 2B). While not routinely used for angular measures, the theorem is allowed for small rotations.[1] The mean difference of pose estimation in six DoF (bias) and mean total difference (total bias) was calculated for all dRSA images included in the analysis in each radiographic setup. Precision was assessed by calculating LoA of the mean difference (bias) and mean total difference (total bias).

Radiographic setups were assessed by evaluating bias and precision for measurements of knee kinematics and individual bone pose in the two unique radiographic setup configurations; uniplanar and biplanar. Results were compared directly for clinical relevance.

For all three outcomes we evaluated method agreement in terms of (1) systematic error (bias) reported as the mean difference in mm and degrees with a 95% confidence interval (CI) and (2) random error (precision) defined by LoA and reported as the mean difference ±1.96 standard deviation, describing the interval in which 95% of differences were expected to fall.

The mean difference (bias) of the BM was compared against the null hypothesis of no difference from zero using a simple one-tailed *t test*. The significance level was set at 0.05. Statistical Software: Release 16.0/IC (StataCorp LLC, TX) was used for calculations, statistical comparisons, and visual representations.

3 | RESULTS

A total of 1520 radiostereometric images (760 uniplanar, 760 biplanar) were analyzed and included for statistical comparison of the automated CT model-based method (BM) and MM. The results in the text below refer to the uniplanar radiographic setup.

3.1 | Method agreement for knee kinematics

The agreement of the BM and MM analysis of knee kinematics in a dRSA recording of one cadaveric specimen during one knee flexion cycle is reported graphically as a general example (Figure 4). The plots show a high method agreement with a very small bias of the BM when compared to the MM. The agreement between BM and MM in knee joint kinematic assessment for all eight cadaveric specimens is demonstrated in Bland–Altman (BA) plots for the 6 DoF (Figure 5).[12,29] The bias and precision for each DoF are listed in a box within each plot (Figure 5). A systematic bias was found for the BM in all 6 DoF ($p < 0.001$); however, BM and MM were still in excellent agreement as bias ranged between −0.04 and 0.04° for all rotations and −0.19 to 0.18 mm for all translations. The poorest precision was ±0.42 mm for anterior–posterior translation and ±0.33° for external–internal rotation (Figure 3).

3.2 | Method agreement for individual bone pose estimation

Femoral bone poses for the BM in comparison to the MM showed a largest observed bias of −0.13 mm for translations and −0.19° for rotations, with precision within ±0.50 mm for translation in medial-lateral axis (Tx) and ±0.34° for rotation about anterior–posterior axis (Ry) (Table 1). Pose of the tibial bone had a bias up to 0.09 mm for translations and −0.21° for rotations, with a precision of ±0.38 mm and ±0.24° for translation in and rotation about the medial-lateral axis (Tx and Rx). Overall, the bias was lower and the precision better for the pose of the tibial bones compared with the femoral bones. Adding to this, less variation of mean total difference (total bias) for tibial bone translations compared to femoral bone translations were found when specimens were considered individually (Figure 6).

3.3 | Agreement of radiographic setup configuration

The biplanar setup was slightly less precise in determining kinematic flexion-extension with a bias of 0.11 mm and precision of ±0.31° compared to 0.03 mm and ±0.24° in the uniplanar setup (Figure 5). However, for external–internal rotation of specimens C and F, the BA plots showed a wider observation cluster in the uniplanar setup compared to the biplanar setup (Figure 5). Overall, no consistent effect on bias or precision of agreement of the BM was found to be caused by radiographic setup configuration (Table 1 and Figure 6).

4 | DISCUSSION

We validated an automated CT bone BM against a *gold standard* marker-model method (MM) for measurement of knee joint kinematics and bone pose estimation in dRSA recordings of cadaveric knees during a knee flexion exercise, in a uniplanar and biplanar radiographic setup. The key findings for evaluation of knee kinematics were a bias no larger than −0.19 mm and 0.11° for all translations and rotations, and precision within ±0.42 mm for translations and ±0.33° for rotations. For evaluation of bone pose estimation total bias was no higher than 0.30 mm and 0.27° with a precision better than ±0.27 mm and ±0.22° for translation and rotation of the femoral bone, and a similar but slightly better precision for the tibial bone. The bias and precision of the uniplanar and biplanar radiographic setup were comparable.

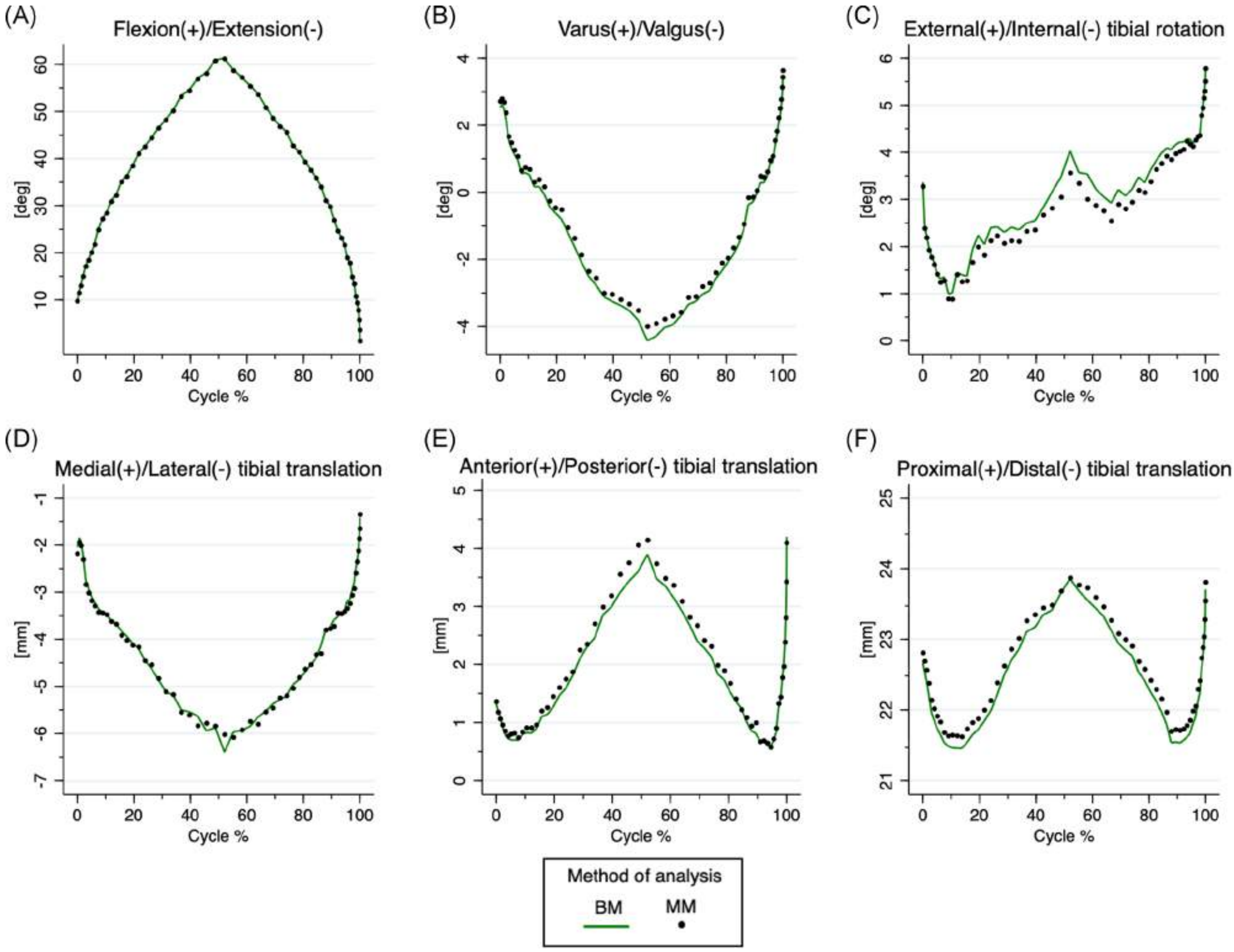

FIGURE 4 Difference during the movement cycle. A comparison between the bone model-based DRR method (BM, solid green lines) and the marker-model method (MM, black dots) for a single recording; Cadaver ID C, uniplanar calibration setup. (A–C) Rotations. (D–F) Translations. (Plots show a single representative recording, for graphs of all trials see supplementary Figures S1 and S2) [Color figure can be viewed at wileyonlinelibrary.com]

4.1 | Method agreement for knee joint kinematics

New methods of analysis should be validated against a gold standard reference, which should ideally be the true measure. In RSA, the best available reference traditionally used for a model-based analysis consists of a cluster of 1 mm tantalum markers surgically inserted into the bone of interest. Such a marker-model is very precise but not a true representation of the geometric structure of the bone undergoing analysis, and does not refer to the ACS. The coordinate system of marker-models must therefore be registered to the bone anatomy to provide a meaningful model of reference for the evaluation of dRSA with anatomical bone models.

Evaluation of knee joint kinematics by the use of CT bone models requires precise registration of the 3D bone models to the 2D bone projection in each successive dRSA image. Stentz-Olesen et al.[30] compared the registration of CT bone surface models to a marker-based method in 89 uniplanar dRSA images. They found similar bias for rotations and translations but inferior clinical precision when compared to the findings of the current study. For all kinematic measurements, clinical precision was found to be about three times as good as previously reported.[30] The surface models utilized by Stentz–Olsen et al[30] contain points in a surface-mesh derived only from compact bone CT-data. We use bone models generated from a volume rendering of CT-data, which include all voxels describing the bone matrix complex. Explanations for improved precision properly lie in the larger amount of data available within the volume model (more robust DRR pose estimation) and large sample size ($n = 760$). In the present study, BA plots showed noticeable clustering of observations for each cadaveric specimen, indicating some influence of specimen properties on method agreement. Variation of observations within each specimen cluster was small which further interprets as a good precision for the BM.

Bey et al[31] applied DRR pose estimation of CT bone volume models to the patellofemoral joint, estimating the pose of the patella

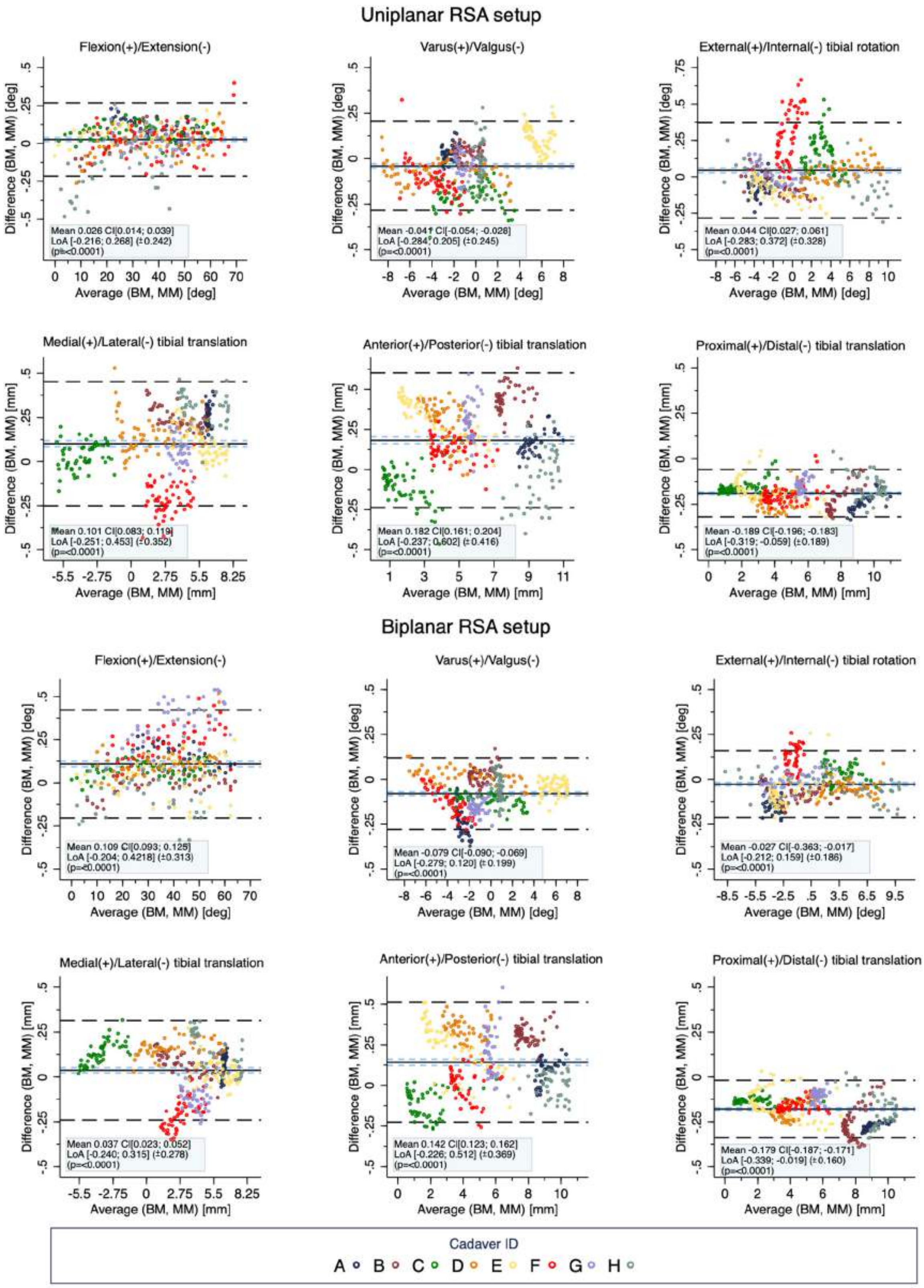

FIGURE 5 Bland–Altman (BA) plots for kinematic measurements in uniplanar and biplanar calibration setups. Scatters demonstrate the agreement between methods of measurement, bone model-based DRR method (BM) versus marker-model method (MM). For all individual observations, points on the plot are identified at (*x*, *y*); (difference between two values, average of two values). The solid black horizontal line represents the mean difference (bias) of all observations plotted, dashed blue lines show CI of the mean differences, and dashed black lines show precision (LoA). The agreement interval is set at mean ± 1.96 SD as defined by Bland and Altman.[29] Upper six BA plots demonstrate agreement between methods in six degrees of freedom (three rotational and three translational) based on data acquired in a uniplanar radiostereometric setup. Lower six BA plots demonstrate agreement based on data acquired in a biplanar setup. The textbox within each subplot presents mean difference (bias), CI of mean difference, and LoA boundaries with clinical precision in parenthesis. A–H are donor specimens. CI, confidence interval; LoA, limits of agreement [Color figure can be viewed at wileyonlinelibrary.com]

relative to the femoral bone in biplane dRSA of cadaveric knee specimens. The small size of the patella puts a biological limit to the amount of volume data available for DRR-based analysis, yet the reported bias was comparable to the findings of the current study, although the random error of dRSA recordings was not reported. Anderst et al[8] compared DRR pose estimation of CT volume bone models to a CT marker-based registration in high-speed biplanar fluoroscopy using a radiographic image resolution of 512 × 512 pixels. They obtained bias for translations and rotations inferior to the results presented in the current study. We suggest that this finding shows how the accuracy of DRR-based analysis is related to radiographic image resolution and quality. Furthermore, the movement velocity of analyzed objects being analyzed was markedly lower in the current study compared with Anderst et al,[8] suggesting that movement velocity could affect accuracy due to within-image blur.

4.2 | Method agreement for individual bone pose

The precision of DRR-based methods depends on the capability of the system to effectively estimate the pose of unique 3D objects from their representation in successive 2D RSA images. Since bones are patient-specific and vary in several parameters such as size, density, and geometry, it is important that the DRR-system is consistent in precision across the registration of individual bone models. Stentz–Olesen et al[30] reported lower bias in pose estimation of the

TABLE 1 Bias of bone model DRR method for individual bone pose estimation

	Translation precision (mm)					Rotational precision (°)				
	Tx	Ty	Tz	Total[a]	*p value*	Rx	Ry	Rz	Total	*p value*
Uniplanar (*n* = 380)										
Femoral bone										
Mean difference	−0.125*	−0.107	−0.085	0.302	<.001	−0.191	−0.026	−0.015	0.273	<.001
±95% CI[b]	0.026	0.011	0.010	0.010		0.012	0.008	0.007	0.016	
SD[c]	0.252	0.101	0.932	0.099		0.120	0.174	0.071	0.114	
±LoA[d]	0.495	0.198	0.183	0.195		0.236	0.341	0.139	0.223	
Tibial bone										
Mean difference	0.094	0.055	0.054	0.226	<.001	−0.211	0.035	−0.003*	0.267	<.001
±95% CI	0.019	0.009	0.004	0.010		0.013	0.011	0.007	0.009	
SD	0.191	0.888	0.037	0.097		0.124	0.110	0.072	0.084	
±LoA	0.375	0.174	0.074	0.191		0.243	0.216	0.141	0.165	
Biplanar (*n = 380*)										
Femoral bone										
Mean difference	0.055	0.066	−0.536	0.227	<.001	−0.126	−0.038	−0.004*	0.198	<.001
±95% CI	0.021	0.011	0.011	0.014		0.014	0.014	0.006	0.011	
SD	0.199	0.100	0.099	0.136		0.140	0.105	0.055	0.105	
±LoA	0.392	0.196	0.195	0.267		0.270	0.206	0.107	0.206	
Tibial bone										
Mean difference	0.106	0.129	0.167	0.304	<.001	−0.232	0.051	−0.054	0.278	<.001
±95% CI	0.019	0.007	0.005	0.009		0.013	0.010	0.008	0.011	
SD	0.191	0.071	0.044	0.839		0.120	0.093	0.073	0.102	
±LoA	0.375	0.135	0.086	0.165		0.236	0.186	0.143	0.201	

Note: n Indicates the number of matched images.

Abbreviations: CI, confidence interval; LoA, limits of agreement.

[a]Mean total difference (total bias) for all specimens, approximated using the Pythagorean theorem.

[b]±95% CI of mean difference.

[c]SD of mean difference.

[d]±LoA set at 1.96 SD; 95% predicted clinical precision.

*Mean difference not different from zero (one-tailed *t test*).

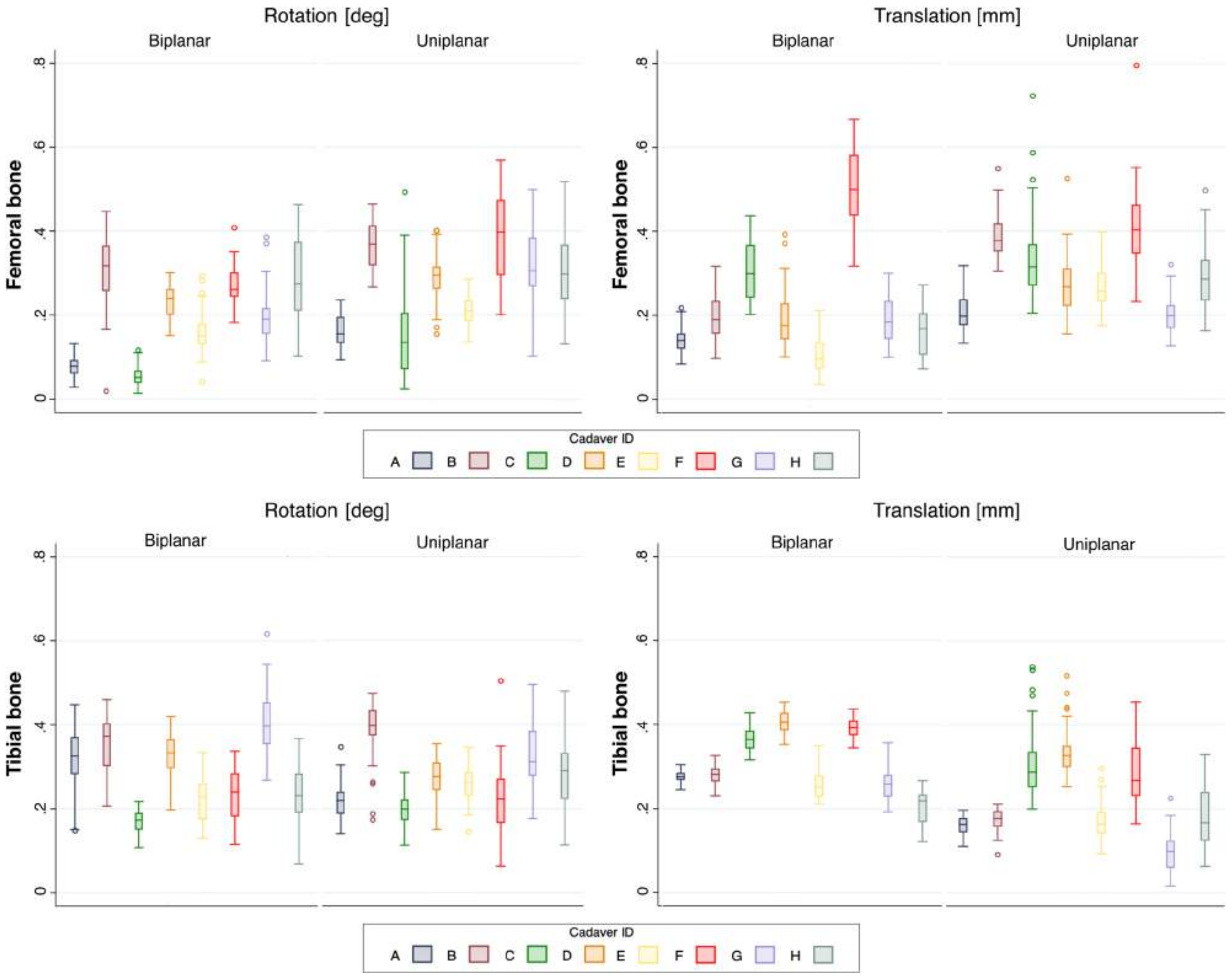

FIGURE 6 Total bias of the bone model DRR method (BM) in the pose of the femoral (top) and tibial bone (bottom). The mean total difference (total bias) for rotations and translations were computed using the Pythagorean theorem for all individual recordings. Uniplanar and biplanar recordings are shown side-by-side for comparison. Boxes are drawn from the 25th percentile (lower hinge) to the 75th percentile (upper hinge). Whiskers extend to upper and lower adjacent values and contain all values not considered outliers. A–H are donor specimens. DRR, digitally reconstructed radiographs [Color figure can be viewed at wileyonlinelibrary.com]

femoral bone against pose estimation of the tibial bone in both translations and rotations. Generally, we found lower bias in all individual pose estimation measurements, and interestingly, and we found pose estimation of the tibial to be more precise than for the femoral bone. No obvious explanation for this finding is evident. The distal femoral bone generally presents more features for DRR-matching than the proximal tibial bone, which should result in a more robust analysis. Supposedly, this finding could simply represent random variation in measurements if methods compared were assumed of equal precision for individual bone pose estimation.

Hansen et al (reference 19) compared software-automated DRR pose estimation of CT volume bone models to marker-based RSA in the assessment of joint kinematics in seven cadaveric hip joints. In DRR-analysis based on the proximal femoral bones, they reported precision for translations and rotations comparable to the findings of the current study.[19] This underlines the general usefulness of the bone model-based DRR method across anatomy and bone geometry.

4.3 | Method agreement for radiographic setup configuration

No obvious trend was observed in bias or precision when comparing results between uniplanar and biplanar setup configurations. Because reported research on DRR-based analysis shows much variation in test protocols, comparison of our results of setup configurations to the literature was not possible nor appropriate. Theoretically, the RSA image pair obtained from biplane projections should show more features and geometric characteristics than the RSA image pair from uniplanar detectors, thus facilitating DRR pose estimation. However, we found no clinically relevant difference in bias and precision of the DRR method when comparing results obtained in either setup.

4.4 | Limitations and strengths

To our knowledge, no other study has evaluated an automatic method of DRR-based assessment of knee joint kinematics against the gold standard of marker-based RSA.

Defining and placing ACS is essential for all BM and MM measurements. The present study compared results based on the unique bony structures of a cohort of eight cadaveric knee joints in two radiographic setup configurations with a large image sample-size. Condition-numbers ensured a high-quality MM reference. We used previously validated methods of placing ACS based on bone geometry.[24,32] Results from the BM are expressed in clinically relevant terms through inheritance use of ACS. When determining the difference between methods, the same ACS is used for the MM reference, since an application of different ACS would have impaired direct comparison of the two methods, BM and MM. The BM offered a close to ten-fold reduction in time taken to analyze resultant images when compared to the MM.

Our study has several limitations. First, a margin of error lies within the registration of the marker positions for the generation of the 3D marker-model used for MM reference. The segmentation of beads is susceptible to missing CT-data, wherefore beads were not necessarily scanned in the exact plane of the bead center coordinate, needed for the marker-model. True bead center coordinate was estimated by fitting virtual spheres to the surface models of beads to obtain remaining bead CT-data from interpolation. Second, biplanar calibration images were acquired separately after each recording. Thus, a small risk of error from disturbing the setup during the acquisition of static phantom calibration images cannot be ruled out. Third, possible influence of having the opposite leg crossing into the field of view in a clinical setting was not examined; however, with the investigated setups we do not experience this to be a problem in the clinical setting. Additionally, dynamic calibration images for the uniplanar setup were of a lower resolution than the static images used for biplanar calibration. It is not known what effect these parameters might have had on the results.

Although highly accurate, marker-based models are equally dependent on the quality of source material and prone to prove faulty under the same circumstances as would the model-based DRR method. Essentially, there is a need for an independent gold standard to perform a test of the absolute accuracy of the model-based DRR method. This effect inevitably becomes more evident as new methods to be validated become increasingly accurate. If methods compared are equally accurate, comparison and evaluation of bias and precision becomes entirely dependent on random variation in measurements.

5 | CONCLUSION

The AutoRSA software package offers an automated and fast noninvasive method of measuring knee joint kinematics and individual bone positioning from dynamic radiostereometric recordings. Bias and precision of the automated method were found to be well within the limits of clinical relevance, and further, it was not found to be sensitive to alteration in configuration of the radiographic setup. The new automatic method is clinically applicable for functional evaluation of native knee joint kinematics and pathomechanics related to conditions, such as ligament instability and bone dysplasia, as well as in the assessment of surgical results.

CONFLICT OF INTERESTS

The authors declare that there are no conflict of interests.

FOUNDING STATEMENTS

This study was supported by The Orthopaedic Research Found at Aarhus University Hospital and the A. P. Møller Foundation.

AUTHOR'S CONTRIBUTIONS

Rasmus Christensen was involved in all aspects of the study and drafted the manuscript. Emil Toft Petersen had an essential role in the study design, RSA analysis, interpretation, and presentation of data. Jonathan Jürgens-Lahnstein and Søren Rytter assisted in data collection, data analysis, and interpretation of data and results. Sepp De Raedt assisted in data analysis. Maiken Stilling made substantial contribution in the study design, data collection and interpretation of data and results. Lars Lindgren contributed to study design and data collection. Annemarie Brüel contributed to the study design and acquisition of cadaveric specimens. All authors revised and approved the final manuscript.

ORCID

Rasmus Christensen http://orcid.org/0000-0002-0704-8934

REFERENCES

1. Selvik G. Roentgen stereophotogrammetry. A method for the study of the kinematics of the skeletal system. *Acta Orthop Scand Suppl*. 1989;232:1-51.
2. Kärrholm J. Roentgen stereophotogrammetry: review of orthopedic applications. *Acta Orthop Scand*. 1989;60:491-503.
3. Valstar ER, Gill R, Ryd L, Flivik G, Börlin N, Kärrholm J. Guidelines for standardization of radiostereometry (RSA) of implants. *Acta Orthop*. 2005;76:563-572.
4. Valstar ER, de Jong FW, Vrooman HA, Rozing PM, Reiber JHC. Model-based Roentgen stereophotogrammetry of orthopaedic implants. *J Biomech*. 2001;34:715-722.
5. Kaptein BL, Valstar ER, Stoel BC, Rozing PM, Reiber JHC. A new model-based RSA method validated using CAD models and models from reversed engineering. *J Biomech*. 2003;36:873-882.
6. Kaptein BL, Valstar ER, Spoor CW, Stoel BC, Rozing PM. Model-based RSA of a femoral hip stem using surface and geometrical shape models. *Clin Orthop Relat Res*. 2006;448:92-97.
7. You B, Siy P, Anderst W, Tashman S. In vivo measurement of 3-D skeletal kinematics from sequences of biplane radiographs: application to knee kinematics. *IEEE Trans Med Imaging*. 2001;20:514-525.
8. Anderst W, Zauel R, Bishop J, Demps E, Tashman S. Validation of three-dimensional model-based tibio-femoral tracking during running. *Med Eng Phys*. 2009;31:10-16.
9. Komistek RD, Dennis DA, Mahfouz M. In vivo fluoroscopic analysis of the normal human knee. *Clin Orthop Relat Res*. 2003;410:69-81.

10. Mahfouz MR, Hoff WA, Komistek RD, Dennis DA. A robust method for registration of three-dimensional knee implant models to two-dimensional fluoroscopy images. *IEEE Trans Med Imaging*. 2003;22:1561-1574.
11. Wu G, Siegler S, Allard P, et al. International Society of Biomechanics. ISB recommendation on definitions of joint coordinate system of various joints for the reporting of human joint motion—part I: ankle, hip, and spine. *J Biomech*. 2002;35:543-548.
12. Grood ES, Suntay WJ. A joint coordinate system for the clinical description of three-dimensional motions: application to the knee. *J Biomech Eng*. 1983;105:136-144.
13. Krčah M, Székely G, Blanc R 2011. Fully automatic and fast segmentation of the femur bone from 3D-CT images with no shape prior. Proceedings, IEEE International Symposium on Biomedical Imaging: From Nano to Macro. https://doi.org/10.1109/ISBI.2011.5872823. Available from: http://xplorestaging.ieee.org/document/5872823
14. de Raedt S, Mechlenburg I, Stilling M, Rømer L, Søballe K, de Bruijne M. Automated measurement of diagnostic angles for hip dysplasia. *Proceedings of SPIE, the International Society for Optical Engineering*. 2013:8670.
15. Boykov Y, Funka-Lea G. Graph Cuts and Efficient N-D Image Segmentation. *Int J Comput Vis*. 2006;70:109-131.
16. Horsager K, Kaptein BL, Rømer L, Jørgensen PB, Stilling M. Dynamic RSA for the evaluation of inducible micromotion of Oxford UKA during step-up and step-down motion. *Acta Orthop*. 2017;88:275-281.
17. Horsager K, Kaptein BL, Jorgensen PB, et al. Oxford medial unicompartmental knees display contact-loss during step-cycle motion and bicycle motion: A dynamic radiostereometric study. *J Orthop Res*. 2018;36:357-364.
18. Bradski G. The OpenCV Library. *Dr. Dobb's J Software Tools*. 2000;25:120-125.
19. Hansen L, de Raedt S, Jørgensen PB, Mygind-Klavsen B, Kaptein B, Stilling M. Marker free model-based radiostereometric analysis for evaluation of hip joint kinematics: a validation study. *Bone Joint Res*. 2018;7:379-387.
20. Hemmingsen CK, Thillemann TM, Elmengaard B, et al. Elbow biomechanics, radiocapitellar joint pressure, and interosseous membrane strain before and after radial head arthroplasty. *J Orthop Res*. 2020;38:510-522.
21. Kaelo P, Ali MM. Some variants of the controlled random search algorithm for global optimization. *J Optim Theory Appl*. 2006;130:253-264.
22. Nelder JA, Mead R. A simplex method for function minimization. *Comput J*. 1965;7:308-313.
23. van der Bom IMJ, Klein S, Staring M, et al. 2011. Evaliation of optimization methods for intensity-based 2D-3D registration in x-ray guided interventions. Proceedings, SPIE, Medical Imaging: Image Processing 796223. https://doi.org/10.1117/12.877655.
24. Miranda DL, Rainbow MJ, Leventhal EL, Crisco JJ, Fleming BC. Automatic determination of anatomical coordinate systems for three-dimensional bone models of the isolated human knee. *J Biomech*. 2010;43:1623-1626.
25. Ryd L, Yuan X, Lofgren H. Methods for determining the accuracy of radiostereometric analysis (RSA). *Acta Orthop Scand*. 2000;71:403-408.
26. Söderkvist I, Wedin P-Å. Determining the movements of the skeleton using well-configured markers. *J Biomech*. 1993;26:1473-1477.
27. Kaptein BL, R Valstar E, Stoel BC, Rozing PM, Reiber JHC. Evaluation of three pose estimation algorithms for model-based roentgen stereophotogrammetric analysis. *Proc Inst Mech Eng H*. 2004;218:231-238.
28. Klein S, Staring M, Murphy K, Viergever MA, Pluim J. Elastix: a toolbox for intensity-based medical image registration. *IEEE Trans Med Imaging*. 2010;29:196-205.
29. Bland JM, Altman DG. Statistical methods for assessing agreement between two methods of clinical measurement. *The Lancet*. 1986;327:307-310.
30. Stentz-Olesen K, Nielsen ET, de Raedt S, et al. Validation of static and dynamic radiostereometric analysis of the knee joint using bone models from CT data. *Bone Joint Res*. 2017;6:376-384.
31. Bey MJ, Kline SK, Tashman S, Zauel R. Accuracy of biplane x-ray imaging combined with model-based tracking for measuring in-vivo patellofemoral joint motion. *J Orthop Surg Res*. 2008;3:38.
32. Nielsen ET, Stentz-Olesen K, de Raedt S, et al. Influence of the anterolateral ligament on knee laxity: a biomechanical cadaveric study measuring knee kinematics in 6 degrees of freedom using dynamic radiostereometric analysis. *Orthop J Sports Med*. 2018;6:232596711878969.

SUPPORTING INFORMATION

Additional Supporting Information may be found online in the supporting information tab for this article.

How to cite this article: Christensen R, Petersen ET, Jürgens-Lahnstein J, et al. Assessment of knee kinematics with dynamic radiostereometry: Validation of an automated model-based method of analysis using bone models. *J Orthop Res*. 2020;1–12. https://doi.org/10.1002/jor.24875

Paper II

Evaluation of automated radiostereometric image registration in total knee arthroplasty utilizing a synthetic-based volumetric implant model and a CT-based volumetric bone model

E.T. Petersen[1-3], T.D Vind[2,3], J.H. Jürgens-Lahnstein[2,3], R. Christensen[2,3], S. de Raedt[3], A. Brüel[5], S. Rytter[2-4], M.S. Andersen[6], M. Stilling[2-4]

[1] *University Clinic for Hand, Hip and Knee Surgery, Holstebro Central Hospital, 7500 Holstebro, Denmark*
[2] *Department of Clinical Medicine, Aarhus University, 8200 Aarhus N, Denmark*
[3] *AutoRSA Research Group, Orthopaedic Research Unit, Aarhus University Hospital, 8200 Aarhus N, Denmark*
[4] *Department of Orthopaedic Surgery, Aarhus University Hospital, 8200 Aarhus N, Denmark*
[5] *Department of Biomedicine, Aarhus University, 8000 Aarhus C, Denmark*
[6] *Department of Materials and Production, Aalborg University, 9220 Aalborg, Denmark*

A B S T R A C T

Radiostereometic analysis (RSA) is an accurate method for rigid body pose (position and orientation) in three-dimensional space. Traditionally, RSA is based on insertion of periprosthetic tantalum markers and manual implant contour selection which limit clinically application. We propose an automated image registration technique utilizing digitally reconstructed radiographs (DRR) of computed tomography (CT) volumetric bone models (*autorsa-bone*) as a substitute for tantalum markers. Furthermore, an automated synthetic volumetric representation of total knee arthroplasty implant models (*autorsa-volume*) to improve previous silhouette-projection methods (*autorsa-surface*). As reference, we investigated the accuracy of implanted tantalum markers (*markers*) or a conventional manually contour-based method (*mbrsa*) for the femur and tibia. The *autorsa-bone* method displayed similar accuracy compared to the gold standard. The *autorsa-volume* did not markedly improve the *autorsa-surface*, and none of these reached the *mbrsa* method. In conclusion, marker-free RSA is feasible with similar accuracy as gold standard utilizing DRR and CT obtained volumetric bone models. Furthermore, utilizing synthetic generated volumetric implant models could not improve the silhouette-based method. However, with a slight loss of accuracy the autorsa methods provide a feasible automated alternative to the semi-automated method.

Introduction

Knee Radiostereometric analysis (RSA) can quantify rigid body pose (position and orientation) in three-dimensional space utilizing a calibrated setup with two crossing x-ray beams, which produce radiographic images from different views.[1,2] Owing to submillimeter accuracy and precision, the RSA technique is widely used to evaluate longitudinal fixation of hip and knee implants as an early surrogacy marker for later aseptic implant loosening.[3–5] Originally, RSA utilized tantalum markers attached on the investigated implants before surgery and inserted into the periprosthetic bone during surgery. There are several downsides to implant marking including expense, need for new regulatory approval of the implants, and a possible influence on fixation.[6] Next, a commercially available RSA method utilizing implant models was introduced and allowed implant tracking without implant-embedded markers at the expense of a slight loss of accuracy.[6,7] Today, this method still requires insertion of periprosthetic tantalum markers and manual implant contour selection in RSA images. Although RSA is a recommended safety measure for fixation of new implants, the requirement for beads as bone reference and lack of full analysis automatization restricts a general use of RSA for monitorization of implant loosening.[1,5,8]

Three-dimensional bone models obtained from computed tomography (CT) has proven to be accurate for two- to three-dimensional (2D/3D) image registration and may replace periprosthetic tantalum markers as reference in RSA.[9] CT scans can be conducted postoperatively and permit RSA migration analysis in any patient. 2D/3D image registration techniques often use intensity or gradient measures to match silhouette projections or digitally reconstructed radiographs (DRR).[9–18] Consequently, these methods are highly dependent on the geometrical shape, the intensities, and contrast to withhold the high accuracy. Theoretically, the registration may be affected by radiopaque metal implants and removal of bone, in terms of reduced bone model geometry and registration information, during insertion of implant components.[12] Previous attempts to replace the markers as reference have not demonstrated feasible results.[19,20]

The current 2D/3D image registration techniques of implants are utilizing silhouette-projections of triangulated surface models and do not reach the accuracy of the marker-method.[7,15–18,21–23] A synthetic volumetric representation of the implant with constant voxel values within the surface-shell may improve the image registration accuracy utilizing DRR registration.

The purpose of this *In vitro* study was to investigate the pose accuracy of implant components from total knee arthroplasty and tibial and femoral bone models from CT scans using silhouette-projections and digitally reconstructed radiographs. As reference, we investigated the accuracy of implanted tantalum markers in the femur and tibia.

Methods

This study utilized eight fresh-frozen donor legs including the hemi-pelvis; male:female ratio 1:1, ages 80–93 (mean 85 years). Relevant approvals were obtained from the Central Denmark Committee on Biomedical Research Ethics (case number 1-10-72-236-19, issued November 21st, 2019), and the Data Protection Agency (case number 1-16-02-410-19, issued December 2nd, 2019).

Preparation and surgical procedure

Before surgery, the knee of each specimen was CT scanned (SOMATOM Definition Flash; Siemens Healthcare, Erlangen, Germany) including 15 cm proximal and distal to the joint line. The scans were carried out using a standard protocol with axial slices at a peak voltage of 120 kVp and exposure of 183 mAs, slice thickness of 0.6 mm, slice increment of 1 mm and pixel spacing of 0.29 × 0.29 mm. The effective dose of the CT was estimated to 0.095 mSv. Subsequently, all specimens were disarticulated at the hip and ankle joints and the proximal femoral and distal tibial bone were dissected for soft tissue to ensure a rigid fixation of the specimen. Approximately 8-13 tantalum beads (X-medics, Sweden) were inserted through a 4 mm drill hole in the cortical bone of the distal femoral and proximal tibial bones using a bead gun (Kulkanon, Wennbergs Finmek AB, Sweden). Beads were placed in a systematic pattern intending a wide-spread 3D marker distribution. We used a standard operative total knee arthroplasty procedure according to the manufacturer's guidelines[24] with an anterior midline incision and medial parapatellar arthrotomy. All specimens received the cemented (Palacos®R+G, Heraeus, Medial GmbH, 61273, Wehrheim, Germany) Triathlon® Knee System (Stryker, Kalamazoo, MI, USA) for the femur, tibia, and patella. One experienced knee arthroplasty surgeon performed the surgical procedures on all specimens.

Table 1 Overview of the radiostereometric analysis methods.

Name	Software	Method	Description	Illustration
marker	MBRSA	Hugh circle detector	The actual marker projections were detected using Hugh circle detector based on manually applied parameters. **Marker-method**: utilizing the actual markers on the stereoradiographs to estimate a 3D position of each marker by minimizing the crossing-line-distance of the marker for each view. **Marker-configuration model**: utilizing a predefined 3D marker-model estimating its 3D pose by minimizing the difference between its projected marker positions and the actual markers on the stereoradiographs.	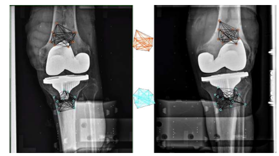
mbrsa	MBRSA	Canny edge detector	Contours were automatically detected in the stereoradiographs by canny edge detection based on manually applied parameters and region of interest. From these the relevant contours of the object of interest were manually selected. Coarser to finer optimization algorithms were applied to estimate the poses by minimizing the error between the virtual projections of the bone models and the manually selected contours.	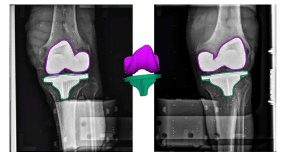
autorsa-surface	AutoRSA	Silhouette-projection	This automated image registration method utilizes silhouette-projection of surface models that are matched to the actual object silhouette-projection using Sobel edge detection algorithm. The similarity metric was determined as the average of the horizontal and vertical gradients normalized cross-correlation between the actual stereoradiographs and the virtually generated projections. Coarser to finer optimization algorithms and image resolution were applied and an automated mask image were used to determine region of interest.	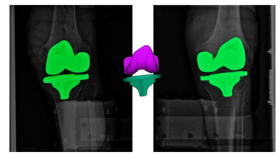
autorsa-volume	AutoRSA	Digitally reconstructed radiographs	This automated image registration method utilizes digitally reconstructed radiographs of synthetic generated volumetric models that are matched to the actual object stereoradiographs using Sobel edge detection algorithm. The similarity metric was determined as the average of the horizontal and vertical gradients normalized cross-correlation between the actual stereoradiographs and the virtually generated projections. Coarser to finer optimization algorithms and image resolution were applied and an automated mask image were used to determine region of interest.	
autorsa-bone	AutoRSA	Digitally reconstructed radiographs	This automated image registration method utilizes digitally reconstructed radiographs of CT-based volumetric models that are matched to the actual object stereoradiographs using Sobel edge detection algorithm. The similarity metric was determined as the average of the horizontal and vertical gradients normalized cross-correlation between the actual stereoradiographs and the digitally reconstructed radiographs. Coarser to finer optimization algorithms and image resolution were applied and an automated mask image were used to determine region of interest and excluding the other implant.	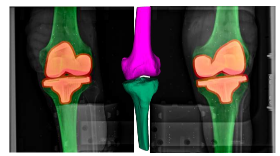

Abbreviations: MBRSA – Model-Based RSA (RSAcore, Leiden, the Netherlands); AutoRSA – AutoRSA software, Orthopedic Research Unit, Aarhus, Denmark; 3D – three-dimensional; CT – computed tomography

Radiographic setup

The stereoradiographs were recorded utilizing a dedicated RSA system (AdoraRSA; NRT X-Ray A/S, Hasselager, Denmark). The system uses two ceiling-mounted x-ray tubes positioned vertically with an inter-tube angle of 40 degrees and a source-to-image distance of 160 cm. The flat panel detectors (CXDI-50RF, Canon Inc., Tokyo, Japan) were embedded in a uniplanar calibration cage (Box 24, Medis Specials, Leiden, Netherlands) containing a fiducial and control layer. In single-image mode, we acquired full detector-size images dimensioned 2,208 x 2,668 pixels with a quadratic pixel width of 0.16 mm using exposure settings of 120 kVp and 1.2 mAs. The dose of one stereoradiograph was estimated to 0.623μSv (Figure 1).

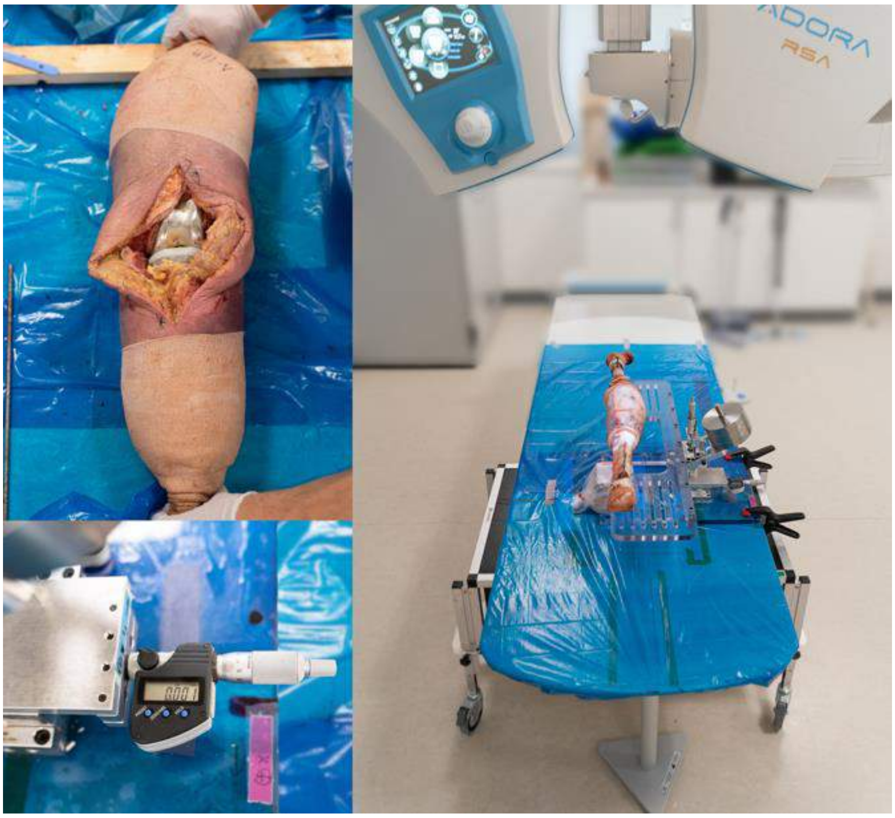

Figure 1 Illustration of the total knee arthroplasty knee before closure, the radiostereometric setup, and a closeup of the micrometer.

Experimental protocol

A customized fixture with an axial movable plexiglass plate was built and ensured rigid fixation of the knee specimen (Figure 1). Accommodating optimal radiographic imaging, a hole was cut out of the plexiglass at the knee level, ensuring free passage of the x-ray beams. We moved the plate in three directions (x, y, z) using digital dial micrometers, each with a resolution of 0.001 mm (Hofmann GmbH, Achim, Germany). The fixture was oriented approximately orthogonal to the reference frame of the RSA setup (calibration cage). First, the knee was positioned anterior-posterior (AP), replicating a patient in a supine position. Second, the knee was positioned in a lateral-medial (LM) view to investigate influence of different view. Recordings were obtained in all directions (x, y, z) at 16 positions. Each series included five recordings at baseline. Second, two recordings were obtained each at 10, 20, 30, 40, 50, 100, 200, 300, 400, 500, 1000, 2000, 3000, 4000, 5000 micrometers. The corresponding measured displacement was established by the difference between the median of the estimated positions at baseline and the corresponding estimated position. The error was determined by subtracting the actual (micrometer) displacement from measured (RSA) displacement.

Analysis of the stereoradiographs

The purpose of RSA was to find 3D spatial measures from 2D projective images to a 3D object. One marker-based (marker) method represented the gold standard of RSA, and four model-based (*mbrsa*, *autorsa-surface*, *autorsa-volume*, and *autorsa-bone*) methods were evaluated (Table 1). We utilized manufacturer-provided computer-aided design models representing the 3D surface models of the femur and tibia implants in all sizes for three of the model-based methods (*mbrsa*, *autorsa-surface*, and *autorsa-volume*). For the *autorsa-*

volume method, we constructed a synthetic volumetric representation of each implant model by assigning the voxels in a 3D isometric volume image inside the surface of the implant model to a value of 3000 and outside values to zero (Figure 2). The volume images with voxel spacing of 0.4x0.4x0.4 were centralized, oriented, and dimensioned according to the implants coordinate systems and bounding boxes using visualization Toolkit (Kitware). For the fourth method (*autorsa-bone*), we obtained volumetric image models from the preoperative CT-scan. Each bone model were identified and extracted individually using a fully automated graph-cut segmentation method.[25–27]

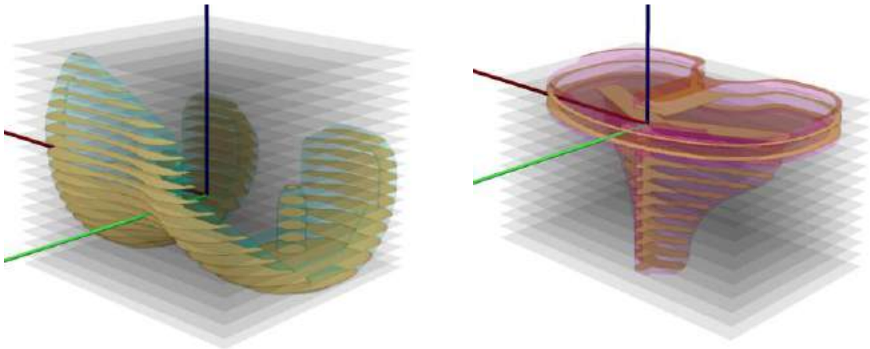

Figure 2 Illustration of the synthetic generated volumetric models. The voxels with the high intensity assigned value of 3000 are represented with the copper-color at each slice. A transparent representation of the surface models is superimposed in each of the volume images to illustrate the outline of the models. Low-resolution volumetric models (slice thickness of 3 mm compared with 0.4 mm) are presented for visualization.

We performed individualized calibration on all stereoradiographs by identifying the fiducial and control markers embedded in the calibration cage using the commercially available software Model-Based RSA (RSAcore, Leiden, The Netherlands). The fiducial markers were used to calculate the focal points of the x-ray sources. All methods were analyzed using the same stereoradiographs making the calibration identical between methods. Hence, the observed differences in displacement between methods was not influenced by the calibration. Model-Based RSA was also applied for the displacement analysis using the inserted tantalum beads (*markers*) and the established semi-automated model-based (*mbrsa*) method.[28]

Marker-based method

The bone-inserted markers at femur and tibia were identified in all images. To accommodate the recommendation of the RSA guidelines, we accounted for 0.35 mm as the upper limit of the mean rigid body error matching and ensured identification of the same markers in all images for one displacement series.[29] The position was estimated as the centroid of the marker positions (*markers*).

Model-based method

Based on manually applied parameters and region of interest, the contours were automatically detected in the stereoradiographs by the Canny Edge Detector (RSAcore, Leiden, The Netherlands). The contours for the femur and tibia implants were then manually selected from these detected contours. Coarser to finer algorithms (IIPM, DIFDHSAnn, and DIFDoNLP) were applied to estimate the model pose by minimizing the error between the virtual projections of the models and the manually selected contours.[30] (*mbrsa*) An effort was made to identify as much of the implant silhouette as possible.

Investigated methods (AutoRSA Software)

We investigated two methods that implemented a pin-hole camera model to accommodate perspective projection like the established methods. One, utilized silhouette-projection of a surface model, and one, utilized digitally reconstructed radiograph (DRR) projection of a volume model. Both methods used ray-casting. While the surface-based (*autorsa-surface*) method only determined the model silhouette, the volume-based (*autorsa-volume* and *autorsa-bone*) method estimated the DRR by calculating the ray's cumulative attenuation by each voxel it passed through the image volume. Image registration processes were accelerated utilizing the graphics processing unit (GPU) for speed improvement.

For the 2D/3D registration purpose, according to previous metric evaluation and initial tests using CT based volumetric models, we found that the normalized gradient correlation worked best when comparing the virtually generated projections to the actual stereoradiographs.[31,32] The gradients were automatically determined using the Sobel edge detection algorithm.[33] This algorithm calculated 2D spatial gradient measures at each pixel utilizing 3x3 convolution kernels, resulting in horizontal and vertical gradient images (Figure 3). The similarity metric was then determined as the average of the horizontal and vertical gradients normalized cross-correlation between the actual radiographs and virtually generated projection (Figure 4).

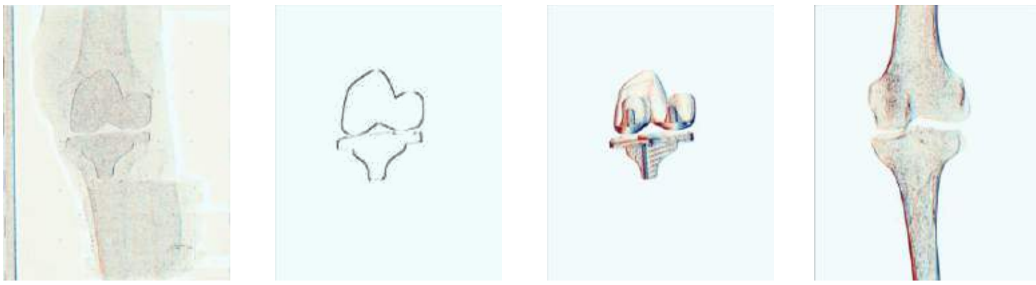

Figure 3 Horizontal Sobel gradient images of the left view. From left; actual radiograph, surface implant projection, digitally reconstructed radiograph implant projection, and digitally reconstructed radiograph bone projection.

The software allowed application of a mask-image to exclude part of the image from the registration process. This benefits the registration in case of non-relevant high image contrasts, which influenced the registration during initial tests. Two methods were optional in combination or separate. A predefined fixed mask-image excluding high intensity objects like metallic object, and a dynamic mask-image ensuring only analysis of the region of interest. The dynamic mask-image were automatically defined as the initial dilated model projection, and thereby exclude the remaining part of the image.

We applied the program's robust optimization scheme that included a two-stage registration process using the implemented nonlinear optimization library NLopt (Steven G. Johson, Boston, Massachusetts). First, a global optimizer (Controlled random search algorithm with local mutations), and second, a refined registration using a local optimizer (Nelder-Mead Simplex).[34,35] We used half resolution images during the global optimizer, and full resolution images with activation of the dynamic mask during the refined local optimizer.

For the *autorsa* methods we analyzed each model separately. First, the femur and then the tibial implant models were analyzed using the surface-based (*autorsa-surface*) and volume-based (*autorsa-volume*) methods. For both methods, we applied the dynamic mask during the refined local optimizer in full image resolution. Second, the bone models were analyzed using the volume-based (*autorsa-bone*) method in the same order. With information of the pre-analyzed implants poses, we utilized the fixed mask to exclude the surgically removed bone and metallic part of the implant from the registration. The fixed mask was produced automatically by dilating the implant silhouette-projection obtained from the previous implant-analysis. The fixed mask was applied during the global optimizer in half resolution and a combination of the fixed and dynamic mask during the refined local optimizer in full resolution. A desktop computer with a quad-core processor (Intel Xeon E5-1620, 3.60 GHz), 8 GB of DDR4 RAM, and a dedicated GPU (GeForce GTX 960, 4 GB GDDR5) completed the registration of a single stereoradiograph in approximately 30 seconds for the *autorsa-surface*, 40 seconds for the *autorsa-volume*, and 85 seconds for the *autorsa-bone* methods.

Figure 4 From left Model-Based RSA implant contour detection, correlation image between the actual radiograph and surface implant projection for the horizontal Sobel gradient images, correlation image between the actual radiograph and implant digitally reconstructed radiographs for the horizontal Sobel gradient images, and correlation image between the actual radiograph and bone digitally reconstructed radiographs for the horizontal Sobel gradient images. Only the left image views are displayed.

Reference frame alignment between systems

While positioning the fixture at the x-ray tubes cross-section, we meticulously oriented the fixture reference frame, defined by the displacements of the three axial micrometers as closely as possible to the RSA reference frame defined by the calibration cage. Even so, the coordinate systems were not completely aligned. To accomplish error-investigation in one direction individually, we defined the axial direction according to a linear fit of the 25 marker-displacements for each series individually. Then, the investigated position coordinate of the models, expressed in the RSA reference frame, were projected to the fitted micrometers axial direction.

Statistical analysis

Accuracy measures of the the RSA registration methods were presented in Bland-Altman plots facilitating the presentation of mean bias and limits-of-agreement (LOA) with a significance level of 0.05. Each of the five methods: Marker-based of bones (*marker*), contour-based of implants (*mbrsa*), surface-based of implants (*autorsa-surface*), volume-based of implants (*autorsa-volume*), and volume-based of bones (*autorsa-bone*), were presented separately for the femur and tibia, respectively. Statistical differences were not investigated between methods. For this study, it is not relevant whether methods are statistically different from one and another. What is relevant, is the accuracy of the method in context of the clinical application. Even so, to accommodate visual overview of the methods, their mean bias and LOA are summarized graphically.

Table 2 Presenting the femur mean and standard deviation of the different views in the three directions. The red text presents the highest standard deviations for each method and view. The bold-red text presents the highest standard deviation for each method in both views.

	Anterior-posterior view			Lateral-medial view		
	x	*y*	*z*	*x*	*y*	*z*
marker	-0.027 (0.043)	-0.011 (0.018)	-0.028 (0.049)	**-0.002 (0.102)**	-0.001 (0.016)	-0.005 (0.041)
mbrsa	-0.027 (0.042)	-0.009 (0.015)	-0.038 (0.052)	**0.004 (0.123)**	-0.004 (0.019)	-0.003 (0.049)
autorsa-surface	-0.027 (0.054)	-0.006 (0.031)	0.036 (0.074)	**-0.018 (0.161)**	0.001 (0.051)	0.026 (0.149)
autorsa-volume	-0.023 (0.049)	-0.013 (0.033)	-0.050 (0.070)	**-0.000 (0.127)**	-0.009 (0.030)	-0.010 (0.049)
autorsa-bone	-0.026 (0.040)	-0.010 (0.021)	-0.027 (0.044)	**-0.003 (0.098)**	-0.004 (0.018)	-0.002 (0.040)

Table 3 Presenting the tibia mean and standard deviation of the different views in the three directions. The red text presents the highest standard deviations for each method and view. The bold-red text presents the highest standard deviation for each method in both views.

	Anterior-posterior view			Lateral-medial view		
	x	*y*	*z*	*x*	*y*	*z*
marker	-0.026 (0.043)	-0.008 (0.013)	-0.035 (0.046)	**0.003 (0.114)**	-0.008 (0.015)	-0.006 (0.043)
mbrsa	-0.026 (0.045)	-0.008 (0.016)	-0.031 (0.056)	**0.011 (0.126)**	-0.009 (0.023)	-0.010 (0.059)
autorsa-surface	-0.020 (0.072)	-0.003 (0.025)	-0.029 (0.058)	**0.007 (0.131)**	-0.010 (0.040)	0.004 (0.131)
autorsa-volume	-0.006 (0.084)	-0.008 (0.039)	-0.032 (0.107)	**0.015 (0.120)**	-0.007 (0.025)	-0.035 (0.105)
autorsa-bone	-0.022 (0.039)	-0.014 (0.020)	-0.024 (0.041)	**-0.002 (0.101)**	-0.010 (0.023)	-0.002 (0.034)

Table 4 Presenting the combined mean and standard deviation of both views in the three directions for the femur and tibia, respectively. The red text presents the highest standard deviations for each method and bone. The bold-red text presents the highest standard deviation for each method in both bones.

	Femur			Tibia		
	x	*y*	*z*	*x*	*y*	*z*
marker	-0.015 (0.077)	-0.006 (0.018)	-0.014 (0.046)	**-0.013 (0.085)**	-0.008 (0.015)	-0.005 (0.041)
mbrsa	-0.012 (0.091)	-0.006 (0.017)	-0.017 (0.053)	**-0.009 (0.094)**	-0.008 (0.020)	-0.018 (0.059)
autorsa-surface	-0.023 (0.117)	-0.002 (0.043)	**0.002 (0.129)**	-0.008 (0.104)	-0.006 (0.034)	-0.009 (0.110)
autorsa-volume	-0.013 (0.094)	-0.011 (0.031)	-0.026 (0.061)	-0.003 (0.102)	-0.007 (0.032)	**-0.034 (0.106)**
autorsa-bone	-0.016 (0.074)	-0.007 (0.020)	-0.011 (0.043)	**-0.013 (0.075)**	-0.012 (0.022)	-0.010 (0.038)

Results

We documented 205 recordings on 8 specimens resulting in a total of 1640 recordings. This included displacement series of two views (AP and LM) in three directions (x, y, z) with one series consisting of 35 stereoradiographs. We excluded 7 series due to non-methodology issues such as a missing image in the recording or unlabeled retakes, resulting in 1395 analyzed stereoradiographs in total.

The results of each registration method are presented as Bland-Altman plots for the femur and tibia separately and revealed no bias for any of the analyzed methods (Figure 5). The best LOA was obtained for the marker and bone registration with similar results for both the femur and tibia. The worst LOA was found for the *autorsa-surface* method for the femoral implant, while the *autorsa-surface* and *autorsa-volume* methods showed equally large LOA for the tibial implant. The *autorsa-volume* method displayed similar LOA for analysis of the femoral implant as the *mbrsa* method. The *mbrsa* method displayed slightly worse LOA values than the marker- and bone-methods (Figure 6).

For future power calculations, elaborated results of the individual directions separately for each view are presented in Table 2 and 3, and data for the two views are combined in Table 4 for femoral and tibial models, respectively. In general, we found worse accuracy in the z direction for the AP view and in the x direction for the LM view, with the LM view being the worst. When the data for the two views are combined the tibia displayed in general slightly worst accuracy.

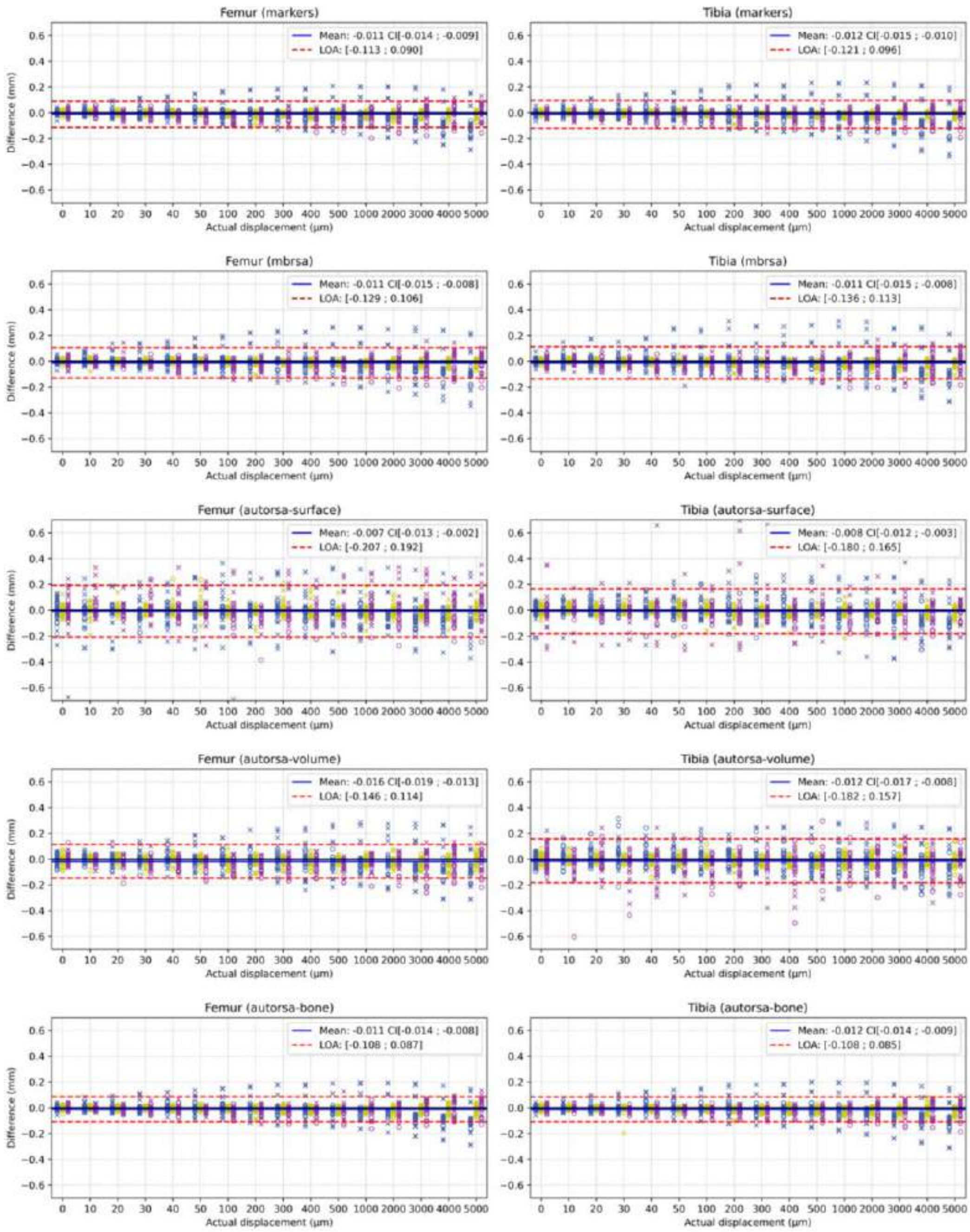

Figure 5 Bland-Altman plots for each method with the colors representing the x (blue), y (yellow), and z (purple). The "o" and "x" represents the anterior-posterior and lateral-medial view, respectively. From top row: *marker*, *mbrsa*, *autorsa-surface*, *autorsa-volume*, and *autorsa-bone*. The first column presents the data of the femur and the second column present data of the tibia.

Discussion

In this study, we evaluated the accuracy of an automated 2D/3D registration method of implant and bone models. Our study adds to previous knowledge with two key findings. First, we evaluated a marker-free bone registration method for an arthroplasty knee joint where the radiopaque implant components occluded or replaced a large part of the bone. It provided similar accuracy compared to the gold standard marker-based method. Second, we evaluate a synthetic volumetric implant model utilizing DRR, which provided more model information to improve registration in radiostereometric analysis.

However, the volumetric implant model and DRR method, in its present form, did not markedly improve the silhouette-projection method.

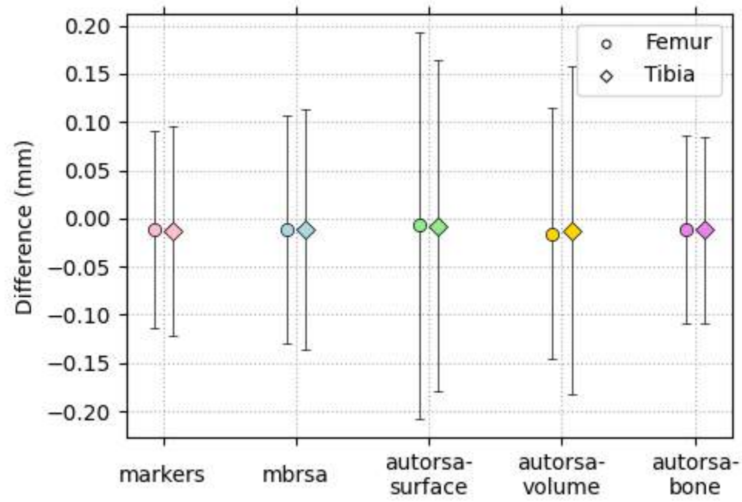

Figure 6 Presentation of the limit-of-agreements for each method for the femur and tibia, respectively.

Various studies have proposed image registration methods for both single and dual radiographic focus systems.[9–18,21–23] The single imaging system are subject to poor out-of-plane performance compared to in-plane[13,21], which can be overcome using a dual focus system.[12,13] When estimating accuracy the definition and establishment of ground truth is crucial. Ideally, the gold standard should be very accurate – at least as accurate as the method being tested, and hopefully much better, while being independent to the investigated method. Most image registration accuracy studies have been oriented towards dynamic studies making radiographic-independent and submillimeter gold standard difficult. Kaptein et al. evaluated static images and used an approach similar to the *marker*- and *mbrsa*-method demonstrating similar in-plane results while our results were superior in out-of-plane direction.[7] Reasons for these differences may be explained by different implants, better optimizers in the software, improved radiographic technology, and image size. Our automated methods showed overall similar or better results to those previously presented by Kaptein et al. when comparing the AP view of the specimens as they also used.

Partial bone registration in artificial joint

Bone-implant interface fixation is considered an important predictor of long-time outcome, and may provide useful information in patients with inexplainable pain and dysfunction of knee arthroplasty.[4] Additionally, inducible micromotion RSA has shown promising results as an instant predictor of long-term loosening, and thereby could eliminate the otherwise required time-expensive follow-up period. Simple RSA recording along with a CT scan provide information to evaluate inducible micromotion without the need for embedded tantalum markers. However, literature on image registration methods of bones within total knee arthroplasty joints are sparse. Seehause et al. and Kim et al. presented bone registration in knees with TKA.[19,20] Their performance measure differs from the present study making comparison difficult. Moreover, Seehause et al. showed migration precision results that exceeded the traditional marker-precision to such a degree that they precluded feasibility of 'completely markerless' migration calculation in the presented form. Kim et al. presented implant and bone translation repeatability ranging between 0.019 to 0.142 and 0.030 to 0.289, respectively. In contrast to our results, Kim et al. found worse bone registration than implant registration. This may be explained by the applied registration methods. They utilized silhouette-projection and canny-edge detection that did not utilize the valuable intensity information of the bone.[9] Additionally, the optimizer may be inhibited to reach the global optima, as the preoperative articulating surface part of the bone silhouette-projection and the postoperative articulating surface part of the actual implant may coincide. Contrary, we utilized bone intensities from DRR registration and eliminated negative influence of the implant by taking advantages of the known implant projection from the pre-completed implant registration.

Synthetic generated volumetric implant model

This study showed that inadequate gradient information was present within the actual stereographs to take advantage of the enhanced information from the DRR. It may be due to the radiopaque nature of the implants. However, the correlation images display that some information were included in the similarity metric, and we saw some improvement in accuracy for the femoral implant in the LM view. Visual inspection of the stereographs also clearly showed intensity differences; thus, we speculate that other similarity metrics may provide improved accuracy. Previously, Mahfouz et al. (2003) presented a similarity metric combining gradient images and the radiographs, and Scarvell et al. (2010) presented a similarity metric using cross-correlation residual entropy (CCRE) of intensity-based edge-enhanced images. CCRE is a mutual information measure that benefits image registration where identical image intensity cannot be presumed, and this is the case for the actual radiograph and the estimated DRR. Continuous research is needed to investigate other similarity metrics.

Limitations

First, establishing a gold standard for accuracy measurements, which is not affected by the radiographic methods is challenging. We used a micrometer to estimate the displacement between recordings; however, a baseline estimate of the zero position was still required. To avoid including other registration methods, we used the median of 5 recordings to estimate a solid baseline and a clinical applicable migration accuracy. With no proportional bias we believe that 5 recordings were sufficient. Second, we used a single implant design. Other TKA designs may influence the accuracy of the method. A more unique design of the implant will be easier to register than a symmetric implant. A difference in implant size will also influence the method accuracy, the bigger the implant the better the results will be. Similar influence of the shape and size of the joint may also affect the accuracy. Third, we used marker-data to establish the alignment between the fixture and the RSA system and therefore may induce uncertainty in the directions. However, only small differences between the orientation of the systems were identified, and we applied the same alignment for each series to all methods ensuring a fair comparison. Fourth, we applied a preoperative CT volumetric bone model without potentially implant artifacts which would be present within a postoperative CT volume. Our experience of postoperative stereoradiographs and the areas of metal artifacts in the CT volume is that these artifacts are anticipated to be hidden behind the implant using the traditional anteroposterior view for the stereoradiographs. Furthermore, mandatory preoperative CT may increase with a direction towards robotic and personalized TKA surgeries.[36–38] Finally, it should be noted that this study does not provide direct information on the rotational accuracy – only translational accuracy in different views were assessed.

Conclusion

In conclusion, marker-free RSA is feasible, with an automated 2D/3D image registration method utilizing CT obtained volumetric bone models and DRR, within a similar accuracy as achieved with the gold standard marker-based RSA. Furthermore, an automated 2D/3D image registration method utilizing synthetic generated volumetric implant models could not improve the silhouette-based method. The automated registration methods exhibit feasible accuracy in relation to the present knowledge within the literature, however, the semi-automated canny-edge detection method exhibit slightly better accuracy.

Acknowledgements: A special thanks to radiographer and photographer Lars Lindgren with data acquisition and photographs.

Conflict of interests: The authors declare no conflict of interests.

Authors contributions: ETP was involved in all aspects of the study and drafted the manuscript. TDV had an essential role in the RSA analysis. JHJ, RC, and SR assisted in data acquisition, data analysis, and interpretation of data. SdR assisted in study design and data interpretation. AB contributed to the study design and acquisition of cadaveric specimens. MSA had an essential role in interpretation, and presentation of data. MS had an essential role in the study design, interpretation, and presentation of data. All authors critically revised and approved the final manuscript.

References

1. Pijls B. Evidence based introduction based introduction of orthopaedic implants RSA, implant quality and patient safety. Published online 2013:1-191. doi:10.13140/RG.2.1.4552.3602
2. Kärrholm J. Radiostereometric analysis of early implant migration – a valuable tool to ensure proper introduction of new implants. *Acta Orthop*. 2012;83(6):551-552. doi:10.3109/17453674.2012.745352
3. Kärrholm J, Borssén B, Löwenhielm G, Snorrason F. Does early micromotion of femoral stem prostheses matter? 4-7-year stereoradiographic follow-up of 84 cemented prostheses. *J Bone Joint Surg Br*. 1994;76(6):912-917.
4. Ryd L, Albrektsson BE, Carlsson L, Dansgard F, Herberts P, Lindstrand A, et al. Roentgen stereophotogrammetric analysis as a predictor of mechanical loosening of knee prostheses. *J Bone Jt Surg Br*. 1995;77(3):377-383.
5. Pijls BG, Valstar ER, Nouta K-A, Plevier JW, Fiocco M, Middeldorp S, et al. Early migration of tibial components is associated with late revision: a systematic review and meta-analysis of 21,000 knee arthroplasties. *Acta Orthop*. 2012;83(6):614-624. doi:10.3109/17453674.2012.747052
6. Valstar ER, De Jong FW, Vrooman H a., Rozing PM, Reiber JHC. Model-based Roentgen stereophotogrammetry of orthopaedic implants. *J Biomech*. 2001;34(6):715-722. doi:10.1016/S0021-9290(01)00028-8
7. Kaptein BL, Valstar ER, Stoel BC, Rozing PM, Reiber JHC. A new model-based RSA method validated using CAD models and models from reversed engineering. *J Biomech*. 2003;36(6):873-882. doi:10.1016/S0021-9290(03)00002-2
8. Nelissen RG, Piljs BG, Kärrholm J, Malchau H, Nieuwenhuijse MJ, Valstar ER. RSA and Registries: The Quest for Phased Introduction of New Implants. *J Bone Jt Surg*. 2011;3:62-65.
9. Christensen R, Petersen ET, Jürgens-Lahnstein J, Rytter S, Lindgren L, De Raedt S, et al. Assessment of knee kinematics with dynamic radiostereometry: Validation of an automated model-based method of analysis using bone models. *J Orthop Res*. Published online 2020. doi:10.1002/jor.24875

10. Moro-Oka TA, Hamai S, Miura H, Shimoto T, Higaki H, Fregly BJ, et al. Can magnetic resonance imaging-derived bone models be used for accurate motion measurement with single-plane three-dimensional shape registration? *J Orthop Res*. 2007;25(7):867-872. doi:10.1002/jor.20355
11. Li G, Van de Velde SK, Bingham JT. Validation of a non-invasive fluoroscopic imaging technique for the measurement of dynamic knee joint motion. *J Biomech*. 2008;41(7):1616-1622. doi:10.1016/j.jbiomech.2008.01.034
12. Zhu Z, Li G. An automatic 2D-3D image matching method for reproducing spatial knee joint positions using single or dual fluoroscopic images. *Comput Methods Biomech Biomed Engin*. 2012;15(11):1245-1256. doi:10.1080/10255842.2011.597387
13. Miranda DL, Schwartz JB, Loomis AC, Brainerd EL, Fleming BC, Crisco JJ. Static and Dynamic Error of a Biplanar Videoradiography System Using Marker-Based and Markerless Tracking Techniques. *J Biomech Eng*. 2011;133(12). doi:10.1115/1.4005471
14. Tsai TY, Li JS, Wang S, Lin H, Malchau H, Li G, et al. A novel dual fluoroscopic imaging method for determination of THA kinematics: In-vitro and in-vivo study. *J Biomech*. 2013;46(7):1300-1304. doi:10.1016/j.jbiomech.2013.02.010
15. Lebel BP, Pineau V, Gouzy SL, Geais L, Parienti JJM, Dutheil JJP, et al. Total knee arthroplasty three-dimensional kinematic estimation prevision. From a two-dimensional fluoroscopy acquired dynamic model. *Orthop Traumatol Surg Res*. 2011;97(2):111-120. doi:10.1016/j.otsr.2011.01.003
16. Wu J, Fatah EEA, Mahfouz MR. Fully automatic initialization of two-dimensional–three-dimensional medical image registration using hybrid classifier. *J Med Imaging*. 2015;2(2):024007. doi:10.1117/1.JMI.2.2.024007
17. Yamazaki T, Watanabe T, Nakajima Y, Sugamoto K, Tomita T, Yoshikawa H, et al. Improvement of depth position in 2-D/3-D registration of knee implants using single-plane fluoroscopy. *IEEE Trans Med Imaging*. 2004;23(5):602-612. doi:10.1109/TMI.2004.826051
18. Guan S, Gray HA, Keynejad F, Pandy MG. Mobile biplane X-Ray imaging system for measuring 3D dynamic joint motion during overground gait. *IEEE Trans Med Imaging*. 2016;35(1):326-336. doi:10.1109/TMI.2015.2473168
19. Seehaus F, Olender GD, Kaptein BL, Ostermeier S, Hurschler C. Markerless Roentgen Stereophotogrammetric Analysis for in vivo implant migration measurement using three dimensional surface models to represent bone. *J Biomech*. 2012;45(8):1540-1545. doi:10.1016/j.jbiomech.2012.03.004
20. Kim Y, Kim K Il, Choi JH, Lee K. Novel methods for 3D postoperative analysis of total knee arthroplasty using 2D-3D image registration. *Clin Biomech*. 2011;26(4):384-391. doi:10.1016/j.clinbiomech.2010.11.013
21. Banks SA, Hodge WA. *Accurate Measurement of Three-Dimensional Knee Replacement Kinematics Using Single-Plane Fluoroscopy*. Vol 43.; 1996.
22. Zuffi S, Leardini A, Catani F, Fantozzi S, Cappello A. A model-based method for the reconstruction of total knee replacement kinematics. *IEEE Trans Med Imaging*. 1999;18(10):981-991. doi:10.1109/42.811310
23. Mahfouz MR, Hoff WA, Komistek RD, Dennis DA. A Robust Method for Registration of Three-Dimensional Knee Implant Models to Two-Dimensional Fluoroscopy Images. *IEEE Trans Med Imaging*. 2003;22(12):1561-1574. doi:10.1109/TMI.2003.820027
24. Stryker. *Triathlon ® Knee System*.; 2015.
25. Krčah M, Székely G, Blanc R. Fully automatic and fast segmentation of the femur bone from 3D-CT images with no shape prior. *Proc - Int Symp Biomed Imaging*. Published online 2011:2087-2090. doi:10.1109/ISBI.2011.5872823
26. Boykov Y, Funka-Lea G. Graph cuts and efficient N-D image segmentation. *Int J Comput Vis*. 2006;70(2):109-131. doi:10.1007/s11263-006-7934-5
27. De Raedt S, Mechlenburg I, Stilling M, Rømer L, Murphy RJ, Armand M, et al. Reliability of computer-assisted periacetabular osteotomy using a minimally invasive approach. *Int J Comput Assist Radiol Surg*. 2018;13(12):2021-2028. doi:10.1007/s11548-018-1802-y
28. Kaptein BL, Valstar ER, Stoel BC. Clinical Validation of Model-based RSA for a Total Knee Prosthesis. *Clin Orthop Relat Res*. 2007;(464):205-209. doi:10.1097/BLO.0b013e3181571aa5

29. Valstar ER, Gill R, Ryd L, Flivik G, Börlin N, Kärrholm J. Guidelines for standardization of radiostereometry (RSA) of implants. *Acta Orthop*. 2005;76(4):563-572. doi:10.1080/17453670510041574
30. Kaptein BL, Valstar ER, Stoel BC, Rozing PM, Reiber JHC. Evaluation of three pose estimation algorithms for model-based Roentgen stereophotogrammetric analysis. 218:231-238.
31. van der Bom IMJ, Klein S, Staring M, Homan R, Bartels LW, Pluim JPW. Evaluation of optimization methods for intensity-based 2D-3D registration in x-ray guided interventions. In: Dawant BM, Haynor DR, eds. *Medical Imaging 2011: Image Processing*. Vol 7962. SPIE; 2011:657-671. doi:10.1117/12.877655
32. Hansen L, De Raedt S, Jørgensen PB, Mygind-Klavsen B, Kaptein B, Stilling M. Marker free model-based radiostereometric analysis for evaluation of hip joint kinematics. *Bone Jt Res*. 2018;7(6):379-387. doi:10.1302/2046-3758.76.BJR-2017-0268.R1
33. Sobel I, Feldman G. A 3x3 Isotropic Gradient Operator for Image Processing. *Stanford Artif Intell Proj*. Published online 1986. https://www.researchgate.net/publication/239398674
34. Kaelo P, Ali MM. Some Variants of the Controlled Random Search Algorithm for Global Optimization. *J Optim Theory Appl 2006 1302*. 2006;130(2):253-264. doi:10.1007/S10957-006-9101-0
35. Nelder JA, Meadf R. *A Simplex Method for Function Minimization*.
36. Saber AY, Marappa-Ganeshan R, Mabrouk A. Robotic Assisted Total Knee Arthroplasty. In: ; 2021.
37. Van der Esch M, Knoop J, van der Leeden M, Roorda LD, Lems WF, Knol DL, et al. Clinical phenotypes in patients with knee osteoarthritis: A study in the Amsterdam osteoarthritis cohort. *Osteoarthr Cartil*. 2015;23(4):544-549. doi:10.1016/j.joca.2015.01.006
38. J Bijlsma JW, J G Lafeber FP, J Bijlsma JW, Berenbaum F, J G Lafeber FP. *Arthritis 1 Osteoarthritis: An Update with Relevance for Clinical Practice*. Vol 377.; 2011. www.thelancet.com

Paper III

Osteoarthritis and Cartilage 30 (2022) 249–259

Osteoarthritis and Cartilage

OARSI OSTEOARTHRITIS RESEARCH SOCIETY INTERNATIONAL

Patients with knee osteoarthritis can be divided into subgroups based on tibiofemoral joint kinematics of gait – an exploratory and dynamic radiostereometric study

E.T. Petersen † ‡ § *, S. Rytter ||, D. Koppens † ||, J. Dalsgaard †, T.B. Hansen † ‡, N.E. Larsen ¶ #, M.S. Andersen ††, M. Stilling ‡ § ||

† University Clinic for Hand, Hip and Knee Surgery, Holstebro Central Hospital, Lægårdvej 12 Holstebro, 7500, Denmark
‡ Department of Clinical Medicine, Aarhus University, Palle Juul-Jensens Boulevard 99 Aarhus N, 8200, Denmark
§ AutoRSA Research Group, Orthopaedic Research Unit, Aarhus University Hospital, Palle Juul-Jensens Boulevard 165 Aarhus N, 8200, Denmark
|| Department of Orthopaedic Surgery, Aarhus University Hospital, Palle Juul-Jensens Boulevard 165 Aarhus N, 8200, Denmark
¶ Department of Radiology, Holstebro Central Hospital, Lægårdvej 12 Holstebro, 7500, Denmark
# Department of Radiology, Aarhus University, Palle Juul-Jensens Boulevard 99 Aarhus N, 8200, Denmark
†† Department of Materials and Production, Aalborg University, Fibigerstræde 16 Aalborg, 9220, Denmark

A R T I C L E I N F O

Article history:
Received 30 June 2021
Accepted 23 October 2021

Keywords:
Knee osteoarthritis
Radiostereometry
Kinematics
Gait analysis
Clustering
Statistical parametric mapping

S U M M A R Y

Objective: Patients with advanced knee osteoarthritis (KOA) frequently alter their gait patterns in an attempt to alleviate symptoms. Understanding the underlying pathomechanics and identifying KOA phenotypes are essential to improve treatments. We investigated kinematics in patients with KOA to identify subgroups of homogeneous knee joint kinematics.
Method: A total of 66 patients with symptomatic KOA scheduled for total knee arthroplasty and 15 age-matched healthy volunteers with asymptomatic, non-arthritic knees were included. We used k-means clustering to divide patients into subgroups based on dynamic radiostereometry-assessed tibiofemoral joint kinematics. Clinical characteristics such as knee ligament lesions and KOA scores were graded by magnetic resonance imaging and radiographs, respectively.
Results: We identified four clusters that were supported by clinical characteristics. *The flexion group* ($n = 20$) consisted primarily of patients with medial KOA. *The abduction group* ($n = 17$) consisted primarily of patients with lateral KOA. *The anterior draw* group ($n = 10$) was composed of patients with medial KOA, some degree of anterior cruciate ligament lesion and the highest KOA score. *The external rotation* group ($n = 19$) primarily included patients with medial collateral and posterior cruciate ligament lesions.
Conclusion: Based on tibiofemoral gait patterns, patients with advanced KOA can be divided into four subgroups with specific clinical characteristics and different KOA-affected compartments. The findings add to our understanding of how knee kinematics may affect the patient's development of different types of KOA. This may inspire improved and more patient-specific treatment strategies in the future.

Introduction

Knee osteoarthritis (KOA) is commonly associated with pain, stiffness, muscle weakness, and joint instability. Thus gait and movement patterns are affected limiting daily activities[1]. Joint pathomechanics in KOA are complex and may affect the entire gait cycle. Even so, most studies have investigated the kinematics in KOA using observer-selected outcomes, i.e., individual discrete time-points, excursion, maximum, and minimum. The entire kinematic trajectory in patients with KOA has never been studied using non-directed hypothesis testing such as statistical parametric mapping (SPM) preventing selection bias[2,3]. This may potentially contribute with patient-specific characteristics of importance for rehabilitation and surgical results.

* Address correspondence and reprint requests to: E. T. Petersen, MSc., Orthopeadic Research Unit Aarhus University Hospital, Palle Juul-Jensens Boulevard 165, J501 Aarhus N, 8200, Denmark. Tel.: 45-22-88-88-60.
E-mail address: emiltp@clin.au.dk (E.T. Petersen).

https://doi.org/10.1016/j.joca.2021.10.011

Classically, kinematic changes in KOA have been reported as comparisons of group categories such as KOA severity[4–6], affected knee compartment[7], anterior cruciate ligament (ACL) deficiency[8], and walking difficulties[9]. However, such predefined categories may promote unnecessary bias and blur kinematic differences due to other unidentified characteristics. A reverse approach may allocate patients with KOA into subgroups based on homogenous kinematic gait trajectories and identify multiple characteristics that affect the kinematic motion patterns between groups. K-means is a centroid-based clustering algorithm using an unsupervised machine-learning approach that previously has been applied on kinematic trajectories[10]. Without prior knowledge of patient or disease characteristics, the algorithm allocates multidimensional data into homogenous subgroups based on an Euclidean distance measure.

Measurement of small kinematic differences requires precise methods. Dynamic radiostereometry (dRSA) can register the three-dimensional bone-pose and accurately measure small kinematic changes in native knees with ligament lesions and reconstructions[7,11–13].

In the present study, we investigated the full-trajectory knee joint kinematics during level gait in patients with advanced KOA to identify: 1) subgroups of KOA patients based on knee kinematics through clustering, and 2) features of knee kinematics unique to the identified subgroup, linking kinematics to patient characteristics describing the subgroup. We compared the results with data from a group of healthy volunteers with asymptomatic non-arthritic knees.

Methods

This study involved the preoperative data of 81 subjects (Table I) who participated in a randomized controlled study investigating the outcome of knee arthroplasty designs (ClinicalTrials NCT03633201). The inclusion period was from 2017 to 2019. A total of 66 patients with radiographic and symptomatic primary KOA were included. The control group comprised 15 local healthy, age-similar volunteers with asymptomatic knees and no radiographic KOA. The inclusion and exclusion criteria are presented in Table II. The study was approved by the Committee on Biomedical Research Ethics of the Central Denmark Region (1-10-72-303-16, issued 28 February 2017) and registered with the Danish Data Protection Agency (1-16-02-582-16, issued 31 October 2016). The study was conducted in accordance with the Helsinki Declaration, and written informed consent was obtained from all participants. The total estimated effective dose exposed to each patient was 0.629 mSv.

Experimental protocol

Participants walked barefoot on a leveled treadmill (Sole F63, Jonesboro, AR, USA) to mimic level gait (Fig. 1). They had a habituation period to get familiar with the test environment, with slowly increasing speed reaching a final speed of 0.83 m/s. This is slightly slower than average walking speed (1.25 m/s)[14] and was chosen to avoid exclusion of gait-disabled patients and facilitate sufficient dRSA data generation throughout the entire gait cycle. When the subject felt comfortable, data collection was initiated. Up to seven coherent gait cycles were obtained. For precaution and anticipating loss of balance during testing, subjects had a rail they could hold on to. Only none-rail-supported gait trials were included for further analysis. An overview of the workflow is illustrated in Fig. 2.

Dynamic radiographic imaging

The gait trials were recorded with a dedicated dRSA system (AdoraRSA; NRT X-Ray A/S, Hasselager, Denmark) with a previously described biplanar setup[13]. The radiation exposure parameters were set at 90 kVp, 600 mA, and a pulse-width of 2.5 ms, utilizing the highest frame rate of 15 Hz without compromising the image size. Simultaneously with the dRSA system, we used a minimum of six OptiTrack Prime 13 motion cameras (NaturalPoint, Corvalis, OR, USA) and Motive software (Motive v.2.0.0, NaturalPoint, USA) to assess the trajectories of skin-attached reflective markers (diameter: 10 mm). Prior to usage, the entire recording area was calibrated using an OptiTrack CW-500 Calibration Wand (NaturalPoint, USA). A custom-programmed Raspberry Pi 3 Model B (Linux Mini PC, Broadcom BCM2837 1.2 GHz Quad-Core 64-bit, 1 Gb LPDDR2 RAM) was used to time-synchronize data from the dRSA and the optical marker systems using pulse information from both systems.

	Patient group	Healthy control group
Inclusion criteria	Age above 18 years but no more than 80 years of age. Informed and written consent. Primary knee osteoarthritis in capable men and women. Indication for cruciate-retaining total knee arthroplasty.	Age above 18 years but no more than 80 years of age. Informed and written consent. Asymptomatic knees and no radiographic osteoarthritis.
Exclusion criteria	Patients with a thigh circumference exceeding 60 cm. Patients with conditions that severely compromise their gait other than knee osteoarthritis in the affected knee. Patients with previous severe fractures at the knee level or severe malalignment at the knee level. Surgically implanted metallic parts and pacemaker. Patients with need for an augmentation and/or stem extension. Patients who cannot perform the exercises.	Patients with a thigh circumference exceeding 60 cm. Patients with conditions that severely compromise their gait. Patients with previous fractures or severe malalignment at the knee level. Surgically implanted metallic parts and pacemaker. Patients who cannot perform the exercises.

Table I Osteoarthritis and Cartilage

Inclusion and exclusion criteria

	Healthy (n=15)	KOA patients (n=66)	G1 (n=20)	G2 (n=17)	G3 (b=10)	G4 (n=19)	P-value*	P-value**
a) Demographics with means and confidence intervals for continuous parameters and percentage for categorical parameters.								
Age	65.1 (60.1;70.1)	63.2 (61.1;65.2)	66.8 (64.2;69.4)^{G2}	57.5 (54.0;60.9)^{G1}	64.3 (56.3;72.3)	63.8 (59.8;67.9)	0.419	0.007
Side (left %)	46.7	54.6	45.0	76.5	30.0	57.9	0.581	0.131
Gender (female %)	26.7	39.4	40.0	41.2	20.0	47.4	0.348	0.536
Height	172.0 (167.3;176.7)	172.5 (170.9;174.6)	173.1 (169.3;176.9)	175.5 (172.4;178.5)	173.2 167.0;179.3)	169.3 (165.3;173.4)	0.794	0.236
Weight	78.1 (71.7;84.4)	86.5 (82.8;90.1)	87.75 (82.5;93.0)	88.3 (80.9;95.7)	81 (71.1;90.9)	86.3 (77.1;95.6)	0.044	0.211
Body Mass Index	26.2 (25.1;27.4)^{P}	29.0 (27.6;30.1)^{H}	29.3 (27.6;31.1)	28.7 (26.3;31.1)	26.8 (24.7;29.0)	30.0 (27.2;32.8)	0.001	0.075
Thigh circumference	51.5 (49.2;53.8)	52.1 (50.7;53.5)	51.9 (49.2;54.6)	53.3 (50.3;56.2)	50.2 (46.6;53.8)	52.2 (49.5;55.0)	0.711	0.700
b) Clinical characteristics with means and confidence intervals for continuous parameters and percentages for categorical parameters (except for the OA Ahlbeck score, which is presented with mean and confidence interval).								
ACL deficiency (0/1/2) %	73 / 27 / 0$^{P, C2, C3}$	30 / 38 / 32^{H}	45 / 35 / 20^{C3}	24 / 41 / 35^{H}	**0 / 30 / 70$^{H, C1}$**	37 / 42 / 21	0.004	<0.001
PCL deficiency (%)	6.7	12.1	10.0	11.8	10.0	15.8	0.544	0.943
MCL deficiency (%)	0.0	7.6	0.0	5.9	0.0	21.5	0.271	0.174†
LCL deficiency (%)	6.8	6.1	5.0	11.8	0.0	5.3	0.930	0.866†
OA Ahlbeck grade	0.7 (0.3;1.0) $^{C1, C2, C3, C4}$	2.8 (2.5;3.1)	2.7 (2.4;3.0)$^{H, C3}$	2.2 (1.8;2.7)$^{H, C3}$	**3.9 (3.4;4.4)$^{H, C1, C2}$**	2.8 (2.2;3.4)^{H}	-†	<0.001
OA medial (%)	53.3	72.7	95.0^{C2}	29.4$^{C1, C4}$	60.0	94.7^{C2}	0.142	<0.001
OA lateral (%)	0.00	9.09	0.00	**35.29**	0.00	0.00	0.225	-†
OA medial+lateral (%)	6.7	16.7	5.0	29.4	40.0	5.3	0.970	0.029
FJS	98.6 (97.1;100.1)$^{P, C1, C2, C3, C4}$	16.0 (12.3;19.7)^{H}	15.3 (9.2;21.4)^{H}	12.3 (6.7;17.8)^{H}	20.0 (3.2;36.8)^{H}	17.9 (10.6;25.2)^{H}	<0.001	<0.001
OKS	47.8 (47.6;48.0)$^{P, C1, C2, C3, C4}$	23.5 (21.9;25.0)^{H}	23.15 (20.4;25.9)^{H}	23.4 (20.3;26.4)^{H}	22.5 (15.7;29.3)^{H}	24.5 (22.0;26.9)^{H}	<0.001	<0.001
KOOS SYMPTOMS	98.6 (97.1;100.0)$^{P, C1, C2, C3, C4}$	48.9 (44.6;53.2)^{H}	49.5 (40.5;58.4)^{H}	40.5 (33.7;47.4)^{H}	52.9 (39.3;66.4)^{H}	53.8 (45.5;62.0)^{H}	<0.001	<0.001
KOOS PAIN	99.6 (99.1;100.2)$^{P, C1, C2, C3, C4}$	43.5 (39.8;47.2)^{H}	39.4 (33.0;45.8)^{H}	42.6 (37.0;48.3)^{H}	46.4 (28.7;64.0)^{H}	46.9 (40.4;53.4)^{H}	<0.001	<0.001
KOOS ADL	99.7 (99.4;100.0)$^{P, C1, C2, C3, C4}$	51.5 (48.1;55.0)^{H}	49.1 (43.3;54.9)^{H}	49.4 (43.1;55.7)^{H}	56.6 (43.1;70.1)^{H}	53.3 (46.6;60.1)^{H}	<0.001	<0.001
KOOS SPORT/REC	96.3 (92.9;99.7)$^{P, C1, C2, C3, C4}$	15.1 (11.5;18.6)^{H}	13.8 (8.4;19.1)^{H}	15.9 (7.5;24.2)^{H}	15.0 (2.0;28.0)^{H}	15.8 (8.8;22.8)^{H}	<0.001	<0.001
KOOS QOL	97.9 (95.8;100.1)$^{P, C1, C2, C3, C4}$	27.4 (24.5;30.3)^{H}	23.4 (19.0;27.9)^{H}	28.3 (22.8;33.8)^{H}	28.1 (16.9;39.3)^{H}	30.3 (24.1;36.4)^{H}	<0.001	<0.001
VAS – gait	0.0 (0.0;0.0)$^{P, C1, C3, C4}$	2.4 (1.5;2.5)^{H}	2.9 (1.7;4.1)^{H}	1.5 (0.5;2.6)	2.3 (1.1;3.5)^{H}	2.9 (1.8;4.0)^{H}	<0.001	<0.001
OPR bilateral	0.0	9.9	15.0	5.9	30.0	5.3	0.156	0.242
c) Kinematic characteristics with overall difference when compared with the healthy group. The superimposed colour-squares, which are identical to those in Figure 6, highlight trajectories with similar differences when compared with the healthy control group.								
Flexion (+) / Extension (-)			**↑ Flexion (sections)**				-	-
Adduction (+) / Abduction (-)			↑ Adduction (full)	**↑ Abduction (full)**	↑ Adduction (full)	↑ Adduction (full)	-	-
Internal rotation (+) / External rotation (-)		↑ External (section)			↑ External (full)	↑ External (full)	-	-
Medial shift (+) / Lateral shift (-)		↑ Lateral (sections)			↑ Lateral (sections)	↑ Lateral (full)	-	-
Anterior drawer (+) / Anterior drawer (-)				↑ Anterior (sections)	**↑ Anterior (full)**	**No anterior**	-	-
Joint distraction (+) / Joint narrowing (-)		↑ Narrowing (full)	↑ Narrowing (full)	↑ Narrowing (full)	↑ Narrowing (full)	↑ Narrowing (full)	-	-

The superscript: H (the healthy group), P (the KOA-patient group) C1 (*the flexion group*), C2 (*the abduction group*), C3 (*the anterior drawer group*), and C4 (*the external rotation group*) show to which groups a significant difference was identified after Bonferroni adjustment.
The bold-cell data illustrate results of high importance.
*Comparison between the healthy group and the entire KOA patient group using either a t-test or a chi-squared test.
**Comparison between the healthy group and the clusters using either one-way analysis of variance, ordinal logistic regression or logistic regression.
†Statistical difference could not be estimated for groups without events.

Table II

Osteoarthritis and Cartilage

Group summary and comparison

Volumetric imaging

All participants underwent a computed tomography (CT) (Revolution EVO, GE Medical Systems, Milwaukee, WI, US) to construct subject-specific bone models (Fig. 3). A helical scan protocol with the reconstruction kernel ‘boneplus’ was used covering 15 cm of the most distal and proximal part of the femur and tibia. Knee scans were acquired with axial slices at a peak voltage of 100 kVp and 200 mAs, a slice thickness of 0.625 mm and a pixel spacing of 0.48×0.48 mm. The CT also included imaging with minor changes to reduce dose exposure of the femoral head (slice thickness of 2.5 mm) and ankle (80 kVp and slice thickness of 2.5 mm) to construct an anatomical coordinate system using the mechanical axis. Bones were segmented using an implemented, fully automated graph-cut segmentation method employing the Insight Segmentation and Registration Toolkit (Kitware, Clifton Park, NY, USA)[15,16]. From the segmentations, both three-dimensional volume and surface bone models were created. The volume model comprised the extracted bone containing the greyscale information of the CT. The surface model was extracted using the marching cubes algorithm and the visualization Toolkit (Kitware). An anatomical coordinate system was assigned to all bone models using a modified version of Miranda *et al.*[17] to implement the mechanical axis[11].

Analysis of dynamic radiographic imaging

The series of stereoradiographs were analyzed using an automated software system developed at our institution (AutoRSA software, Orthopaedic Research Unit, Aarhus, Denmark). The software utilized a digitally reconstructed radiographic (DRR) registration method to estimate bone pose from virtually generated projections using mathematical optimization algorithms, as previously described in more detail[13,16,18]. The optimal pose was found by minimizing the difference between virtually generated DRR images from a 3D volume to actual stereoradiographs using a normalized gradient correlation approach[13,18,19]. Prior to the DRR registration process, the automated bone pose initialization between frames deviated from previously described studies[13,16,18] by utilizing the skin-attached marker trajectories.

Quantification of knee joint kinematics

We implemented the joint coordinate system [Fig. 3(e)] initially defined by Grood and Suntay[20] to describe the knee joint kinematics, but using the modified equations proposed by Dabirrahmani and Hogg[21] to account for possible hyper-extension and hyper-flexion. The relative motion in all six degrees-of-freedom

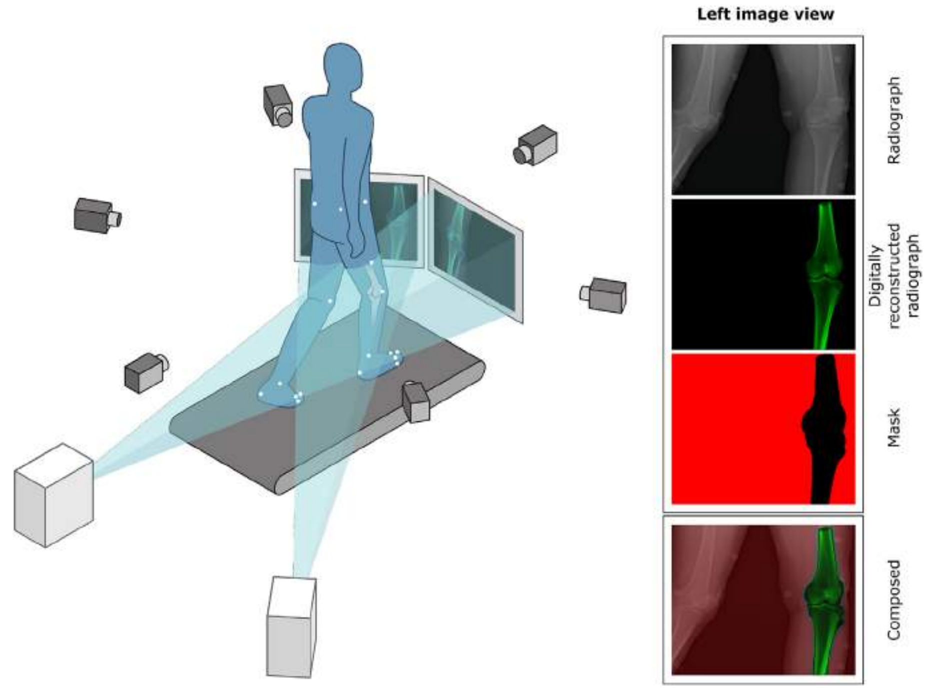

Fig. 1

Osteoarthritis and Cartilage

Illustration of the treadmill setup. Utilizing the largest recording area possible, we used a biplanar setup where the detectors were placed on individual stands with a relative angle of 40°; one in front of the subject and one to the side of the limb of interest. The source image distance was approximately 240 cm (frontal view) and 280 cm (side view). The source object distance was approximately 190 cm (frontal view) and 220 (side view). The system was acting in a plane parallel to the floor at a patient-specified height to centralize the knee joint in the radiographic images throughout the entire recording. The setup was mirrored for left/right knees to accommodate having the investigated knee as close as possible to the side view. The six optical cameras were positioned strategically surrounding the subject to avoid occluded markers during analysis of the skin-attached reflective markers. The markers (white dots) were attached at the subjects' pelvis, lower limb, and feet; three cluster markers at the thigh, two at the knee epicondyles, three cluster markers at the shank, two at the ankle malleolus, one at the heel, three at the metatarsales (1, 3, 5), and one at the first distal phalanx. The mask image was used for a refined optimization on each frame excluding irrelevant pixel values surrounding the DRR overlay image area of interest.

(rotation and translation) of the body-fixed anatomical coordinate systems was computed for each frame. The translation was quantified in mm with medial tibial shift, tibial anterior drawer, and joint distraction as positive directions. Rotations were measured in sequence as presented and quantified in degrees with flexion, adduction, and tibial internal rotation as positive directions. Kinematic values were divided into gait cycles, starting and ending with two successive initial foot contacts of the ipsilateral limb. We used the approach of O'Conner *et al.*[22] to identify initial contact using the optical markers on foot. To estimate each subjects' most representative gait cycle pattern, we time-normalized the kinematic measures to 21 points representing the gait cycle from 0 to 100% and calculated the median across trials for each subject.

Clinical characteristics

Based on conventional radiographs, KOA was classified according to the Ahlbeck score (grade 1–5). Those without KOA were classified as grade 0. Additionally, we registered the affected tibiofemoral compartment as lateral or/and medial. Knee ligament lesions were assessed with high accuracy and repeatability using detailed magnetic resonance imaging (1.5 T Avanto, SIEMENS, Erlangen, Forchheim, DE)[23]. We applied a modified version of the Osteoarthritis Initiative protocol[24] based on GE scanner recommendations (T2 SAG de3D DESS WE acquisition with 0.7 mm slice thickness and T1 COR fl3D WE with 1.5 mm slice thickness). We evaluated the following knee ligaments: ACL, posterior cruciate ligament (PCL), medial collateral ligament (MCL) and lateral collateral ligament (LCL). The ACL was graded as: 0 (no lesion), 1 (partial lesion), and 2 (full lesion). PCL, MCL, and LCL were registered as 0 (intact) or 1 (with lesion). The clinical outcome measures were assessed by the Oxford Knee Score (OKS), the Forgotten Joint Score (FJS) and the Knee Osteoarthritis Outcome Score (KOOS).

Subgroup allocation

The median kinematic trajectories of each patient were used to construct a 126 by 66 feature matrix (M) containing the 126 trajectory kinematic feature points (6 kinematic parameters × 21 time-points) for each of the 66 patients. Feature point ordering was consistent across all participants in the matrix. For the purpose of clustering, each feature was standardized to avoid different weightage between features. Each feature was subtracted by the respective mean values and divided by the standard deviation.

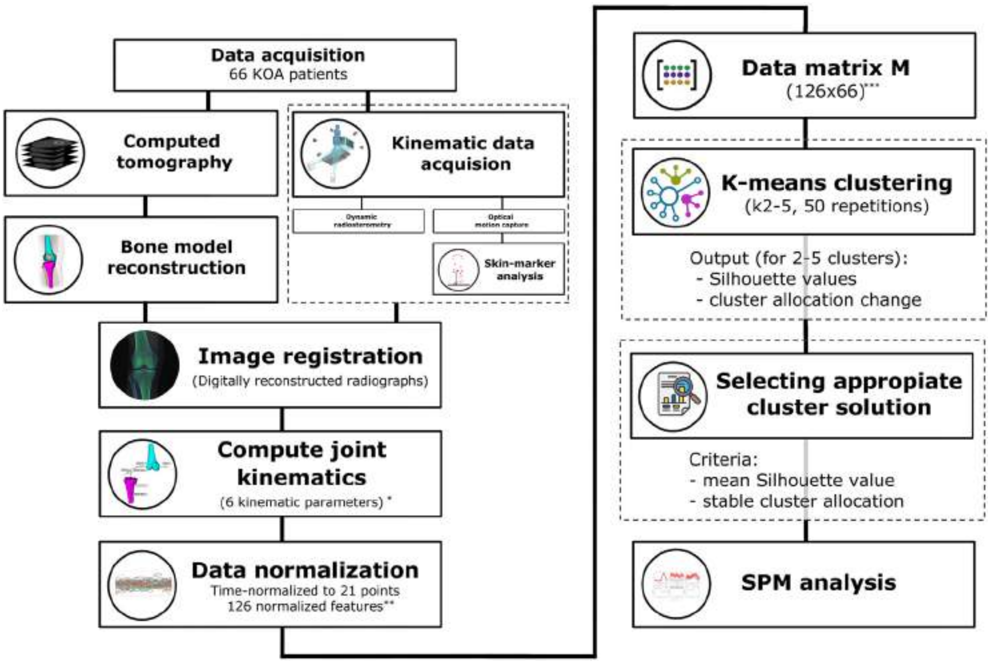

Fig. 2 Osteoarthritis and Cartilage

Illustration of the data analysis workflow. KOA – knee osteoarthritis, SPM – statistical parametric mapping. * The 6 kinematic parameters: flexion/extension, adduction/abduction, external/internal tibial rotation, lateral/medial tibial shift, anterior/posterior tibial translation, and joint distraction/narrowing. ** The 126 features (6 × 21) include the 6 kinematic parameters concatenated after time-normalization to 21 points representing the gait cycle from 0 to 100%. *** The data matrix M (126 × 66) were constructed of the 126 features (6 kinematic parameters × 21 time-points) and the 66 patients.

Subgroup allocation was performed with skleans[25] implementation of k-means clustering in Python. K-means clustering is an iterative algorithm randomly allocating every data point to the nearest subgroup, while minimizing the sum of squared Euclidian distance between every data point and its subgroup's centroid. Due to random seeding of the initial allocation, the k-means algorithm may not reach the global optimum, but instead converge to a local optimum. To handle this limitation, each clustering process was based on 50 repetitions with different, randomly allocated seeds. The repetition with the lowest sum of squared Euclidian distance was chosen as the final allocation of one *clustering process*. Another challenge of the k-means approach is to determine the number of subgroups, *k*. To do so, we investigated repeatability and quality for *k* number of subgroups ranging from two to five. Subgroup repeatability was evaluated based on repeating ten *clustering processes* for each of which we tracked differences in subgroup allocations with increasing *k*-subgroups. Subgroup quality of the two to five k-subgroups was assessed using the Silhouette value of the *clustering process* with the lowest sum of squared error of 10 repetitions (considered as the best). The Silhouette value is a measure of similarity describing how well subjects is allocated within a subgroup in relation to all other subgroups. The value ranges from −1 to 1 with a larger value indicating a stronger association with its allocated subgroup, whereas a more negative value indicates a stronger association with other subgroups. Of these four subgroup allocations, the one with the best repeatability and quality was used in the subsequent analysis.

Statistical analysis

Differences in knee joint kinematics across the entire gait cycles were examined using one-dimensional SPM with the open-source code spm1d (spm1d.org, v.0.4.2) for Python (Python Software Foundation, v.3.6). SPM allows for examining the entire one-dimensional time series of kinematic trajectories, avoiding selection bias and allowing for non-directed hypothesis testing instead of reducing the dataset to a certain observation or alternatively risking false hypothesis testing due to multiple repeated measurements[2,3]. SPM uses Gaussian random field theory to calculate the threshold that only the significance level of equivalently smooth Gaussian random fields would cross when the null hypothesis is true. QQ-plots revealed that our kinematic data were not normally distributed. Thus, we used statistical non-parametric mapping (SnPM), which deals with smoothness implicitly and estimates the test statistics through permutation[26]. First, a Hotelling test was implemented on the entire vector field. Then, the post-hoc Hotelling test was applied to each vector component if the vector field level reached statistical significance.

We compared demographically and clinically characteristic differences between groups using one-way analysis of variance (ANOVA) for continuous variables, ordinal logistic regression for categorical variables, and logistic regression for binary variables. When significant differences were detected, Bonferroni correction was applied for group differences. Visual inspection of QQ-plots verified normally distributed data.

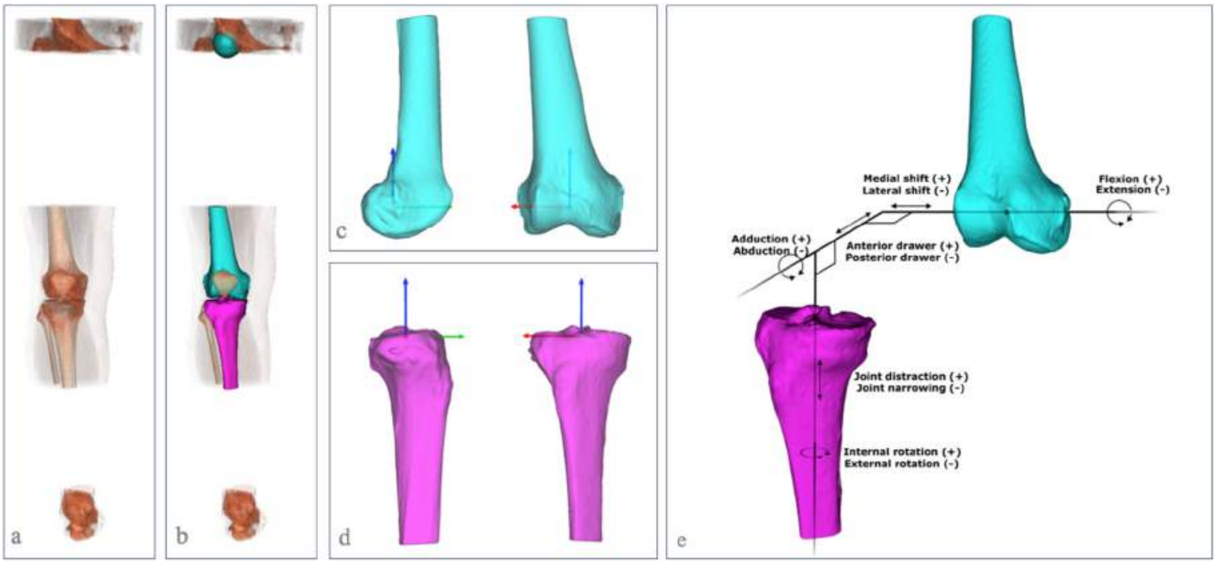

Fig. 3 Osteoarthritis and Cartilage

Illustration of the right leg of a CT (a), bone segmentation along with marked hip and ankle centres (b), anatomical coordinate system (c–d), and knee joint coordinate system (e). (a) Volume rendering of a hip-knee-ankle CT. (b) Bone segmentation of the femur (cyan) and tibia (magenta). The hip joint centre (cyan) was defined as the centre of a sphere fitted to the cortical bone of the femoral head using least square. The ankle centre (magenta) was defined as the midpoint between the ankle malleolus that was manually selected at the CT volume-rendered model. (c–d) 3D bone models of the femur (c) and tibia (d) bones in a sagittal and frontal view illustration the anatomical coordinate system. Femur: the lateral–medial axis was defined as the centre line of a cylinder placed using a least-square fit to the knee condyles, the proximal–distal axis was defined as an orthogonal projection from the medial–lateral axis to the centre of a sphere at the femoral head. The anterior-posterior axis was defined as the cross product of the medial–lateral axis and the proximal–distal axis. The origin was defined as the midpoint between the medial–lateral axis surface intersections. Tibia: the origin was defined as the centroid of the tibial plateau proximal of the largest cross section. The medial–lateral axis was defined as the first principal component axis. The proximal–distal axis was defined as an orthogonal projection from the medial–lateral axis to the midpoint between the ankle malleoli. The anterior-posterior axis was defined as the cross product of the medial–lateral axis and the proximal–distal axis. (e) Illustration of the knee joint coordinate system used for kinematic pose assessment of the femoral and tibial bones considered in relation to each.

Results

Subgroup allocation

The quality and repeatability analyses are presented in Fig. 4. Silhouette values [mean (standard deviation, SD)] across ten k-means cluster repetitions were: $k = 2$ [0.178 (0.002)]; $k = 3$ [0.140 (0.006)]; $k = 4$ [0.128 (0.004)]; and $k = 5$ [0.125 (0.005)]. The individual subgroup allocation across the ten consecutive repetitions showed identical subgroup allocation for $k = 2$. Individual data allocation was more variable for $k = 3$ and $k = 4$ with three and ten individuals switching subgroups, respectively. No consistent pattern of subgroup allocation could be identified for the $k = 5$ solution. Noticeably, the second ($k = 3$) and third ($k = 4$) solutions allocated two identical subgroups (G3,G4), whereas the third ($k = 4$) solution separated the remaining subgroup into two subgroups (G1,G2). All of this indicates that four subgroups may represent the optimal solution for separating the current dataset into the largest number of subgroups with the highest quality and reasonable repeatability. Consequently, the third ($k = 4$) solution was chosen for further analysis; G1 ($n = 20$), G2 ($n = 17$), G3 ($n = 10$), and G4 ($n = 19$).

Kinematic and clinical characteristics

The tibiofemoral joint kinematic trajectories for the entire patient cohort showed increased tibial external rotation, tibial lateral shift, and joint narrowing compared to the healthy group (Fig. 5). The four gait-trajectory-based subgroups (G1,G2,G3,G4) are compared to the healthy group in Fig. 6 and Table IIc (color-code highlight the main differences). The in-between subgroup kinematic comparison can be found in the Supplementary material. Clinical differences and a schematic overview of the most relevant differences between subgroups and the healthy control group are presented in Table II.

G1 – The flexion group

This was the only subgroup revealing different knee flexion when compared with the healthy group. Increased knee flexion was identified at initial contact, terminal stance, and terminal swing phase. Additionally, throughout the entire gait cycle, this subgroup showed greater adduction and joint narrowing than the healthy group. The clinical characteristics revealed that this subgroup consisted primarily of cases with medial tibiofemoral osteoarthritis. In relation to the other subgroups, this group displayed a

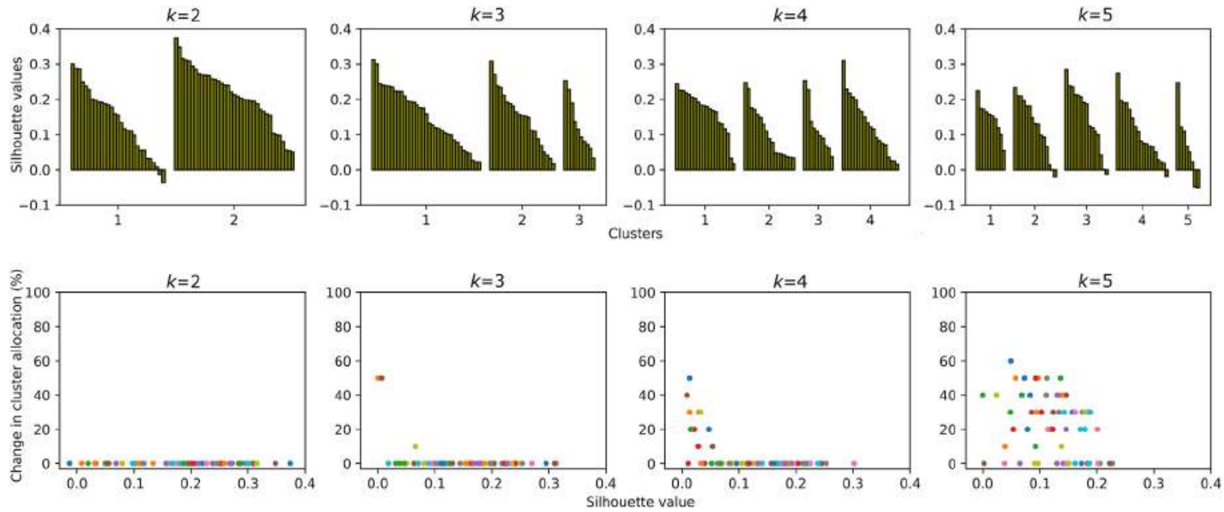

Fig. 4

Presentation of cluster allocation for *k*-values ranging from 2 to 5. Top row: Silhouette values of each subject of the repetition that showed the best mean square error of the ten repetitions. Bottom row: Change in cluster allocation across the ten repetitions with respect to each subject's silhouette value.

larger flexion angle than *the anterior group* (loading response and initial swing phase) and *the external rotation group* (swing phase). Additionally, this subgroup displayed the largest internal rotation of any group.

G2 – The abduction group

This was the only subgroup revealing greater abduction than the healthy group. This was identified throughout the entire gait cycle. In addition, this subgroup showed greater joint narrowing throughout the gait cycle and anterior drawer during the loading response and terminal swing phase. The clinical characteristics revealed that it was the only subgroup that included cases with lateral tibiofemoral osteoarthritis. In relation to the other subgroups, this group displayed the largest abduction. In addition, it revealed a larger anterior drawer than *the flexion group* (stance, initial swing, and terminal swing) and *the external rotation group* (initial contact to mid-stance and terminal stance). It was only exceeded in this respect by *the anterior drawer group.*

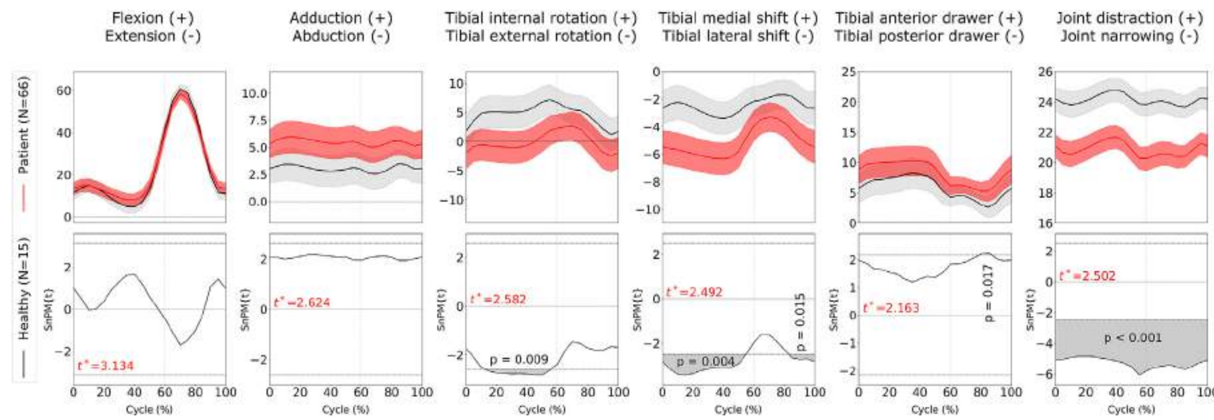

Fig. 5

Kinematic comparison of the entire patient group with the healthy control group. The top row presents the mean trajectories of the two groups with confidence interval as the shaded area. The bottom row presents the ***post hoc*** non-parametric scalar field ***t*** tests (SnPM{t}), depicting where patients show higher (+) and lower (–) than healthy subjects. The thin dotted lines indicate the critical thresholds for significance. The grey-shaded areas illustrate when critical threshold is exceeded thus determining a significant difference.

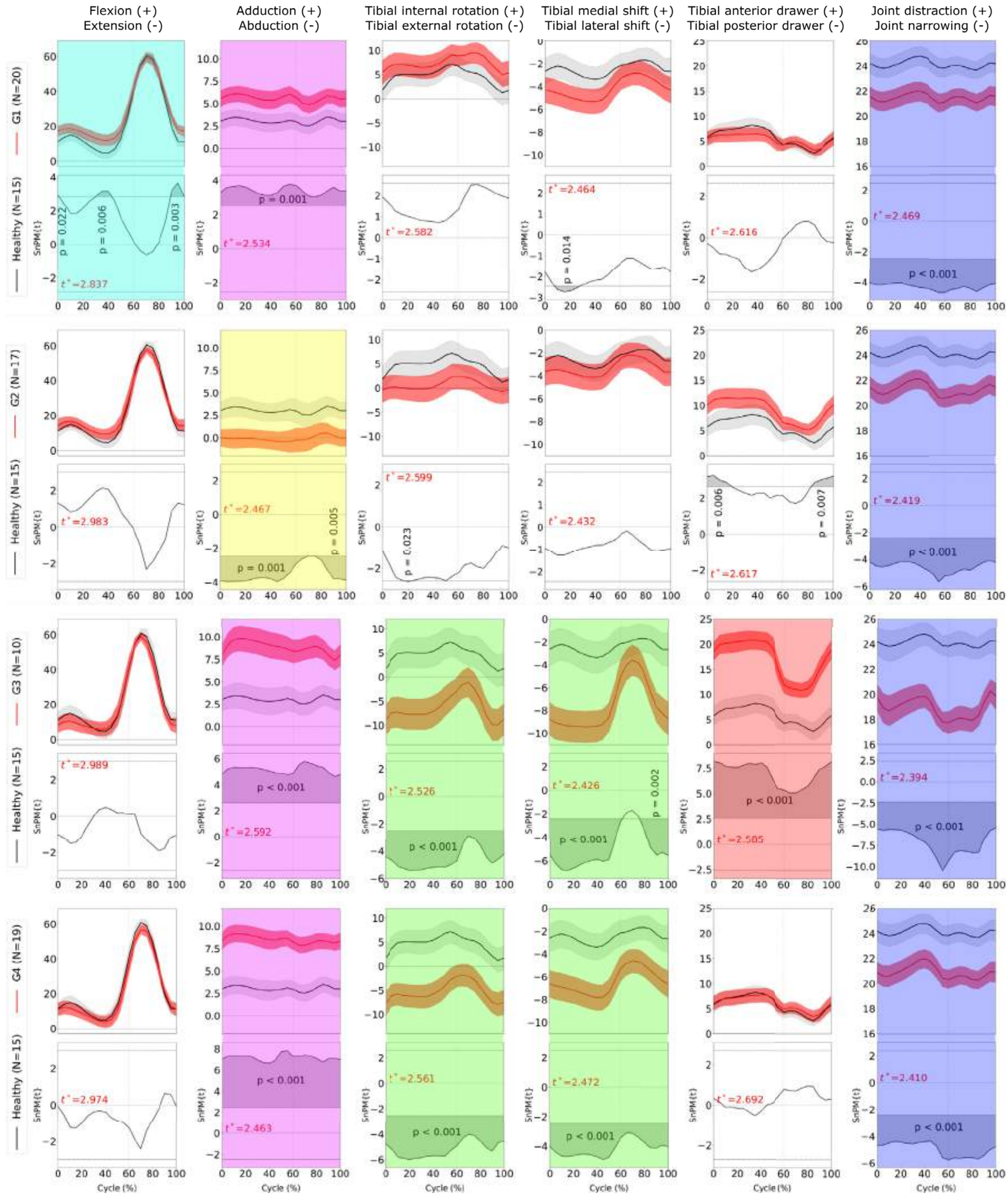

Fig. 6 Osteoarthritis and Cartilage

Statistical parametric mapping of all kinematic parameters (flexion/extension, adduction/abduction, internal/external tibial rotation, medial/lateral tibial shift, anterior/posterior tibial drawer, joint distraction/narrowing) for each cluster compared with the healthy control group. For each cluster comparison, the top row presents the mean trajectories of the two groups with confidence interval shown as the shaded area. The bottom row presents the ***post hoc*** non-parametric scalar field ***t*** tests (SnPM{t}), depicting where patients show more (+) and less (−) than healthy controls. The thin dotted lines indicate the critical thresholds of significance. The grey-shaded areas illustrate when the critical threshold exceeds; thus, a significant difference is present. The superimposed colour-squares highlight trajectories with similar differences when compared with the healthy control group: cyan presents increased flexion angle trajectories; magenta presents increased adduction angle trajectories; yellow presents abduction angle trajectories; green presents increased tibial external rotation and tibial lateral shift trajectories; red presents increased tibial anterior drawer; blue presents increased joint narrowing. The significance level was set to 5%.

G3 – The anterior drawer group

This was the only subgroup revealing severe anterior drawer throughout the gait cycle. Furthermore, this subgroup showed the largest external tibial rotation and lateral tibial shift throughout the motion (similar to G4) and larger adduction and joint narrowing compared with the healthy group. The clinical characteristics revealed that this subgroup was primarily composed of cases with medial tibiofemoral osteoarthritis, with partial and total ACL lesion and the largest KOA score of any group. In relation to the other subgroups, this group displayed the largest anterior drawer and, during the swing phase, the largest joint narrowing. In addition, like *the external rotation group,* it showed the largest adduction, external rotation, and tibial lateral shift. For this subgroup, increased lateral tibial shift was not observed during mid swing, whereas increased external rotation was not found during mid-swing, but this only applied when compared with *the abduction group*.

G4 – The external rotation group

This subgroup revealed, similar to G3, more external tibial rotation and lateral tibial shift, but no anterior drawer was observed compared with the healthy group. In addition, this subgroup showed more adduction and joint narrowing throughout the gait cycle. The clinical characteristics of this subgroup included the cases with the largest proportion of MCL and PCL lesions. In relation to the other subgroups, this group displayed, like *the anterior drawer group*, largest adduction, external rotation, and tibial lateral shift. For this subgroup, increased lateral shift was not observed during the swing phase compared with *the abduction group*, whereas increased external rotation was observed only when compared with *the abduction group*. Similar to lateral shift, no difference in external rotation was found during mid-swing between this subgroup and *the abduction group*.

All subgroups reported larger VAS pain scores during gait than the healthy group, with exception of *the abduction group* due to large variation in this group. However, no differences between subgroups were identified. Similarly, all subgroups had poorer clinical scores than the healthy group. Although the entire KOA patient group displayed greater Body Mass Index (BMI) than the healthy group and *the adduction group* included younger patients than *the flexion group* did, no other differences between groups were found in terms of potentially confounding variables (age, height, weight, side, and gender) (Table II).

Discussion

In patients with advanced KOA, we identified four clusters with homogeneous knee joint kinematics during gait that relate well with clinical characteristics but were clearly different from the knee joint kinematics of healthy volunteers without KOA. Our study differs from previous studies in three ways. First, we recorded the entire gait cycle using the accurate and precise dRSA method to assess knee kinematics (limits of agreement below 0.3° for rotation and 0.4 mm for translation)[13] rather than using traditional motion capture techniques that are often inhibited by soft-tissue artifacts. Second, we applied SPM, which allows examination of an entire kinematic trajectory thereby minimizing the risk of type-II errors and selection bias, which can be a problem with discrete-point comparisons. Third, we separated the patient cohort reversely by homogenous kinematics which present potential KOA phenotypes instead of applying the more often used predetermined clinical characteristics.

Previous gait studies of patients with KOA have compared various KOA group compositions to various control groups. KOA groups have been compared with healthy controls[4,27] and patients with medial tibiofemoral osteoarthritis have been compared with both healthy controls[5] and healthy controls with varus knee alignments[8]. Additionally, various discrete time-points and parameters during different gait phases have been used for group comparisons[4,5,8,27]. Thus, direct comparison with our results is challenging. However, a frequently chosen time point when comparing KOA and healthy groups is initial contact of the foot to the ground. At initial contact, diverse kinematic behaviors have been reported for patients with KOA compared with healthy controls: in patients with KOA, knee flexion has been identified as greater[5,27], lower[4], and similar[8] to that of healthy controls. Among these studies, three have investigated adduction and internal rotation. They found greater adduction[4,5,8], whereas the internal rotation showed both lower[4,5] and similar[8] rotations. Bytyqi *et al.*[8] and Zeng *et al.*[5] further investigated tibial anterior translation and found similar and lower translations, respectively. Only Zeng *et al.*[5] investigated the two remaining parameters, finding a greater tibial lateral shift and joint narrowing. The literature here presents various results based on various group comparisons. Thus, perhaps patients with KOA should not be assessed as a homogeneous group. Our results may explain this behavior and enhance our understanding of the KOA population as a heterogeneous group.

When comparing the entire KOA cohort with the healthy control group, we found increased tibial lateral shift, and joint narrowing at initial contact, whereas increased tibial external rotation first occurred later during stance. Thus, we cannot confirm the previous observations[4,5,8,28] which associate patients with KOAs with altered flexion, adduction, or anterior drawer. The likely reason for this is the large variation in kinematic trajectories in the KOA cohort. Thus, when the KOA cohort was clustered, we found statistically significant, clinically relevant differences for all kinematic parameters compared with the healthy control group. This suggests that the cohort of KOA patients comprises different kinematic phenotypes and that divergence in the results of previous investigations of the KOA group as a whole is due to the specific composition of kinematic subgroups included but not controlled for. This statement is substantiated by the fact that *the abduction group* (G2) was not observed until the number of subgroups increased from three to four. The identified kinematic characteristics of each subgroup could be linked to specific clinical characteristics. For example, *the flexion group* (G1), *the anterior drawer group* (G3), and *the external rotation group* (G4) revealed increased adduction. It displayed the largest portion of patients with medial tibiofemoral OA, whereas *the abduction group* (G2) revealed the largest proportion of patients with lateral tibiofemoral OA. Mechanically, this can be explained by the fact that reduced medial cartilage thickness increases a varus knee posture and, conversely, reduced lateral cartilage thickness increases a valgus knee posture[29]. Additionally, *the abduction group* (G2) and *the anterior drawer group* (G3) were the only subgroups revealing increased anterior drawer and larger ACL lesion grades than the healthy group. Additionally, *the anterior drawer group (G3)* showed the most prominent increase in anterior drawer and the largest proportion of patients with ACL rupture. Furthermore, *the anterior drawer group* (G3) also displayed the largest Ahlbeck score, representing a link between the well-established coherence of anterior-posterior knee instability and the development of KOA[30].

A systematic review[31] found that the course of pain and physical functioning in KOA were diverse and described a high heterogeneity across studies. The authors also suggested that KOA populations consist of subgroups or phenotypes. Our findings support this. However, the cluster scores and clinical outcome variables in our study indicate further subgroup overlap. Other subgroups and phenotypes have previously been identified. Knoop *et al.*[32] (later confirmed by Holla *et al.*[33]) identified three subgroups with distinct trajectories of physical functioning over time (good, moderate, and poor). Esch *et al.*[34] identified five homogeneous clinical phenotypes (minimal joint disease phenotype, strong muscle strength phenotype, severe radiographic KOA phenotype, obese phenotype, and depressive mood phenotype). Another systematic review proposed six other phenotypes (chronic pain, inflammatory, metabolic syndrome, metabolic bone/cartilage, mechanical overload, and minimal joint disease). These phenotypes may potentially explain some of the variation in clinical outcomes within the identified subgroups in our study. Thus, further investigation is needed, including multiple characteristics, e.g., clinical, biomechanical, psychosocial, and genetic factors, categorizing and identifying phenotypes that embrace the heterogeneous pathology and multifactorial nature of patients with KOA.

Overall, TKA is a successful treatment for pain reduction in patients with KOA. However, up to 20% of treated patients are, dissatisfied with the outcome[35], and more than 50% have residual knee symptoms[36]. Although considerable effort has been devoted to increase patient satisfaction, this has not yet been accomplished. The natural knee joint is heterogenic in shape, size, and function. Gait kinematic phenotyping within KOA patients may help us better understand the contributory and persistent causes of TKA patients' dissatisfaction with outcomes. Maybe, various patient groups should undergo different interventions or treatment with specific implant designs. Treatment targeted more specifically towards selective phenotypes has also previously been suggested to lead to improved outcomes[37]. To clarify this, new research on the groups identified in this study needs to be conducted.

Some limitations of our study warrant discussion. First, the gait pattern on the treadmill may be different from that over ground. However, some reports have declared that only minimal differences in kinetic and kinematic parameters were found between treadmill and over-ground gait[38,39]. Barefoot walking may influence the load on the lower extremity joints within the subjects, but conditions were similar for the KOA group and the healthy group. Thus, we do not expect this to have influenced either the results or the conclusion. Second, inevitably, crossing leg coursed leg-projection overlap during dRSA acquisition. However, our setup ensured that one of the radiographic views were always free of overlay and we did not see a negative effect of leg-overlay on accuracy in the entire gait cycle. Third, the requirement of a maximum thigh circumference may have excluded obese subjects whom have showed altered kinematics.[40]

In conclusion, we found that patients with advanced KOA can be clustered into four subgroups based on homogeneous gait patterns. For these subgroups, we determined a meaningful relationship to different KOA-affected compartments, KOA progression and ligament lesions. A better understanding of knee joint pathomechanics in patients with KOA allows for phenotyping of subgroups, which may inspire improved and more patient-specific treatment strategies in the future.

Contributors

ETP was involved in all aspects of the study and drafted the manuscript. SR, DK, and JD operated the patients, whereas NEL and SR examined and labelled the clinical characteristics. SR, MSA and MS had an essential role in the study design, interpretation, and presentation of data. All authors contributed to data interpretation and manuscript revision.

Competing interest statement

The authors have no conflicts of interest to declare.

Acknowledgements

We thank for the financial support we received from: Aarhus University, The Danish Rheumatism Association, Toyota-Fonden, Købmand Sven Hansen og Hustru Ina Hansens Fond, and Søster og Verner Lipperts Fond. The study sponsors have no conflicts of interest to declare.

Supplementary data

Supplementary data to this article can be found online at https://doi.org/10.1016/j.joca.2021.10.011.

References

1. Davis MA, Ettinger WH, Neuhaus JM, Mallon KP. Knee osteoarthritis and physical functioning: evidence from the NHANES I epidemiologic followup study. J Rheumatol 1991;18(4):591–8.
2. Pataky TC. One-dimensional statistical parametric mapping in Python. Comput Methods Biomech Biomed Engin 2012;15(3):295–301, https://doi.org/10.1080/10255842.2010.527837.
3. Pataky TC, Robinson MA, Vanrenterghem J. Vector field statistical analysis of kinematic and force trajectories. J Biomech 2013;46(14):2394–401, https://doi.org/10.1016/j.jbiomech.2013.07.031.
4. Nagano Y, Naito K, Saho Y, Torii S, Ogata T, Nakazawa K, *et al.* Association between in vivo knee kinematics during gait and the severity of knee osteoarthritis. Knee 2012;19(5):628–32, https://doi.org/10.1016/j.knee.2011.11.002.
5. Zeng X, Ma L, Lin Z, Huang W, Huang Z, Zhang Y, *et al.* Relationship between Kellgren-Lawrence score and 3D kinematic gait analysis of patients with medial knee osteoarthritis using a new gait system. Sci Rep 2017;7(1):1–8, https://doi.org/10.1038/s41598-017-04390-5.
6. Zeni JA, Higginson JS. Differences in gait parameters between healthy subjects and persons with moderate and severe knee osteoarthritis: a result of altered walking speed? Clin Biomech 2009;24(4):372–8, https://doi.org/10.1016/j.clinbiomech.2009.02.001.
7. Farrokhi S, Tashman S, Gil AB, Klatt BA, Fitzgerald GK. Are the kinematics of the knee joint altered during the loading response phase of gait in individuals with concurrent knee osteoarthritis and complaints of joint instability? A dynamic stereo X-ray study. Clin Biomech 2012;27(4):384–9, https://doi.org/10.1016/j.clinbiomech.2011.10.009.
8. Bytyqi D, Shabani B, Lustig S, Cheze L, Karahoda Gjurgjeala N, Neyret P. Gait knee kinematic alterations in medial osteoarthritis: three dimensional assessment. Int Orthop 2014;38(6):1191–8, https://doi.org/10.1007/s00264-014-2312-3.
9. Na A, Piva SR, Buchanan TS. Influences of knee osteoarthritis and walking difficulty on knee kinematics and kinetics. Gait Posture 2018;61:439–44, https://doi.org/10.1016/j.gaitpost.2018.01.025.
10. Kuntze G, Nettel-Aguirre A, Ursulak G, Robu I, Bowal N, Goldstein S, *et al.* Multi-joint gait clustering for children and youth with diplegic cerebral palsy. PLoS One 2018;13(10), https://doi.org/10.1371/journal.pone.0205174.
11. Nielsen ET, Stentz-Olesen K, de Raedt S, Jørgensen PB, Sørensen OG, Kaptein B, *et al.* Influence of the anterolateral ligament on knee laxity: a biomechanical cadaveric study measuring knee kinematics in 6 degrees of freedom using dynamic radiostereometric analysis. Orthop J Sport Med 2018;6(8), https://doi.org/10.1177/2325967118789699.

12. Gray HA, Guan S, Thomeer LT, Schache AG, de Steiger R, Pandy MG. Three-dimensional motion of the knee-joint complex during normal walking revealed by mobile biplane x-ray imaging. J Orthop Res 2019;37(3):615–30, https://doi.org/10.1002/jor.24226.
13. Christensen R, Petersen ET, Jürgens-Lahnstein J, Rytter S, Lindgren L, De Raedt S, *et al*. Assessment of knee kinematics with dynamic radiostereometry: validation of an automated model-based method of analysis using bone models. J Orthop Res 2020, https://doi.org/10.1002/jor.24875. Published online.
14. Bohannon RW, Williams Andrews A. Normal walking speed: a descriptive meta-analysis. Physiotherapy 2011;97(3):182–9, https://doi.org/10.1016/j.physio.2010.12.004.
15. Krčah M, Székely G, Blanc R. Fully automatic and fast segmentation of the femur bone from 3D-CT images with no shape prior. Proc - Int Symp Biomed Imaging 2011:2087–90, https://doi.org/10.1109/ISBI.2011.5872823. Published online.
16. Hemmingsen CK, Thillemann TM, Elmengaard B, de Raedt S, Nielsen ET, Mosegaard SB, *et al*. Elbow biomechanics, radiocapitellar joint pressure, and interosseous membrane strain before and after radial head arthroplasty. J Orthop Res 2020;38(3):510–22, https://doi.org/10.1002/jor.24488.
17. Miranda DL, Rainbow MJ, Leventhal EL, Crisco JJ, Fleming BC. Automatic determination of anatomical coordinate systems for three-dimensional bone models of the isolated human knee. J Biomech 2010;43(8):1623–6, https://doi.org/10.1016/j.jbiomech.2010.01.036.
18. Hansen L, De Raedt S, Jørgensen PB, Mygind-Klavsen B, Kaptein B, Stilling M. Marker free model-based radiostereometric analysis for evaluation of hip joint kinematics. Bone Joint Res 2018;7(6):379–87, https://doi.org/10.1302/2046-3758.76.BJR-2017-0268.R1.
19. van der Bom IMJ, Klein S, Staring M, Homan R, Bartels LW, Pluim JPW. Evaluation of optimization methods for intensity-based 2D-3D registration in x-ray guided interventions. In: Dawant BM, Haynor DR, Eds. Medical Imaging 2011: Image Processing. SPIE; 2011:657–71, https://doi.org/10.1117/12.877655.
20. Grood ES, Suntay WJ. A joint coordinate system for the clinical description of three-dimensional motions: application to the knee. J Biomech Eng 1983;105(2):136–44, http://www.ncbi.nlm.nih.gov/pubmed/6865355. Accessed July 31, 2015.
21. Dabirrahmani D, Hogg M. Modification of the Grood and Suntay joint coordinate system equations for knee joint flexion. Med Eng Phys 2017;39:113–6, https://doi.org/10.1016/j.medengphy.2016.10.006.
22. O'Connor CM, Thorpe SK, O'Malley MJ, Vaughan CL. Automatic detection of gait events using kinematic data. Gait Posture 2007;25(3):469–74, https://doi.org/10.1016/j.gaitpost.2006.05.016.
23. Koch JEJ, Ben-Elyahu R, Khateeb B, Ringart M, Nyska M, Ohana N, *et al*. Accuracy measures of 1.5-tesla MRI for the diagnosis of ACL, meniscus and articular knee cartilage damage and characteristics of false negative lesions: a level III prognostic study. BMC Musculoskelet Disord 2021;22(1), https://doi.org/10.1186/s12891-021-04011-3.
24. Peterfy CG, Schneider E, Nevitt M. The osteoarthritis initiative: report on the design rationale for the magnetic resonance imaging protocol for the knee. Osteoarthritis Cartilage 2008;16(12):1433–41, https://doi.org/10.1016/j.joca.2008.06.016.
25. Pedregosa F, Varoquaux G, Gramfort A, Michel V, Thirion B, Grisel O, *et al*. In: Scikit-Learn: Machine Learning in Python 2011;vol. 12, http://scikit-learn.sourceforge.net.
26. Nichols TE, Holmes AP. Nonparametric Permutation Tests for Functional Neuroimaging: A Primer with Examples. Published online 2001, https://doi.org/10.1002/hbm.1058.
27. Favre J, Jolles BM. Gait analysis of patients with knee osteoarthritis highlights a pathological mechanical pathway and provides a basis for therapeutic interventions. EFORT Open Rev 2016;1(10):368–74, https://doi.org/10.1302/2058-5241.1.000051.
28. Heiden TL, Lloyd DG, Ackland TR. Knee joint kinematics, kinetics and muscle co-contraction in knee osteoarthritis patient gait. Clin Biomech 2009;24(10):833–41, https://doi.org/10.1016/j.clinbiomech.2009.08.005.
29. Eckstein F, Wirth W, Hudelmaier M, Stein V, Lengfelder V, Cahue S, *et al*. Patterns of femorotibial cartilage loss in knees with neutral, varus, and valgus alignment. Arthritis Care Res 2008;59(11):1563–70, https://doi.org/10.1002/art.24208.
30. Wallace DT, Riches PE, Picard F. The assessment of instability in the osteoarthritic knee. EFORT Open Rev 2019;4(3):70–6, https://doi.org/10.1302/2058-5241.4.170079.
31. De Rooij M, Van Der Leeden M, Heymans MW, Holla JFM, Häkkinen A, Lems WF, *et al*. Prognosis of pain and physical functioning in patients with knee osteoarthritis: a systematic review and meta-analysis. Arthritis Care Res 2016;68(4):481–92, https://doi.org/10.1002/acr.22693.
32. Knoop J, Van Der Leeden M, Thorstensson CA, Roorda LD, Lems WF, Knol DL, *et al*. Identification of phenotypes with different clinical outcomes in knee osteoarthritis: data from the osteoarthritis initiative. Arthritis Care Res 2011;63(11):1535–42, https://doi.org/10.1002/acr.20571.
33. Holla JFM, Van Der Leeden M, Heymans MW, Roorda LD, Bierma-Zeinstra SMA, Boers M, *et al*. Three trajectories of activity limitations in early symptomatic knee osteoarthritis: a 5-year follow-up study. Ann Rheum Dis 2014;73(7):1369–75, https://doi.org/10.1136/annrheumdis-2012-202984.
34. Van der Esch M, Knoop J, van der Leeden M, Roorda LD, Lems WF, Knol DL, *et al*. Clinical phenotypes in patients with knee osteoarthritis: a study in the Amsterdam osteoarthritis cohort. Osteoarthritis Cartilage 2015;23(4):544–9, https://doi.org/10.1016/j.joca.2015.01.006.
35. Bourne RB, Chesworth BM, Davis AM, Mahomed NN, Charron KDJJ. Patient satisfaction after total knee arthroplasty: who is satisfied and who is not? Clin Orthop Relat Res 2010;468(1):57–63, https://doi.org/10.1007/s11999-009-1119-9.
36. Nam D, Nunley RM, Barrack RL. Patient dissatisfaction following total knee replacement: a growing concern? Bone Jt J 2014;96B(11):96–100, https://doi.org/10.1302/0301-620X.96B11.34152.
37. Bijlsma JWJ, Berenbaum F, Lafeber FPJG. In: Arthritis 1 Osteoarthritis: An Update with Relevance for Clinical Practice 2011;vol. 377, www.thelancet.com.
38. Riley PO, Paolini G, Della Croce U, Paylo KW, Kerrigan DC. A kinematic and kinetic comparison of overground and treadmill walking in healthy subjects. Gait Posture 2007;26(1):17–24, https://doi.org/10.1016/j.gaitpost.2006.07.003.
39. Levine D, Richards J, Whittle MW. Whittle's Gait Analysis 2012.
40. Li J, Tsai T, Brentzel K, Ahn YJ, Felson DT. Three-dimensional knee joint kinematics in obese individuals with knee pain during treadmill gait. PLos One 2017;12(3):1–11, https://doi.org/10.1371/journal.pone.0174663.

Paper IV

In vivo kinematic comparison of Medial Congruent and Cruciate Retaining polyethylene designs in total knee arthroplasty - A randomized controlled study of gait using dynamic radiostereometry

E.T. Petersen[1-3], S. Rytter[2-4], D. Koppens[1,4], J. Dalsgaard[1], T.B. Hansen[1,2], M.S. Andersen[5], M. Stilling[2-4]

[1] *University Clinic for Hand, Hip and Knee Surgery, Holstebro Central Hospital, 7500 Holstebro, Denmark*
[2] *Department of Clinical Medicine, Aarhus University, 8200 Aarhus N, Denmark*
[3] *AutoRSA Research Group, Orthopaedic Research Unit, Aarhus University Hospital, 8200 Aarhus N, Denmark*
[4] *Department of Orthopaedic Surgery, Aarhus University Hospital, 8200 Aarhus N, Denmark*
[5] *Department of Materials and Production, Aalborg University, 9220 Aalborg, Denmark*

A B S T R A C T

Objective: Total knee arthroplasty is a successful treatment for patients with painfully disabling knee osteoarthritis. New implant designs attempt to normalize kinematics patterns that may improve functional performance and patient satisfaction. The purpose of the study was to compare functional kinematics and congruency of two different polyethylene bearings: a more medial congruent anatomic design and a symmetric design.

Methods: In this double-blinded randomized study, 66 patients with knee osteoarthritis were included randomly in two groups: Medial Congruent (MC, n=31) and Cruciate Retaining (CR, n=33). Clinical characteristics such as knee ligament lesion and knee osteoarthritis score were graded on preoperative magnetic resonance imaging and radiographs, respectively. Dynamic radiostereometric analysis was used to assess tibiofemoral joint kinematics and articulation congruency at one-year follow-up. Patient-reported outcome measures were assessed preoperatively and at one-year follow-up.

Results: Compared to the CR bearing, the MC bearing displayed an offset with greater anterior tibial drawer during the entire motion, and more tibial external rotation from mid-swing to the end of the gait cycle at one-year follow-up. Further, the congruency area in the joint articulation was larger during approximately 80% of the gait cycle for the MC bearing compared with the CR. The patient-reported outcome measures improved but there were no differences between groups. In addition, there were no difference in clinical characteristics and there were no knee revisions or recognised deep infections during follow-up.

Conclusion: The study demonstrates that the MC bearing design changes tibiofemoral kinematics and increases the area of congruency compared with the CR bearing. This may control joint kinematics and contribute to a more stabilized knee motion that may restore patient's confidence in knee function during daily activities.

Introduction

Knee osteoarthritis (KOA) is a chronic disorder resulting in degenerative changes to the joint, and is commonly associated with pain, stiffness, reduction in range-of-motion, and muscle weakness that limits daily activities [11]. The prevalence of disabling knee pain caused by KOA in adults above the age 55 years is 10%, and a quarter of those affected are severely disabled [46]. Total knee arthroplasty (TKA) is widely accepted as a well-documented and successful treatment for patients with end-stage KOA [24, 39]. However, within the first five years after surgery, 6% of patients require revision [43], 19% are unsatisfied with the outcome one year after knee surgery [2, 7], and more than 50% may have residual knee symptoms [38]. Considerable effort has been devoted in improving TKA designs in an attempt to reducing the number of dissatisfied TKA patients, however, this has not yet been successful.

There is emerging evidence that achieving normalized kinematic patterns in prosthetic knees will improve functional knee performance [8, 54]. The native knee is characterised by a medial compartment that has a better articular congruence due to a relatively stationary centre of rotation acting as a pivot point compared to lateral compartment that has less congruency with more motion. This is caused by a larger medial femoral condyle and a concave medial tibial plateau compared to a smaller lateral femoral condyle and a flat or slightly convex lateral tibial plateau [35]. It is the articular surface congruency and the ligaments that guide the kinematics and balance of the knee joint by controlling the interaction between the tibial plateau and the femoral condyles. This makes the knee to one of the most complex weight-bearing joints in the body, concerning movement pattern, stability, and functionality. Persona® The Personalized Knee® System (Zimmer Biomet, Warsaw, Indiana, USA) is a design that attempts to address these challenges. The prosthetic knee system provides various implant sizes, shapes, and constraint options, which improve the surgeon's options for implant fitting and ligament balancing. In addition, the polyethylene bearing of the tibial implant is available with an anatomic prosthetic knee design, Persona® Medial Congruent® Articular Surface (MC), in which the articular surface design resembles the native surface of the tibial plateau and expectedly promotes kinematics during the knee movements, which are closer to native knees than the standard symmetrical polyethylene bearing prosthetic knee design, Persona® Cruciate Retaining (CR) [56]. However, the MC bearing design is yet to be investigated dynamically during gait using dynamic radiostereometric analysis (dRSA), which is the gold standard for In vivo three-dimensional knee joint kinematic estimates [9, 15, 18, 41].

The purpose of this study was to compare functional kinematics and congruency of two different polyethylene bearings: a more medial congruent anatomic design and a symmetric design using dRSA during gait at one-year follow-up after TKA surgery. We hypothesized that 1) the tibiofemoral kinematics are different between the MC bearing and the CR bearing, and that 2) the MC bearing enhance articular congruency compared to the CR bearing.

Methods

This study represents a double-blinded randomized controlled study, investigating two different designs of Vitamin E Infused Technology polyethylene bearings for TKA at one year follow-up (clinicaltrials.gov NCT03633201). We determined the appropriate group sizes with a post-hoc power analysis using data variation from published knee kinematics with TKA [20]. Assuming a threshold for observing a difference of three degrees (for rotation) and three millimetres (for translation), an alpha value of 0.05, and a power of 0.80, group sizes of n = 29 were required. Sixty-six subjects were enrolled in the period from 2017 to 2019 with inclusion and exclusion criteria that are presented in Table 1. The subjects were randomized into two groups with different polyethylene cruciate retaining bearings: an asymmetric medial congruent design – the MC and a symmetric less congruent design – the CR, both from the same manufacturer (Zimmer Biomet, Warsaw, Indiana USA). Block randomization (blocks of 10) was performed during surgery using concealed opaque envelopes. Both bearings were compatible with the same femur, tibia, and patella implants (Zimmer Biomet, Warsaw, Indiana, USA). Hence, the only difference between the groups was the bearings' shape and congruency. The study was approved by the Committee on Biomedical Research Ethics of the Central Denmark Region (1-10-72-303-16, issued 28 February 2017) and registered with the Danish Data Protection Agency (1-16-02-582-16, issued 31 October 2016). The study was conducted following the Helsinki Declaration, and all patients gave written informed consent. The consort diagram is presented in Figure 1.

Surgical procedure

Standard operative procedure with an anterior midline incision and medial parapatellar arthrotomy was used in all patients and with surgeries performed according to the manufacturer's surgical technique [57]. All patients received cemented CR femoral implants (standard or narrow), tibial implants with either a MC or CR bearing, and patella resurfacing with all-polyethylene patella implants. The MC bearing is designed with a higher anterior lip, a more posterior dwell point, and with a more congruent articulation with the femur implant compared to the CR bearing (Figure 2). The patients followed the same postoperative routine rehabilitation regime and were discharged according to well-defined clinical and functional criteria. The surgical procedures were performed by three experienced knee arthroplasty surgeons.

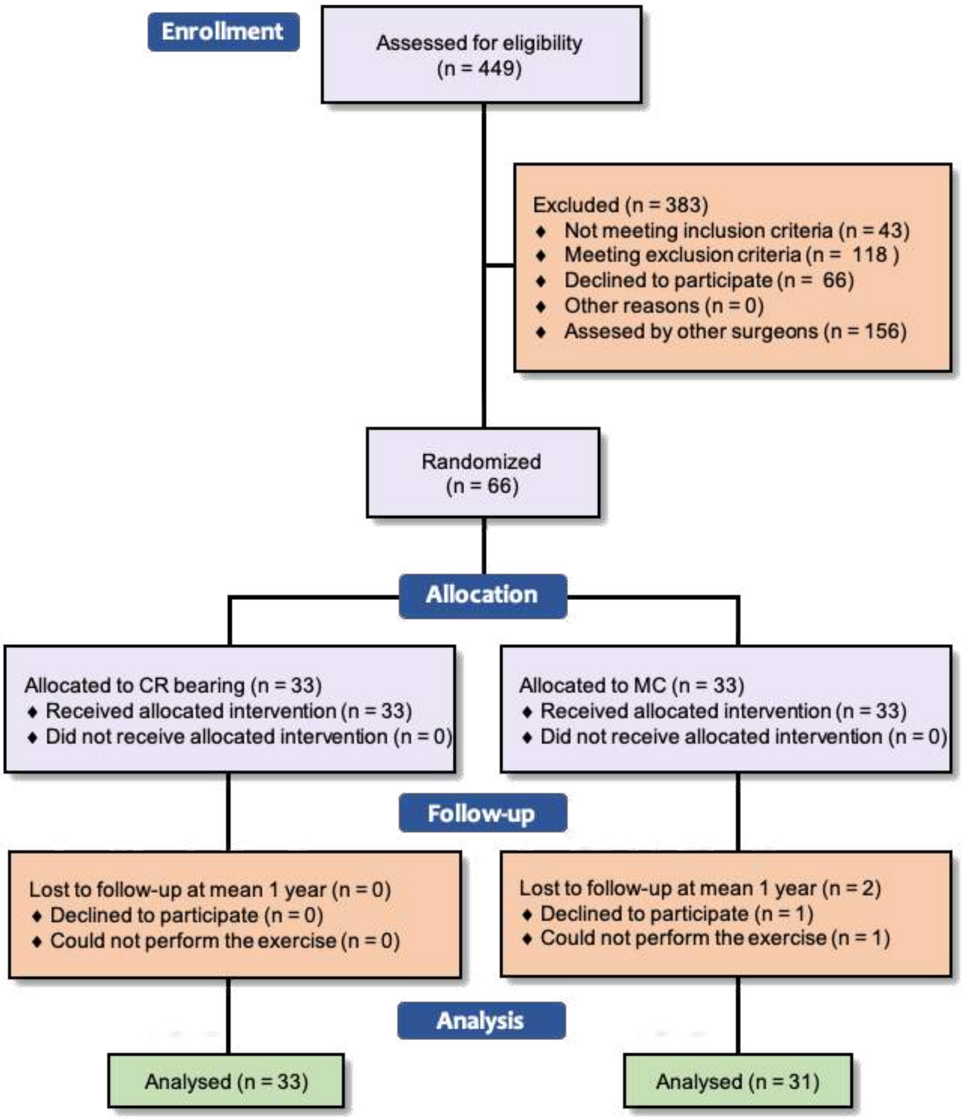

Figure 1 Consort flow chart. All available data were used in the statistical analysis. A complete dataset was collected for 33 patients in the CR bearing group and 31 patients in the MC bearing group.

Experimental protocol

One year after TKA surgery, participants walked barefooted on a horizontal treadmill (Sole F63, Jonesboro, AR, USA), imitating gait. Once the participant had completed a habituation period (gradually speeding to a final speed of 0.83 m) to familiarize with the lab environment and felt comfortable, the data acquisition was initiated. The walking speed is slightly slower than average (1.25 m/s) [5] to facilitate sufficient dRSA recordings throughout the entire gait cycle. Up to seven coherent gait cycles were obtained. As a precautionary measure and anticipation of balance loss during testing, subjects had a rail they could hold on to. Only none-rail-supported gait trials were included for further analysis. Immediately after completing the gait trials, we registered, the patients pain intensity during the trial using a horizontal visual-analogue-scale (ranging 0-10), and the patients strength using a leg-extension-power-rig (Bio-Med International, Nottingham, UK) [1, 30]. The visual- analogue -scale and leg-extension-power-rig were also registered preoperatively.

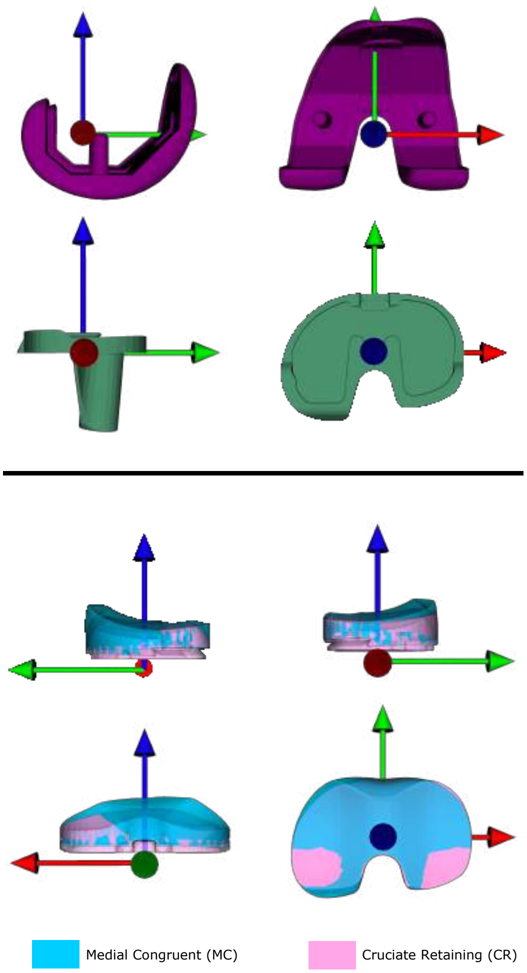

Figure 2 Implant models; a) Illustration of the implant surface models in a sagittal (left column) and an axial view (right column) represented in their coordinate system. Medial-lateral (X, red), anterior-posterior (Y, green), and proximal-distal (Z, blue). For the femur: The origin was defined as the centre of a least square fitted cylinder to the medial and lateral articulating surfaces. X-Y plane was parallel to the inner most distal bone contact surface, and the X-Z plane was parallel to the inner bone contact surface of the posterior flanges. For the tibia: The origin was defined medial-lateral as the centre of a circle fitted to the inner central locking mechanism, and anterior-posterior as the anteroposterior midpoint. The X-Y plane was parallel to the lower part of the baseplate. Y-Z plane was defined perpendicular to the X-Y plane coinciding the midpoint of the anterior locking mechanism. The first two rows illustrate the femoral and tibial implants. The next two rows, third and fourth, illustrate the two bearings along with the tibia implant: first, the Cruciate Retaining (CR) bearing (pink), and second, the Medial Congruent (MC) bearing (light blue). b) Superimposed illustration of the two bearings, CR and MC, displaying the design differences in a medial (top left), lateral (top right), frontal (bottom left), and axial (bottom right) view.

Dynamic radiographic imaging and analysis

We utilized a dedicated dRSA system (AdoraRSA; NRT X-Ray A/S, Hasselager, Denmark) that was time-synchronized with an optical motion capture system (OptiTrack, NaturalPoint, Corvalis, OR, USA) to record the gait trials. The biplanar dRSA setup with minimum six infrared cameras (OptiTrack Prime 13) is presented in Figure 3 and were identical to the system previously described [48]. The series of

Table 1. Inclusion and exclusion criteria

	Knee osteoarthritis patient group
Inclusion criteria	Age above 18 years but no more than 80 years of age.
	Informed and written consent.
	Primary knee osteoarthritis in capable men and women.
	Indication for cruciate retaining total knee arthroplasty.
Exclusion criteria	Patients with a thigh circumference exceeding 60 cm.*
	Patients with conditions that severely compromise their gait other than KOA in the affected knee.
	Patients with previous severe fractures at the knee level or severe malalignment at the knee level.
	Surgically implanted metallic parts and pacemaker.*
	Patients with need for an augmentation and/or stem extension.
	Patients who cannot perform the exercises.

*Inevitable criteria for magnetic resonance imaging (MRI) acquisition. Abbreviation: KOA – knee osteoarthritis

stereoradiographs were analysed using an automated software system developed at our institution (AutoRSA software, Orthopaedic Research Unit, Aarhus, Denmark). The software utilizes virtually generated silhouette-projections of three-dimensional triangular surface models to the image-plane. The optimal model pose was found by minimizing the difference between the virtually generated projection image and the actual stereoradiographs using a normalized gradient correlation approach [6, 22]. The mathematical optimization algorithms have been previously described in more detail [22, 25]. The manufacturer supplied the three-dimensional triangular implant surface models containing approximately 5,000 vertices each.

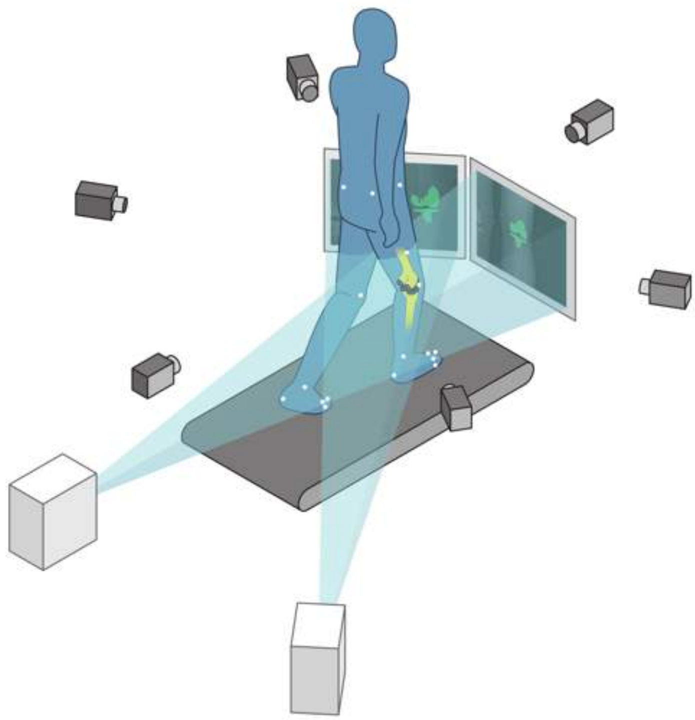

Figure 3 Illustration of the gait analysis setup utilizing a biplanar radiostereometric setup where the detectors were placed on individual stands with a relative angle of 40 degrees; one in front of the subject and one to the side of the limb of interest. The setup was mirrored for left/right knees to accommodate having the investigated knee as close as possible to the side view. The six optical cameras were positioned strategically surrounding the subject to avoid occluded markers during analysis of the skin-attached reflective markers (white dots). The markers were attached at the subjects' pelvis, lower limb, and feet; three cluster markers at the thigh, two at the knee epicondyles, three cluster markers at the shank, two at the ankle malleolus, one at the heel, three at the metatarsales (1, 3, 5), and one at the first distal phalanx.

Quantification of tibiofemoral joint kinematics and articulation

Tibiofemoral joint kinematics

We implemented the joint coordinate system initially defined by Grood and Suntay [19] to describe the tibiofemoral joint kinematics, using the modified equations that Dabirrahmani and Hogg [10] proposed to account for possible hyperextension and hyperflexion. For each frame, we computed the relative motion in all six degrees-of-freedom (rotation and translation) of the body-fixed coordinate systems. The kinematics were determined using the manufacturer-provided implant models and their coordinate systems as presented in Figure 2. The translation was quantified in mm with medial tibial shift, tibial anterior drawer, and joint distraction as positive directions. Rotations were measured in sequence as presented and quantified in degrees with flexion, adduction, and tibial internal rotation as positive directions [49].

In addition, we measured the range-of-motion of the femoral low-point kinematics relative to the tibia implant for each timepoint during the gait cycle. The femoral low-point kinematics were defined as the lowest point of the femur implant relative to the tibia implant. These points were determined for the medial and lateral compartment separately. Hence, the range-of-motion describe the joint constrain achieved between the femoral and tibial implants for the medial and lateral compartment, respectively.

Tibiofemoral joint articulation

We estimated the joint articulation by constructing a distance map between the femoral implant and tibial bearing. Since the tibial bearing is radiolucent, we assumed a rigid relationship to the radiopaque tibial implant to estimate its pose. The distance map was obtained by assigning each mesh point on the tibial bearing with the value of its shortest distance to the femur implant model within a distance range limit of -0.5 to +0.5 mm. The distance map was computed for each frame. Since patients received different implant sizes and bearing types, we scaled each bearing to a fixed width of 68 mm, which represented a mid-implant size, to facilitate direct comparison between patient groups. Subsequently, we defined a 70x70 point grid with a point distance of 1 mm. It was centralized about the proximal-distal axis and oriented in the coronal plane of the tibial implant coordinate system. The grid points were coloured according to the cell colour of which its orthogonal projection intersected with the bearing (Figure 4).

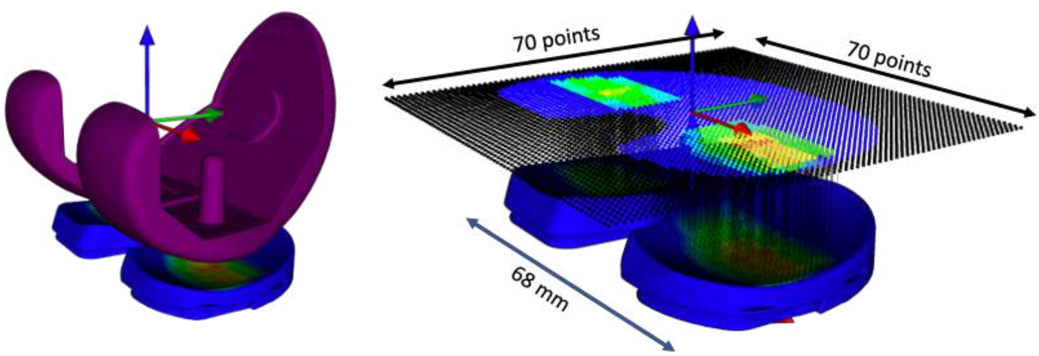

Figure 4 Quantification of joint articulation; left) Illustration of the distance colormap determined by the shortest distance from each point on the tibial bearing to the femoral implant. The spacing between the bearing and implant is increased for visualisation purpose. right) Illustration of the 3D colormap transformation to the 2D point grid that are used in the statistical parametric mapping (SPM) analysis to quantify the difference between the Medial Congruent (MC) and Cruciate Retaining (CR) bearing.

Time normalization

Kinematic values and articulation distance maps were divided into gait cycles - starting and ending with two successive initial foot contacts of the ipsilateral limb. We used the approach of O'Conner et al. [42] to identify initial contact using the optical markers placed on the foot. To estimate each subject's most representative gait cycle pattern, we time-normalized the kinematic measures to 21 discrete points representing the gait cycle from 0-100% and calculated the median across trials for each subject.

Clinical characteristics, PROMs, and operative complications

Preoperatively, we classified KOA according to the Ahlbäck score (grade 1-5) based on conventional weight-bearing radiographs. Additionally, we registered the affected tibiofemoral compartment as lateral or/and medial. Knee ligament lesions were assessed using detailed magnetic resonance imaging (1.5 T Avanto, SIEMENS, Erlangen, Forchheim, DE). We applied a modified version of the Osteoarthritis Initiative protocol [47] based on GE scanner recommendations (T2 SAG de3D DESS WE acquisition with 0.7 mm slice thickness and T1 COR fl3D WE with 1.5 mm slice thickness). We evaluated the following knee ligaments: anterior cruciate ligament (ACL), posterior cruciate ligament (PCL), medial collateral ligament (MCL), and lateral collateral ligament (LCL). The ACL was graded as 0 (no lesion), 1 (partial lesion), and 2 (total lesion). PCL, MCL, and LCL were registered as 0 (intact) or 1 (with lesion). The patient-reported outcome measures (PROMs) were assessed preoperative and at one-year follow-up by the Oxford Knee Score (OKS) [12], the Forgotten Joint Score (FJS) [3], and the Knee Osteoarthritis Outcome Score (KOOS) [51]. Furthermore, we registered any postoperative complications during the one-year follow-up period.

Statistical analysis

Differences in tibiofemoral joint kinematics and articulation across the entire gait cycles were examined using one-dimensional SPM with the open-source code spm1d (spm1d.org, v.0.4.2) for Python (Python Software Foundation, v.3.6). Statistical parametric mapping (SPM) allows for examining the entire one-dimensional time series of kinematic trajectories, avoiding selection bias, and allowing for non-directed hypothesis testing instead of reducing the dataset to a specific observation or risking false hypothesis testing due to multiple repeated measurements [44, 45]. For the two-dimensional articulation measure, we performed SPM analysis on the entire grid-map at each time point during the gait cycle. SPM analysis uses Gaussian random field theory to calculate the threshold that only the significance level of equivalently smooth Gaussian random fields would cross when the null hypothesis is true. QQ-plots revealed not normally distributed kinematic data. Thus, we used statistical non-parametric mapping (SnPM), which deals with smoothness implicitly and estimates the test statistics through permutation[40]. First, a Hotelling test was implemented on the entire vector field. Next, if statistical significance was reached at the vector field level, the post-hoc Hotelling test was applied to each vector component. We compared demographically, clinically characteristic, PROMs, visual-analogue-scale, leg-extension-power, and contact point range-of-motion differences between groups using Student's T-test for continuous variables, ordinal logistic regression for categorical variables, and chi-squared for binary variables. Visual inspection of QQ-plots verified normally distributed data.

Results

Tibiofemoral joint kinematics and articulation

The comparison of the tibiofemoral joint kinematic trajectories for the MC and CR bearings are presented in Figure 5. The MC bearing displayed an offset with a statistically significantly greater anterior tibial drawer during the entire motion, and more tibial external rotation from the mid-swing to end of the gait cycle.

The congruency area in the joint articulation was statistically significantly greater during approximately 80% of the gait cycle for the MC bearing compared with the CR. (Figure 6). This included most of the stance phase and the mid-swing to the end of the gait cycle. The greater congruency occurred during the same gait phases for both knee compartments; for the lateral compartment, it was pronounced mostly medially, whereas for the medial compartment, the area of congruency moved during the gait cycle. For the medial compartment, the greater area of congruency was pronounced posterolateral at initial contact of the foot. During loading response, the greater congruency area moved to also include the anterolateral area of the bearing until it resolved during pre-swing, first posterolaterally and next anterolaterally. During mid-swing, the greater congruency area appeared again, this time anterolateral and moved posterolateral during the terminal swing. Furthermore, the femoral low-point kinematics for the MC bearing group showed 1.8 mm [CI 0.8;2.8] ($p<0.001$) smaller range-of-motion for the medial compartment when compared to the CR bearing (Table 2C).

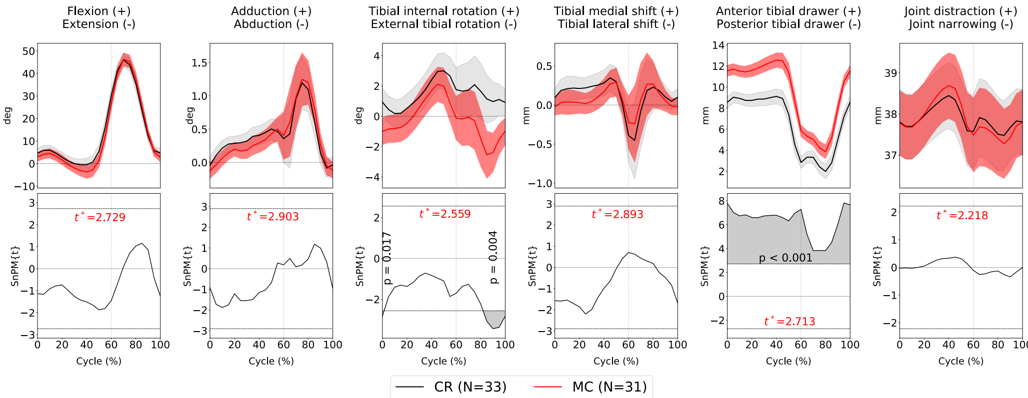

Figure 5 Statistical parametric mapping of tibiofemoral joint kinematics. Kinematic comparison of the MC bearing group (red) with the CR bearing group (gray). The top row presents the mean trajectories of the two groups with confidence interval as the shaded area. The bottom row presents the post hoc non-parametric scalar field t tests (SnPM{t}), depicting where the MC group show higher (+) and lower (-) than the CR group. The thin dotted lines indicate the critical thresholds for significance. The grey-shaded areas illustrate when critical threshold is exceeded thus determining a significant difference.

Clinical characteristics, PROMs, and complications

Between groups, no differences were found in demographics, clinical characteristics, implant size, or implant type ($p>0.320$). Furthermore, the three surgeons operated a similar number of patients in both groups ($p=0.367$). Both groups improved significantly regarding PROMs ($p<0.001$), visual-analogue-scale ($p<0.001$), and leg-extension-power-rig ($p<0.004$). However, no differences in improvement were found between groups ($p>0.351$). In the first year after TKA, five patients had knee manipulations under anaesthesia for joint stiffness, five in the MC group and two in the CR group ($p=0.197$). Among those an intraarticular corticosteroid injection was performed in one patient per group. Aspiration of the knee due to joint effusion was performed in three patients, one in the MC group and two in the CR group, but cultures were negative for bacterial growth, and there were no knee revisions or recognized deep infections during the one-year follow-up period.

Discussion

One year after surgery, the MC bearing group displayed greater anterior drawer throughout the entire gait cycle, greater tibial external rotation from mid-swing to the end of the gait cycle, and a greater congruency area between the tibial bearing and femoral implant for approximately 80% of the gait cycle compared with the CR bearing group.

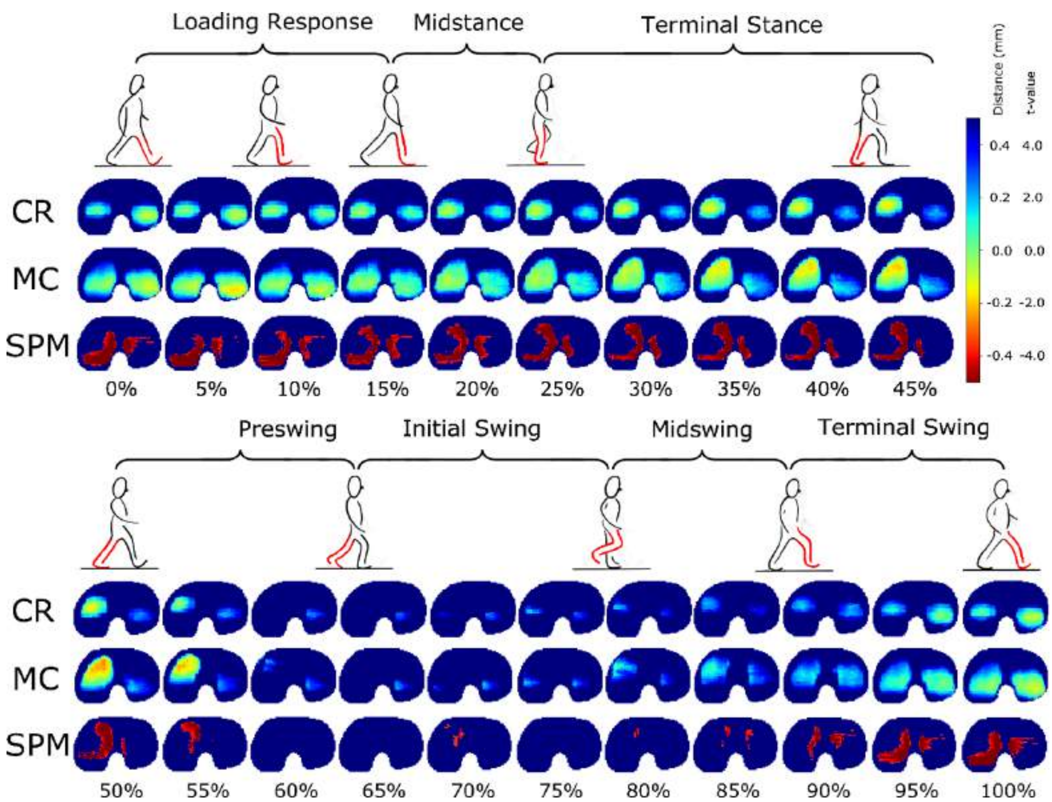

Figure 6 Statistical parametric mapping of tibiofemoral joint articulation. Illustration of the tibiofemoral articulation analysis of a right knee throughout the gait cycle represented by the distance point grid (70x70 pixels). The columns represent each of the 21 normalized discrete time points corresponding to the same time points as used for the kinematic analysis. The rows represent from the top Cruciate Retaining (CR) bearing, Medial Congruent (MC) bearing, and the results of the statistical parametric mapping (SPM) analysis. The red areas of the SPM row represents where the statistical significance was reached between the MC and CR grid-point maps.

Tibiofemoral joint kinematics

The MC bearing was designed with an increased anterior lip height and a more posterior dwell point when compared to the CR. According to a simulation study, investigating different sagittal and coronal congruency levels in artificial tibiofemoral joint, the tibial anteroposterior translation and internal rotation are the parameters that depends primarily on sagittal congruency [55]. This support our findings of the observed differences between the MC and CR bearing within these two parameters, and that these

Table 2. Group summary and comparison

	CR (n=33)	MC (n=31)	P-value*
2a) Demographics with means and confidence intervals for continuous parameters and percentage for categorical parameters.			
Age (years)	62.0 (59.2;65.9)	64.8 (61.8;67.9)	0.182
Side (left %)	45.5	64.5	0.126
Gender (female %)	39.4	38.7	0.955
Height (cm)	173.5 (170.5;176.6)	171.9 (169.5;174.5)	0.420
Weight (kg)	87.9 (82.7;93.2)	85.9 (80.5;91.2)	0.576
Body Mass Index (kg/m²)	29.2 (27.6;30.7)	29.0 (27.2;30.8)	0.913
Thigh circumference (cm)	52.9 (50.9;54.8)	51.4 (49.3;53.6)	0.484
2b) Clinical characteristics with means and confidence intervals for continuous parameters and percentages for categorical parameters (except for the KOA Ahlbäck score, which is presented with mean and confidence interval).			
ACL lesion (0/1/2) %	27 / 36 / 36	35 / 42 / 23	0.474
PCL lesion (%)	12.1	12.9	0.925
MCL lesion (%)	9.1	6.5	0.694
LCL lesion (%)	9.1	3.2	0.333
KOA Ahlbäck grade	3.0 (2.6;3.4)	2.6 (2.2;3.0)	0.071
KOA medial (%)	64.6	80.7	0.130
KOA lateral (%)	12.1	6.5	0.437
KOA medial+lateral (%)	21.2	12.9	0.379
FJS (preop)	16.1 (11.0;21.2)	16.5 (10.5;22.4)	0.522
OKS (preop)	24.3 (22.2;26.5)	23.1 (20.8;25.4)	0.775
KOOS SYMPTOMS (preop)	47.4 (41.5;53.4)	51.0 (44.1;57.9)	0.417
KOOS PAIN (preop)	42.5 (37.5;47.5)	45.4 (39.6;51.2)	0.438
KOOS ADL (preop)	49.7 (44.5;54.9)	53.7 (48.9;58.6)	0.250
KOOS SPORT/REC (preop)	14.8 (9.9;19.8)	16.1 (10.6;21.6)	0.726
KOOS QOL (preop)	29.0 (25.0;32.9)	26.8 (22.4;31.3)	0.459
VAS – gait (preop)	2.3 (1.6;3.1)	2.5 (1.6;3.5)	0.729
LEPR (preop) (W/kg)	1.5 (1.3;1.7)	1.5 (1.3;1.7)	0.731
FJS (follow-up)	55.4 (43.6;67.3)	58.9 (47.7;70.2)	0.668
OKS (follow-up)	39.0 (36.2;41.8)	39.0 (36.4;41.8)	0.986
KOOS SYMPTOMS (follow-up)	71.4 (64.6;78.2)	75.0 (68.6;81.4)	0.441
KOOS PAIN (follow-up)	82.9 (76.2;89.6)	82.6 (76.8;88.5)	0.946
KOOS ADL (follow-up)	83.2 (77.4;88.9)	84.8 (79.3;90.3)	0.672
KOOS SPORT/REC (follow-up)	46.5 (38.5;54.5)	49.5 (39.2;59.8)	0.638
KOOS QOL (follow-up)	64.4 (55.8;72.9)	65.3 (58.0;72.7)	0.306
VAS – gait (follow-up)	0.2 (-0.1;0.4)	0.0 (-0.0;0.1)	0.354
LEPR (follow-up) (W/kg)	1.8 (1.5;2.0)	1.8 (1.6;2.0)	0.712
2c) Range-of-motion of the femoral low-point kinematics. Measured for both the lateral and medial compartment in both directions; x (lateral [+] and medial [-]) and y (anterior [+] and posterior [-]). The means and confidence intervals are presented for each group.			
Lateral low-point (x)	1.9 (1.7;2.1)	1.8 (1.6;2.0)	0.381
Lateral low-point (y)	4.7 (4.1;5.3)	4.0 (3.5;4.5)	0.076
Medial low-point (x)	1.4 (1.2;1.6)	1.4 (1.2;1.6)	0.883
Medial low-point (y)	6.4 (5.6;7.2)	4.6 (4.1;5.1)	**<0.001**

ACL: anterior cruciate ligament, PCL: posterior cruciate ligament, MCL: medial collateral ligament, LCL: lateral collateral ligament, KOA: knee osteoarthritis, , FJS: forgotten joint score, OKS: oxford knee score, KOOS: knee osteoarthritis outcome score, ADL: activity of daily living, QOL: quality of life, VAS: visual-analogue-scale, LEPR: leg extension power rig, W/kg; watt/kilogram, MUA: manipulation under anaesthesia , preop: preoperative, follow-up: 1 year follow-up.
Demographics, clinical characteristics, and preoperative proms have previously been published [51].

kinematic differences may be a result of the enhanced sagittal congruency design of the MC bearing.

The combination of these design features may act as a constraint of the femoral condyles to move anteriorly, which results in an anterior appearance (anterior off-set) of the tibial component and MC bearing relative to the femur. Thus, the shape of the MC bearing seems to prevent the so-called "paradoxical motion" phenomenon [13], which is an abnormal kinematic motion, where the femur slides anteriorly relative to tibia. Paradoxical motion is associated with mid-flexion instability, which is more evident for CR bearing designs and has been shown to be a contributing factor for dissatisfaction in these TKA patients [23, 34]. This is supported in a recent intraoperative investigation of a passive knee flexion movement of the MC and CR bearings of the *Persona®* knee using an image-free navigation system that identified anterior constraint of the femoral component on the MC bearing when compared to the CR at 30 and 45 degrees of knee flexion [53]. The results of the present study showed a similar but constant difference in anterior offset between MC and CR bearings during patients' active gait cycle one year after surgery and confirm that the MC bearing prevents paradoxical motion. This may improve mid-flexion stability and result in more satisfied TKA patients. We suggest further research to investigate the active mid-flexion instability for the MC bearing as well as more demanding tasks that also include deeper knee flexion.

The MC bearing design contributed to a greater tibial external rotation compared to the CR design during the extension phase of the swing. This phenomenon, referred to as the "screw-home movement" [21], occurs for the native knee during the last 10-15 degrees of an open-chain extension. It is caused by tension in the ACL, the shape of the medial femoral condyle, and a lateral oriented tension in the patella tendon as the quadriceps muscle pull slightly lateral near full knee extension. In most TKA designs, the ACL is removed during surgery. The continuation of the screw-home movement in the TKA with a MC bearing must therefore relate to the bearing design and congruency acting as a joint stabilizer. In the intraoperative kinematic study of passive knee motion, Tsubosaka et al. found less internal rotation near full knee extension for the MC bearing compared with the CR bearing and concluded that MC bearings have a more effective screw-home movement [53]. The kinematic assessment of active gait in the present study confirms these results.

Tibiofemoral joint articulation

Investigations of the tibiofemoral joint articulation contact confirmed more congruency for the MC bearing design than for the CR bearing design. In addition, we found that the area of greater congruency moved during the gait cycle. Previous studies have described several occurrences of anteroposterior directed movement within the tibiofemoral joint during stance [14, 28, 29]. They describe three load cases (Figure 7); at initial contact and during late midstance, a posterior load of the femur on the tibia corresponding to the extensor mechanism pulling at tibia (case 1); during loading response, the femur apply an anterior load on tibia corresponding to the braking action of tibia (case 2); during terminal stance and pre-swing, an anterior load of the femur on tibia is applied, corresponding to the increased moment from the centre of gravity's forward movement and contraction of the gastrocnemius (case 3). We observed that the greater area of congruency for the MC bearing were positioned and moved correspondingly to these knee load cases. However, we did not observe occurrence of load case 1 during the later midstance as the knee extends back (no greater posterior congruency area of the MC). An explanation may be due to the single-leg support, where the entire load of the body and the knee flexion angle may result in complete congruence between the bearing and the femoral implant. Importantly, the greater congruency is not necessarily a result of anteroposterior relative movement of the femur and tibia implants, but more likely a greater anteroposterior constraint. This statement is supported by the femoral low-point kinematics showing lower medial range-of-motion for the MC bearing when compared to the CR bearing. Thus, the MC bearing may provide increased intrinsic stability of the knee and thereby potentially reduce demands to ligaments and muscles as being other knee stabilizers.

Figure 7 Tibiofemoral load cases. Load case 1: a posterior load of the femur on the tibia corresponding to the extensor mechanism pulling at the tibia. Load case 2: an anterior load of the femur on tibia corresponding to the braking action of tibia. Load case 3: an anterior load of the femur on the tibia, corresponding to the increased moment from the centre of gravity’s forward movement and contraction of the gastrocnemius.

Knees with MC bearings have previously been shown to have a tendency of more extended knees at heel strike, and midstance compared with a posterior-stabilized knee design [17]. The same tendency of more extended knees during walking were also found for a different medial pivot TKA bearing design [36]. The lesser knee extension may be a consequence of more quadriceps and hamstring co-contraction that previously has been reported in patients following ACL reconstruction or TKA as a strategy to limit their demands to the quadriceps [4, 32, 37]. Our results confirm this tendency of more extended knees during these phases for the MC bearing group compared with the CR group. Thus, we speculate that the articulation design of the bearing potentially provides less requirement for the stabilizing quadriceps and hamstring co-contraction, but further biomechanical investigations are needed to confirm this relationship.

Clinical characteristics and PROMs

Clinical studies have reported excellent results for the MC bearing design although not significantly different compared to other designs [26, 27, 52]. Interestingly, one study identified a potential benefit for the MC design with better clinically assessed knee flexion range-of-motion [27]. However, though not statistically significant, this contradicts with our finding of more cases with manipulation under anaesthesia in the MC group when compared to the CR. With the mechanical findings of more a constrained knee, it is important that it does not inhibit the range-of-motion of the knee. Thus, further investigations concerning this are needed.

A meta-analysis study interestingly reported that patients with different designs inserted bilaterally preferred their medial pivot design over other designs and found it to be more stable and ‘normal’ [16]. However, we cannot conclude whether the mechanical differences in this study represents superior clinical outcome. Further research is still needed to establish associations of mechanical MC bearing design improvements, clinical outcomes, and patient satisfaction.

Limitations

We acknowledge that this study had some limitations. First, the gait pattern on the treadmill may be different from that during overground walking. However, some reports have declared that only minimal differences in kinetic and kinematic parameters were found between treadmill and overground walking [31, 50]. Barefoot walking may influence the load on the lower extremity joints within the subjects, but conditions were similar between groups. Thus, we do not expect this to affect neither the results, nor the conclusion. Second, leg-projection overlay during dRSA acquisition was inevitable. However, our setup ensured that one of the radiographic views were always free of overlay. We did not see a negative effect of leg-overlay on accuracy in the entire gait cycle. Third, the requirement of a maximum thigh circumference to ensure high quality of dRSA analysis have likely excluded very obese subjects with different knee kinematics [33]. However, the results provide important information on the kinematic advantages of MC bearings that may be used to improve future TKA designs.

Conclusion

We conclude that the design of the MC bearing changes tibiofemoral kinematics and enhances the area of congruency compared with the CR bearing design. This may result in improved control of the paradoxical motion, produce a more effective screw-home movement, and contribute to a more stabilized knee motion that may restore patient's confidence in knee function during daily activities, and potentially lead to improved patient satisfaction.

Conflict of interest: The authors have no conflicts of interest to declare.

Funding: Aarhus University, The Danish Rheumatism Association, Toyota-Fonden, Købmand Sven Hansen og Hustru Ina Hansens Fond, and Søster og Verner Lipperts Fond. Furthermore, Zimmer Biomet provided financial support for dynamic radiostereometric analysis investigations but had no role in collection, evaluation, or interpretation of the study data. The study sponsors have no conflicts of interest to declare.

Authors contribution: ETP was involved in all aspects of the study and drafted the manuscript. SR, DK, and JD operated the patients. SR examined and labelled the clinical characteristics. SR, TBH, MSA, and MS had an essential role in the study design, interpretation, and presentation of data. All authors contributed to data interpretation and manuscript revision.

References

1. Aalund PK, Larsen K, Hansen T, Bandholm T (2013) Normalized knee-extension strength or leg-press power after fast-track total knee arthroplasty: which measure is most closely associated with performance-based and self-reported function? Arch Phys Med Rehabil Arch Phys Med Rehabil 94:384–390
2. Baker PN, Van Der Meulen JH, Lewsey J, Gregg PJ (2007) The role of pain and function in determining patient satisfaction after total knee replacement - data from the national joint registry for England and Wales. J Bone Jt Surg [Br] 8989:893–900

3. Behrend H, Giesinger K, Giesinger JM, Kuster MS (2012) The "Forgotten Joint" as the Ultimate Goal in Joint Arthroplasty. Validation of a New Patient-Reported Outcome Measure. J Arthroplasty Churchill Livingstone Inc. 27
4. Benedetti MG, Catani F, Bilotta TW, Marcacci M, Mariani E, Giannini S (2003) Muscle activation pattern and gait biomechanics after total knee replacement. Clin Biomech 18:871–876
5. Bohannon RW, Williams Andrews A (2011, September) Normal walking speed: A descriptive meta-analysis. Physiotherapy
6. Van Der Bom IMJ, Klein S, Staring M, Homan R, Bartels LW, Pluim JPW (2011) Evaluation of optimization methods for intensity-based 2D-3D registration in x-ray guided interventions. In Dawant BM, Haynor DR (eds) Med Imaging 2011 Image Process SPIE, pp 657–671
7. Bourne RB, Chesworth BM, Davis AM, Mahomed NN, Charron KDJJ (2010) Patient satisfaction after total knee arthroplasty: Who is satisfied and who is not? Clin Orthop Relat Res Springer New York 468:57–63
8. Causero A, Di Benedetto P, Beltrame A, Gisonni R, Cainero V, Pagano M (2014) Design evolution in total knee replacement: which is the future? Acta Biomed 85:5–19
9. Christensen R, Petersen ET, Jürgens-Lahnstein J, Rytter S, Lindgren L, De Raedt S, Brüel A, Stilling M (2020) Assessment of knee kinematics with dynamic radiostereometry: Validation of an automated model-based method of analysis using bone models. J Orthop Res John Wiley and Sons Inc
10. Dabirrahmani D, Hogg M (2017) Modification of the Grood and Suntay Joint Coordinate System equations for knee joint flexion. Med Eng Phys 39:113–116
11. Davis MA, Ettinger WH, Neuhaus JM, Mallon KP (1991) Knee osteoarthritis and physical functioning: Evidence from the NHANES I epidemiologic followup study. J Rheumatol 18:591–598
12. Dawson J, Fitzpatrick R, Murray D, Carr A (1998) Questionnaire on the perceptions of patients about total knee replacement. J Bone Joint Surg Br England 80:63–69
13. Dennis DA, Komistek RD, Colwell CE, Ranawat CS, Scott RD, Thornhill TS, Lapp MA (1998) In Vivo Anteroposterior Femorotibial Translation of Total Knee Arthroplasty: A Multicenter Analysis. Clin. Orthop. Relat. Res. Number Lippincott Williams & Wilkins
14. Dyrby CO, Andriacchi TP (2004) Secondary motions of the knee during weight bearing and non-weight bearing activities. J Orthop Res 22:794–800
15. Farrokhi S, Tashman S, Gil AB, Klatt BA, Fitzgerald GK (2012) Are the kinematics of the knee joint altered during the loading response phase of gait in individuals with concurrent knee osteoarthritis and complaints of joint instability? A dynamic stereo X-ray study. Clin Biomech Elsevier Ltd 27:384–389
16. Fitch DA, Sedacki K, Yang Y (2014) Mid- to long-term outcomes of a medial-pivot system for primary total knee replacement: a systematic review and meta-analysis. Bone Joint Res Bone Joint Res 3:297–304
17. Ghirardelli S, Asay JL, Leonardi EA, Amoroso T, Indelli PF, Andriacchi TP (2021) Kinematic comparison between medially congruent and posterior-stabilized third-generation tka designs. J Funct Morphol Kinesiol MDPI AG 6
18. Gray HA, Guan S, Thomeer LT, Schache AG, de Steiger R, Pandy MG (2019) Three-dimensional motion of the knee-joint complex during normal walking revealed by mobile biplane x-ray imaging. J Orthop Res John Wiley and Sons Inc. 37:615–630
19. Grood ES, Suntay WJ (1983) A joint coordinate system for the clinical description of three-dimensional motions: application to the knee. J Biomech Eng 105:136–44
20. Guan S, Gray HA, Schache AG, Feller JA, de Steiger R, Pandy MG (2017) In vivo six-degree-of-freedom knee-joint kinematics in overground and treadmill walking following total knee arthroplasty. J Orthop Res J Orthop Res 35:1634–1643
21. Hallén LG, Lindahl O (1966) The screw-home movement in the knee-joint. Acta Orthop Informa Healthcare 37:97–106
22. Hansen L, De Raedt S, Jørgensen PB, Mygind-Klavsen B, Kaptein B, Stilling M (2018) Marker free model-based radiostereometric analysis for evaluation of hip joint kinematics. Bone Jt Res 7:379–387

23. Hasegawa M, Naito Y, Yamaguchi T, Wakabayashi H, Sudo A (2018) Factors Contributing to Patient Satisfaction and Expectations following Computer-Assisted Total Knee Arthroplasty. J Knee Surg J Knee Surg 31:448–452
24. Hawker G, Wright J, Coyte P, Paul J, Dittus R, Croxford R, Katz B, Bombardier C, Heck D, Freund D (1998) Health-related quality of life after knee replacement. J Bone Jt Surg (American Vol 80:163–173
25. Hemmingsen CK, Thillemann TM, Elmengaard B, de Raedt S, Nielsen ET, Mosegaard SB, Stentz-Olesen K, Stilling M (2020) Elbow Biomechanics, Radiocapitellar Joint Pressure, and Interosseous Membrane Strain Before and After Radial Head Arthroplasty. J Orthop Res J Orthop Res 38:510–522
26. Indelli PF, Morello F, Ghirardelli S, Fidanza A, Iannotti F, Ferrini A (2020) No clinical differences at the 2-year follow-up between single radius and J-curve medial pivot total knee arthroplasty in the treatment of neutral or varus knees. Knee Surgery, Sport Traumatol Arthrosc Springer Science and Business Media Deutschland GmbH 28:3949–3954
27. Indelli PF, Risitano S, Hall KE, Leonardi E, Migliore E (2019) Effect of polyethylene conformity on total knee arthroplasty early clinical outcomes. Knee Surgery, Sport Traumatol Arthrosc Springer Verlag 27:1028–1034
28. Kozanek M, Hosseini A, Liu F, Van de Velde SK, Gill TJ, Rubash HE, Li G (2009) Tibiofemoral kinematics and condylar motion during the stance phase of gait. J Biomech 42:1877–1884
29. Lafortune MA, Cavanagh PR, Sommer HJ, Kalenak~i A (1992) Three-dimensional kinematics of the human knee during walking. J. &mechanics
30. Lee JS, Hobden E, Stiell IG, Wells GA (2003) Clinically important change in the visual analog scale after adequate pain control. Acad Emerg Med Acad Emerg Med 10:1128–1130
31. Levine D, Richards J, MW W (2012) Whittle's Gait Analysis.
32. Lewek M, Rudolph K, Axe M, Snyder-Mackler L (2002) The effect of insufficient quadriceps strength on gait after anterior cruciate ligament reconstruction. Clin Biomech Elsevier 17:56–63
33. Li J, Tsai T, Brentzel K, Ahn YJ, Felson DT (2017) Three-Dimensional Knee Joint Kinematics in Obese Individuals with Knee Pain during Treadmill Gait. PLoS One 12:1–11
34. Martin JW, Whiteside LA The Influence of Joint Line Position on Knee Stability After Condylar Knee Arthroplasty.
35. Masouros SD, Bull AMJ, Amis AA (2010) (i) Biomechanics of the knee joint. Orthop Trauma Elsevier Ltd 24:84–91
36. Miura K, Ohkoshi Y, Ino T, Ukishiro K, Kawakami K, Suzuki S, Suzuki K, Maeda T (2020) Kinematics and center of axial rotation during walking after medial pivot type total knee arthroplasty. J Exp Orthop Springer Science and Business Media Deutschland GmbH 7
37. Mizner RL, Snyder-Mackler L (2005) Altered loading during walking and sit-to-stand is affected by quadriceps weakness after total knee arthroplasty. J Orthop Res 23:1083–1090
38. Nam D, Nunley RM, Barrack RL (2014) Patient dissatisfaction following total knee replacement: A growing concern? Bone Jt J 96B:96–100
39. Nemes S, Rolfson O, A WD, Garellick G, Sundberg M, Karrholm J, Robertsson O (2015) Historical view and future demand for knee arthroplasty in Sweden. Acta Orthop 86:426–431
40. Nichols TE, Holmes AP (2001) Nonparametric Permutation Tests For Functional Neuroimaging: A Primer with Examples.
41. Nielsen ET, Stentz-Olesen K, de Raedt S, Jørgensen PB, Sørensen OG, Kaptein B, Andersen MS, Stilling M (2018) Influence of the Anterolateral Ligament on Knee Laxity: A Biomechanical Cadaveric Study Measuring Knee Kinematics in 6 Degrees of Freedom Using Dynamic Radiostereometric Analysis. Orthop J Sport Med SAGE Publications Ltd 6
42. O'Connor CM, Thorpe SK, O'Malley MJ, Vaughan CL (2007) Automatic detection of gait events using kinematic data. Gait Posture 25:469–474
43. Odgaard A, Hospital G (2016) Dansk Knæalloplastikregister, Årsrapport 2016.
44. Pataky TC (2012) One-dimensional statistical parametric mapping in Python. Comput Methods Biomech Biomed Engin 15:295–301
45. Pataky TC, Robinson MA, Vanrenterghem J (2013) Vector field statistical analysis of kinematic and force trajectories. J Biomech 46:2394–2401
46. Peat G, McCarney R, Croft P (2001) Knee pain and osteoarthritis in older adults: a review of community burden and current use of primary health care. Ann Rheum Dis 60:91–7

47. Peterfy CG, Schneider E, Nevitt M (2008) The osteoarthritis initiative: report on the design rationale for the magnetic resonance imaging protocol for the knee. Osteoarthr Cartil Elsevier Ltd 16:1433–1441
48. Petersen ET, Rytter S, Koppens D, Dalsgaard J, Hansen TB, Larsen NE, Andersen MS, Stilling M (2021) Patients with knee osteoarthritis can be divided into subgroups based on tibiofemoral joint kinematics of gait – an exploratory and dynamic radiostereometric study. Osteoarthr Cartil
49. Petersen ET, Rytter S, Koppens D, Dalsgaard J, Hansen TB, Larsen NE, Andersen MS, Stilling M (2021) Patients with knee osteoarthritis can be divided into subgroups based on tibiofemoral joint kinematics of gait – an exploratory and dynamic radiostereometric study. Osteoarthr Cartil 1st revisi
50. Riley PO, Paolini G, Della Croce U, Paylo KW, Kerrigan DC (2007) A kinematic and kinetic comparison of overground and treadmill walking in healthy subjects. Gait Posture 26:17–24
51. Roos E (1998) The Knee Injury and Osteoarthritis Outcome Score. 1–5
52. Sabatini L, Risitano S, Parisi G, Tosto F, Indelli PF, Atzori F, Massè A (2018) Medial Pivot in Total Knee Arthroplasty: Literature Review and Our First Experience. Clin Med Insights Arthritis Musculoskelet Disord SAGE Publications 11
53. Tsubosaka M, Ishida K, Kodato K, Shibanuma N, Hayashi S, Kurosaka M, Kuroda R, Matsumoto T (2021) Mid-flexion stability in the anteroposterior plane is achieved with a medial congruent insert in cruciate-retaining total knee arthroplasty for varus osteoarthritis. Knee Surgery, Sport Traumatol Arthrosc Springer Science and Business Media Deutschland GmbH 29:467–473
54. Victor J, Bellemans J (2009) A comparative study on the biomechanics of the native human knee joint and total knee arthroplasty. Dep Orthop Fac Med PhD:168
55. Zhang Q, Chen Z, Zhang J, Hu J, Peng Y, Fan X, Jin Z (2019) Insert conformity variation affects kinematics and wear performance of total knee replacements. Clin Biomech Elsevier 65:19–25
56. Zimmer Biomet (2017) Persona® The Personalized Knee® - Medial Congruent® bearing design rationale. Warsaw
57. Zimmer Biomet (2017) Persona® The Personalized Knee® - Surgical Technique.